CATALYTIC ASYMMETRIC CHLOROFUNCTIONALIZATION REACTIONS:
MECHANISTIC DISCOVERIES AND ADVANCEMENTS

By

Aritra Sarkar

A DISSERTATION

Submitted to
Michigan State University
in partial fulfillment of the requirements
for the degree of

Chemistry–Doctor of Philosophy

2020

ABSTRACT

CATALYTIC ASYMMETRIC CHLOROFUNCTIONALIZATION REACTIONS:
MECHANISTIC DISCOVERIES AND ADVANCEMENTS

By

Aritra Sarkar

This thesis presents the mechanistic exploration of various catalytic asymmetric alkene halofunctionalization reactions. The mechanistic studies were focused on asymmetric halofunctionalization reactions that are catalyzed by the well-known, commercially available catalyst $(DHQD)_2PHAL$. Chemical kinetics were a central part of this investigation as the study entailed exploration of various kinetic properties, such as rate law equations, effects of isotopic substitution, and competition studies, to obtain key mechanistic insights into these reactions. The kinetic studies were complemented with computational modeling that led to the proposal of detailed catalytic models.

Chapter 1 introduces the inherent mechanistic challenges in a successful catalytic asymmetric alkene halofunctionalization reaction and also serves as an introduction to the kinetic tools that will be utilized in the following chapters to investigate the mechanism of the reactions. Chapter 2 presents the mechanistic investigation of $(DHQD)_2PHAL$ catalyzed asymmetric chlorolactonization of alkene carboxylic acids and illustrates the mechanistic model of catalysis for this reaction. Chapter 3 presents the mechanistic investigation of $DHQD)_2PHAL$ catalyzed asymmetric chloroetherification of alkene amides reaction. Interestingly, despite being driven by the same catalyst and chlorine source, evidences pointed to the two reactions having dramatically divergent mechanistic pictures.

ACKNOWLEDGEMENTS

I am incredibly grateful for the constant support from my friends and colleagues here at Michigan State University. First and foremost, I want to thank my advisor Prof. Babak Borhan, without whom the work presented thesis would not be possible. I will be forever grateful for his constant support and his trust in my ability to steer this research in directions I found most exciting. Babak is also an extraordinary mentor and teacher, and over the years, my interactions with him has greatly shaped how I communicate scientific ideas. Babak's endless guidance and unfaltering patience have allowed me to grow as a researcher and as a person.

Few people have been as instrumental to my research projects as Dr. Dan Holmes and Dr. Li Xie at the Max T. Rogers facility at MSU. From early days of my projects to the last, Dan and Li has spent endless hours training me on various NMR instruments and helping me to get my kinetic experiments up and running. I have spent numerous hours with them, brainstorming about ideas, discussing projects and various NMR technique. I will always be in debt to Dan and Li for their incredible support as mentors and friends.

I am grateful for the support provided by my committee members: Prof. Ned Jackson, Prof. William D. Wulff and Prof. Dan Jones. Ned has been my default go-to person whenever I am stuck on a mechanistic question or when I am out of ideas. The hours I have spent in Ned's office with me, Ned and Babak, bouncing new ideas back and forth were some of the most exciting moments of graduate research. Every week of my graduate school I have looked forward to Prof. Wulff's database meetings, not only was it a fantastic opportunity to learn about new reactions and it also taught me how

iii

TABLE OF CONTENTS

LIST OF TABLES

LIST OF FIGURES

KEY TO SYMBOLS AND ABBREVIATIONS

Å	Angstrom
cm^{-1}	wavenumber
h	hour
mg	milligram
g	gram
M	molar
°C	degree Celsius
K	kelvin
mM	millimolar
mmol	millimole
μL	microliter
mL	milliliter
L	liter
min	minutes
exp	experiment
conc.	concentration
rxn	reaction
eq	equation
ln	natural logarithm
kcal/mol	kilocalorie per mole
ppm	parts per million

MS	molecular sieves
dr	diastereomeric ratio
er	enantiomeric ratio
ee	enantiomeric excess
aq	aqueous
ZPE	zero-point energy
ΔE	difference in energy
ΔG	difference in Gibbs free energy
ΔH	difference in enthalpy
ΔS	difference in entropy
Δt	difference in time
xs	excess
k_{obs}	observed rate constant
LA	Lewis acid
LB	Lewis base
cat	catalyst
Nuc	nucleophile
$CHCl_3$	chloroform
$CDCl_3$	deuterated chloroform
MeCN	acetonitrile
CD_3CN	deuterated acetonitrile
MeOH	methanol
CD_3OH	deuterated methanol

CH_2Cl_2	dichloromethane
H_2O	water
D_2O	deuterium oxide
Et_2O	diethyl ether
EtOH	ethanol
ROH	alcohol
Hex	*n*-hexane
*n*PrOH	*n*-propanol
nPrNO$_2$	1-nitropropane
THF	tetrahydrofuran
HCl	hydrogen chloride
HFIP	1,1,1,3,3,3-hexafluoroisopropanol
TFE	1,1,1-trifluoroethanol
Na_2CO_3	Sodium carbonate
NaHCO3	sodium bicarbonate
NaOH	sodium hydroxide
K_2CO_3	potassium carbonate
Na_2SO_3	sodium sulfite
$Na_2S_2O_3$	sodium thiosulfate
Na_2SO_4	sodium sulfate
CaH_2	calcium hydride
(DHQD)$_2$PHAL	Hydroquinidine 1,4-phthalazinediyl diether
(DHQ)$_2$PHAL	Hydroquinine 1,4-phthalazinediyl diether

NCS	N-chlorosuccinimide
NBS	N-bromosuccinimide
NIS	N-iodosuccinimide
DCDMH	1,3-dichloro-5,5-dimethylhydantoin
MCDMH	3-chloro-5,5-dimethylhydantoin
DMH	5,5-dimethylhydantoin
DCH	1,3-dichlorohydantoin
MCH	3-chlorohydantoin
DCDPH	1,3-dichloro-5,5-diphenylhydantoin
DBDMH	1,3-dibromo-5,5-dimethylhydantoin
HalA	halenium affinity
NAAA	nucleophile assisted alkene activation
Ad_E3	termolecular electrophilic addition
NMR	nuclear magnetic resonance
ROESY	rotating frame overhauser effect spectroscopy
COSY	correlation spectroscopy
HSQC	heteronuclear quantum coherence
HMBC	heteronuclear multiple bond correlation
NOE	nuclear overhauser effect
DOSY	diffusion ordered spectroscopy
IR	infrared
HPLC	high performance liquid chromatography
UV	ultraviolet

Vis	visible
HRMS	high resolution mass spectrometry
ESI	electrospray ionization
RPKA	reaction progress kinetic analysis
VTNA	variable time normalized analysis
v	rate of reaction
KIE	kinetic isotopic effect
DFT	density functional theory
TS	transition state
H-bonding	hydrogen bonding

Chapter 1. Catalytic asymmetric alkene halofunctionalization reaction and kinetic approaches for mechanistic studies

Catalytic asymmetric alkene halofunctionalization reactions are a rapidly evolving area. Despite recent developments and the flurry of reports in this area, the mechanism for catalysis remains largely unexplored. This chapter aims to introduce the possible mechanistic scenarios for the uncatalyzed halofunctionalization reactions and illustrate the challenges in attaining catalyst-controlled selectivity in product formation. This was followed with a discussion on the working models for catalysis that have been proposed in literature thus far. The second part of the Chapter 1 presents an introduction to various kinetic analysis protocols and tools that will be utilized throughout the thesis to explore the mechanism of the catalytic processes.

1.1 Catalytic asymmetric halofunctionalization reaction

Alkene halogenation are a well-known class of reactions that pertains to addition of halogen atoms to olefinic centers leading to the formation of organohalides (Figure 1.1). The apparent familiarity of alkene halogenation reaction for anyone associated in the area of chemical sciences stems from its early incorporation into organic chemistry textbooks.[1] While, earliest reports of halogenation reactions dates back to the 19th century,[2] currently, these halogenation reactions are some of the very first reactions taught to sophomore level undergraduate students. Perhaps the most commonly depicted mechanism for these addition reactions is where the alkene attacks the electrophilic halogen center (X) leading to the formation of a cationic haliranium intermediate, which in turn is captured by a nucleophile (Y) (Figure 1.1).[3] If the nucleophile (Y) involved in the second step is a halide, the reaction is a dihalogenation reaction. However, one may also

envision a more generalized scenario, where the nucleophile is not restricted to a halide, but can also be a nucleophile such as water, alcohol, carboxylic acids or amines. To encompass all these scenarios, a more generalized term coined for these reactions is the alkene halofunctionalization reaction.
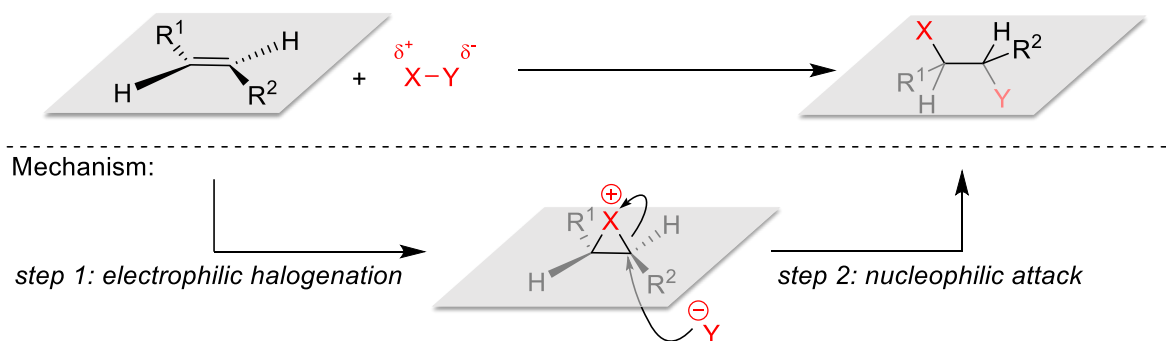
Figure 1.1 Alkene halogenation reaction. A classical depiction of electrophilic halogenation of alkene via a cyclic haliranium ion intermediate.

The utility of halofunctionalization reactions stems from versatility, as not only this reaction allows one to quickly introduce multiple functional groups in an olefinic moiety, but the nature of the carbon-halogen bond enables introduction of other functional groups (substitution reactions, coupling reactions etc.[4-6] A catalytic asymmetric version of halofunctionalization would augment the utility of this reaction by providing an efficient means to rapidly access various chiral motifs.[7, 8] Despite the potential application of catalytic asymmetric halofunctionalization reactions, their appearance is surprisingly recent in modern literature. In 2010, Borhan and co-workers reported one of the very first, practical, catalytic asymmetric halofunctionalization reaction.[9] This reaction, which was catalyzed by an organocatalyst (DHQD)₂PHAL, involved the chlorination and cyclization 1,1-disubstituted alkene carboxylic acids (Figure 1.2) to generate chiral chlorolactones. Since this report, example of halofunctionalizations in the literature has burgeoned over

the last decade,[10-17] further underscoring the interest of the scientific community to find efficient ways to halofunctionalization simple olefins.

a)

b)

55-86%, 43-90% ee
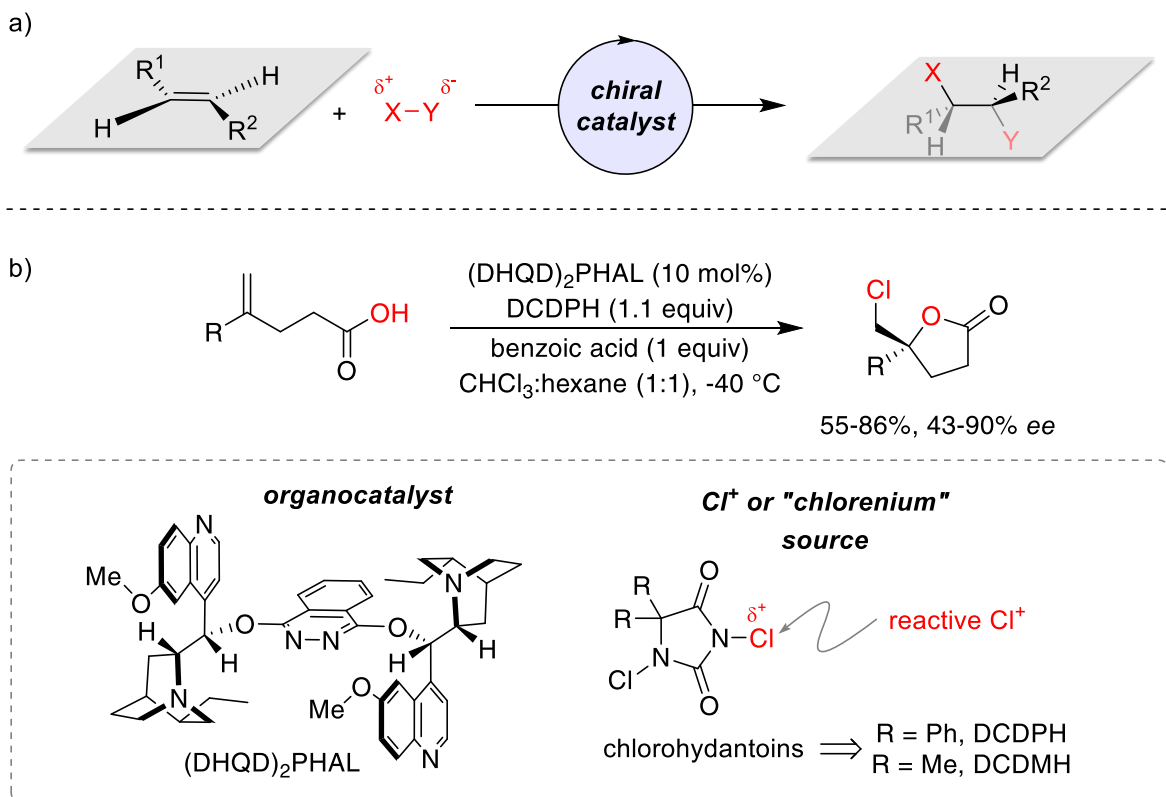
Figure 1.2 Catalytic asymmetric halofunctionalization of alkene. (a) A schematic depiction of catalytic asymmetric halofunctionalization of alkene to make chiral organohalides. (b) Catalytic asymmetric chlorolactonization of alkene carboxylic acids.

Despite the rapid growth in this emerging area of catalytic asymmetric halofunctionalization significant challenges remain, both in terms of rational catalyst design and in expanding the applicability and substrate scope.[10, 11] These challenges have prevailed in part due to the dearth in mechanistic insights into these catalytic asymmetric halofunctionalization process. While many of these reported catalytic asymmetric halofunctionalizations have put forth hypothesized working models, most of these models have little mechanistic support. A detailed mechanistic analysis of catalytic asymmetric halofunctionalization would not only illuminate the catalytic process, but also

3

could provide critical information that can potentially be leveraged to improve existing reactions or even design new asymmetric transformations.

1.2 Challenges in asymmetric stereoinduction: A non-trivial mechanism of addition

The most simplistic mechanistic picture for halofunctionalization consists of a two-step addition of halenium and nucleophile to an olefin, via a three membered halonium (or haliranium) intermediate (Figure 1.1), as proposed originally by Roberts and Kimball,[3] and later experimentally supported by Olah.[18-20] While this interpretation is not incorrect, it often represents only a segment of the various mechanistic possibilities. While NMR studies by Olah and coworkers have shown evidence for the existence of these cyclic haliranium intermediates, significant evidences have also favored an open β-halocarbenium ion intermediate[21-25] as shown in Figure 1.3, This is especially true for chlorine due to its high electronegativity as compared to bromine and iodine. Studies have also shown that in the absence of any significant electronic bias in an olefinic center, the successively formed β-halocarbenium ion can be in an equilibrium with its regioisomeric form, as well as with the cyclic halirenium form. Furthermore, Brown and coworkers have also demonstrated that these cyclic haliranium intermediates can engage in a halenium exchange equilibrium with unreacted olefins at a rate comparable to that of diffusion-controlled reaction the.[26-28]

β-chlorocarbenium isomer

Classical *interpretation*

cyclic haliranium ion

olefin to olefin halenium transfer

β-chlorocarbenium isomer
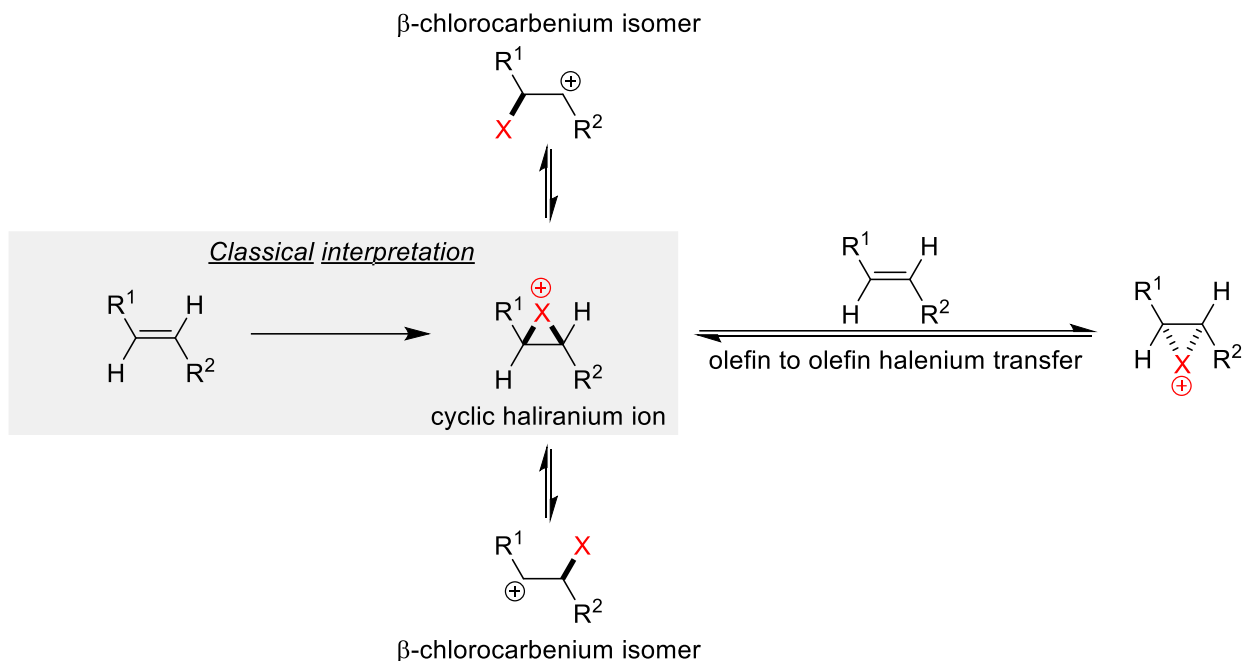
Figure 1.3 Mechanism of alkene halogenation. Above is a depiction of the various outcomes of electrophilic halogenation of alkene and the fate of a classical cyclic haliranium ion intermediate

Once all these pathways are taken into account, the overall mechanism of an olefin halofunctionalization process becomes far less trivial than what is often interpreted in a typical undergraduate textbook. The key challenges in attaining any form of selectivity (regio-, diastereo-, or enantioselectivity) in a halofunctionalization reaction thus lies in its unique mechanistic possibilities. To envision this better, consider a simplified scenario of a catalytic asymmetric halofunctionalization reaction via the irreversible formation cyclic haliranium intermediate (Figure 1.4a). Achievement of high enantioselectivity will hinge on the catalyst's ability to control the delivery of the halenium ion in a face selective manner in the first step. A high diastereoselectivity is also expected if this is the only mechanism, as the nucleophiles will presumably attack the haliranium intermediate from the opposite face of the halenium addition, leading to an anti-addition. But the regioselectivity of the nucleophile attack will either have to be controlled by the internal

5

bias of the alkene or the catalyst. This will lead to a successful regio- and stereoselectivity in this simplified scenario for a catalystic asymmetric halofunctionalization reaction. If the possibility of an olefin to olefin halenium transfer is now factored in (Figure 1.4b), one is suddenly faced with a precarious scenario where this rapid exchange completely scrambles the stereocenter set by the catalyst in cyclic haliranium intermediate, which in turn would lead to a complete or partial racemic product mixture. The prospect of this unfortunate outcome has been elegantly demonstrated by Denmark and co-workers.[29] They showed that by doping a process that involved a stereoselective, nucleophilic trapping of an in-situ generated chiral bromonium intermediates with external olefins led to a noticeable loss of the stereoselectivity, via olefin to olefin halenium transfer. The results from their study immediately underscores the challenge posed by such olefin to olefin halenium transfer processes towards the development of a successful catalytic asymmetric halofunctionalization reaction.
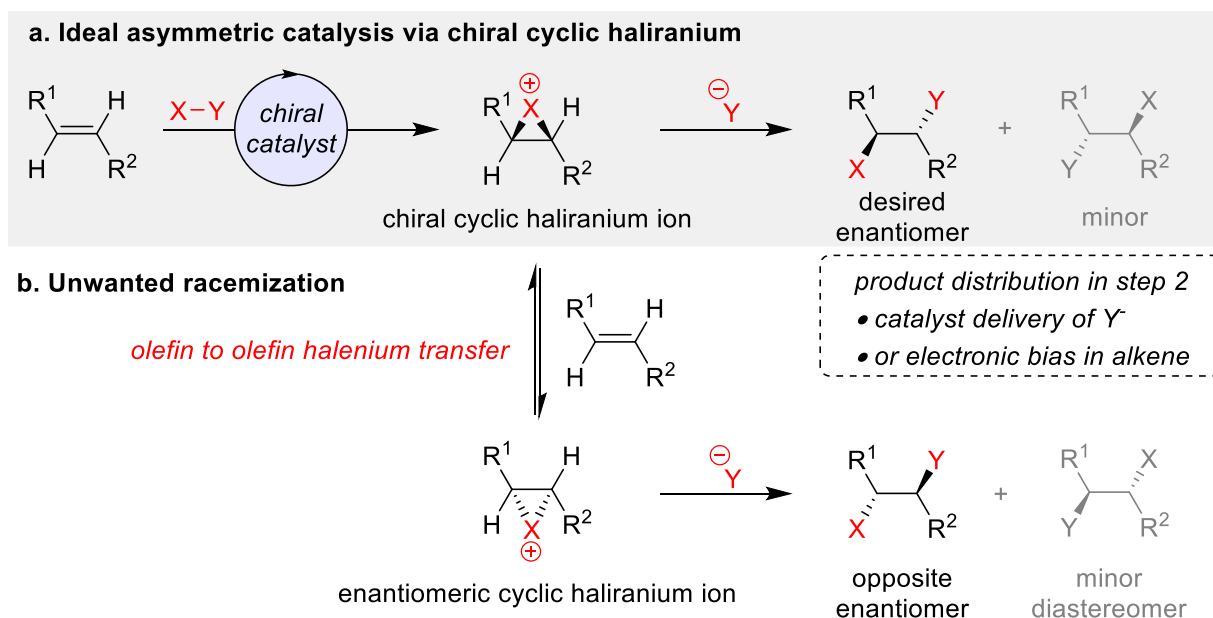
Figure 1.4 Challenges in catalytic asymmetric halofunctionalization via cyclic haliranium intermediate. (a) Depiction of an ideal catalytic asymmetric halofunctionalization reaction via a cyclic haliranium intermediate. Note that so long as

(Figure 1.4 (cont'd)) alkene's electronic bias controls the regioselectivity of addition in step 2, the catalyst only needs to control the face-selectivity of step 1. (b) Depicts an unwanted racemization pathway, that may rescind face-selectivity set by the catalyst.

Now consider another simplistic scenario where the reaction is a two-step process via the irreversible formation of a β-halocarbenium ion intermediate (Figure 1.5a). In this scenario, face selectivity in the addition of the halenium ion as well as the nucleophile has to be catalyst controlled in order to obtain any enantioselectivity or diastereoselectivity. The regioselectivity has to be controlled either by the alkene's internal electronic/steric bias or by the catalyst. This scenario by itself is not trivial as now the catalyst has to serve the purpose of a bifunctional catalyst controlling the selectivity of addition of both the nucleophile and the electrophile separately in both step 1 and step 2. Failure of the catalyst to control the selectivity both step 1 and step 2 simultaneously would lead to a loss of diastereoselectivity as shown in Figure 1.5b and Figure 1.5c.
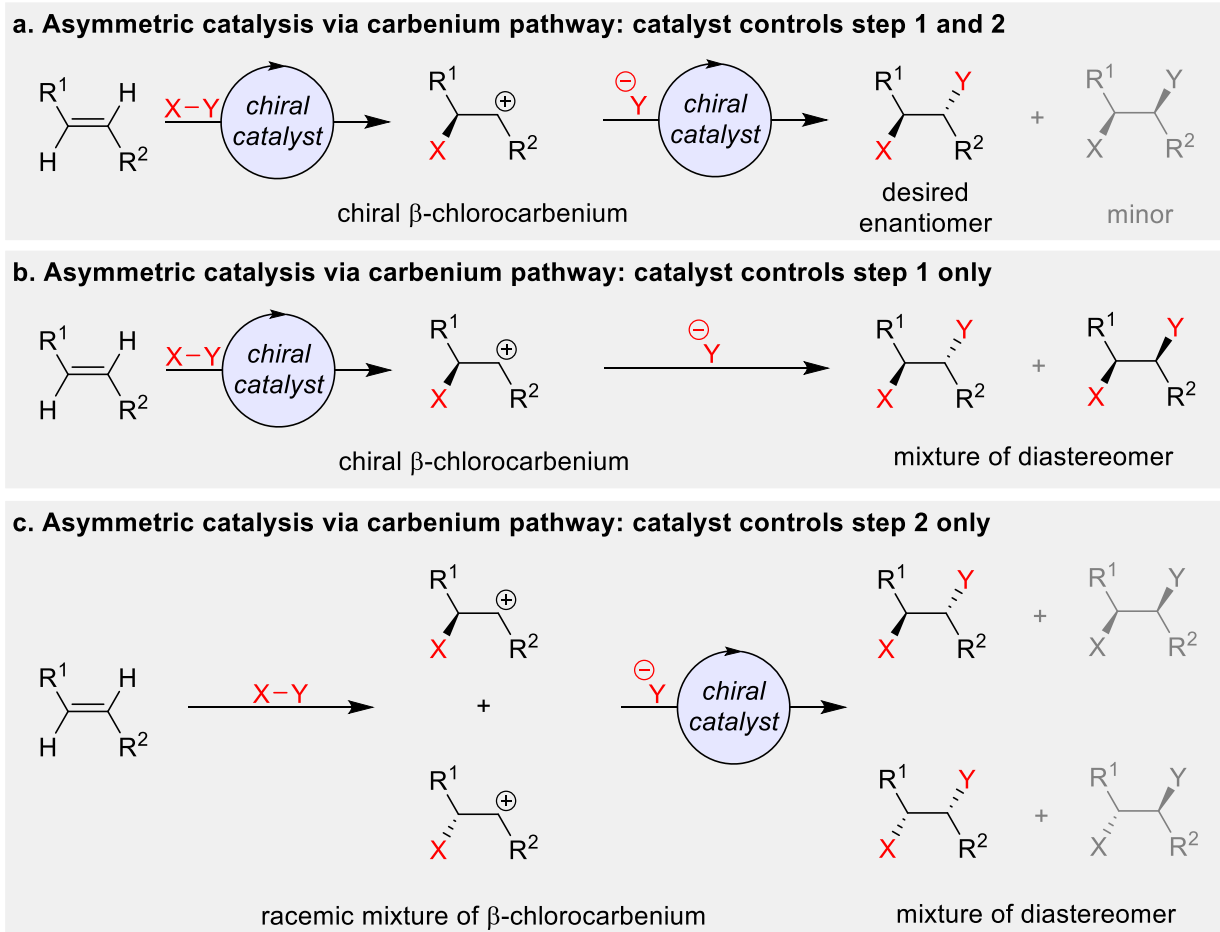
Figure 1.5 Challenges in catalytic asymmetric halofunctionalization via a β-halocarbenium pathway. (a) Depiction of an ideal catalytic asymmetric halofunctionalization reaction via β-halocarbenium pathway. To selectively generate only one stereoisomer, the catalyst must exert selectivity in both step 1 and step 2. (b) Failure of catalyst to control face selectivity of nucleophile in step 2 will lead to a loss in diastereoselectivity. (c) Failure of catalyst to control face selectivity of the halenium in step 1 will lead to a mixture of diastereomer.

Nonetheless, this model becomes exponentially more convoluted once the reversibility of the halenium addition step and the possibility of the simultaneous existence of multiple β-halocarbenium regioisomers and cyclic haliranium intermediates are factored in. If the multiple β-halocarbenium regioisomer have comparable lifetimes, one could potentially scramble the regioselectivity in the products. If the olefin-to-olefin halenium transfer is at play, even the face selectivity of the halenium would be lost. Thus, even if a catalyst exerts perfect selectivity in step 1 and step 2 of the addition, the rapid

8

equilibria between the different intermediates could lead to a complete loss of selectivity. Figure 1.6 attempts to illustrate this loss of selectivity by considering all of these possibilities.
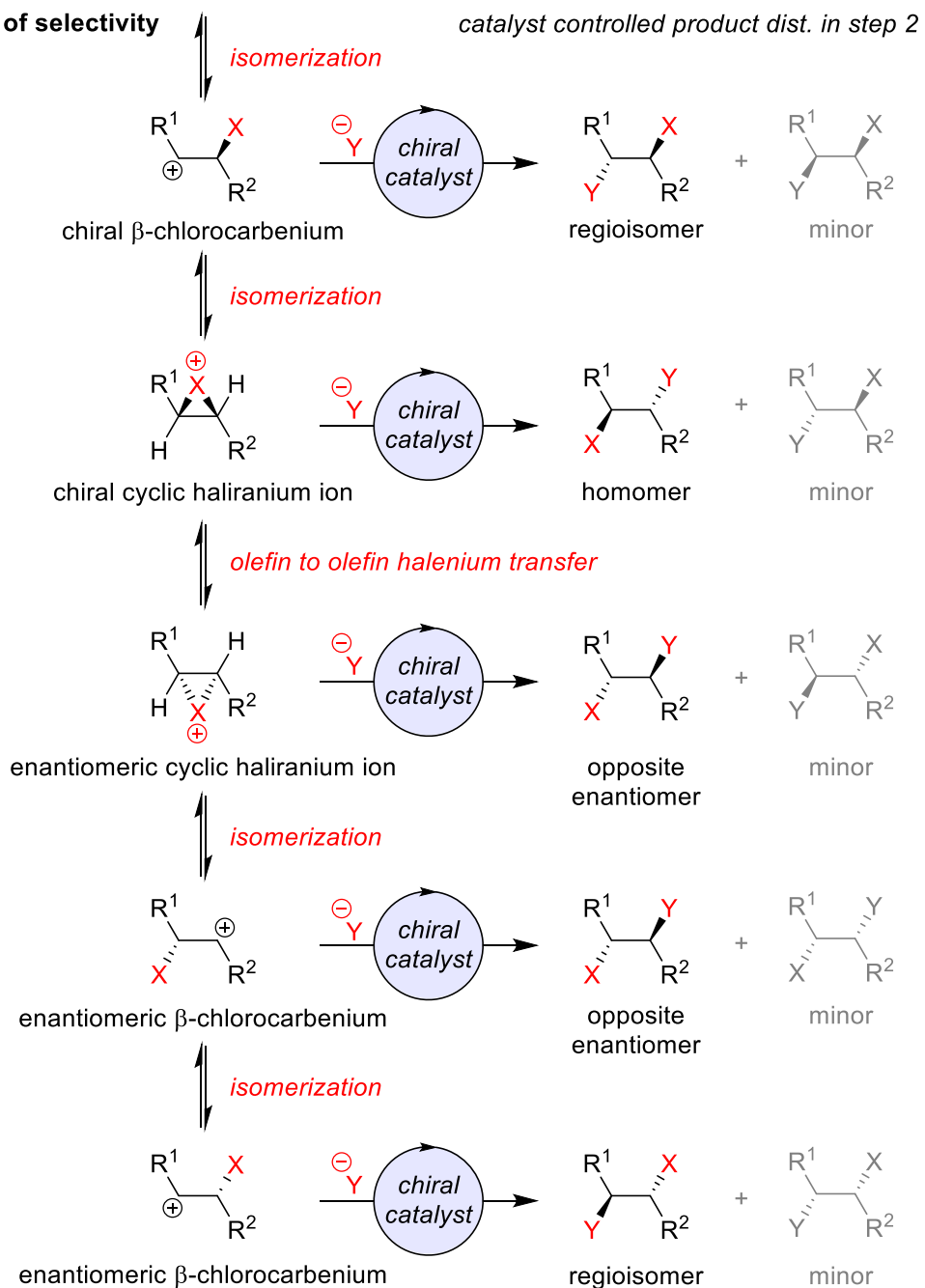
Figure 1.6 Challenges in catalytic asymmetric halofunctionalization. (a) Depiction of an ideal catalytic asymmetric halofunctionalization reaction via β-halocarbenium pathway. (b) Various pathways to lose all selectivity despite the catalyst successfully controlling

(Figure 1.6 (cont'd)) the face-selective delivery of both the halenium (step 1) and nucleophile (step 2).

The above exercise hopefully demonstrates how addition of these mechanistic possibilities to the classical halofunctionalization pathway (via a cyclic haliranium intermediate) can disproportionately increase the challenges in developing a successful catalytic asymmetric halofunctionalization reaction.

1.3   Another mechanistic possibility: concerted addition pathway

The above mechanistic models for halofunctionalization focused on a stepwise addition process which is initiated by the alkene's attack on the electrophilic halenium, however, recent reports have shed light on the possibility of an alternative mechanistic scenario. Independent investigations by Borhan and co-workers as well as by Denmark and co-workers have provided strong experimental evidence in favor of a one-step concerted Ad_E3-type addition mechanism (Figure 1.7).[30, 31] In this concerted addition pathway, the alkene engages both the electrophilic halenium ion as well as the nucleophile simultaneously.

a. Concerted addition pathway for halofunctionalization
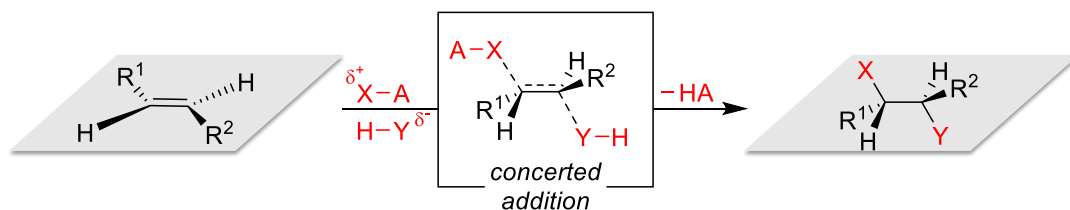
b. Concerted addition for chlorolactonization *One-step concerted addition*
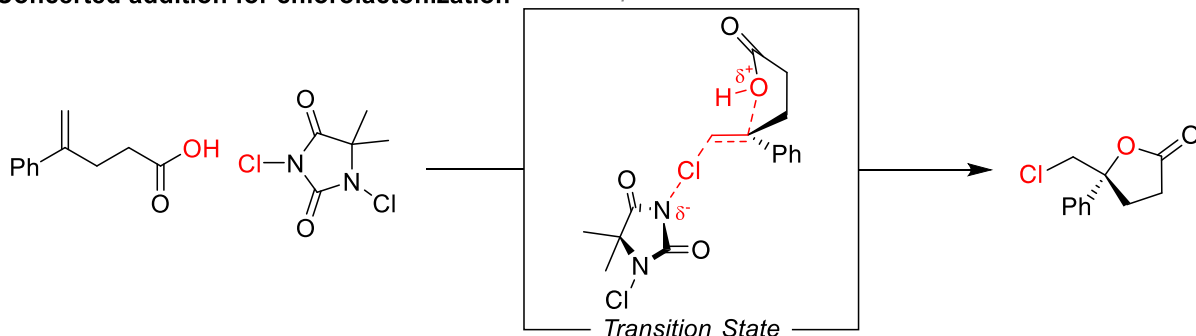
Figure 1.7 A concerted addition pathway for halofunctionalization. (a) Depiction of a concerted addition pathway for halofunctionalization of an alkene. (b) Uncatalyzed chlorolactonization reaction has been shown to take a concerted addition pathway for addition.

The operation of this concerted addition pathway was perhaps first hinted at during the development of a parameter called halenium affinity, which as the name suggests provides a measure of the affinity of a species toward binding to a halenium ion (shown in Figure 1.8a).[32] Halenium affinity of a species can easily be calculated using relatively inexpensive density functional models and relates to the ground state enthalpic difference between the halogenated and the de-halogenated species. In a system with multiple Lewis basic centers competing for a halenium ion, halenium affinity calculation can accurately predict the location of the halenium ion (Figure 1.8b). Halenium affinities can also be calculated for species that at a glance might not appear as typical Lewis bases, such as alkenes, where the halogenated species would be either the cyclic haliranium or the β-halocarbenium ions. A few of these reported halenium affinity calculations[32] are shown in Figure 1.8c.

12

a. Halenium affinity

LB + X⁺ ⇌ LB—X

lewis base *halenium* *halogenated adduct*
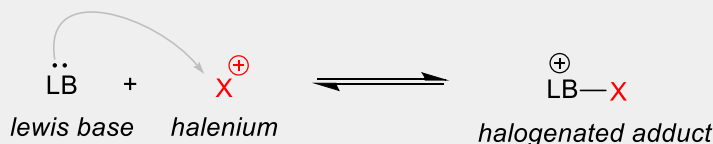
Halenium affinity of the lewis base can be calculated from the following equation

$$HalA\ (X) = -\Delta E_{elec} - \Delta ZPE - \Delta E_{vib} + \frac{5}{2}RT$$

b. Predicting reactivity using halenium affinity

Y–X + Z⁻ ⇌ Y⁻ + Z–X

HalA (X) of Z⁻ > HalA (X) of Y⁻

Y–X + Z⁻ ⇌ Y⁻ + Z–X

HalA (X) of Z⁻ < HalA (X) of Y⁻
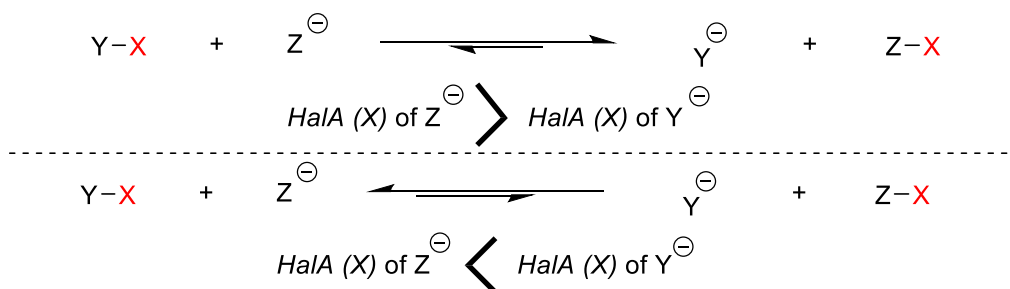
c. Shown below are halenium affinities of select species relevant to halofunctionalization

252.1   275.7   290.1   171.3   C¹ site: 173.8
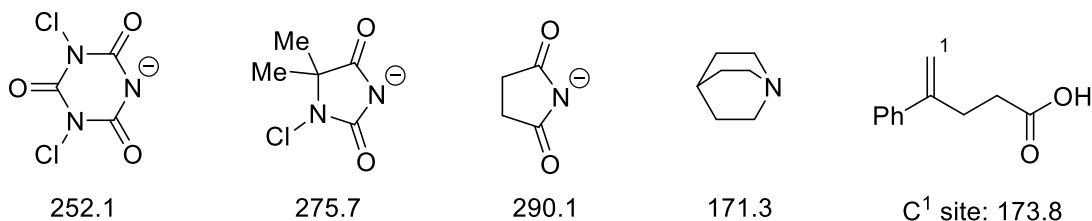
The above HalA (Cl) values are calculated in gas phase (DFT-B3LYP/6-31G*)
The values are taken from Kumar *et al. J. Am. Chem. Soc.* **2014**, *136*, 13355

Figure 1.8 Halenium affinities. (a) Depiction of a general definition for halenium affinity. (b) The halogenating ability of a species may be predicted based on halenium affinity calculation. Higher the halenium affinity of a dehalogenated species, worse it is as a halogenating agent. (c) Shown are the reported halenium affinities of several species. The halenium affinity values (in kcal/mol) were calculated with density functionals B3LYP/6-31G* and in gas phase.

Halenium affinity calculation is a tool that enabled one to predict whether a halogenating agent would be thermodynamically potent to halogenate an alkene. However, attempting to directly apply halenium affinities to predict alkene reactivities led to some unanticipated results. For example, certain alkenes, such the one shown in Figure 1.9a, were predicted to be unreactive towards the used halogenating agents yet

13

they reacted readily.[30] Understanding this unusual reactivity led to a detailed investigation into the reactive conformations of these alkenes, which in-turn revealed a novel addition pathway via a concerted addition mechanism.

For the chlorolactonization reaction, the reactive alkene precursor (Figure 1.9c) was found to be in a biased conformation where the nucleophile (carboxylic acid) is positioned in a way where it is poised for a simultaneous attack on the alkene as it captures the halenium. This reactive precursor conformation of the alkene (often dubbed the nucleophile activated alkene) is often a few kcal/mol unit higher in energy as compared to the fully relaxed alkene. However, it does kinetically enable the alkene to capture the halenium ion by simultaneously compensating the charge development on the alkenoic center by the nucleophile's engagement and obviating the formation of high-energy, cationic intermediates altogether. The nucleophile's engagement in the process to enable the halogenation of an otherwise unreactive alkene led to the process being dubbed nucleophile-assisted alkene activation or NAAA. This concerted addition pathway in chlorolactonization reaction that was hinted at by halenium affinity calculations of the folded and the unfolded alkenes (Figure 1.9b) were supported with various kinetic isotopic effect studies (not shown here).[30]

It is important to note that while halenium affinity is a thermodynamic parameter, NAAA, is a purely kinetic phenomenon as it pertains to the nucleophile's effects on the transition state of the reaction, as it lowers the activation energy barrier in the process. However, it has been shown that one may be able to factor in the effect of NAAA into halenium affinity calculations and thereby predict alkene reactivity, by measuring

halenium affinities of conformational minima in alkenes that well represent NAAA conformation of the concerted addition.[30]

a. Halenium predicted uncatalyzed chlorolactonization reaction

lower HalA (158.8)

HalA prediction: reaction not feasible
Observed: product was obtained

higher HalA (181.1)
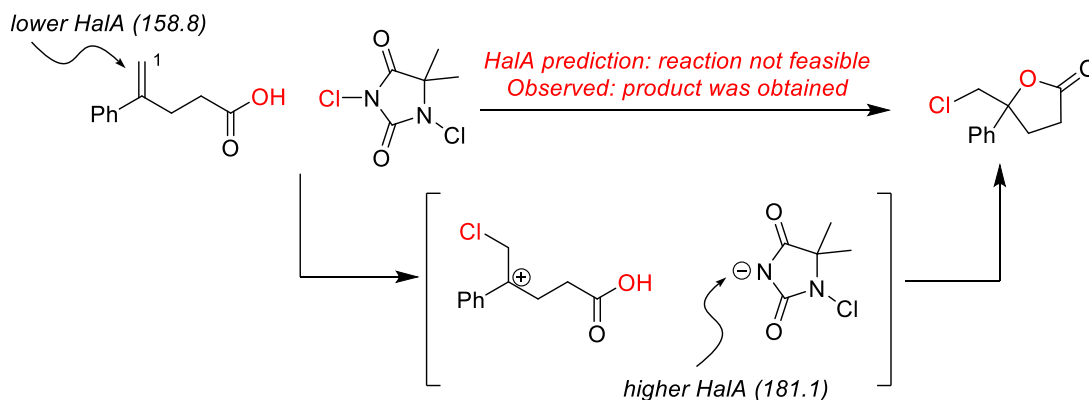
b. Halenium affinity calculations that led to the discovery of concerted NAAA addition pathway

181.1

C^1 site: 158.8

173

folded conformation

C^1 site: 173.3
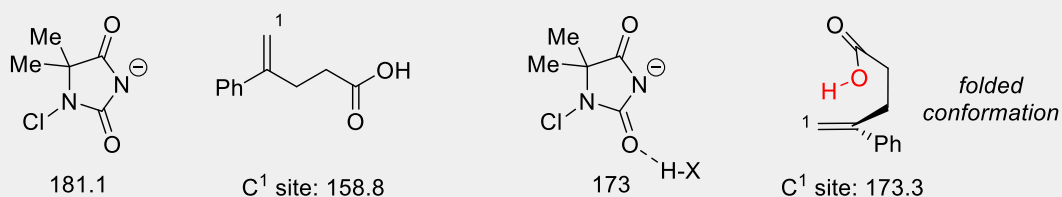
HalA (Cl) calculations in DFT-B3LYP/6-31G*/SM8(CHCl$_3$)
The values (in kcal/mol) are taken from Kumar *et al. J. Am. Chem. Soc.* **2016**, *138*, 8114

c. Discovery of a concerted addition pathway for uncatalyzed chlorolactonization

open conformation (unreactive)

disfavored (by 14.2 kcal/mol)

folded conformation (reactive)

One-step concerted addition

favored

Transition State
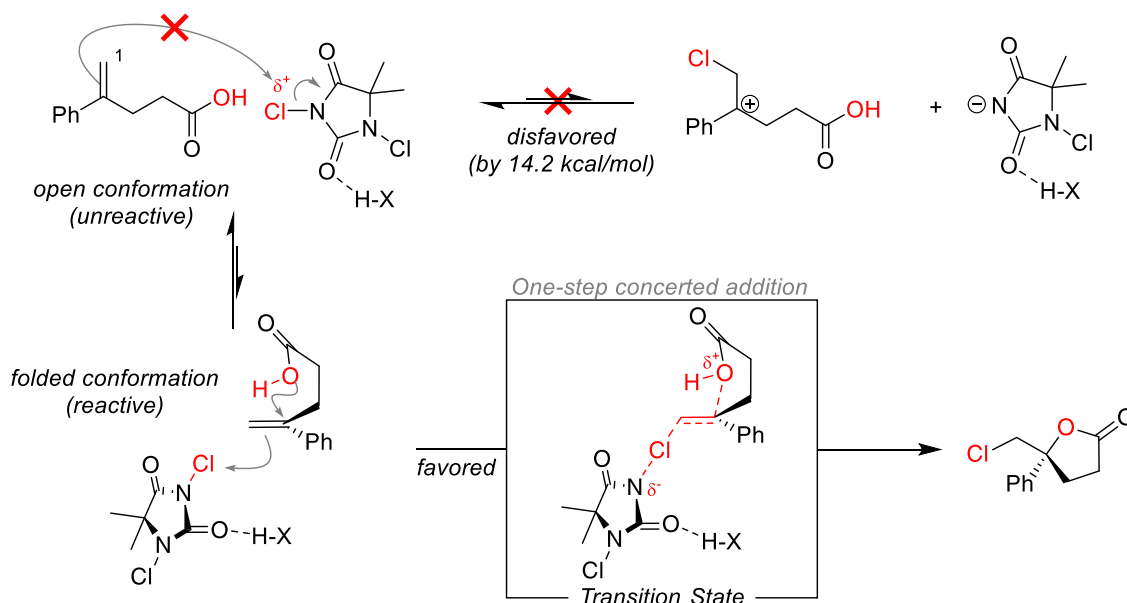
Figure 1.9 Discovery of concerted NAAA addition pathway for chlorolactonization reaction. (a) Halenium predicted reactivity of chlorolactonization (b) Halenium affinity

15

(Figure 1.9 (cont'd)) calculations that indicated a folded conformation of the alkene was necessary for effective halenium transfer from the halogen source to the alkene. (b) Depiction of the feasibility of the concerted pathway versus the stepwise addition pathway.

To summarize, there are multiple possible pathways for alkene halofunctionalization. Evidences have shown the possibility of both stepwise and concerted addition pathways, as well as several unwanted pathways for isomerizations and racemizations. However, these studies have only explored either uncatalyzed reaction systems or reactions that are not asymmetric halofunctionalizations. The mechanism of the catalytic asymmetric halofunctionalization yet remains unexplored. Nonetheless, these detailed studies lay the foundation for the rest of the chapters as we explore more of the catalytic asymmetric reaction systems.

1.4   Role of the catalyst

To understand the catalytic version of an uncatalyzed reaction one must first probe the role served by the catalyst, specifically with regards to the stereoinduction in the product in an asymmetry catalysis. Denmark and co-workers have elegantly summarized a set of four plausible catalytic models to account for the role of the catalyst in various reported catalytic asymmetric halofunctionalization reactions.[10] While these models certainly do not cover every possible catalytic behavior, it represents a good starting framework to build more complex models, and are highlighted briefly. The catalytic models are as follows:

Chiral Lewis base catalytic systems (type I). As the name suggests, in these systems the chiral catalyst has a chiral Lewis basic center that is halogenated first and in turn delivers the halenium ion over to the reacting alkenoic center in a stereoselective manner (Figure 1.10a). Perhaps the simplest of the catalytic models, reactions that are

16

hypothesized to obey this model also represent some of the oldest/earliest efforts towards catalytic asymmetric halofunctionalization reactions.[10] In reality, the catalysts in these models are chiral mediators for the halenium source rather than actual catalyst, as every example either uses stoichiometric or super-stoichiometric amount of the chiral "catalyst" (Figure 1.10b).[33] A reason for this could be that these chiral mediators could do not successful accelerate the "catalytic" pathway over the background reaction, in other words, catalyst-halenium complexation do not lead to an activated halenium complex.
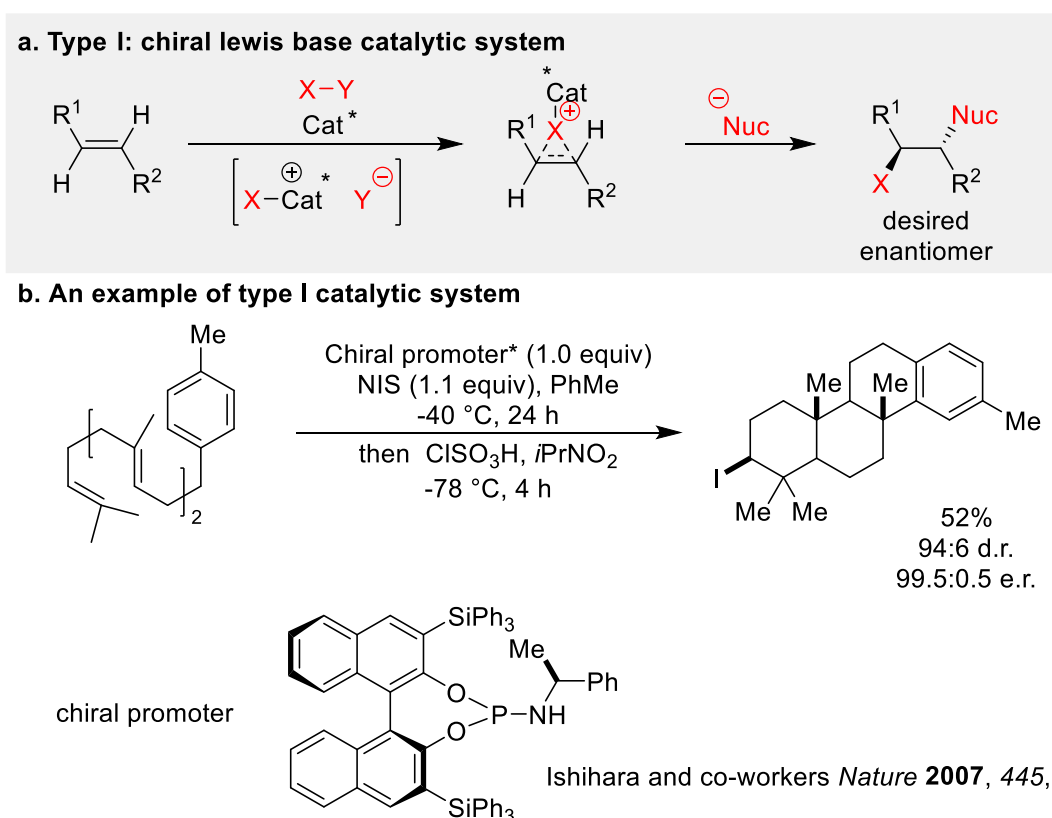
Figure 1.10 Chiral lewis base catalyst system (type I). (a) Depicts the mechanism of halenium delivery for catalyst in type I model. (b) An example of a catalytic system hypothesized to be following a type I mechanistic model is one reported by Ishihara and co-workers.

Chiral ion-pairing catalytic systems (type II): This is a variation of the first system, where the chiral catalyst and the halenium ion source forms a tight adduct, either through ion-pairing or a hydrogen bonded complex (Figure 1.11). This chiral adduct is now a more

potent halenium donor (as compared to the naked halenium source) and ferries the halenium to the reacting alkene center leading to the halofunctionalization. A majority of the reported catalytic asymmetric halofunctionalization reactions are hypothesized to follow this pathway; an example of this type is shown in Figure 1.11b.[34]
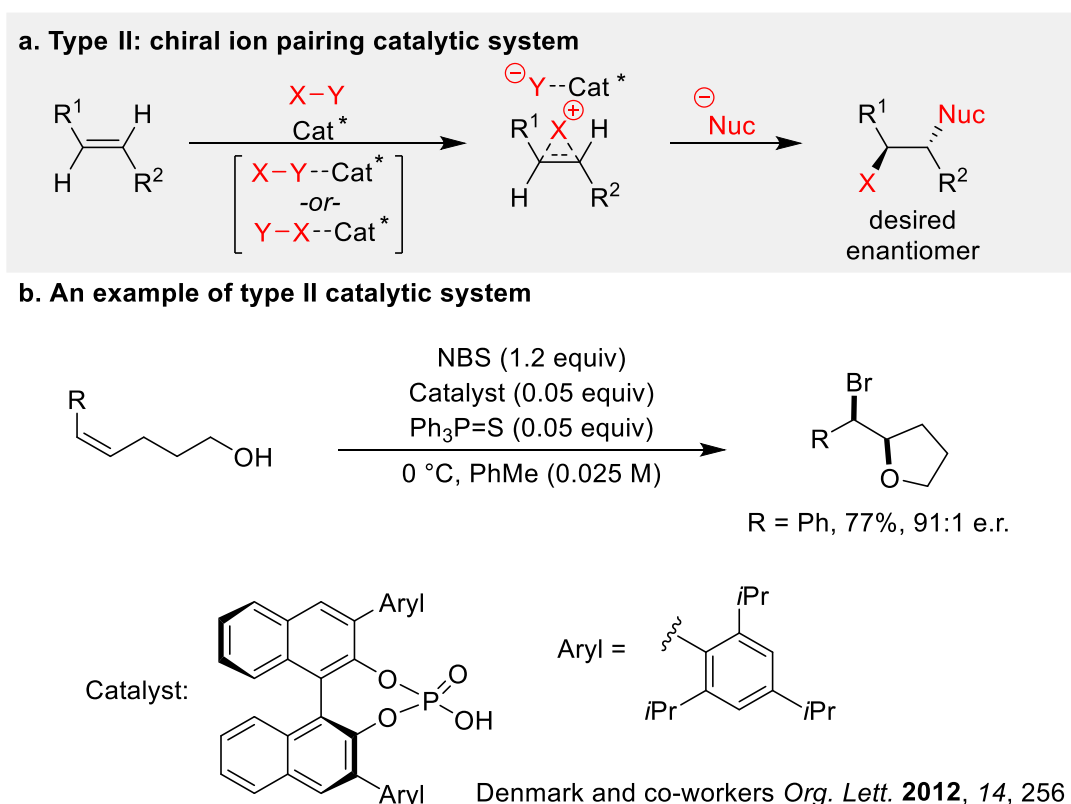
Figure 1.11 Chiral ion pairing catalyst system (type II). (a) Depicts the mechanism of halenium delivery and stereoinduction for catalyst in type II model. (b) An example of a catalytic system hypothesized to be following a type II mechanistic model is one reported by Denmark and co-workers.

Hydrogen bonded substrate-catalyst complex (type III): In both the type 1 and 2 systems, the catalyst creates a chiral halenium source, leading to its facial discrimination in halenium delivery. In type 3 systems, the alkene substate is bound within the catalytic cavity via hydrogen bonding, this enables the incoming halogen source to stereo-differentiation between the two faces of the alkene (Figure 1.12). While the face-selectivity of the alkene is determined by its binding to the catalyst, the enhanced reactivity of

catalytic pathway over the background reaction, that is presumably arising from the activation of the halenium source is more difficult to rationalize.[10] To justify the reactivity of these catalytic systems, the catalyst-alkene complex is typically depicted to further pre-organize with the halenium source into ternary complexes leading to an activated complex. An example of a reaction hypothesized to follow this mechanism is reported by Nicolaou and co-workers is shown in Figure 1.12b.[35] Note that perhaps the success of these catalytic systems can be better explained in many cases by invoking the possibility of a concerted (NAAA) pathway, where the catalyst-bound nucleophilic site of the alkene is more activated for a concerted addition. This will be explored further in chapter 2 for chlorolactonization reaction, another reaction hypothesized to follow the same type III mechanistic model.
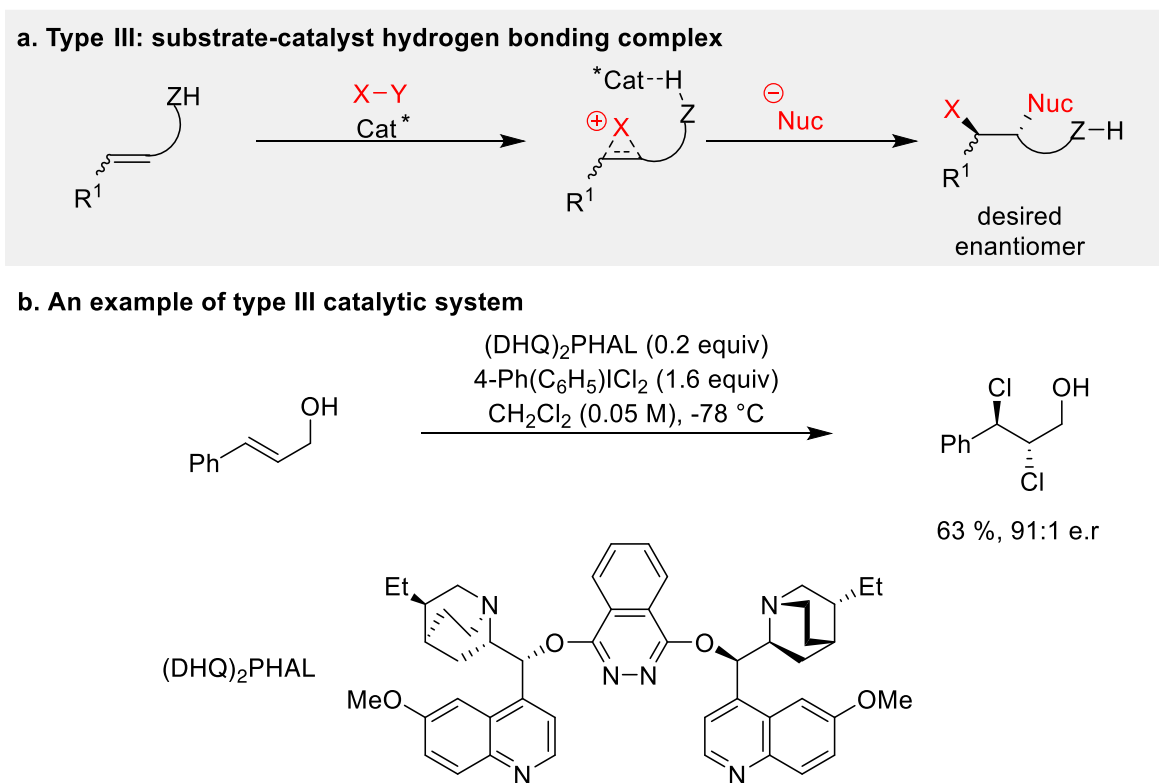
Nicolaou and co-workers *J. Am. Chem. Soc.* **2011**, *133*, 8134

Figure 1.12 Substrate-catalyst hydrogen bonded complex (type III). (a) Depicts the mechanism of halenium delivery and stereoinduction for catalyst in type III model. (b) An

19

(Figure 1.12 (cont'd)) example of a catalytic system hypothesized to be following a type III mechanistic model is one reported by Nicolaou and co-workers.

Bound substrate via Lewis acid-base adduct (type IV): Quite similar to type three systems, these are also heavily preorganized systems where the catalyst, alkene and the halenium source are arranged via Lewis acid-base interactions (Figure 1.12). The catalytic asymmetric halofunctionalization reactions reported by Burn and co-workers, for instance, are hypothesized to obey this model (Figure 1.13).[7, 36]

a. Type IV: Lewis acid-base complex

b. An example of type IV catalytic system
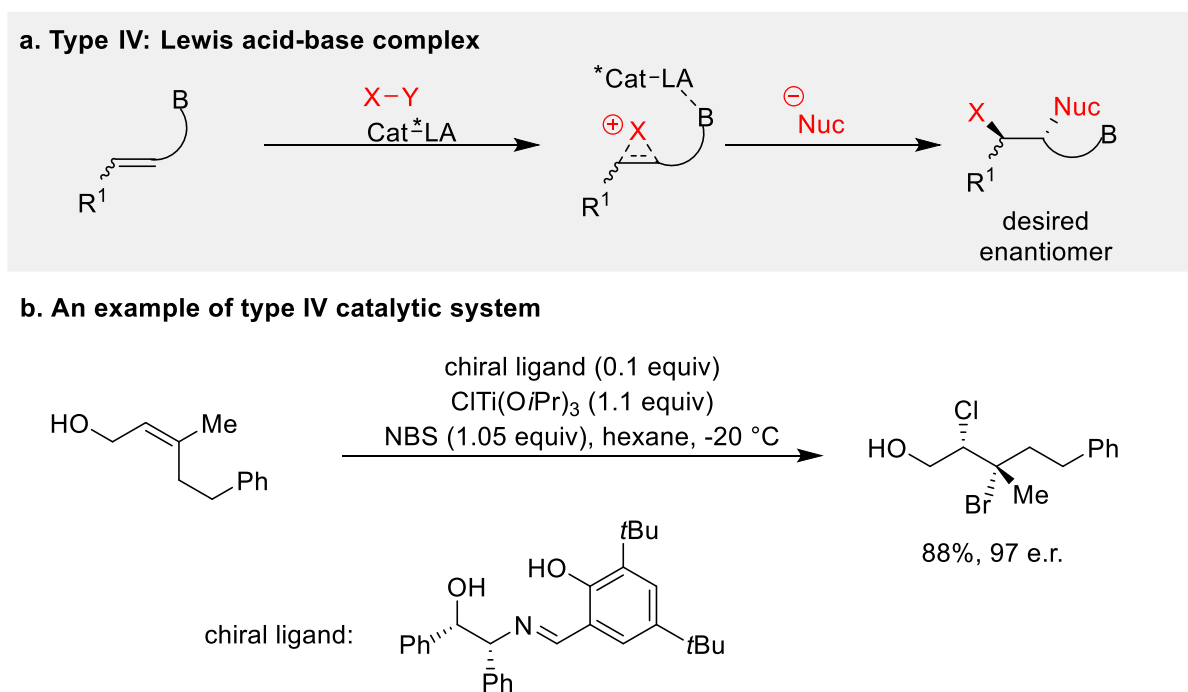
Burns and co-workers *J. Am. Chem. Soc.* **2015**, *137*, 3795

Figure 1.13 Substrate-catalyst Lewis acid-base complex (type IV). (a) Depicts the mechanism of halenium delivery and stereoinduction for catalyst in type III model. (b) An example of a catalytic system hypothesized to be following a type IV mechanistic model is one reported by Burns and co-workers.

A few cautionary notes, while the above models are elegant and logical from a chemical sense, they are mostly formulated based on preexisting knowledge of uncatalyzed processes. The reactions that have been allotted to different models, are done so with only little, or in some cases no experimental investigations into the

20

mechanism, but using mostly one's chemical intuition. In fact, Denmark and co-workers have also pointed this out for several reactions where the proposed mechanisms were found to have conflicting interpretations.[10] Furthermore, the models have been proposed with mostly a haliranium intermediate pathway in mind.

1.5 (DHQD)$_2$PHAL catalyzed asymmetric halofunctionalization reaction

With an exploration of the possible mechanism of addition in halofunctionalization and roles of catalyst for a catalytic asymmetric version, let us return to the (DHQD)$_2$PHAL catalyzed halofunctionalization reaction mentioned earlier in the chapter. (DHQD)$_2$PHAL is a dimeric cinchona alkaloid that has found remarkable success in its role as chiral organocatalyst for various chlorofunctionalization reactions. Since the report of catalytic asymmetric chlorolactonization (Figure 1.2) in 2010 by Borhan and co-workers,[9] a number of catalytic asymmetric chlorofunctionalization have been reported to have used (DHQD)$_2$PHAL as the chiral catalyst.[37-43] These chlorofunctionalization reactions are typically categorized into two types based on the location of the nucleophile, 1) cyclization reactions where the nucleophile are tethered to the alkene or are intramolecular (Figure 1.14a), and 2) reactions that use external nucleophiles or are intermolecular (Figure 1.14b). Examples of the former include chlorolactonization,[9] chlorocyclization of alkene amides,[37] chlorocyclization of alkene carbamates,[38] while some examples of the latter class are chloroetherifications,[41] dichlorinations,[42] and chloroamidations.[43]
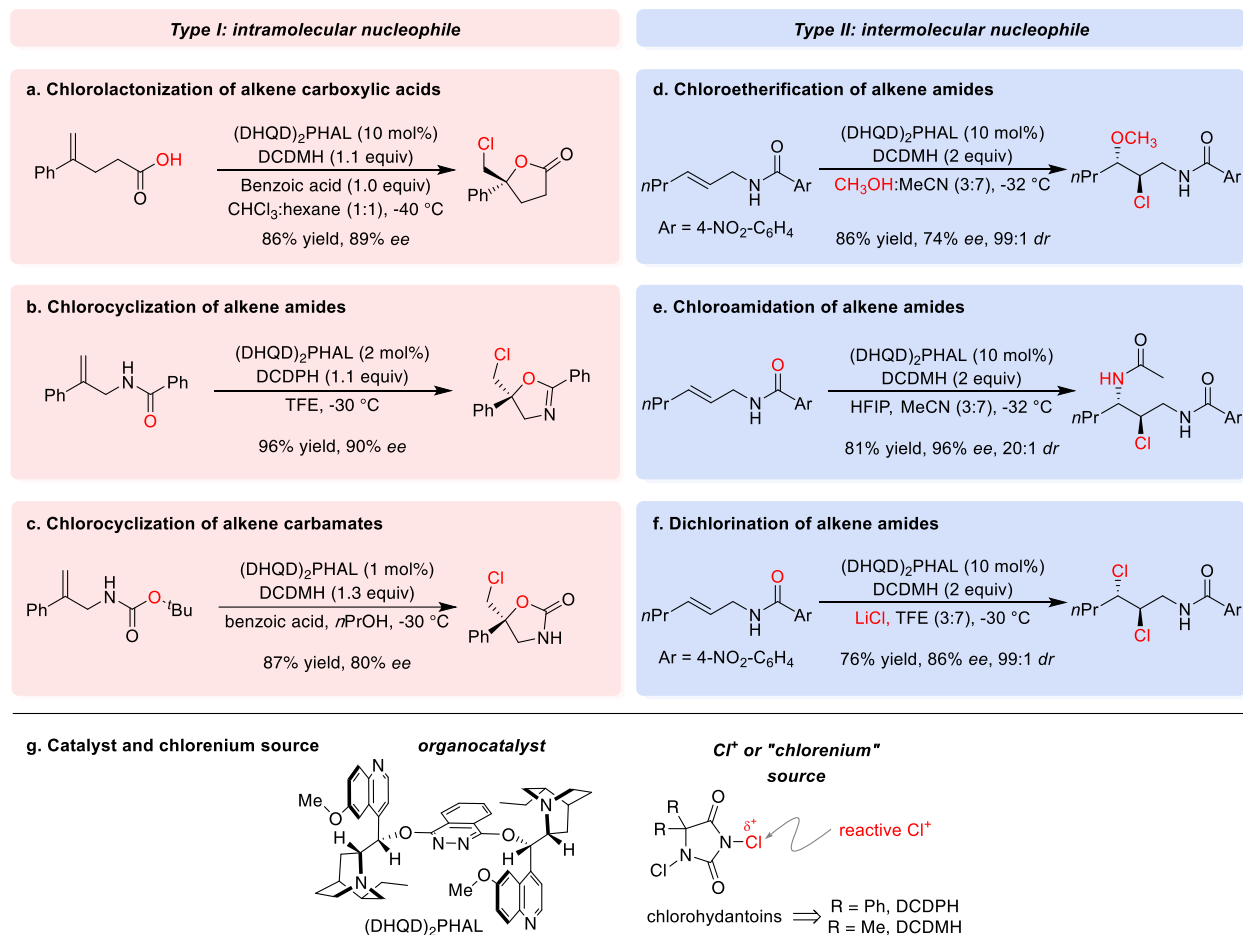
Figure 1.14 (DHQD)₂PHAL catalyzed asymmetric alkene chlorofunctionalization reaction. Type I systems (a) Chlorolactonization of alkene carboxylic acids. (b) Chlorocyclization of alkene amides. (c) Chlorocyclization of alkene carbamates. Type II systems (d) chloroetherification of alkene amides. (e) Chloroamidation of alkene amides. (f) Dichlorination of alkene amides. (g) Catalyst and chlorine source utilized for these chlorofunctionalization reactions.

Despite the success of (DHQD)₂PHAL as a chiral catalyst for catalytic asymmetric chlorofunctionalization reactions, little is still known about the mechanism of the reaction. Based on a few preliminary investigations on the chlorolactonization reaction,[10] the model for (DHQD)₂PHAL catalyzed reactions have been hypothesized to be that of type III (Figure 1.12), where the substrate is presumably sitting in the catalytic cavity, while the chlorenium source delivers the halogen in a face selective manner. However, there is a lack of any rigorous investigations to rule out alternative mechanistic possibilities.

Investigations of the face selectivity of these reactions have also led to some interesting revelations that are hard to explain with a single generalized mechanism. For instance, the alkene face selectivity of the nucleophile is completely different in the cyclization of alkene carboxylic acid (chlorolactonization) versus the cyclization of alkene amides.[44, 45] Interestingly, the alkene carboxylic acid was found to undergo a syn-addition, which is difficult to explain with the classical mechanistic model of addition via a cyclic haliranium intermediate. However, the amide cyclization was found to proceed as an anti-addition (Figure 1.15a). This difference is surprising given the two reaction systems are driven by the same catalyst and similar chlorenium source, the only major difference between the two systems being the amide vs carboxylic acid serving as the nucleophile and polar protic vs non-polar solvent environment. Perhaps more interesting is the cyclization of alkene carbamate,[38, 45] where only a change from a polar protic to non-polar solvent changes the face selectivity of the nucleophile, leading to syn-addition in the former case and anti-addition in the latter (Figure 1.15b). In this case the polar protic conditions led to improved selectivity at lower temperatures while the non-polar conditions had improved selectivity at a more elevated temperature. Furthermore, all polar reactions were found to have severely enhanced rate while most non-polar reactions were much slower.
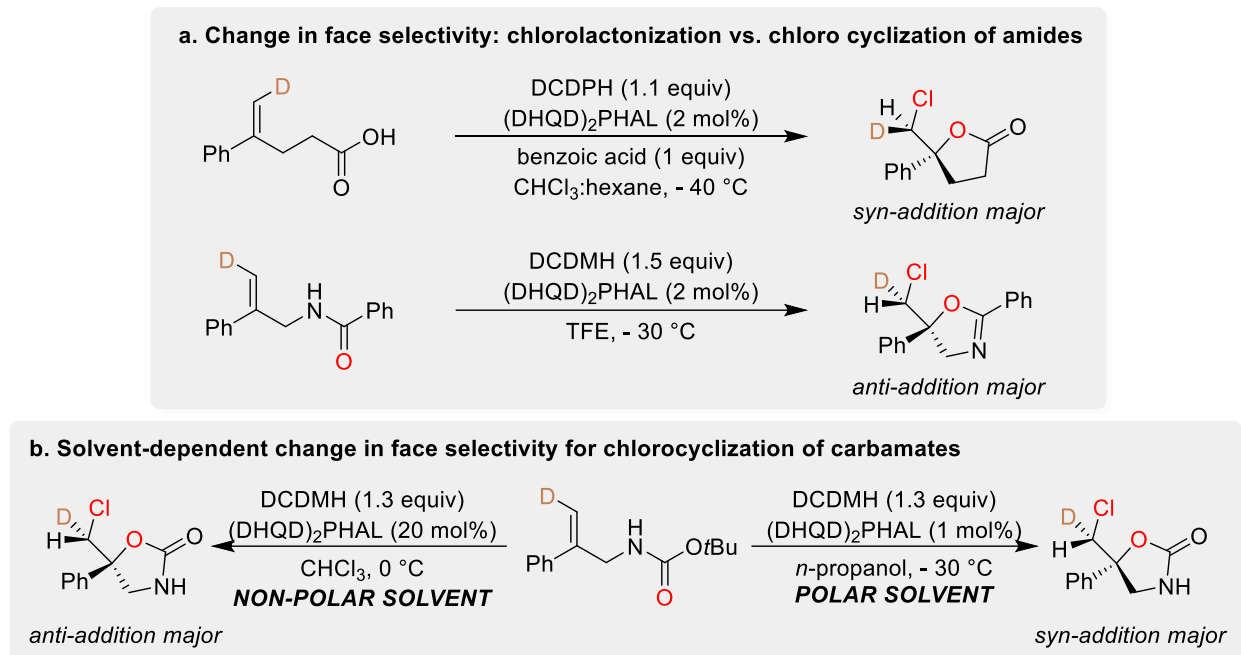
Figure 1.15 Prior mechanistic studies for dissecting the face selectivities. (a) Change in nucleophile face selectivity for chlorolactonization vs chlorocyclization of alkene amide. (b) Solvent dependent change in nucleophile face selectivity in chlorocyclization of alkene carbamates.

These differences pointed to a non-trivial mechanistic scenario which needed a thorough mechanistic investigation. Some reasonable questions about the mechanism of these catalytic asymmetric halofunctionalization reactions may be:

1) What is the mechanism of addition?

2) What role does the catalyst serves?

3) How does the catalytic pathway lower the activation energy barrier?

4) How does is the asymmetric induction taking place?

5) Is the mechanism same for all of the reactions listed in Figure 1.14?

To answer these questions, we have conducted an in-depth mechanistic study using chemical kinetics as our primary tool for mechanistic exploration. The mechanism will be explored in the form of two catalytic asymmetric chlorofunctionalization reactions 1) Chlorolactonization reaction, which will be the subject of Chapter 2, 2)

24

Chloroetherification reaction, which will be the subject of Chapter 3. Kinetics is an integral, albeit not the only tool utilized for our mechanistic studies. Thus, the following sections of this chapter will discuss some of the early and recent kinetic techniques that are relevant to our investigations.

1.6   Kinetic studies

Chemical kinetics is an area of study that measures and analyzes the temporal-concentration profile of reacting components for the reaction under study.[46] Often these studies are associated with divulging the empirical function linking the concentration of each reacting component to the reaction rate, also known as the rate law equation. The studies leading to a rate equation can provide critical information relating to the mechanism of the reaction under study. Although finding the rate law equation will be the primary goal of our mechanistic studies, the study of chemical kinetics encompasses numerous other tools for mechanistic investigation, including the effect of isotopic substituent on reaction rates (kinetic isotopic effects),[47] finding activation parameters[48-50] (Eyring plots), etc. As such, chemical kinetics has historically been an indispensable tool for mechanistic investigations.[51] In the following section, we will discuss how obtaining a rate law equation can allow for the development of mechanistic models.

1.7   Reaction rate and the rate law equation

Kinetic experiments that measure the temporal change in concentration of various components in a reaction can provide one with the rate of the reaction. While detailed discussion on the definition of the rate of a reaction can be found in several advanced texts,[51-53] to accomplish a meaningful transition into kinetic studies in the following

sections, we will briefly introduce the idea of rate using a simple example. Consider a simple chemical transformation:

$$aA + bB \rightarrow cC + dD \hspace{4cm} \text{rxn (1.0)}$$

For the above reaction A, B, C and D are the chemical components while *a, b, c* and *d* are the stoichiometric coefficients of each component that allows a balanced chemical equation. The rate of the above reaction can be defined in terms of the concentration of the substrates and products as follows:

$$rate = -\frac{1}{a}\frac{d[A]}{dt} = -\frac{1}{b}\frac{d[B]}{dt} = \frac{1}{c}\frac{d[C]}{dt} = \frac{1}{d}\frac{d[D]}{dt} \hspace{2cm} \text{eq (1.1)}$$

Where [A], [B], [C] and [D] are the concentration of the respective components at time t. Thus, rate of a reaction is defined by the concentration change of each component per unit time, normalized with their stoichiometry of consumption in the reaction.[51-53] The rate can often be represented as a function of the concentration of the various reacting components as shown in equation (1.2).

$$rate = f([A], [B]) \hspace{5cm} \text{eq (1.2)}$$

These functions f([A],[B]), are known as the rate law equation for representative reaction. The mathematical form of this rate function can be derived from the mechanistic model of the reaction, and conversely, the form of the rate equation function reflects the mechanistic model. This is demonstrated by using a simplified reaction (Rxn 2) in Figure 1.16, where one may notice how two different reaction mechanism for the same transformation yields different rate law equations. Thus, experimentally determining this mathematical form of the rate law can illuminate the mechanism of the reaction.

$$A \quad + \quad B \longrightarrow C \quad + \quad D \qquad \qquad ....Rxn\ (2)$$

Model reaction 1:

$$A + B \underset{k_{-1}}{\overset{k_1}{\rightleftharpoons}} I \xrightarrow[\text{slow step}]{k_2} C + D$$

Model reaction 2:

$$A \underset{k_{-1}}{\overset{\substack{k_1 \\ \text{slow step}}}{\rightleftharpoons}} I \xrightarrow[k_2]{B} C + D$$

Rate of the reaction:

$$\text{rate} = \frac{d[C]}{dt} = k_2[I]$$

Rate of the reaction:

$$\text{rate} = \frac{d[C]}{dt} = k_2[I][B]$$

Since step 2 is slow, step 1 can be presummed to be in an equilibrium. Thus,

$$K_{eq} = \frac{k_1}{k_{-1}} = \frac{[I]}{[A][B]}$$

Rearranging the above equation provides I

$$[I] = K_{eq}[A][B]$$

Since step 1 is slow, I is consumed as soon as it is formed. Thus one may assume steady state for I,

$$\frac{d[I]}{dt} = k_1[A] - k_2[I][B] - k_{-1}[I] = 0$$

Rearranging the above equation provides I

$$[I] = \frac{k_1[A]}{k_2[B] + k_{-1}}$$

Rate law equation:

$$\text{rate} = k_2[I] = k_2K_{eq}[A][B]$$

Rate law equation:

$$\text{rate} = k_2[I] = \frac{k_2k_1[A][B]}{k_2[B] + k_{-1}}$$

Figure 1.16 Different rate equation for different mechanistic models . This figure depicts different mechanistic scenarios may lead to different rate equation for the same reaction.

It is, however, important to note that the form of a rate equation is always not unique to a singular mechanism, in other words, multiple mechanistic scenarios can lead to the same form of rate equation. This is shown in Figure 1.17, despite the two-rate equation being different, they have similar form, that is the rate of the reaction is $k_{obs}[A][B]$. Thus, it is often necessary to complement these kinetic studies with other investigations, such as kinetic isotopic effect studies, to establish a reaction mechanism with a greater degree of certainty. Nonetheless, determination of the rate law sets a stringent boundary conditions, often dramatically cutting the number of mechanistic possibilities to only a select few.

Model reaction 1:

$$A + B \underset{k_{-1}}{\overset{k_1}{\rightleftharpoons}} I \xrightarrow[\text{slow step}]{k_2} C + D$$

Model reaction 3:

$$A + B \underset{k_{-1}}{\overset{\overset{k_1}{\text{slow step}}}{\rightleftharpoons}} I \xrightarrow{k_2} C + D$$

Rate of the reaction:
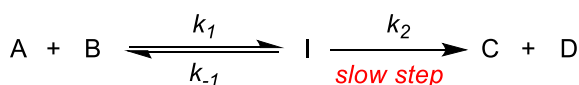
$$rate = \frac{d[C]}{dt} = k_2[I]$$

Rate of the reaction:

$$rate = \frac{d[C]}{dt} = k_2[I]$$

Since step 2 is slow, step 1 can be presummed to be in an equilibrium. Thus,

$$K_{eq} = \frac{k_1}{k_{-1}} = \frac{[I]}{[A][B]}$$

Rearranging the above equation provides I

$$[I] = K_{eq}[A][B]$$

Since step 1 is slow, I is consumed as soon as it is formed. Thus one may assume steady state for I,

$$\frac{d[I]}{dt} = k_1[A][B] - k_2[I] - k_{-1}[I] = 0$$

Rearranging the above equation provides I

$$[I] = \frac{k_1[A][B]}{k_2 + k_{-1}}$$

Rate law equation:

$$rate = k_2[I] = k_2K_{eq}[A][B]$$

Rate law equation:

$$rate = k_2[I] = \frac{k_2k_1[A][B]}{k_2 + k_{-1}}$$

Figure 1.17 Similar rate equation for different mechanistic models. This figure depicts how two different mechanistic scenarios could also lead to rate equation of similar form.

1.8   Empirical rate law and order of components

An experimentally determined rate law, for a generic reaction such as the one in Rxn 1, is typically represented in the following form,

$$rate = k_{obs}[A]^{\alpha}[B]^{\beta} \qquad\qquad\qquad eq\ (1.3)$$

The k_{obs} is the experimentally observed rate constant for the reaction. The powers α and β are known as the 'order' of the components A and B respectively. The orders of each component of a reaction can have positive, negative, integer or non-integer values, and are unrelated to their stoichiometric coefficients in the reaction. When order of a component is zero (zeroth order), rate of the reaction has no concentration dependence on that component, when order of a component is one (first order), rate of the reaction has linear dependence on that component and so on. The summation of the order of each

component represent the overall order of the reaction, for instance, if order of every component is zero (a rare occurrence) the overall reaction is a zero-order reaction. Determining the orders not only allows one to define the empirical rate equation but are also highly informative about the reaction's mechanism. Hence, determination of orders via kinetic experiments for various chlorofunctionalization reactions will be a key part of the following chapters. Discussion on the zeroth, first and second order reactions, their mechanistic implications and case studies etc. can easily be found in any undergraduate[54, 55] as well as advanced texts[51-53] on reaction kinetics and will not be discussed further.

Note that the empirical rate law can have a different, more simplified linear form compared to the one derived from a proposed mechanistic model. However, the derived rate equation can always be reduced to its empirically determined form at certain concentration limits (also known as limiting form) or with certain reasonable approximations. To understand this, consider reaction model 2 in Figure 1.16. The rate law equation derived from the mechanistic model has the following form,

$$rate = \frac{d[C]}{dt} = \frac{k_2 k_1 [A][B]}{k_2[B]+k_{-1}} \qquad \text{eq (1.4)}$$

However, if k_{-1} is insignificantly small under the reaction condition (due to large B or k_2), the above equation 1.4 can be approximated to the following form equation (1.5) similar to the generalized empirical rate equation.

$$rate = \frac{k_2 k_1 [A][B]}{k_2[B]+k_{-1}} \approx k_1[A] \qquad \text{eq (1.5)}$$

Once the empirical rate law is determined using kinetic experiments, one may leverage the above fact to ensure that the proposed mechanism is correct, as the rate

law derived from the correct mechanistic model will conform with the experimental rate law.

Despite the proven utility of chemical kinetics to determine reaction mechanism, it is often underutilized among synthetic organic chemist due to two reasons: 1) Challenges in reaction monitoring, 2) The often-cumbersome mathematics that are associated with kinetic analysis to find the order of components. These two points will be addressed in the next section in more detail to illustrate how recent development has simplified kinetic measurements and kinetic analysis.

1.9   Reaction monitoring and kinetic measurements

The first step towards any kinetic study is establishing a protocol for consistent measurement of the reaction progress for the reaction under study. This involves choosing the appropriate spectroscopic tools/instrumentation for quantitative analysis, as well as a standard reaction condition that is suitable for the kinetic study. This step can often be deceptively challenging, and the challenges may be unique to each reaction system, as will be displayed with examples from our own studies.
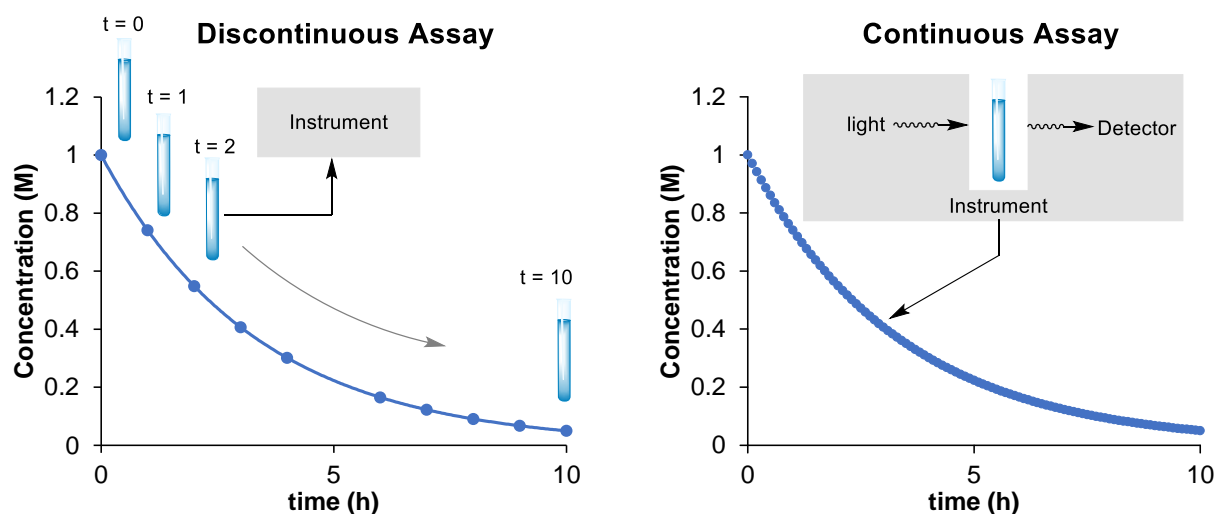
Figure 1.18 Reaction monitoring techniques. (a) Reaction monitoring using a discontinuous assay. (b) Reaction monitoring using a continuous assay.

30

Perhaps the most common approach towards monitoring reaction progress is via measurement of the concentration decay and growth of the substrate and product, respectively, over time. The measurements can be done using a discontinuous assay or a continuous assay method (Figure 1.18).[52] A discontinuous assay would involve direct extraction and analysis of reaction aliquots from benchtop reactions at designated time intervals. However, advent of modern spectroscopic tools now also allows for a continuous assay that allows for direct in-situ reaction monitoring of the concentration of each component (example NMR and React-IR spectroscopy). Both the discontinuous assay and the continuous assay methods have their own advantages and disadvantages. For instance, continuous in-situ reaction monitoring typically provides greater number of data points, which is especially convenient for fast reactions, and are less prone to human error due to the entire experiment being in-situ once initiated. On the other hand, a discontinuous assay via time course sampling can provide greater flexibility for measurements as the reaction condition is not restricted to the instrument's own limitations (monitoring a reaction with no available deuterated analog of the solvent). Once a concentration-time profile is obtained from the kinetic measurements, one may either directly analyze to find properties of interest (order of components, rate constants etc.) or convert the concentration-time profile to a rate-concentration profile for further analysis (discussed more in next section). Alternative to a concentration measurement, direct rate measurement can also be performed, using techniques such a reaction calorimetry.

This thesis will present kinetic studies of various (DHQD)$_2$PHAL catalyzed asymmetric chlorofunctionalization reactions. The kinetic studies are the result of in-situ

reaction monitoring using NMR spectroscopy and, in some cases, react-IR. Reaction

monitoring of each chlorofunctionalization reaction presented its own unique set of

challenges. Some of these challenges and experimental techniques used to overcome

them are discussed in the following paragraphs.

Chlorolactonization of alkene carboxylic acids
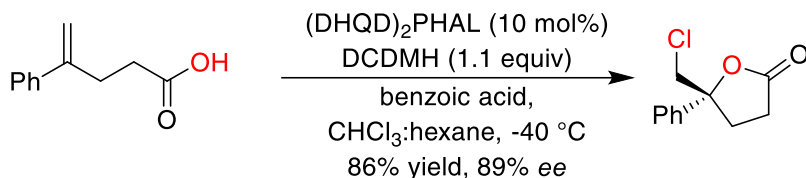
Figure 1.19 Challenges in reaction monitoring of chlorolactonization of alkene carboxylic acids. Challenges in reaction monitoring (shown in right box) is specifically for reaction monitoring using NMR

Chlorolactonization of alkene carboxylic acids: The original optimized reaction

condition,[9] which involved a 1:1 mixture of chloroform:hexane was reoptimized to use

only chloroform as the solvent, while maintaining a comparable selectivity and yield

(Figure 1.19). This was done to easily monitor this reaction using ^{1}H NMR spectroscopy

without involving any solvent suppression in the spectra.
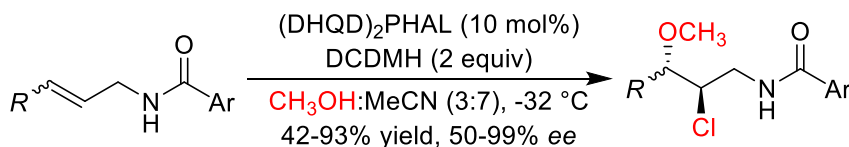
Chloroetherification of alkene amides

Figure 1.20 Challenges in reaction monitoring of chloroetherification of alkene amides. Challenges in reaction monitoring (shown in right box) are for both for NMR and React-IR.

Chloroetherification of alkene amides: The biggest challenge for

chlorofunctionalization of any alkene amide[41] (Figure 1.20) system was found to be their

fast rate. Chloroetherification reaction at room temp or even when lowered down to -30

°C reaction went to completion in <30 min in most cases. Attempts to slow the reaction by lowering the catalyst loading did not yield helpful result (which ultimate presented an important mechanistic clue, discussed more in chapter 3). Attempts to slow reaction rate by lowering temperature further was also not feasible since lowering temperature below -30 °C often lead to substrate (alkene amide) precipitation. This was exacerbated from the instrument limitations as the NMR and React-IR cooling systems used did not allow for maintaining a consistent temperature when temperature was lowered below -30 °C. Lowering rate by lowering the overall reactant concentration was avoided due to the low starting concentration of reactants (40 mM). These problems were compounded by the fact that the reaction uses a solvent mixture of methanol-acetonitrile (3:7). Fortunately, deuterated versions of both solvents are cheap, commercially available, and miscible. However, the presence of multiple deuterium signals increased the time necessary for properly locking and shimming the samples at the beginning of the kinetic runs, leading to a loss of a significant number of data points at the start of the reaction. Further challenges included the slow relaxation of some of the protons of interest in these solvents (up to ~3 secs). React-IR is a good alternative for capturing fast reaction processes due to the instrument's rapid response. Resorting to react-IR as a means of reaction monitoring, however, presented its own set of challenges. For instance, the reaction lacked high intensity infrared active functional groups that changed during the course of the reaction. The change of alkene to chloroalkane was not directly visible in the IR, however, we were able to monitor and quantify (albeit with difficulty) the chlorinating agent and its byproduct. This although, not ideal did provide one of the first ways to monitor the chloroetherification reaction. Ultimately, screening substrates led to a less reactive alkene

that further mitigated some of the problems by slowing the reaction rate enough for reaction monitoring with NMR. The standard conditions and protocols for chloroetherification will be discussed further in the experimental section of Chapter 3.

Chloroamidation of alkene amides
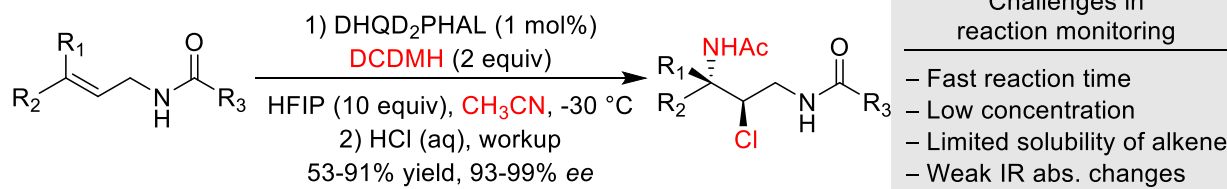
Figure 1.21 Challenges in reaction monitoring of chloroamidation of alkene amides. Challenges in reaction monitoring (shown in right box) are for both for NMR and React-IR.

Chloroamidation of alkene amides: Monitoring catalytic asymmetric chloroamidation[43] reaction were accompanied with challenges similar to chloretherification due to its comparably fast rate (Figure 1.21). Similar to chloroetherification, use of appropriate substrate allowed for reaction monitoring with NMR and react-IR. Monitoring the catalytic asymmetric chlorocyclization of alkene amides and alkene carbamates are perhaps more challenging due to their faster rate and their use of fluorinated alcoholic solvents which are not ideal for NMR use. Currently, efforts are underway in the Borhan lab to develop standard conditions appropriate for continuous reaction monitoring for the latter two reactions.

1.10   Kinetic analysis to find order of components

Once a standard condition is established for reaction monitoring, the data is then subjected to kinetic analysis for extracting various kinetic properties of the reaction. As discussed before, determining the order of each components can provide valuable information about the mechanism of a reaction. While determining order of a component is relatively simple (ex: using method of half-life) when there is only one component

involved in the reaction (rate law has the form rate = k[A]^n), this is rarely the case for most organic reactions. Determining the order of each components when there are multiple components involved in the reaction can be especially tricky. Thus, various protocols are reported in the literature for treating of kinetic data to extract information relating to order of each components, some of which will be discussed in the following sections.

1.10.1 Method of isolation

Method of isolation is a protocol well utilized in older literature to determine order of components. This technique involves an assay of varying the initial concentration of the particular reaction component whose order is of interest while maintaining saturation with every other reaction component.[53] This is explained with a simple example as follows. Consider the following reaction:

$$A + B \rightarrow C + D \hspace{4cm} \text{rxn (2.0)}$$

Let's assume the rate equation for this reaction 2 is as follows:

$$rate = k[A]^\alpha[B]^\beta \hspace{4cm} \text{eq (1.6)}$$

Table 1.1 Set of experiments for finding the order of components using method of isolation

Exp	[A] (M)	[B] (M)
1	1	10
2	2	10
3	10	1
4	10	2

To determine the order of A one may run a minimum two experiments (exp 1 and 2, Table 1.1), with different concentration of A. For each of these experiments the equivalence of B is set to be at least 10 times (or more) than that of A. As the reaction progresses, both A and B are consumed, but the change in concentration of B is negligible

35

leading to B having a pseudo order (an approximately constant impact on rate). Thus, the above rate equation is reduced to rate being a function of A only.

$$rate = k'[A]^\alpha \qquad\qquad \text{eq (1.7)}$$

Where, $k' = k[B]^\beta \approx constant$ eq (1.8)

Thus, by measuring the impact on rate for the two reaction with two different initial concentration of A (exp 1 and 2, Table 1.1) one may deduce the order of A. Conversely, one can determine the order of B by saturating the reaction with A and measuring the impact of two different initial concentration of B on the rate.

While this method is relatively simple and intuitive, it has several obvious drawbacks. For example, it might not be feasible to drastically increase the concentration of components due to factors like precipitation. Furthermore, using this abnormal stoichiometry, which is often different from original reaction conditions, could change the mechanism of the reaction, yielding misleading results.

1.10.2 Method of initial rate

Method of initial rate, as the name suggests leverages on the change of rate at the very beginning of the reaction (t → 0) with change in initial concentration of the reaction component to find its order. Let us consider the same last example to understand the method.

$$A + B \rightarrow C + D \qquad\qquad \text{rxn (2.0)}$$
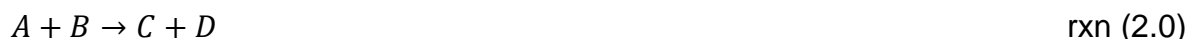
Where the rate equation is as follows:

$$rate = v = k[A]^\alpha[B]^\beta \qquad\qquad \text{eq (1.9)}$$

Based on equation 1.1, rate can be represented as,

$$v = -\frac{d[A]}{dt} = -\frac{d[B]}{dt} = \frac{d[C]}{dt} = \frac{d[D]}{dt} = k[A]^\alpha[B]^\beta \qquad\qquad \text{eq (1.10)}$$

The (measurable) rate at the very beginning of the reaction when $t \to 0$, that is the initial rate v_i, can be approximately represented in terms of the known initial concentration of the reaction components

$$\lim_{t \to 0} v = v_i \approx k[A]_i^{\alpha}[B]_i^{\beta} \qquad \text{eq (1.11)}$$

Thus, if one were to estimate the order of A, one may run at least two experiments with different initial concentration of A, say A_1 and A_2 (Table 1.2), while maintaining an otherwise identical reaction condition including the same initial concentration of B. The initial rate for the two system can be approximately defined as

$$v_{i,1} \approx k[A_1]_i^{\alpha}[B]_i^{\beta} \qquad \text{eq (1.12)}$$

$$v_{i,2} \approx k[A_2]_i^{\alpha}[B]_i^{\beta} \qquad \text{eq (1.13)}$$

Table 1.2 Set of experiments for finding the order of A using method of initial kinetics

Exp	[A] (M)	[B] (M)
1	A_1	B
2	A_2	B

Dividing the above two equation above leads to equation

$$\frac{v_{i,1}}{v_{i,2}} = \frac{[A_1]_i^{\alpha}}{[A_2]_i^{\alpha}} = \left(\frac{[A_1]_i}{[A_2]_i}\right)^{\alpha} \qquad \text{eq (1.14)}$$

Taking a log of both side and rearranging the above equation can easily reveal the order (α) of A in terms of the initial concentration of A and the initial rates.

$$\alpha = \frac{\log\left(\frac{v_{i,1}}{v_{i,2}}\right)}{\log\left(\frac{[A_1]_i}{[A_2]_i}\right)} \qquad \text{eq (1.15)}$$

For the above equation, A_1 and A_2 are known as they represent the initial concentration of A (Table 1.2). Thus, initial rates $v_{i,1}$ and $v_{i,2}$ are the only values needed to be measured to determine the order (α) of A.

The advantage of this method over the method of isolation is that the kinetic experiments can be performed under conditions that are relatively similar to the original reaction conditions. Furthermore, as the measurements only rely on measurements of parameters under the initial reaction, a rigorous instrumental setup for continuous reaction monitoring to monitor the entire reaction profile is not entirely necessary.

Unfortunately, this method is not without its disadvantages either. The first and rather more obvious disadvantage is that by focusing entirely on the initial conditions, one is discarding the kinetic information of the entire later part of the reaction. This is especially important for enzyme kinetics where drastic change in substrate concentration can often lead to a change in enzyme activity or even molecularity. By relying solely on this method, one may lose information on such late stage processes. There are other kinetic methods known in literature, such as Selwyn's test for detecting enzyme inactivation,[56] which one may complement with the initial rate measurements. However, these tests again require an instrumental setup for a complete kinetic profiling of the reaction.

The second, less obvious disadvantage of this method stems from the challenges in the measurability of the initial rate. Initial rate, by definition, has to be measured from the small change in the concentration of a components, say dA with small change in time dt, when time is closes to zero (t → 0). An approximation often used for calculating these changes is that dA ≈ ΔA and dt ≈ Δt which give the following equation for the initial rate in terms of A.

$$v_i = -\frac{d[A]}{dt} \approx -\frac{\Delta[A]}{\Delta t} = \frac{[A]_t - [A]_i}{t - t_i}$$
eq (1.16)

As long we know the concentration of A at time t (A_t) one might think its easy to calculate the initial rate, while the reality is less trivial. For instance, the measured span of time (and concentration) will always be larger that of the ideal theoretical value. And since rate only decrease over time (in most reactions), the measured initial rate will always be smaller than the actual initial rate. In fact, the measured initial rate is most likely not the initial rate at all but rather an average of a series early rate values. Perhaps more accurate approach for this is by plotting the concentration vs time profile of A vs t and then extracting the initial rate from the tangent of the plot at the origin (that is when A and t are both nearly zero). Nonetheless, accurate measurement of the curvature from the initial data points is not trivial. Early reaction events such as brief incubation periods, could contribute to the inaccurate estimation of the real initial rate.[52]

1.10.3 Method of reaction progress kinetic analysis (RPKA)

Reaction progress kinetic analysis or RPKA is a graphical kinetic analysis protocol that has found extensive following in the modern literature to solve various mechanistic problems.[57, 58] At its core, the philosophy of RPKA protocol is to analyze the measured kinetic profile(s) of a reaction (concentration vs time or rate vs time), and present it in a graphical form that allows for direct extraction of relevant kinetic information, such as order of components. To illustrate this in its simplest case let us consider the following reaction.

$A \rightarrow P$
<div align="right">rxn (3.0)</div>

The empirically measured rate equation for the above reaction will have the form,

$Rate = k_{obs}[A]^n$
<div align="right">eq (1.17)</div>

a. Measured data

b. Graphical rate equation
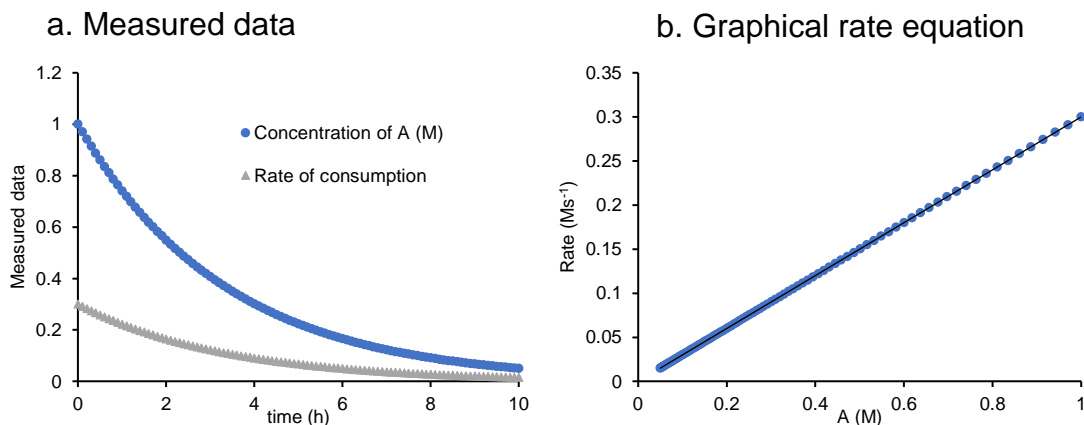
Figure 1.22 Graphical analysis of rate law equation. (a) Plot of measured data (rate or concentration) against time. (b) Plot of rate against concentration. The straight line through the origin in this plot indicates first order in A, providing direct information on the nature of the rate law.

For the above Figure 1.22, the left plot represents the measured data, that is, either a rate vs time or concentration vs time profile. While the plot by itself does not intuitively provide any information about, say the rate law of the reaction, replotting the same information in a rate vs concentration plot (also known as graphical rate equations), shows a linear relationship between rate and concentration of A. The linearity of this plot immediately and intuitively provides the user with a rate equation (Rate = k[A]) and this graphical analysis to find the rate equation would be a reaction progress kinetic analysis. For any RPKA study, there are really only two requirements: 1) one must have some means to be able to monitor a significant amount of reaction progress (preferably using a continuous assay) 2) One needs a computer equipped with a graphical software that supports basic data analysis functions such as curve-fitting (such as excel).

Due to the over-simplicity of the above example and the fact that these plots are shown regularly in undergraduate physical chemistry courses, the novelty of the approach will probably not be apparent unless we consider a more complex kinetic scenario. Thus, let us look at the RPKA analysis of the the following reaction.

$A + B \rightarrow C + D$ (initial conc. of A, B, C, D are 2M, 3M, 0M, 0M)   rxn (4.0)

We have illustrated that whenever we have a multicomponent reaction such as the one above (rxn 4) obtaining the order of each component using the method of isolation or the method of initial rates involves several caveats. The novelty of RPKA really stems from its simple and intuitive graphical approach to solving rate equations for multi-component reactions, while avoiding the compromises of the classical kinetic analysis approaches. Let us assume that the reaction has the following rate equation,

$$Rate = k_{obs}[A]^1[B]^1$$ eq (1.18)

Based on the above rate equation, rate has a first order dependence on the concentration of both A and B (overall second order). If we were to determine this relationship using RPKA, based on the last example we could take the following steps. First measure the concentration-time profile, then plot this as a rate vs concentration for A or B (Figure 1.23). However, now the rate vs A or B would have a parabolic plot that fails to intuitively present the order of each components.
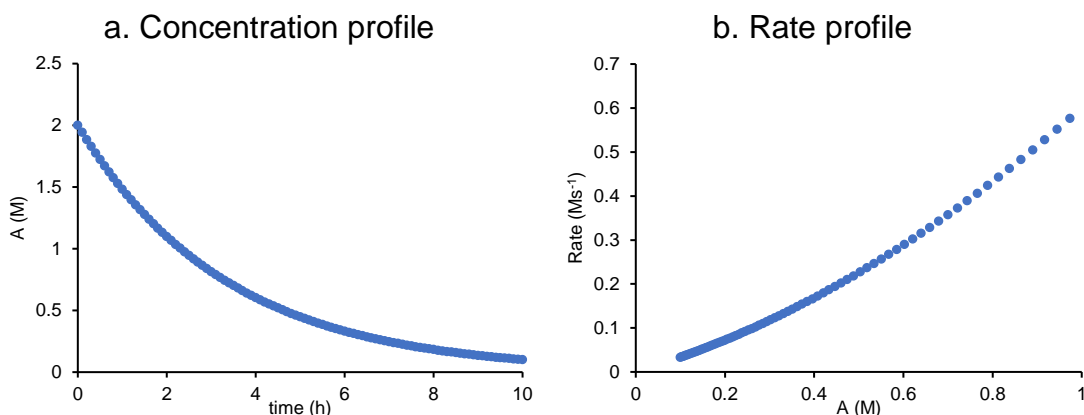
Figure 1.23 Kinetic profile of a second order reaction. (a) Concentration vs time plot. (b) Rate vs concentration plot.

Fitting functions generated from a second order rate law can be developed and used to establish that this reaction is a second order reaction but that would require a

more complex mathematical analysis. The goal of RPKA is to present a simple and more visually intuitive approach for synthetic organic chemists. RPKA would suggest plotting the following functions instead would directly provide a meaningful information,

$$\frac{Rate}{[A]^1} = k_{obs}[B]^1 \qquad \text{-or-} \qquad \frac{Rate}{[B]^1} = k_{obs}[A]^1 \qquad\qquad \text{eq (1.19)}$$

The above function now presents a simple form where the left-hand side of the equation represents a [A] or [B] 'normalized' rate function, that is only a function of the other component [B] or [A] (right-hand side). Provided the order of both A and B is one, plotting either of these equations should be a straight line through the origin as shown in Figure 1.24. Conversely, the linear nature of the plot of Rate/[A] against B, determined through experiments will support a first order in both A and B.
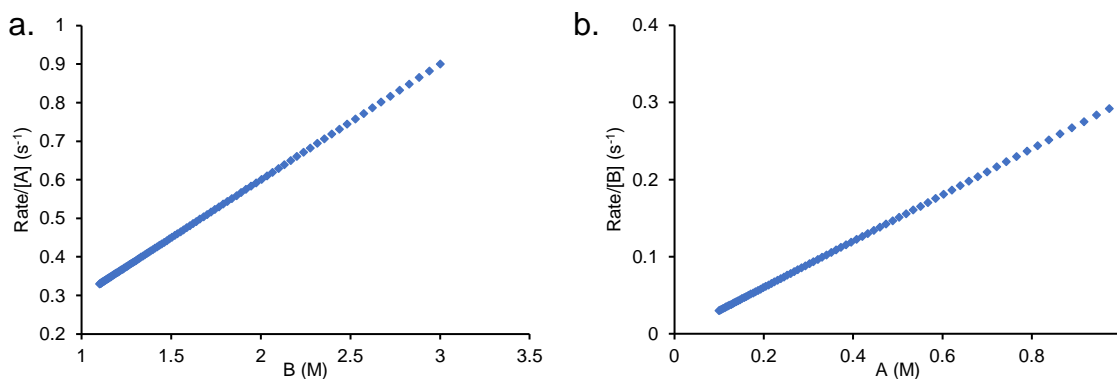
Figure 1.24 RPKA analysis of rate law. (a) The rate axis has been normalized for the concentration effect of A leading to its displayed linearity. (b) The rate axis has been normalized for the concentration effect of B.

Thus, the linearity in the above graphical rate equation plot, directly informed us about the order of the reaction components A and B, and theoretically for this kinetic scenario, a single experiment is sufficient to deduce the order. A generalized approach to determine order for more complex cases using experiments known as different excess experiments will be discussed in the next section. This linearization approach (heavily inspired by the Lineweaver-Burk plot[59]) laid a simple, direct insight into physical

parameters, such as orders of components, to establish the rate law equation. Furthermore, this approach does not require any unnatural saturation conditions and the order can be measured in terms of the entire span of the reaction and requires few experiments, thus negating the pitfalls of the method of isolation or the initial rates.

$A + B \rightarrow C + D$ (initial conc. of A, B, C, D are 2M, 3M, 0M, 0M)   rxn (4.0)
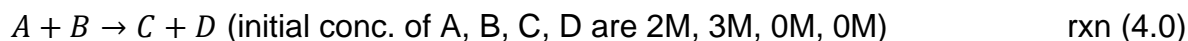
Another common scenario for rxn (4) is where the order of one of the components is zero, while the order of the other is one. Let's say order of A is one while B is zero.

$Rate = k_{obs}[A]^1[B]^0$ eq (1.20)

In this case, the above equation (1.20) would be reduced to the following

$$\frac{Rate}{[A]^1} = k_{obs}[B]^0 = k_{obs} = constant$$

a.

b.
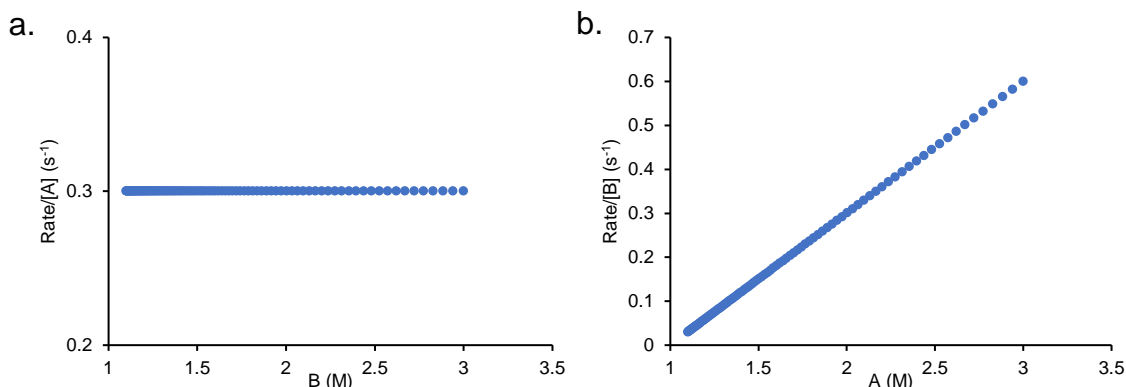
Figure 1.25 RPKA analysis of rate law for a reaction of overall order of 1. (a) Since rate is independent of the concentration of B (zero order), removing the effect of A on rate lead to a function (rate/[A]) that does not change with the concentration of B. (b) The plot of rate against the concentration of A also generates a straight line through the origin, indicating a zero order effect of B and first order effect of A on rate.

Thus, in the above case, the Rate/[A] function is a constant and should not change with [B]. Hence, plotting Rate/[A] against B would still yield a straight line but now the line would be horizontal or parallel to the axis of B, this is shown in Figure 1.25. And the

reverse would be true if order of A was zero and B was one. This again demonstrates how from the nature of this plot one can quickly extract the order.

The RPKA technique is not restricted to integer orders (such as 0 or 1 as shown above), rather any value of order (positive, negative, integer or fraction) can be determined using RPKA in a similarly intuitive fashion and will be discussed in the following section. While a comprehensive review articulating the generalized approaches to kinetic analysis using RPKA[57, 58] is beyond the scope of this chapter, the following paragraph illustrates a few key approaches that will be utilized in the following chapters.

Different excess experiments: To understand the generalized approach for finding the order of components, let us consider the following catalytic reaction (5),

$$A + B \xrightarrow{cat} C + D \qquad\qquad \text{rxn (5.0)}$$

The reaction will have the following general rate equation,

$$Rate = k_{obs}[A]^{\alpha}[B]^{\beta} \qquad\qquad \text{eq (1.21)}$$

Where, $k_{obs} = k'[cat]^{\gamma}$ and $k' = composite\ rate\ constant$ eq (1.22)

For the above rate equation, the composite rate constant is composed of rate constants from multiple elementary steps. To interrogate the general order of A and B (α and β), let us first introduce a term excess (xs). Excess or xs is defined as B − A is a constant throughout the entire reaction (provided A reacts only with B and vice versa). To determine the order of A and B using RPKA, we need to run a at least two experiments with different values of excess, hence these experiments are named "different excess experiments". Table 1.3 which presents a set of different excess experiments.

Table 1.3 Set of different excess experiments for finding order of components using RPKA

Exp	[A] (M)	[B] (M)	xs (M) = B − A
1	2	3	1
2	2	4	2
3	3	3	0
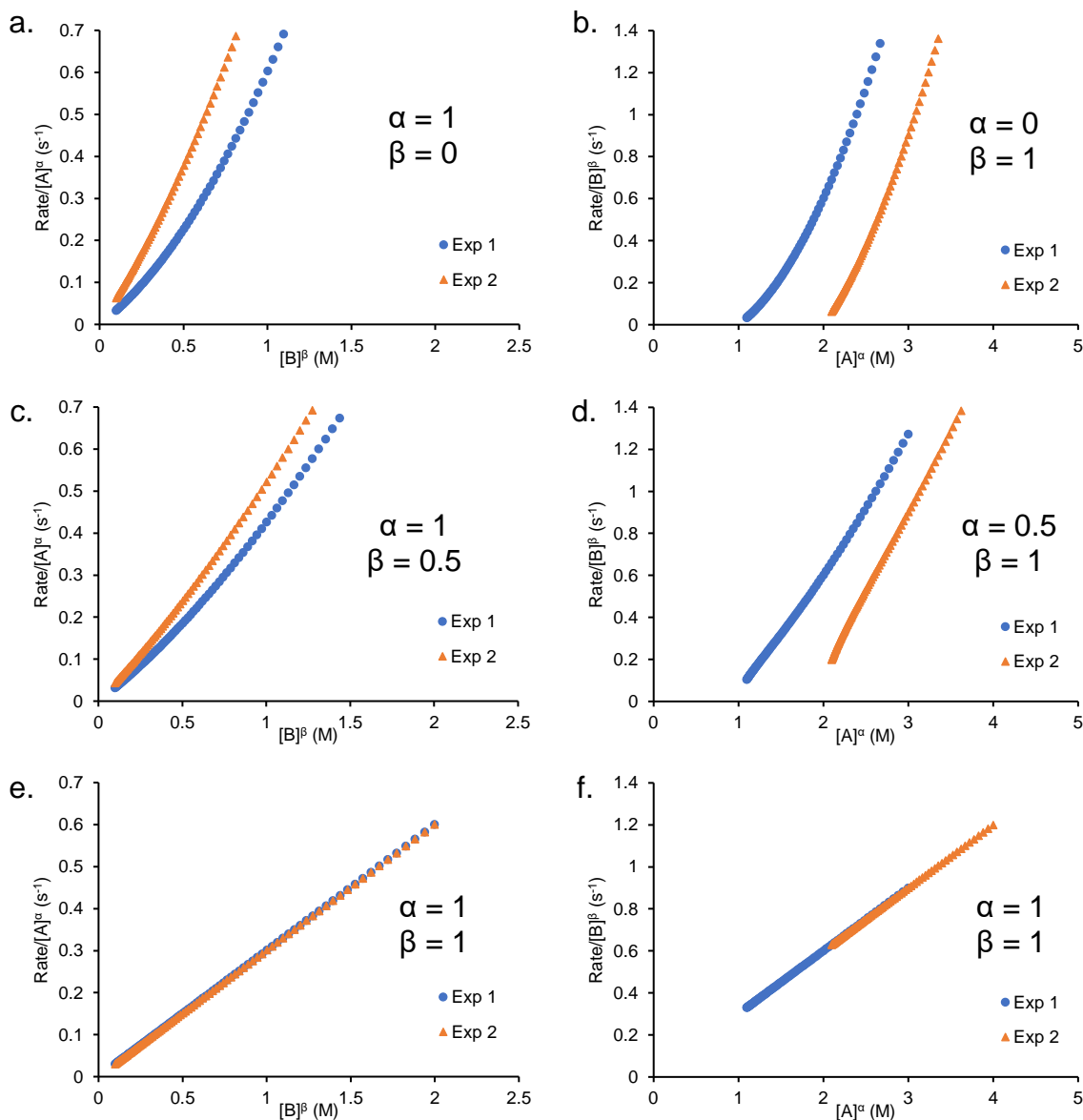
Figure 1.26 Reaction progress kinetic analysis of different excess experiments to find the order of components. The figure (a)-(f) demonstrates how the curvature and overlay of the plots for experiment 1 and 2 (Table 1.3) changes with change in the order of A and B (α and β). The overlay and linearization occur for correct value of α and β in figure (e) and (f) revealing the correct values to be 1 for both.

To understand how these different excess experiments can be leveraged to find the order, let us go back the general rate equation (1.21). Similar to before, the rate expression can be rearranged to the following forms,

$$\frac{Rate}{[A]^\alpha} = k_{obs}[B]^\beta \qquad \textit{-or-} \qquad \frac{Rate}{[B]^\beta} = k_{obs}[A]^\alpha \qquad\qquad\qquad \text{eq (1.23)}$$

Once again, the left-hand side (Rate/[A]$^\alpha$ or Rate/[B]$^\beta$) will become a "linear" function of concentration of one component B or A, only when raised to their respective power of β or α. If one conducts a set of two experiments with different excess of B (experiment 1 and 2, Table 1.3), and plot of the above two functions should be linear, and overlay provided the correct values of α and β are used. Now, α or β will be unknown to the investigator in the beginning, however, once a kinetic profile for the reaction is obtained experimentally (experiment 1, Table 1.3), the data can be easily converted to the above form using a plotting software (like excel) and the investigator may start their analysis by choosing a random values for α and β. Once this is done, the α and β (unknown variables) can be changed manually until the two plot linearizes and overlays, which only occurs for the correct value of α and β. This process of analysis is demonstrated in Figure 1.26, notice how the plots do not overlay for Figure 1.26a and Figure 1.26b, however both of the plot becomes linear and overlay when value for α and β is chosen to be 1 in Figure 1.26e and Figure 1.26f. This indicates the correct power of both A and B are 1.

Thus, one can see how only two kinetic experiments (different excess) provided the order of both A and B regardless of their value via analysis of overlay. The need for fewer experiments further adds to the appeal of using RPKA protocols for kinetic analysis. Of course, one may also complement or verify this further with a third different excess,

with a different value of A instead (experiment 3, Table 1.3). It is also important to point out that the slope of these plots now directly represents the observed rate constants for these reactions, providing the user with another important parameter from the same set of experiments. Finally, one may also determine catalyst order in the same manner, by defining the term rate/[cat]$^\gamma$ and plotting it against the concentration of A or B. For experiments run under different concentration of the catalyst, the plots must overlay when using the correct order of the catalyst γ.

Note another benefit of having the "excess" defined is, now one may represent the entire rate equation in terms of either A or B as the excess is a constant.

$$Rate = k_{obs}[A]^\alpha[A + xs]^\beta \qquad\qquad\qquad\qquad \text{eq (1.24)}$$

$$Rate = k_{obs}[B - xs]^\alpha[B]^\beta \qquad\qquad\qquad\qquad \text{eq (1.25)}$$

This means, while useful, it is not necessary to be able to individually monitor the concentration of both A and B, one may simply replace A or B by the other in terms of its excess as shown below. This further simplifies the experimental setup for the above graphical analysis.

$$\frac{Rate}{[A]^\alpha} = k_{obs}[A + xs]^\beta \qquad \textit{-or-} \qquad \frac{Rate}{[B-xs]^\alpha} = k_{obs}[B]^\beta \qquad\qquad \text{eq (1.26)}$$

Same excess experiments: Using RPKA one can also extract other valuable mechanistic information about a reaction, such as, the presence of catalyst deactivation or product inhibition. This can be done using a set of experiments called the same excess experiments. To understand this let us consider the same reaction (Rxn 5). One may run two experiments (Table 1.4, exp 1 and 2) with the same excess (xs) values but different initial concentration of A and B.

Table 1.4 Set of same excess experiments

Exp	[A] (M)	[B] (M)	Catalyst (M)	xs = B − A	additive
1	2	3	0.1	1	-
2	3	4	0.1	1	-
3	2	3	0.1	1	C, 1 M
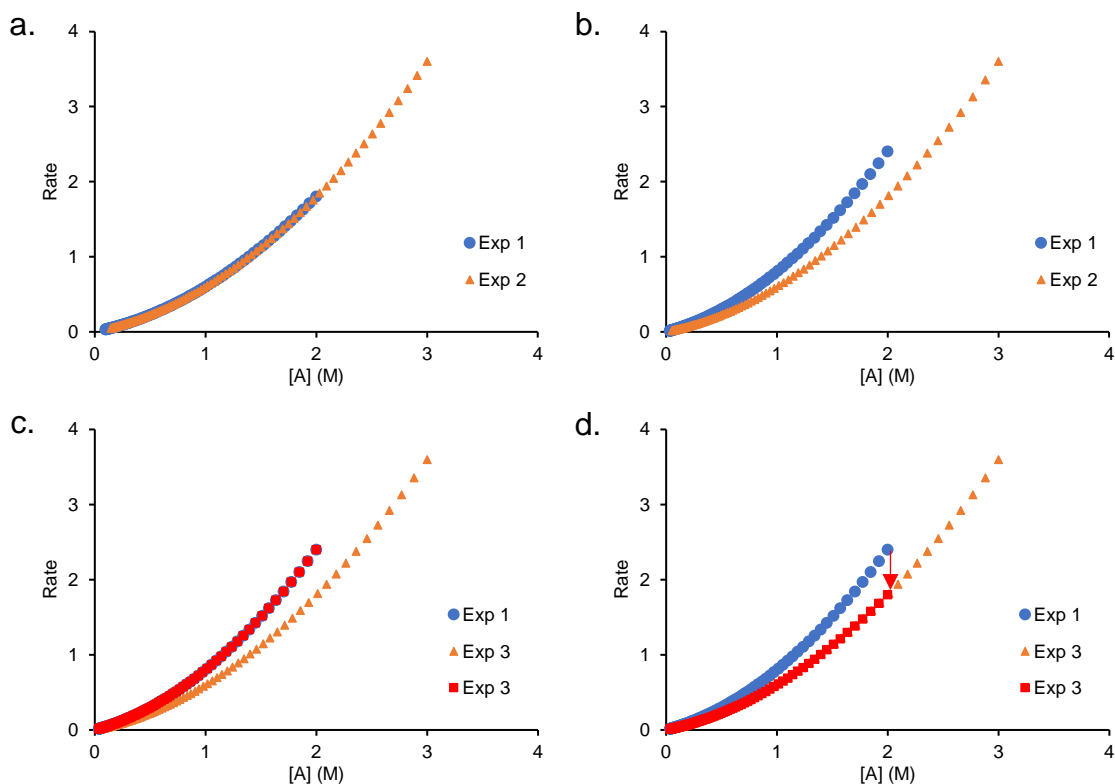
Figure 1.27 Reaction progress kinetic analysis of same excess experiments. (a) In this case, the overlay of experiment 1 and 2 (Table 1.4) indicate that there is no product inhibition or catalyst deactivation occurring. (b) The non-overlay of experiment 1 and 2 indicate either product inhibition or catalyst deactivation. (c) The overlay of experiment 3 with 1 indicate catalyst deactivation. (d) The overlay of experiment 3 with 2 indicate product inhibition.

Figure 1.27 presents the simulated plot of the experiments in Table 1.4. Notice that as the reaction progresses, the concentration of A and B in experiment 2 (3 and 4 M respectively), at some point of time, will match that of the reaction in experiment 1 (2 and 3 M respectively). In other words, they are essentially the same experiment with different initial points and their kinetic profiles are expected to overlay as shown in Figure 1.27a. However, when experiment 2 reaches the experiment 1's initial condition, there are two

key differences between them. First the catalyst in experiment 2 has undergone a few turnovers, and second some product has been generated and is now present in the reaction mixture. If the profile of reaction 1 and 2 do not match or overlay, like the one shown in Figure 1.27b, it is the result of either catalyst deactivation or product inhibition from the generated product.

The actual cause behind this can further be verified by running experiment 1 with the product (let us say, C, Table 1.4, experiment 3) added in as an additive from the beginning. If this new experiment (exp 3, Table 1.4) has the same profile as experiment 1, as shown in Figure 1.27c, product has no influence on the rate and the difference is due to catalyst deactivation. However, if exp 3 is now overlays with experiment 2, as shown in Figure 1.27d, that would indicate the different between exp 1 and 2 arises from product inhibition. This demonstrates how these experiments are key to illuminating various off-cycle catalytic activities and will be used for studing chlorofunctionalization reaction as well in later chapters.

The above sections have briefly illustrated the power of RPKA studies to extract kinetic information with little compromise. To summarize the advantages this technique

1) Involves relatively simple mathematical transformations

2) Does not require advanced kinetic simulation software

3) Reactions can be studies under conditions similar to optimized conditions

4) Involves analysis of the entire kinetic profile

There are, however, some disadvantages, for instance, the "overlay" of different plots utilized for extracting information are completely based on visual analysis and there is no straight-forward way of determining the error in an overlay.[60] For reaction monitoring,

most often spectroscopic instruments are employed that directly generate a concentration profile. To create the above shown graphical rate equation plots, the concentration-time data needs to be converted into the rate. Rate is generally determined by taking a differential of these concentration-time profiles but doing so can sometime introduce noise and artifacts in the rate data and thereby in the graphical plots. To circumvent this, one may couple the instrument that directly monitors concentration (such as a react-IR or NMR) with another instrument that directly collects rate data (such as reaction calorimeter, which provides rate in the form of instantaneous heat flow). However, this will further complicate the instrumental setup, will increase the number of experiments necessary and doing so is not always feasible. Nonetheless, the advantages of RPKA arguably far outweigh the drawbacks as is demonstrated from its extensive implementation in both academia[61-66] and industry.[67-71]

1.10.4 Method of variable time normalized analysis (VTNA)

VTNA or variable time normalized analysis is a more recent iteration of the RPKA analysis that leverages on the same type of experiments (different excess, same excess etc.) to find order of reaction components.[60, 72-74] However, instead of graphical rate plots it extracts the same information directly from the measured concentration-time profiles, with little graphical manipulation. This allows for circumventing the issues in analysis of rate profiles as discussed at the end of RPKA, as one may now directly conduct the analysis of orders from the measured concentration profile.

To understand the VTNA analysis, let us revisit the Rxn (5)

$$A + B \xrightarrow{cat} C + D \qquad\qquad\qquad\text{rxn (5.0)}$$

The rate equation for which can be represented as,

$$v = -\frac{d[A]}{dt} = k_{obs}[A]^{\alpha}[B]^{\beta} \qquad\qquad\qquad\qquad \text{eq (1.27)}$$

Following the footsteps of RPKA the above rate equation (1.27) could be rearranged to the following form leading to its analysis in the graphical form

$$\frac{v}{[A]^{\alpha}} = -\frac{1}{[A]^{\alpha}}\frac{d[A]}{dt} = k_{obs}[B]^{\beta} \qquad\qquad\qquad \text{eq (1.28)}$$

The left side of above equation (1.28) is represented in terms of rate, which is a differential term and not often directly measured, rather it is generally derived from the differential of the concentration-time profile. To change it to a form where each variable is in the form of concentration or time (which can be directly measured in most scenario), the above equation must be taken to its integral form. This was done as follows,

$$\int_{A_0}^{A} -\frac{d[A]}{[A]^{\alpha}} = \int_{t=0}^{t=t} k_{obs}[B]^{\beta} dt \qquad\qquad\qquad \text{eq (1.29)}$$

Notice that the equation (1.29) now appears in a relatively complex integral form, however, the integrations need not be solved. The aim here is to reduce the integral rate equation to a form where effect of concentration of the various components are 'normalized' for the different excess experiments, provided the orders are correct. Looking at the above equation, the left side is only a function of A as shown below,

$$f(A) = \int_{A_0}^{A} -\frac{d[A]}{[A]^{\alpha}} \qquad\qquad\qquad\qquad\qquad \text{eq (1.30)}$$

Therefore, the right side of equation (1.29) by virtue of equality to the left side, is also just a function of A,

$$f(A) = \int_{t=0}^{t=t} k_{obs}[B]^{\beta} dt \qquad\qquad\qquad\qquad\qquad \text{eq (1.31)}$$

Plot of A vs time (t) for the two different excess experiments 1 and 2 (Table 1.5) will yield a non-overlaying plot as shown in Figure 1.28a, due to the effect of the concentration of B on the rate (provided order of B is not zero). Since the above integral

function (1.31) represents a function of only A, the two different excess experiments (Table 1.5) where only the initial concentration of B is varied should yield overlaying plots when plotted A vs $f(A)$ or rather A vs $\int B^\beta dt$. However, this overlay will only occur when the B in $\int B^\beta dt$ for the above equation (1.31) is raised to its correct order β as f(A) is defined by the correct order of B. This is shown by the analysis of overlay by changing the value of β in Figure 1.28b, Figure 1.28c, and Figure 1.28d the order of B is 1. Thus, if $\int B^\beta dt$ is measurable, we will have another scenario of a reaction progress kinetic analysis whereby conducting a different excess experiment, allows for measuring the order of B by merely changing β until the two experimental plots overlay as shown in Figure 1.28. $\int B^\beta dt$ is called the normalized time axis where the effect of the concentration of B has been normalized from the time axis.

Table 1.5 Set different experiments for finding order of components using VTNA

Exp	[A] (M)	[B] (M)	xs (M) = B − A
1	2	3	1
2	2	4	2
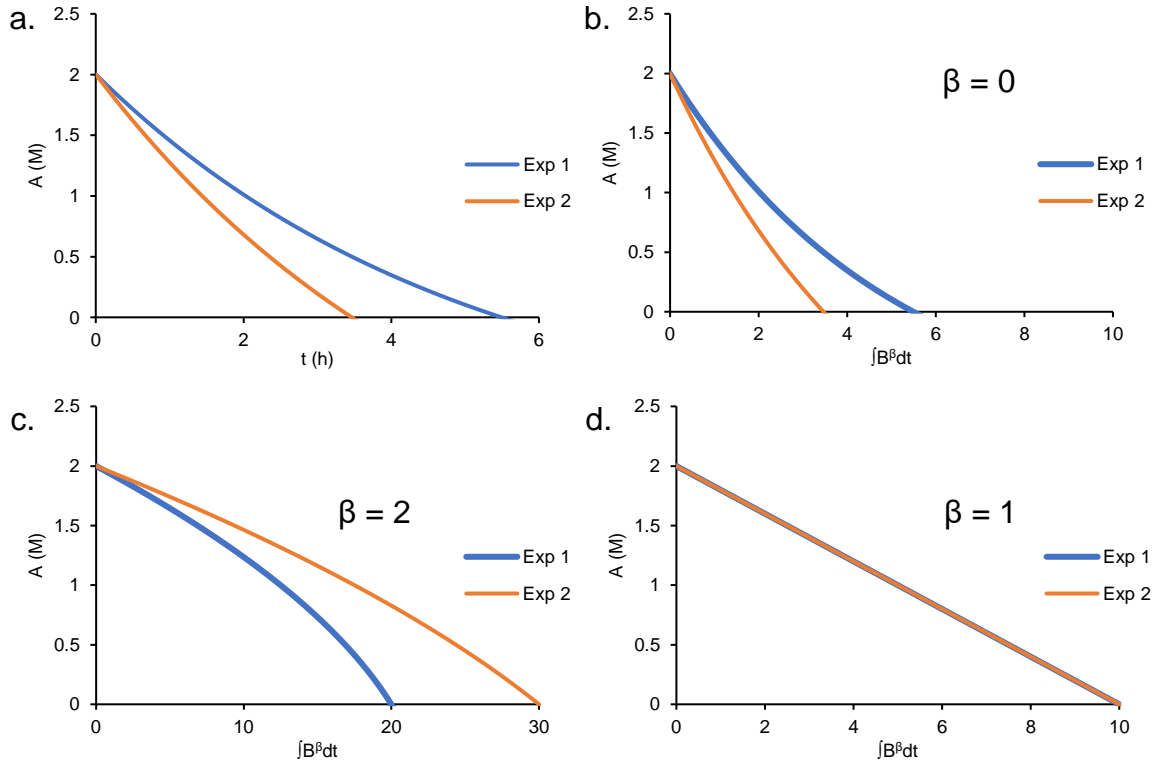
Figure 1.28 Variable time normalized analysis of different excess experiments to find order of components. (a) This plot represents a typical concentration vs time plot. Figure (b)-(d) demonstrates how the curvature and overlay of the time normalized plots for experiment 1 and 2 (Table 1.4) changes with change in the order of A and B (α and β). The overlay occurs for correct value of β in figure (d) which is found to be 1. Note that the linearization of the plot is not general and stem from the fact that the order of A was chosen to be zero for the simulated plot.

The function ∫B^β dt would be difficult to evaluate from its integral form, however, it can be simplified readily using the trapezoid approximation. This simplifies the equation 1.31 as follows

$$f(A) = \int_{t=0}^{t=t} k_{obs}[B]^\beta dt = \Sigma \left(\frac{B_i + B_{i-1}}{2}\right)^\beta (t_i - t_{i-1}) \qquad \text{eq (1.32)}$$

Now that the integral function above has been reduced to a summation function, it can be deduced readily if the concentration values of B and time is known. Since, the summation expression 1.32 is relatively large, it will be abbreviated as follows,

$$\Sigma \left(\frac{B_i + B_{i-1}}{2}\right)^\beta (t_i - t_{i-1}) = \Sigma [B]^\beta \Delta t \; (abbreviated \; form) \qquad \text{eq (1.33)}$$

53

The function $\sum B^\beta \Delta t$ represents the time normalized axis and the overlay of plots for a set of simulated different excess experiment is shown in Figure 1.29. Again, based on the overlay of plots in Figure 1.29d, one may conclude that the order of B is 1. (Note: the linearity of the plot in Figure 1.29d is not general. The linearity in this plot stems from the fact that for the simulated kinetics, the order of A was kept as zero, and normalizing the time axis for the concentration effect of B gave the decay profile an overall zero order trend. A non-zero order of A will bring a curvature to the plot, however, there will still be an overlay for the correct value of β).
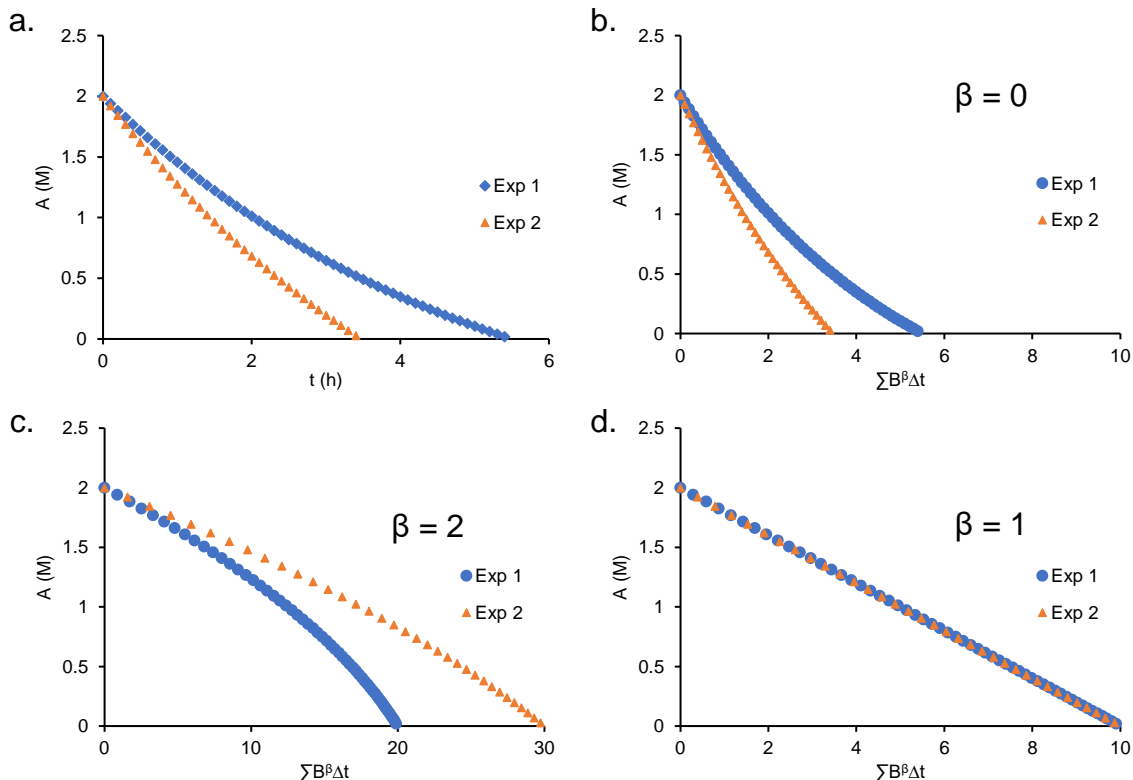
Figure 1.29 Variable time normalized analysis of different excess experiments using summation function. The interpretation of the plots in this figure is identical to the last. The difference is that the time normalized axis for all plot is now a summation function (instead of integral) which can be derived more easily with plotting software like excel. Figure (b)-(d) demonstrates how the curvature and overlay of the time normalized plots for experiment 1 and 2 (Table 1.4) changes with change in the order of A and B (α and β). The overlay occurs for correct value of β in figure (d) which is found to be 1.

This principle can be applied to any of the component as long as their concentration can be (directly or indirectly) measured. For instance, order of A can be determined by plotting $\sum A^\alpha \Delta t$ against B or even C or D. This can also be extended for determining catalyst order where instead of representing the time normalized axis as $\int [cat]^\gamma dt$, it can simply be represented as $[cat]^\gamma t$, since the concentration of the catalyst generally remains constant.

Same excess experiments can also be conducted and analyzed using VTNA to determine the presence of product inhibition or catalyst deactivation. This is done by comparing and the concentration profiles of a set of same excess experiments. The concentration profile of two reactions for two same excess experiments (See exp 1 and experiment 2, Table 1.6) will be offset at first based on how the starting time is chosen (Figure 1.30a). To determine whether catalyst deactivation or product inhibition affected the concentration profile for experiment 1 and 2 (Table 1.6) one must shift the experiment 1 along the time axis until the start time for the experiment 1 fall along the profile for the experiment 2. This is shown in Figure 1.30b. By doing so, if the two concentration profile of exp 1 now follows that of exp 2, then there is no product inhibition or catalyst deactivation (Figure 1.30b). Alternatively, Figure 1.30c and Figure 1.30d shows a scenario where time-shifting the concentration profile of exp 1 and 2 (Table 1.6) does not lead to an overlay of the two profiles. This difference now must arise from either product inhibition of catalyst deactivation. Conducting a third experiment (experiment 3, Table 1.6) with identical conditions as exp 1 but with added product could now lead to one of two scenarios. If the profile of exp 3 continues to match profile of experiment 1 the difference

is due to catalyst deactivation. However, if the profile of experiment 3 now matches that

of experiment 2, then this indicated product inhibition, slowing the reaction down.

Table 1.6 Set of 4 kinetic experiments for finding order of components using method of isolation

Exp	[A] (M)	[B] (M)	Catalyst (M)	xs = B – A	additive
1	2	3	0.1	1	-
2	3	4	0.1	1	-
3	2	3	0.1	1	D, 1 M
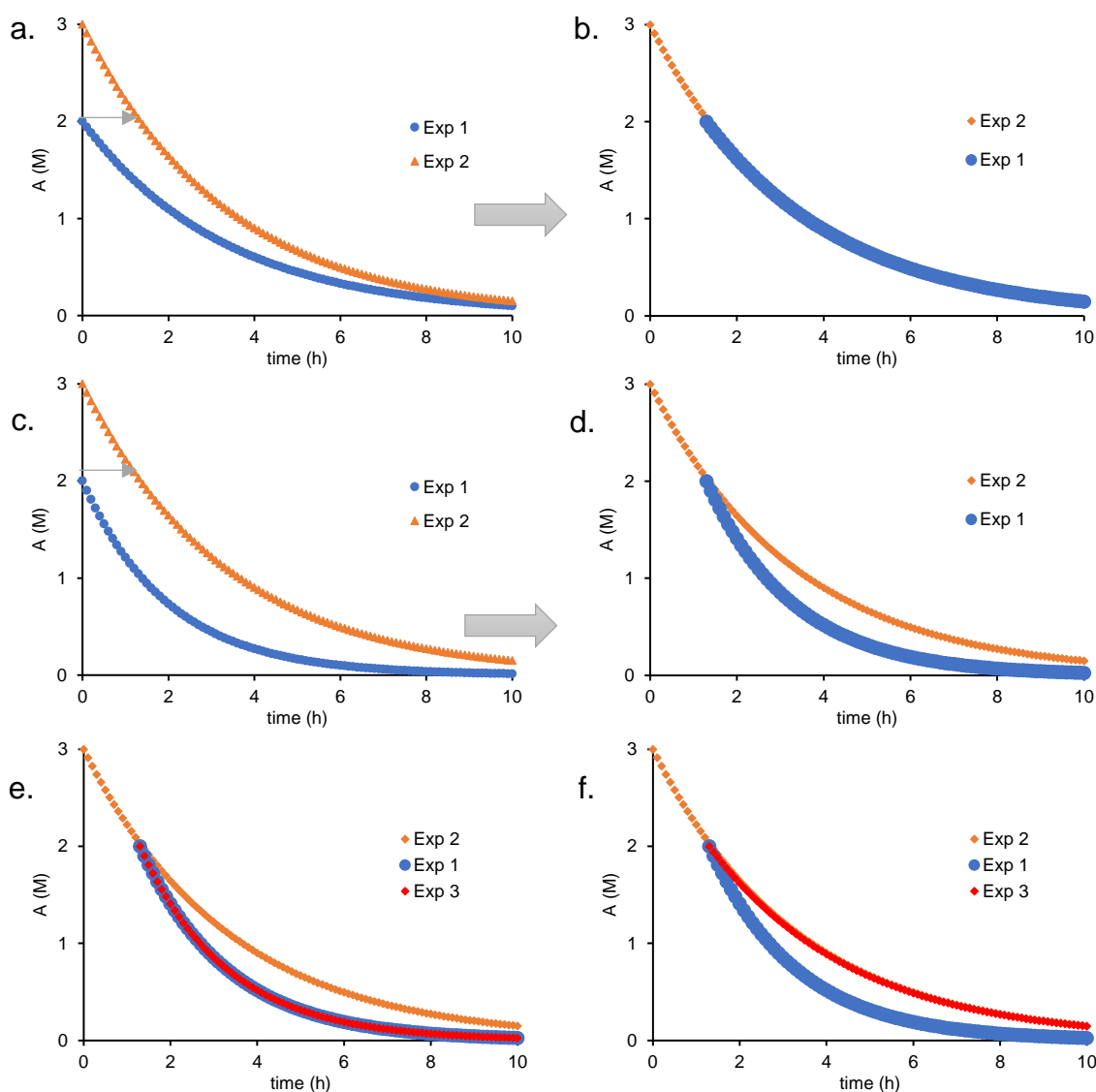
Figure 1.30 Time normalized analysis of same excess experiments. (a) A set of same excess experiments to probe catalyst deactivation or product inhibition. (b) Shifting the experiment 1 (Table 1.6) along the time axis led to complete overlay indicating no catalyst

56

(Figure 1.30 (cont'd)) deactivation or product inhibition. (c) An alternative result for the same set of same excess experiment. (d) Shifting the experiment 1 along the time axis in this case did not lead to overlay indicating either catalyst deactivation or product inhibition. (e) A time shifted experiment 3 overlays with experiment 1 indicates catalyst deactivation. (f) A time shifted experiment 3 overlays with experiment 2 indicates product inhibition.

The above RPKA/VTNA studies have hopefully demonstrated how one may quickly extract kinetic information of a reaction using relatively few experiments. VTNA studies, being fundamentally similar to the previous graphical rate based RPKA studies, also have similar drawbacks,[60] however, it improves on the RPKA for experimental setups where direct measurement of rate is not possible.

These RPKA and VTNA methods will be used rigorously in the successive chapters to deduce the rate law equation and consequently, the mechanism and catalytic cycles of various $(DHQD)_2PHAL$ catalyzed asymmetric chlorofunctionalization reactions.

REFERENCES

REFERENCES

1.   Gilman, H., *Organic Chemistry: An Advanced Treatise*. Wiley: New York, 1938; Vol. 1.

2.   Wislicenus, J.; Moldenhauer, W., Ueber das Cholesterindibromür. *Justus Liebigs Ann. Chem.* **1868,** *146*, 175-180.

3.   Roberts, I.; Kimball, G. E., The Halogenation of Ethylenes. *J. Am. Chem. Soc.* **1937,** *59*, 947-948.

4.   Kambe, N.; Iwasaki, T.; Terao, J., Pd-catalyzed cross-coupling reactions of alkyl halides. *Chem. Soc. Rev.* **2011,** *40* (10), 4937-4947.

5.   Gu, J.; Wang, X.; Xue, W. C.; Gong, H. G., Nickel-catalyzed reductive coupling of alkyl halides with other electrophiles: concept and mechanistic considerations. *Org. Chem. Front.* **2015,** *2* (10), 1411-1421.

6.   Das, R.; Kapur, M., Transition-Metal-Catalyzed Site-Selective C-H Halogenation Reactions. *Asian J. Org. Chem.* **2018,** *7* (8), 1524-1541.

7.   Landry, M. L.; Burns, N. Z., Catalytic Enantioselective Dihalogenation in Total Synthesis. *Acc. Chem. Res.* **2018,** *51* (5), 1260-1271.

8.   Chung, W. J.; Vanderwal, C. D., Stereoselective Halogenation in Natural Product Synthesis. *Angew. Chem. Int. Ed. Engl.* **2016,** *55* (14), 4396-434.

9.   Whitehead, D. C.; Yousefi, R.; Jaganathan, A.; Borhan, B., An Organocatalytic Asymmetric Chlorolactonization. *J. Am. Chem. Soc* **2010,** *132* (10), 3298-3300.

10.   Denmark, S. E.; Kuester, W. E.; Burk, M. T., Catalytic, Asymmetric Halofunctionalization of Alkenes-A Critical Perspective. *Angew. Chem. Int. Ed.* **2012,** *51* (44), 10938-10953.

11.   Cresswell, A. J.; Eey, S. T. C.; Denmark, S. E., Catalytic, Stereoselective Dihalogenation of Alkenes: Challenges and Opportunities. *Angew. Chem. Int. Ed.* **2015,** *54* (52), 15642-15682.

12.   Tan, C. K.; Zhou, L.; Yeung, Y. Y., Organocatalytic Enantioselective Halolactonizations: Strategies of Halogen Activation. *Synlett* **2011,** (10), 1335-1339.

13.   Murai, K.; Fujioka, H., Recent progress in organocatalytic asymmetric halocyclization. *Heterocycles* **2013,** *87* (4), 763-805.

14.   Tan, C. K.; Yeung, Y. Y., Recent advances in stereoselective bromofunctionalization of alkenes using N-bromoamide reagents. *Chem. Commun.* **2013,** *49* (73), 7985-96.

15.   Nolsoe, J. M. J.; Hansen, T. V., Asymmetric Iodolactonization: An Evolutionary Account. *Eur. J. Org. Chem.* **2014,** *2014* (15), 3051-3065.

16.   Chen, J.; Zhou, L., Recent Progress in the Asymmetric Intermolecular Halogenation of Alkenes. *Synthesis-Stuttgart* **2014,** *46* (5), 586-595.

17.   Cheng, Y. A.; Yu, W. Z.; Yeung, Y. Y., Recent advances in asymmetric intra- and intermolecular halofunctionalizations of alkenes. *Org. Biomol. Chem.* **2014,** *12* (15), 2333-2343.

18.   Olah, G. A.; Bollinger, J. M., Stable Carbonium Ions 57. Halonium ion Formation via Neighboring Halogen Participation. Trimethyl- and 1,1-Dimethylene halonium Ions. *J. Am. Chem. Soc.* **1968,** *90* (4), 947-953.

19.   Olah, G. A.; Bollinger, J. M.; Brinich, J., Stable carbonium ions. 62. Halonium Ion Formation via Neighboring Halogen Participation: Ethylenehalonium, Propylenehalonium, and 1,2-Dimethylethylenehalonium Ions. *J. Am. Chem. Soc.* **1968,** *90* (10), 2587-2594.

20.   Olah, G. A.; Bollinger, J. M.; Brinich, J., Stable Carbonium Ions. 76. 2,2-Dimethyltetramethylene Halonium Ions And a Study of Ha logen Participation in Protonated Methyl Gamma-Halopropyl Ketones and 5-halo-1-pentynes. *J. Am. Chem. Soc.* **1968,** *90* (25), 6988-6992.

21.   Olah, G. A.; Bollinger, J. M.; Brinich, J. M.; Mo, Y. K., Stable Carbocations. 126. Attempted Preparation of Trimethylenehalonium Ions. Preference For Three- and Five-Membered Ring Halonium Ion Formation. *J. Am. Chem. Soc.* **1972,** *94* (4), 1164-1168.

22.   Olah, G. A.; Westerman, P. W.; Melby, E. G.; Mo, Y. K., Onium Ions. 10. Structural Study of Acyclic and Cyclic Halonium Ions by Carbon-13 Nuclear Magnetic Resonance Spectroscopy. Question of Intra- and Intermolecular Equilibration of Halonium Ions With Haloalkylcarbenium Ions. *J. Am. Chem. Soc.* **1974,** *96* (11), 3565-3573.

23.   Berman, D. W.; Anicich, V.; Beauchamp, J. L., Stabilities of Isomeric Halonium ions C2H4X+ (X = Chlorine, Bromine) by Photoionization Mass Spectrometry and Ion Cyclotron Resonance Spectroscopy. General Considerations of the Relative Stabilities of Cyclic and Acyclic Isomeric Onium Ions. *J. Am. Chem. Soc.* **1979,** *101* (5), 1239-1248.

24.   Yamabe, S.; Tsuji, T.; Hirao, K., Substituent Effects on Chloronium-Ion Intermediates. *Chem. Phys. Lett.* **1988,** *146* (3-4), 236-242.

25.   Haubenstock, H.; Sauers, R. R., Computational studies of benzyl-substituted halonium ions. *Tetrahedron* **2005,** *61* (35), 8358-8365.

26.   Brown, R. S.; Nagorski, R. W.; Bennet, A. J.; McClung, R. E. D.; Aarts, G. H. M.; Klobukowski, M.; McDonald, R.; Santarsiero, B. D., Stable Bromonium and Iodonium Ions of the Hindered Olefins Adamantylideneadamantane and Bicyclo[3.3.1]nonylidenebicyclo[3.3.1]nonane. X-Ray Structure, Transfer of Positive Halogens to Acceptor Olefins, and ab Initio Studies. *J. Am. Chem. Soc.* **1994,** *116* (6), 2448-2456.

27.   Neverov, A. A.; Brown, R. S., Br+ and I+ transfer from the halonium ions of adamantylideneadamantane to acceptor olefins. Halocyclization of 1,omega-alkenols and alkenoic acids proceeds via reversibly formed intermediates. *J. Org. Chem.* **1996,** *61* (3), 962-968.

28.   Strating, J.; Wieringa, J. H.; Wynberg, H., The Isolation of a Stabilized Bromonium Ion. *Journal of the Chemical Society D-Chemical Communications* **1969,** (16), 907-908.

29.   Denmark, S. E.; Burk, M. T.; Hoover, A. J., On the Absolute Configurational Stability of Bromonium and Chloronium Ions. *J. Am. Chem. Soc.* **2010,** *132* (4), 1232-1233.

30.   Ashtekar, K. D.; Vetticatt, M.; Yousefi, R.; Jackson, J. E.; Borhan, B., Nucleophile-Assisted Alkene Activation: Olefins Alone Are Often Incompetent. *J. Am. Chem. Soc.* **2016,** *138* (26), 8114-8119.

31.   Denmark, S. E.; Ryabchuk, P.; Burk, M. T.; Gilbert, B. B., Toward Catalytic, Enantioselective Chlorolactonization of 1,2-Disubstituted Styrenyl Carboxylic Acids. *J. Org. Chem.* **2016,** *81* (21), 10411-10423.

32.   Ashtekar, K. D.; Marzijarani, N. S.; Jaganathan, A.; Holmes, D.; Jackson, J. E.; Borhan, B., A New Tool To Guide Halofunctionalization Reactions: The Halenium Affinity (HalA) Scale. *J. Am. Chem. Soc.* **2014,** *136* (38), 13355-13362.

33.   Sakakura, A.; Ukai, A.; Ishihara, K., Enantioselective halocyclization of polyprenoids induced by nucleophilic phosphoramidites. *Nature* **2007,** *445* (7130), 900-903.

34.   Denmark, S. E.; Burk, M. T., Enantioselective Bromocycloetherification by Lewis Base/Chiral Bronsted Acid Cooperative Catalysis. *Org. Lett.* **2012,** *14* (1), 256-259.

35.   Nicolaou, K. C.; Simmons, N. L.; Ying, Y.; Heretsch, P. M.; Chen, J. S., Enantioselective Dichlorination of Allylic Alcohols. *J. Am. Chem. Soc.* **2011,** *133* (21), 8134-8137.

36.   Hu, D. X.; Seidl, F. J.; Bucher, C.; Burns, N. Z., Catalytic Chemo-, Regio-, and Enantioselective Bromochlorination of Allylic Alcohols. *J. Am. Chem. Soc.* **2015,** *137* (11), 3795-3798.

37.   Jaganathan, A.; Garzan, A.; Whitehead, D. C.; Staples, R. J.; Borhan, B., A Catalytic Asymmetric Chlorocyclization of Unsaturated Amides. *Angew. Chem. Int. Ed.* **2011,** *50* (11), 2593-2596.

38.   Garzan, A.; Jaganathan, A.; Marzijarani, N. S.; Yousefi, R.; Whitehead, D. C.; Jackson, J. E.; Borhan, B., Solvent-Dependent Enantiodivergence in the Chlorocyclization of Unsaturated Carbamates. *Chem. Eur. J.* **2013,** *19* (27), 9015-9021.

39.   Jaganathan, A.; Staples, R. J.; Borhan, B., Kinetic Resolution of Unsaturated Amides in a Chlorocyclization Reaction: Concomitant Enantiomer Differentiation and Face Selective Alkene Chlorination by a Single Catalyst. *J. Am. Chem. Soc.* **2013,** *135* (39), 14806-14813.

40.   Jaganathan, A.; Borhan, B., Chlorosulfonamide Salts Are Superior Electrophilic Chlorine Precursors for the Organocatalytic Asymmetric Chlorocyclization of Unsaturated Amides. *Org. Lett.* **2014,** *16* (14), 3616-3619.

41.   Soltanzadeh, B.; Jaganathan, A.; Staples, R. J.; Borhan, B., Highly Stereoselective Intermolecular Haloetherification and Haloesterification of Allyl Amides. *Angew. Chem. Int. Ed.* **2015,** *54* (33), 9517-9522.

42.   Soltanzadeh, B.; Jaganathan, A.; Yi, Y.; Yi, H.; Staples, R. J.; Borhan, B., Highly Regio- and Enantioselective Vicinal Dihalogenation of Allyl Amides. *J. Am. Chem. Soc.* **2017,** *139* (6), 2132-2135.

43.   Steigerwald, D. C.; Soltanzadeh, B.; Sarkar, A.; Morgenstern, C.; Staples, R. J.; Borhan, B., Ritter-Enabled Catalytic Asymmetric Chloroamidation of Olefins. *J. Am. Chem. Soc.* **2020**, Submitted.

44.   Yousefi, R.; Ashtekar, K. D.; Whitehead, D. C.; Jackson, J. E.; Borhan, B., Dissecting the Stereocontrol Elements of a Catalytic Asymmetric Chlorolactonization: Syn Addition Obviates Bridging Chloronium. *J. Am. Chem. Soc.* **2013,** *135* (39), 14524-14527.

45.   Marzijarani, N. S.; Yousefi, R.; Jaganathan, A.; Ashtekar, K. D.; Jackson, J. E.; Borhan, B., Absolute and relative facial selectivities in organocatalytic asymmetric chlorocyclization reactions. *Chem. Sci.* **2018,** *9* (11), 2898-2908.

46.   Laidler, K. J., Chemical-Kinetics and the Origins of Physical Chemistry. *Arch. Hist. Exact Sci.* **1985,** *32* (1), 43-75.

47.   Lars, M.; Hundley, S. W., Reaction Rates of Isotopic Molecules. John Wiley & Sons: 1979; pp 91-102.

48.   Evans, M. G.; Polanyi, M., Some applications of the transition state method to the calculation of reaction velocities, especially in solution. *Trans. Faraday Soc.* **1935,** *31* (1), 0875-0893.

49.   Eyring, H., The Activated Complex in Chemical Reactions. *J. Chem. Phys.* **1935,** *3* (2), 107-115.

50.   Laidler, K. J.; King, M. C., The Development of Transition-State Theory. *J. Phys. Chem.* **1983,** *87* (15), 2657-2664.

51.   Carpenter, B. K., *Determination of Organic reaction mechanisms*. John Wiley & Sons Inc.: New York, 1984.

52.   Cornish-Bowden, A., *Fundamentals of Enzyme kinetics*. 4th Ed. ed.; Wiley-Blackwell: Weinheim, Germany, 2012.

53.   Laidler, K. J., *Chemical Kinetics*. 3rd Ed. ed.; Harper & Row: New York, 1987.

54.   I.N., L., *Physical Chemistry*. 6th Ed. ed.; McGraw-Hill: New York, 2009.

55.   McQuarrie, D. A.; Simon, J. D., Physical Chemistry: A Molecular Approach. 1st Ed. ed.; University Science Books: California, 1997.

56.   Selwyn, M. J., A Simple Test for Inactivation of an Enzyme During Assay. *Biochim. Biophys. Acta* **1965,** *105* (1), 193-195.

57.   Blackmond, D. G., Reaction progress kinetic analysis: A powerful methodology for mechanistic studies of complex catalytic reactions. *Angew. Chem. Int. Ed.* **2005,** *44* (28), 4302-4320.

58.   Blackmond, D. G., Kinetic Profiling of Catalytic Organic Reactions as a Mechanistic Tool. *J. Am. Chem. Soc.* **2015,** *137* (34), 10852-66.

59.   Lineweaver, H.; Burk, D., The determination of enzyme dissociation constants. *J. Am. Chem. Soc.* **1934,** *56*, 658-666.

60.   Nielsen, C. D. T.; Bures, J., Visual kinetic analysis. *Chem. Sci.* **2019,** *10* (2), 348-353.

61.   Kutateladze, D. A.; Strassfeld, D. A.; Jacobsen, E. N., Enantioselective Tail-to-Head Cyclizations Catalyzed by Dual-Hydrogen-Bond Donors. *J. Am. Chem. Soc.* **2020,** *142* (15), 6951-6956.

62.   Baxter, R. D.; Sale, D.; Engle, K. M.; Yu, J. Q.; Blackmond, D. G., Mechanistic Rationalization of Unusual Kinetics in Pd-Catalyzed C-H Olefination. *J. Am. Chem. Soc.* **2012,** *134* (10), 4600-4606.

63.   Hill, D. E.; Pei, Q. L.; Zhang, E. X.; Gage, J. R.; Yu, J. Q.; Blackmond, D. G., A General Protocol for Addressing Speciation of the Active Catalyst Applied to Ligand-

Accelerated Enantioselective C(sp(3))-H Bond Arylation. *ACS Catal.* **2018,** *8* (2), 1528-1531.

64.   Bures, J.; Armstrong, A.; Blackmond, D. G., Curtin-Hammett Paradigm for Stereocontrol in Organocatalysis by Diarylprolinol Ether Catalysts. *J. Am. Chem. Soc.* **2012,** *134* (15), 6741-6750.

65.   Bures, J.; Dingwall, P.; Armstrong, A.; Blackmond, D. G., Rationalization of an Unusual Solvent-Induced Inversion of Enantio-meric Excess in Organocatalytic Selenylation of Aldehydes. *Angew. Chem. Int. Ed.* **2014,** *53* (33), 8700-8704.

66.   Bures, J.; Armstrong, A.; Blackmond, D. G., Explaining Anomalies in Enamine Catalysis: "Downstream Species" as a New Paradigm for Stereocontrol. *Acc. Chem. Res.* **2016,** *49* (2), 214-222.

67.   Dechert-Schmitt, A. M.; Garnsey, M. R.; Wisniewska, H. M.; Murray, J. I.; Lee, T.; Kung, D. W.; Sach, N.; Blackmond, D. G., Highly Modular Synthesis of 1,2-Diketones via Multicomponent Coupling Reactions of Isocyanides as CO Equivalents. *ACS Catal.* **2019,** *9* (5), 4508-4515.

68.   Daponte, J. A.; Guo, Y. J.; Ruck, R. T.; Hein, J. E., Using an Automated Monitoring Platform for Investigations of Biphasic Reactions. *ACS Catal.* **2019,** *9* (12), 11484-11491.

69.   Ji, Y. N.; Li, H. M.; Hyde, A. M.; Chen, Q. H.; Belyk, K. M.; Lexa, K. W.; Yin, J. J.; Sherer, E. C.; Williamson, R. T.; Brunskill, A.; Ren, S. M.; Campeau, L. C.; Davies, I. W.; Ruck, R. T., A rational pre-catalyst design for bis-phosphine mono-oxide palladium catalyzed reactions. *Chem. Sci.* **2017,** *8* (4), 2841-2851.

70.   Ji, Y. N.; Plata, R. E.; Regens, C. S.; Hay, M.; Schmidt, M.; Razler, T.; Qiu, Y. P.; Geng, P.; Hsiao, Y.; Rosner, T.; Eastgate, M. D.; Blackmond, D. G., Mono-Oxidation of Bidentate Bis-phosphines in Catalyst Activation: Kinetic and Mechanistic Studies of a Pd/Xantphos-Catalyzed C-H Functionalization. *J. Am. Chem. Soc.* **2015,** *137* (41), 13272-13281.

71.   Lehnherr, D.; Ji, Y. N.; Neel, A. J.; Cohen, R. D.; Brunskill, A. P. J.; Yang, J. Y.; Reibarkh, M., Discovery of a Photoinduced Dark Catalytic Cycle Using in Situ LED-NMR Spectroscopy. *J. Am. Chem. Soc.* **2018,** *140* (42), 13843-13853.

72.   Bures, J., A Simple Graphical Method to Determine the Order in Catalyst. *Angew. Chem. Int. Ed.* **2016,** *55* (6), 2028-2031.

73.   Bures, J., Variable Time Normalization Analysis: General Graphical Elucidation of Reaction Orders from Concentration Profiles. *Angew. Chem. Int. Ed.* **2016,** *55* (52), 16084-16087.

74.   Bures, J., What is the Order of a Reaction? *Top. Catal.* **2017,** *60* (8), 631-633.

Chapter 2. Mechanism of catalytic asymmetric chlorolactonization of alkene carboxylic acids

Electrophilic halofunctionalization reactions have undergone a resurgence sparked by recent discoveries in the field of catalytic asymmetric halocyclizations. To build mechanistic understanding of these asymmetric transformations, a toolbox of analytical methods has been deployed, addressing the roles of catalyst, electrophile (halenium donor), and nucleophile in determining rates and stereopreferences. The test reaction, (DHQD)$_2$PHAL-catalyzed chlorocyclization of 4-aryl-4-pentenoic acids with 1,3-dichloro-5,5-dimethylhydantoin (DCDMH), is revealed to be first order in catalyst and chlorenium ion donor and zero order in alkenoic acid substrate under synthetically relevant conditions. The simplest interpretation is that rapid substrate-catalyst binding precedes rate-limiting chlorenium attack, controlling the face selec-tivity of both chlorine attack and lactone closure. ROESY and DFT studies, aided by crystal structures of carboxylic acids bound by the catalyst, point to a plausible resting state of the catalyst-substrate complex predisposed for asymmetric chlorolactonization. As revealed by our earlier labeling studies, these findings suggest modes of binding in the (DHQD)2PHAL chiral pocket that explain the system's remarkable control over rate- and enantioselection-determining events. Though a comprehensive modeling analysis is beyond the scope of the present work, quantum chemical analysis of the fragments' interactions and candidate reaction paths point to a one-step concerted process with the nucleophile playing a critical role in activating the olefin for concomitant electrophilic attack.

2.1   Introduction

Electrophilic olefin halocyclizations (Figure 2.1a) are long-known workhorse organic transformations,[1] now returning to prominence as their catalytic asymmetric variants offer a powerful strategy for enlarging the chiral pool.[2-47] In early work on 4-aryl-4-pentenoic acids, we found Sharpless's ligand, (DHQD)$_2$PHAL, to be an efficient mediator for asymmetric chlorolactonization (Figure 2.1b).[38, 48] Since then, reports from our own and other labs have confirmed the efficacy of cinchona alkaloid dimers in a range of asymmetric halofunctionalizations.[17-19, 22, 39-41, 49-52] With the growing list of examples, mechanistic insight into the catalytic activation and stereoinduction in these processes is necessary to support the design of new reactions and catalyst scaffolds. Taking (DHQD)$_2$PHAL-catalyzed asymmetric chlorolactonization of 4-aryl-4-propenoic acid as a test reaction, we present here kinetic, spectroscopic, structural, and computational studies leading to a mechanistic model.

a. Generalized Halofunctionalization Reaction
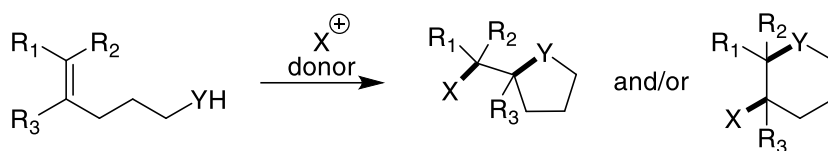
b. Halocyclization using Model Substrate 2-1
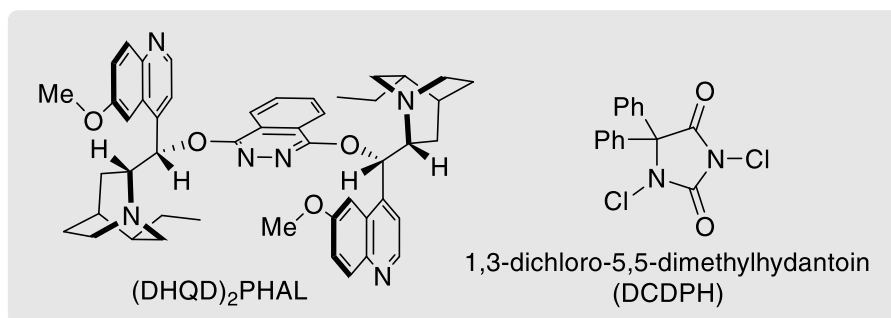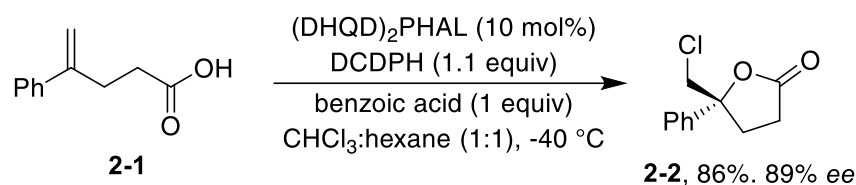
Figure 2.1 Halocyclization reactions. a. Generalized depiction of halocyclization reactions; b. Catalytic asymmetric chlorolactonization of 4-aryl-4-pentenoic acid **2-1** mediated by (DHQD)₂PHAL

Our recent labeling and spectroscopic analyses[53, 54] revealed the absolute and relative face selectivities of Cl (electrophile) and O (nucleophile) addition across the double bond in **2-1** (Figure 2.2) as well as the rate and stereochemical effects of varying the chlorohydantoins (chlorenium ion donors).[53, 54] The cumulative findings of this work led to the following conclusions:

1. Catalyst templated addition across the olefin **2-1** shows both a strong pro-*R* preference (>20:1) for chlorenium ion attachment at C-6, and closure favoring the 5*R* over the 5*S* lactone by a factor of >10:1. The net result is predominant *syn* Cl, O addition across the olefinic π-bond in **2-1-D**, obviating the potential intermediacy of a 3-membered cyclic chloronium ion (Figure 2.2).

Figure 2.2 Stereochemical outcomes of chlorolactonization reaction. Summary of observed stereoselectivities with deuterated substrate analog **2-1-D**, highlighting the syn addition as the major product of the catalytic reaction

2. In principle, the two new bonds in the major product stereoisomer **2-2-D** could be formed stepwise, *via* a carbocation intermediate, or concertedly (Figure 2.2).

3. In either mechanistic case, the catalyst templates the ring closure. Catalyst binding, mainly *via* hydrogen bonding and van der Waals interactions, presumably limits the conformational choices of substrate **2-1**, guiding the enantioselective cyclization.

(DHQD)₂PHAL (10 mol%)
chlorohydantoin (1.1 equiv)
benzoic acid (1 equiv)
CHCl₃, -40 °C

2-1 → **2-2**

$$y = -0.0706x + 19.273$$
$$R^2 = 0.9853$$

ΔΔG = RTln(k_X/k_H) (kcalmol⁻¹)

HalA (Cl) (kcalmol⁻¹)

chlorohydantoin

HalA (Cl) decreases — rate increases
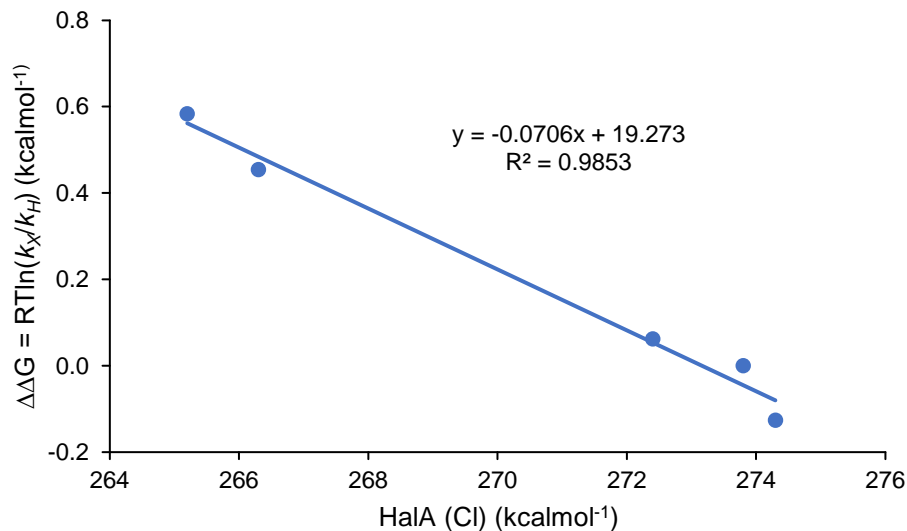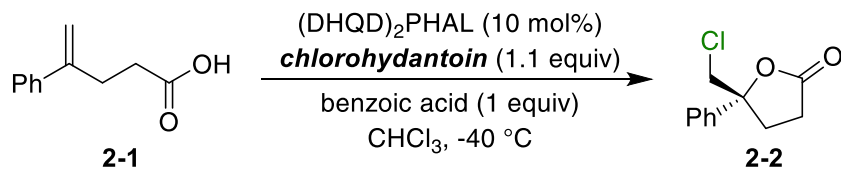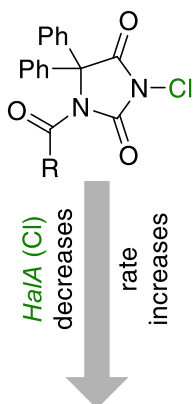
Ar	*HalA* (Cl)[a] kcal/mol	%yield	%ee	k_{Ar} (s⁻¹)
4-Me-C₆H₄	274.3	86	88	1.6×10^{-6}
C₆H₅	273.8	78	88	2.1×10^{-6}
2-F-C₆H₄	272.4	67	88	2.4×10^{-6}
4-CN-C₆H₄	266.3	78	84	5.6×10^{-6}
4-NO₂-C₆H₄	265.2	71	86	7.4×10^{-6}

[a]Calculated at the B3LYP/6-31G*/SM8 (CHCl₃) level of theory.

Figure 2.3 Chlorohydantoin effect on rate of chlorolactonization reaction. Electronic perturbation at the *N*1 substituent of chlorohydantoins affecting the rate of chlorolactonization. The plot represents the linear variation of ΔΔG‡ = RTln(k_{Ar}/k_{Ph}), relating experimentally determined rate constants (k_{Ar}) with the theoretically calculated absolute *HalA*(Cl) values.

4.   As depicted in Figure 2.3, we have probed the effects of tuning the chlorenium source in our asymmetric chlorolactonization protocol. By preparing and studying a series of previously unknown N-aroylated N-chlorohydantoins, we have shown that N1 substituents inductively activate delivery of the N3 chlorine to the substrate during

the course of the chlorolactonization. The reaction rates of these electronically perturbed chlorinating agents vary as predicted by their HalA values (halenium affinity).[55] The linearity and low slope of the $\Delta\Delta G\ddagger$ [=RTln(kAr/kPh)] vs HalA plot suggests an early transition state for chlorine transfer. Furthermore, chiral chlorohydantoins in these reactions display classic match-mismatch behaviors.[54] These results indicate direct involvement of the chlorohydantoins in the rate and stereoselectivity-determining events in the asymmetric chlorocyclization.

These preliminary mechanistic findings call for a full investigation of the reaction mechanism to identify the modes of interaction among the participants, and to map out the catalytic cycle of this (DHQD)$_2$PHAL catalyzed asymmetric chlorolactonization.

2.2   Kinetic studies

Kinetic investigation of multistep organic reactions can provide key insights into reaction mechanisms by revealing the order of individual components in the rate-determining step (RDS). As articulated in recent years by Blackmond and co-workers,[56-59] Reaction Progress Kinetic Analysis (RPKA) exploits modern reaction monitoring methods and easily accessible fitting and graphing software to improve the ease and accuracy of analyses over classical approximation methods. A great advantage of RPKA is that it can probe practical reactions such as halofunctionalization under their native conditions, unlike classical kinetic treatments that require e.g. the unbalanced concentrations used in pseudo first order studies. In this work, RPKA results place critical boundary conditions on the mechanisms proposed for this asymmetric chlorolactonization.

70

In the original optimized reaction, 4-phenyl-4-pentenoic acid **2-1** at 0.051 M concentration was cyclized in the presence of 0.056 M 1,3-dichloro-5,5-diphenylhydantoin (DCDPH) as the chlorine source, along with 10 mol% (DHQD)$_2$PHAL as the chiral catalyst. The highest enantioinduction was observed in a 1:1 chloroform:hexane mixture as solvent with benzoic acid as an additive at 0.051 M (Figure 2.1b).[38]

To follow the kinetics of this reaction, NMR analysis proved optimal as the reagent and products displayed well-resolved peaks under the reaction conditions. The following modifications to the standard protocol were introduced to simplify the mixture for kinetic studies: (i) deuterated chloroform was employed instead of 1:1 chloroform:hexane; (ii) 4 mol% of the catalyst was used to slow the reaction, enabling capture of the important early data points. This approach allowed time for temperature equilibration in the probe and shimming, while retaining ≥85% of the starting material at the initial point of measurement; (iii) 1,3-dichloro-5,5-dimethylhydantoin (DCDMH) was employed since the originally used DCDPH results in the insoluble byproduct 1-chloro-5,5-diphenylhydantoin, adversely affecting the spectra of the evolving reaction mixture. (iv) to reduce the complexity of the initial kinetic studies, benzoic acid was omitted, although, as described in the experimental section, and later in the manuscript, including benzoic acid was illuminating with respect to the order of the substrate. These adjustments for the kinetic studies led to only a 5% drop in *ee* and presumably do not qualitatively change the reaction mechanism.

A detailed RPKA analysis of the chlorolactonization reaction revealed the following results (see SI for detailed experimental analysis and a brief theoretical description of RPKA in the context of asymmetric halogenation):

a)   The asymmetric chlorolactonization is *zero order* in alkene carboxylic acid **2-1**.

b)   The reaction shows *first order* dependence with respect to the catalyst (DHQD)$_2$PHAL and the chlorenium ion donor-DCDMH.

c)   The reaction does not suffer from any catalyst deactivation or product inhibition, as demonstrated by 'the same excess' experiments.

d)   Addition of an external carboxylic acid such as benzoic acid or an inert alkenoic acid, that can potentially compete with the substrate's binding to the catalyst's active site, retards the overall rate of the reaction.

The above observations can be summarized as follows:

$$Rate = k\ [(DHQD)_2PHAL]^1[DCDMH]^1[\mathbf{2-1}]^0$$

The fact that the reaction is zeroth order in substrate **2-1** (4-phenylpent-4-enoic acid) suggests that the catalyst is saturated, binding **2-1** rapidly to the basic quinuclidine moiety to form the strongly hydrogen-bonded acid-base adduct. As detailed further below, this **resting state** species is a 1:2 complex of (DHQD)$_2$PHAL and **2-1.**

Quantum chemical modeling of the reaction components and their interactions finds that quinuclidine has a substantially stronger affinity for alkenoic acid **2-1** (-15.8 kcal/mol) than for DCDMH (-10.6 kcal/mol; see shaded box in Figure 2.4). It is thus not surprising that alkene **2-1** outcompetes DCDMH for binding to the catalyst. NMR evidence further supports this conclusion: 1,3-dichlorohydantoin with (DHQD)$_2$PHAL shows splitting of the CH$_2$ hydrogens into a diastereotopic pair, implying a complex formed with

the chiral catalyst. However, addition of **2-1** completely reverses this complexation, returning the hydantoin spectrum to that of uncomplexed reagent.[38]

Pairwise Association Energies ΔH (kcal/mol)

| quinuclidine---2-**1** | -16.8 | DCDMH---**1** (interaction at CO$_2$H) | -7.3 | DCDMH---**1** (interaction at alkene) | -4.0 |
| quinuclidine---DCDMH | -13.3 | | | | |

Resting state

Proposed Catalytic cycle

(DHQD)$_2$PHAL

Step 1

2-1

DCDMH

Step 2 Path A **Slow step**

Step 2' Path B slow step

2-A

2-B

Step 3

MCDMH + **2-2**

Path B — *or* — *Path A*

Transition state 2-B

Intermediate 2-A
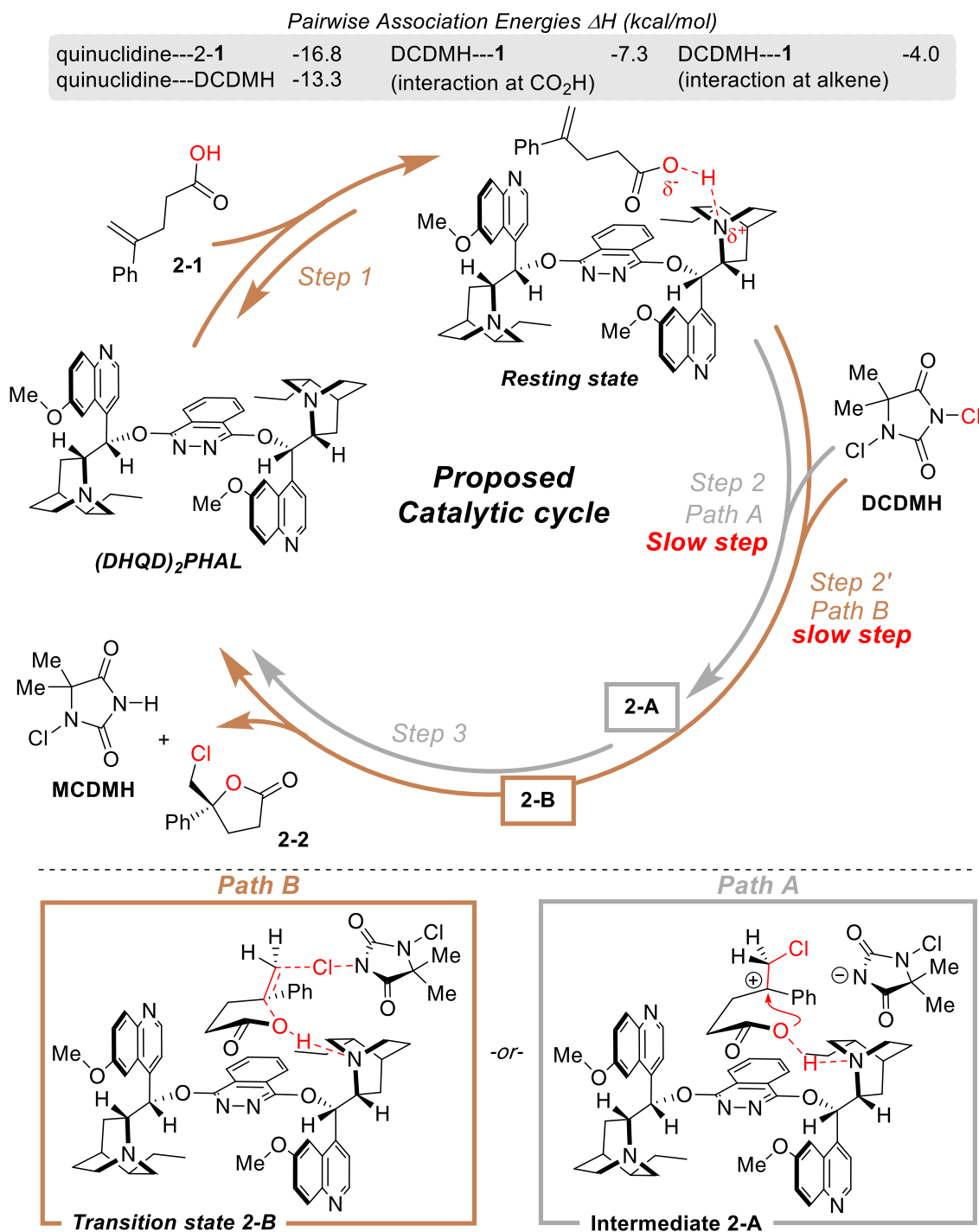
Figure 2.4 Catalytic cycle for chlorolactonization reaction. Putative catalytic cycle for (DHQD)$_2$PHAL catalyzed chlorolactonization of alkenoic acid **2-1** (in the absence of benzoic acid additive). Path A depicts a stepwise addition via a carbocationic intermediate

(Figure 2.4 (cont'd)) **2-A**. Path B depicts a possible one step concerted addition to the alkene **2-1**. NMR studies and computational modeling of the proposed intermediates and transition states are detailed in the following section. The top table insert displays calculated binding enthalpies of alkene **2-1**, DCDMH and quinuclidine (a truncated model for the catalyst). These pairwise association energies argue for the validity of the resting state. For clarity, only one alkenoic acid is shown bound to the catalyst, although experimental results indicate two molecules are bound at one time.

Collision of suitable conformations of the **resting state** complex (DHQD)$_2$PHAL-**2-1** with DCDMH results in chlorenium transfer to the alkene in a rate determining step (RDS, see SI for the detailed kinetic model that leads to the rate law and proposed catalytic cycle). This process may follow either of two paths: (a) formation of a *β-*chloromethyl carbenium ion **intermediate 2-A** (Path A, Figure 2.4), or (b) a concerted addition *via* **transition state 2-B**, to directly access the products (Path B, Figure 2.4). This latter Ad$_E$3-type process is an example of nucleophile assisted alkene activation (*NAAA*).[60]

In the absence of (DHQD)$_2$PHAL or quinuclidine catalysts, the DCDMH and alkene **2-1** are essentially unreactive at -40 °C. Therefore, apart from controlling the enantioselectivity by providing a chiral pocket, the catalyst must also activate the alkene or the DCDMH (or both). To promote the stepwise pathway leading to **intermediate 2-A**, the catalyst must activate the DCDMH to form the proposed chlorocarbenium ion intermediate. Rapid cyclization, guided by the catalyst, would then afford the product. On the other hand, the concerted pathway via **transition state 2-B** hinges on the activation of the alkene, irrespective of additional activation of the chlorenium source.

In the case of stepwise cyclization, the cation closure (step three in Figure 2.4) could not be rate limiting as this would predict a buildup of cation intermediate, which is not observed. Also, reversible formation of the carbocation should scramble the stereochemistry of the alkene =CHD site in deuterium labeled substrate **2-1-D** (see

74

Scheme 1), a process ruled out by the finding that recovered starting materials retain their stereochemical integrity. In the alternative event of a concerted addition *via NAAA* (**transition state 2-B**), the concerted chlorenium ion attack and ring closure would directly form the chlorolactone product. In either case (Path A or B), the chlorenium ion delivery to the olefin (step 2 or 2') must be part of the rate-determining step.

The kinetic studies also helped clarify the role of the benzoic acid additive, which marginally increases the enantioselectivity. We surmise that its presence aids in maintaining the rigidity of the C_2-symmetric (DHQD)$_2$PHAL catalyst (see next section for validation of this hypothesis by NMR and X-ray studies), and perhaps also aids in shuttling the protons required to neutralize the byproduct hydantoin anions, especially toward the end of the reaction when the concentration of **2-1** is low. Consistent with this idea, benzoic acid addition at an equimolar ratio to substrate lowers the rate of chlorolactonization (see SI for experimental details); presumably benzoic acid competes with 4-phenylpent-4-enoic acid **2-1** for binding in the catalyst's active site. This interpretation gained support from RPKA studies with benzoic acid added, which raised the measured order of the alkene from zero to 0.5 in the rate equation. This change is expected due to the fact that alkene **2-1** has to compete with the benzoic acid for binding in the catalyst, making its concentration relevant with respect to the rate. The following is the observed rate law in presence of benzoic acid:

$$Rate = k \, [(DHQD)_2PHAL]^1 [DCDMH]^1 [\mathbf{2-1}]^{0.5}$$

To further explore the proposed catalytic cycle, we resorted to competition studies (Figure 2.5). Prior analysis of the catalytic asymmetric chlorolactonization methodology revealed that 4-(4-(trifluoromethyl)phenyl)pent-4-enoic acid **2-3** is one tenth as reactive

as **2-1**.[38] Nonetheless, the trifluoromethyl substituent should not interfere with binding, as other sterically comparable substrates behaved well under the same reaction conditions. If substrate **2-3** binds to the catalyst to form an unreactive analogue of the **resting state**, it should serve as a competitive inhibitor, decreasing the concentration of the reactive complex with substrate **2-1**. Indeed, as shown in Figure 2.5, the chlorolactonization of **2-1** was slowed dramatically (decreased by 58%) upon addition of one equivalent of **2-3** to a 1:1 mixture of **2-1** and DCDMH with 1.5 mol% catalyst.

A similar competition study was performed between 4-phenylpent-4-enoic acid **2-1** and 4-(3-nitrophenyl)pent-4-enoic acid **2-4**, known to be a slow substrate. With a 1:1:1 mixture of substrates **2-1**, **2-4** and DCDMH under 1.5 mol% catalyst loading, the rate of the chlorolactonization of **2-1** was decreased by 71% (Figure 2.5). At a 1:1 ratio of inhibitor **2-4** to substrate **2-1**, a 50% decrease in rate would suggest similar binding affinity of **2-4** and **2-1** with (DHQD)$_2$PHAL; the larger observed inhibition suggests a stronger complexation with **2-4**. Perhaps this hints at the presence of weak aromatic stacking interaction contributing to the binding, which is expected to be stronger for **2-4**.

Further evidence supporting the idea that chlorine delivery from the hydantoin to **2-1** is rate-determining may be found in the effects of structural variations in the hydantoin chlorenium donors. As noted earlier (Figure 2.3), the *N*3 chlorine is activated when the *N*1 substituent of DCDMH is an electron withdrawing group (EWG). As quantified by the *HalA* values, stronger EWGs on *N*1 accelerate the reaction, consistent with chlorine delivery to **2-1** in the RDS. A related result is that chiral chlorohydantoins show match/mismatch effects in reaction, pointing to direct involvement of the chlorenium delivery reagent in the chlorocyclizations.[54]
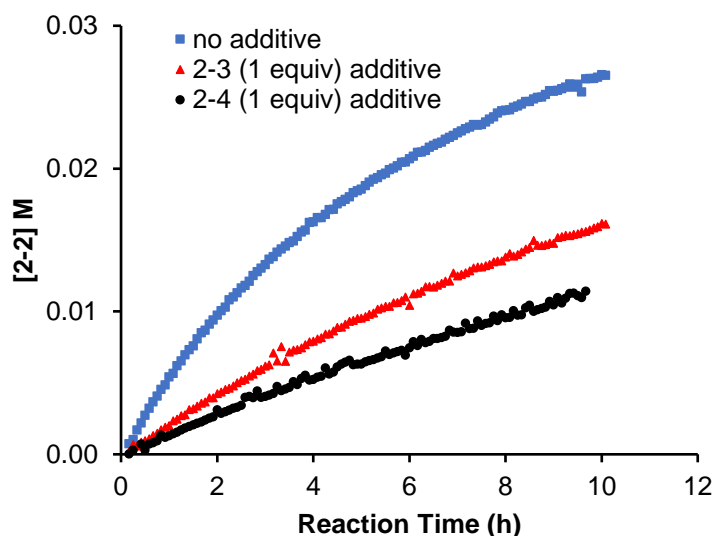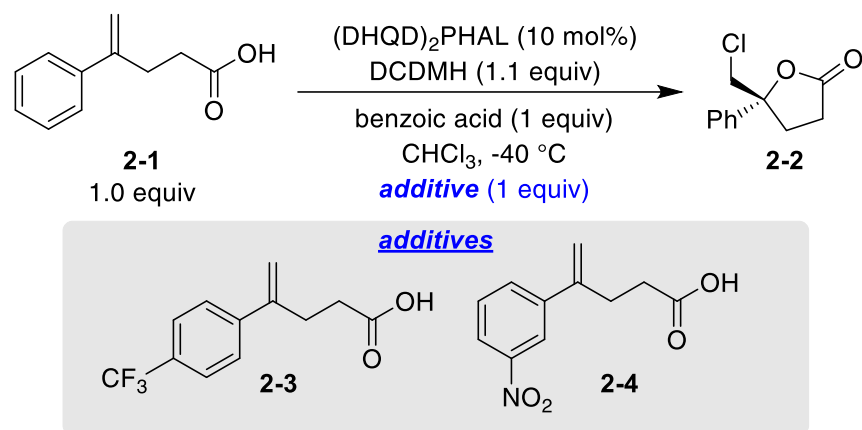
Figure 2.5 Competition studies on chlorolactonization reaction. Rate of formation of product **2-2** in presence of alkenoic acids **2-3** and **2-4**. The reduced rates imply **2-3** and **2-4** are competitive inhibitors of the catalyst, presumably binding to the active site and retarding the binding of substrate **2-1**.

To probe the involvement of the carboxylic acid moiety in the rate determining step, chlorocyclization of the deuterated 4-phenylpent-4-enoic acid **2-1-OD** (RCO_2D) was studied and compared to the same reaction with unlabeled substrate **2-1**. An inverse isotope effect ($k_H/k_D = 0.82$, see experimental sections for more detail) was measured, suggesting that the carboxylate plays a direct role in the reaction. Considering *Path A*, the change from H to D should not lead to the observed KIE, as the electrophilic transfer of the chlorenium ion is ostensibly insensitive to the nature of the hydrogen-bonded

nucleophile. On the other hand, the concerted *Path B* via **transition state 2-B** would presumably be accelerated by the H to D change, as the carboxylate oxygen's, and therefore the alkene's nucleophilicity is more activated as a consequence of the increased acidity of **2-1-OD** vs **2-1-OH**.

Overall, reaction progress kinetic analysis (RPKA), competition, reagent, and isotope studies find that (a) rate is first order in catalyst and in DCDMH, but zero order in substrate; (b) chlorenium donor ability and asymmetry characteristics affect reaction rates; and (c) the carboxylic acid's hydrogen isotope also modulates reaction rate. The implication is that the rate-determining step involves chlorenium transfer and the carboxylic acid's degree of deprotonation.

2.3   Resting state of the catalyst

With the elementary steps of the catalytic cycle deduced from the kinetic findings, we undertook NMR and computational studies to gain structural insight into intermediates and transition states along the reaction paths. Our first target in this process was the **resting state** (catalyst-substrate complex) of the catalytic cycle.

A comprehensive conformational search of the free catalyst using molecular mechanics and density functional simulations revealed three low energy conformational orientations for the two sidechains on the phthalazine (see SI for computational details). These showed H_aCCH_b dihedral angles of roughly 80° and 170°, consistent with prior NMR and theoretical work.[61-63] Figure 2.6a shows a DFT-B3LYP/6-31G* (gas) minimized structure of $(DHQD)_2PHAL$ with a H_aCCH_b dihedral of 169.4°. This is consistent with the NMR of free $(DHQD)_2PHAL$, where the H_b resonance exhibits a *ddd* with three equivalent 9 Hz coupling constants. Dihedral angles between H_b and the methylene protons in the

quinuclidine ring lead to the anticipated 9 Hz coupling. Thus, the third 9 Hz coupling of H_b is ascribed to its interaction with H_a, resulting from the *anti* orientation of the two protons.
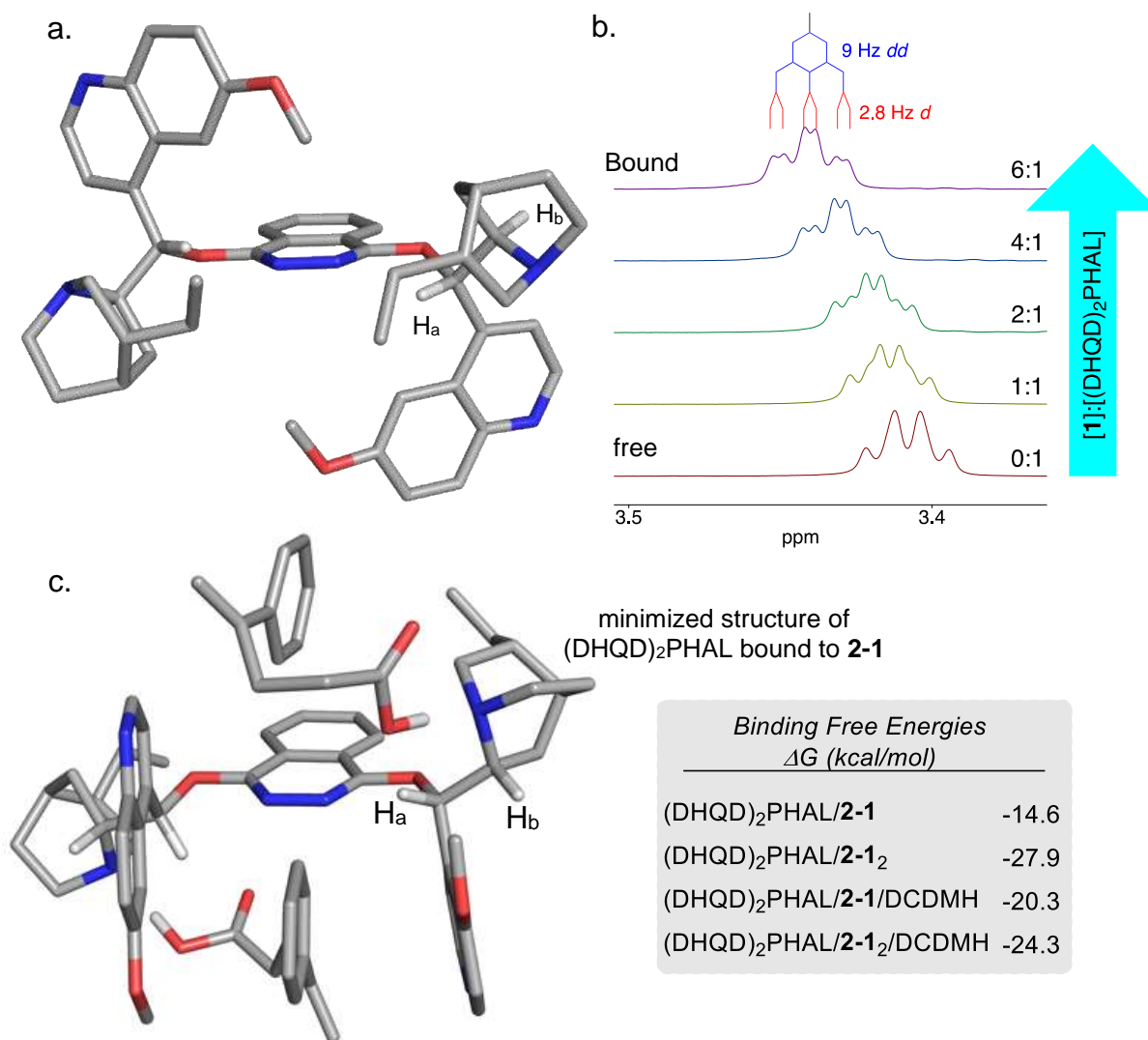
Figure 2.6 Conformational changes observed upon binding of 2-1 to (DHQD)₂PHAL.
(a) represents the minimized structure of free (DHQD)$_2$PHAL with $H_a CCH_b$ dihedral angle ~170°, supported by the 9 Hz coupling of H_b with H_a. (b) ^{1}H NMR titration induces a change in the H_b/H_a coupling from 9 to <3 Hz with the addition of the alkenoic acid **2-1**. (Figure 2.6 (cont'd)) (c) The model depicts a minimized structure of the catalyst bound to two alkenoic acid **2-1**, where the two $H_a CCH_b$ dihedral angle are 73.8° and 80.7°. The dihedral angles of the bound catalyst fit well with the observed smaller coupling constant for H_a/H_b. Computed binding free energies for complexation of the first and second alkenoic acids **2-1**, and for DCDMH with (DHQD)$_2$PHAL are shown in the shaded box.

79

Titration of (DHQD)$_2$PHAL with substrate **2-1** lowers the catalyst's H$_a$-H$_b$ coupling constant from 9 to <3 Hz, suggesting a conformation with an averaged H$_a$CCH$_b$ dihedral angle close to 90° (Figure 2.6b). This geometry, as depicted in Figure 2.6c, also orients the quinuclidine N toward the chiral cleft of the catalyst. Furthermore, the 1:1 catalyst complex exhibits broad peaks which sharpen on addition of another equivalent of alkenoic acid suggesting that in the **resting state**, the catalyst binds two alkenes. Finally, conformational searching using the MMFF94 force field, followed up by B3LYP-D3/6-31G*/postSMD(CHCl$_3$) structural optimization of the (DHQD)$_2$PHAL bound with two alkenoic acids found calculated binding free energies for the first and second molecules of **2-1** in (DHQD)$_2$PHAL of -14.6 and -13.3 kcal/mol, respectively. Among the lowest energy complex minima, the structure shown at right in Figure 2.6 is used here as the **resting state** catalyst model; this structure has H$_a$CCH$_b$ dihedral angles of 73.8° and 80.7°, consistent with the <3 Hz coupling of H$_a$ with H$_b$ in the NMR of the fully saturated complex.

Given the desymmetrization observed in the NMR of dichlorohydantoin interacting with the catalyst, one might expect that DCDMH binding would compete for the catalyst active site. However, for both the empty and singly occupied forms of the catalyst, the -14.6 and -13.3 kcal/mol binding energies of an additional acid substantially outcompete the -5.7 kcal/mol binding free energy of a molecule of DCDMH. Interacting with the doubly occupied **resting state**, the association of DCDMH is even weaker, as shown by the free energy values in Figure 2.6c.

Table 2.1 ^{1}H NMR analysis of alkenoic acid 2-5 and its complexes with (DHQD)$_2$PHAL and quinuclidine at -40 ºC in CDCl$_3$.
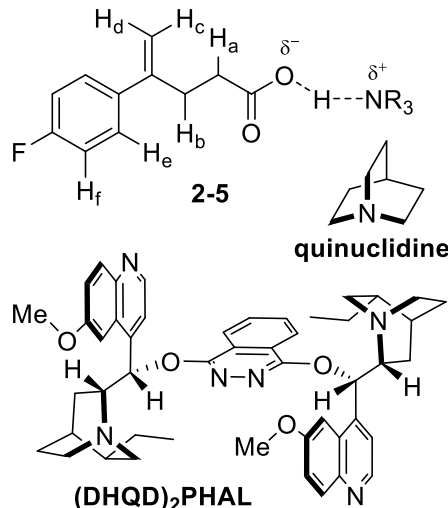
Protons on **2-5**	**2-5** only (ppm)	**2-5** with (DHQD)$_2$PHAL Δppm	**2-5** with quinuclidine Δppm
H_a	2.52	-0.52	-0.19
H_b	2.80	-0.43	-0.06
H_c	5.06	-0.46	-0.04
H_d	5.25	-0.54	-0.04
H_e	7.36	-0.23	+0.04
H_f	7.01	-0.29	-0.06

NR$_3$ = (DHQD)$_2$PHAL or quinuclidine

Further structural data on the **resting state** complex were obtained from NMR studies of a 2:1 mixture of 4-(4-fluorophenyl)pent-4-enoic acid **2-5** and (DHQD)$_2$PHAL in CDCl$_3$ carried out at -40 °C. Carboxylic acid **2-5** was used as a substitute for **2-1** since its aromatic protons (ortho to fluorine) do not overlap with the aromatic protons of the catalyst. Table 2.1 compares the ^{1}H NMR chemical shifts of the substrate with and without (DHQD)$_2$PHAL present. It is notable that the vinylic protons and also two methylene groups of the alkenoic acid **2-5** are shielded by ~0.5 ppm upon complexation with catalyst. We interpret this shielding as a combination of two effects: (a) deprotonation of the carboxylic acid and (b) binding in the cleft of the catalyst. To distinguish these contributions, ^{1}H NMR spectra of **2-5** were taken with quinuclidine in CDCl$_3$. There, it was the methylene group adjacent to the carboxylate moiety that showed the highest upfield shift (0.19 ppm). The other protons' shifts showed at most slight changes (~0.04 ppm). Thus, acid-base complex formation does not account fully for the large shielding seen with the catalyst–bound substrate.

To further probe the interactions between the substrate and the catalyst, ROESY experiments using the methods described by Bodenhausen *et al.*[64-66] found correlations between protons of **2-5** and (DHQD)$_2$PHAL offering further insights into binding. As depicted in Figure 2.7, ROESY correlations, leading to average distances are grouped into intramolecular and intermolecular correlations. The distances derived for the intramolecular interactions fit well with the minimized structure of the catalyst, illustrated in Figure 2.6. Probing intermolecular interactions, the OMe sidechains of the quinoline group (H$_n$) showed contacts with the substrate's methylene (H$_r$ and H$_t$) and phenyl protons (H$_k$). This also matches well with the calculated **resting state** model, depicted in Figure 2.6c, where the calculated distances fall well within the ROESY measured values (H$_n$/H$_t$ 2.6 Å calc'd, 3.0 Å expt, H$_n$/H$_r$ 2.5 calc'd, 3.2 Å expt, H$_n$/H$_k$ 2.9 Å calc'd, 3.8 Å expt). The ROESY verified model for the **resting state** shown in Figure 2.6c illustrates carboxylate binding to the protonated quinuclidine moiety, positioning the vinylic protons in the shielding regions of the quinoline rings, which leads to their observed upfield shifts.

ROESY Correlations of (DHQD)$_2$PHAL + **2-5**
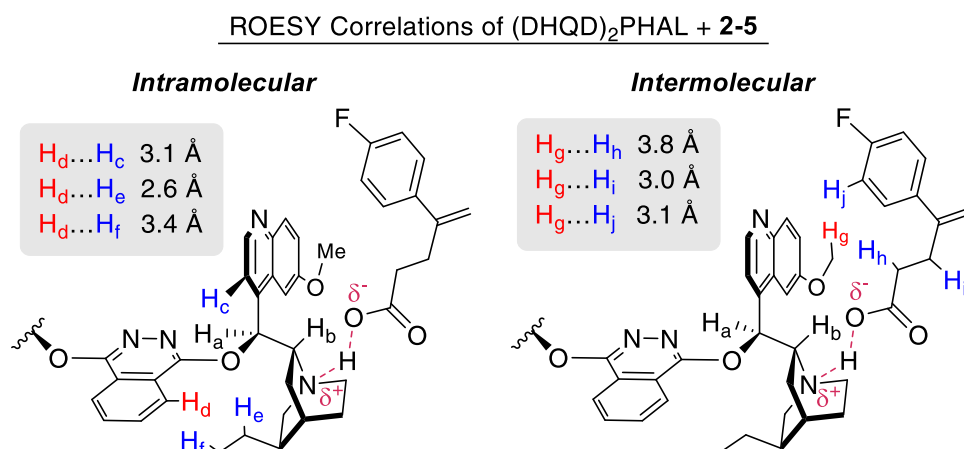
Figure 2.7 Structural investigation of resting complex using ROESY NMR. Intramolecular and intermolecular ROESY correlations of **2-5** bound to (DHQD)$_2$PHAL. The intramolecular correlations place the ethyl group near the phthalazine ring, while the methoxy shows close intermolecular relations with the substrate methylene units. These interactions are present in the lowest energy conformation of (DHQD)2PHAL.

As a C_2 symmetric cinchona alkaloid, (DHQD)$_2$PHAL can potentially bind to two substrates at the same time (as depicted in Figure 2.6). Consistent with this idea, when (DHQD)$_2$PHAL is treated with only one equivalent of the alkenoic acid **2-1**, the ^{1}H NMR peak broadening at room temperature clearly suggests loss of structural symmetry due to partial occupancy of the substrate. The spectra sharpen up in the presence of two equivalents of **2-1**. These results support a picture in which (DHQD)$_2$PHAL requires two substrates (or other carboxylic acids) to maintain its conformational rigidity in the C_2-symmetric *anti*-open form. On the other hand, addition of four equivalents of alkenoic acid to (DHQD)$_2$PHAL resulted in an averaged spectrum for the substrates, indicating fast equilibrium (on the NMR time scale) between bound and free forms of the alkenoic acid, while the catalyst's spectra remained sharp. Similar behavior is seen with benzoic acid (see SI for NMRs of (DHQD)$_2$PHAL with benzoic acid).

To further explore the stoichiometry of complexation, (DHQD)$_2$PHAL was treated with two equivalents of a 1:1 mixture of alkenoic acids **2-1** and **2-4**. This NMR experiment showed shielding behavior for both **2-1** and **2-4** similar to that seen in 2:1 substrate:catalyst mixtures with the individual substrates. If catalyst had only a single binding site, such mixtures should show more shielding of resonances of the more tightly bound alkenoic acid. Since the same degree of chemical shift is observed in the above case with the spectra being well-resolved, it appears that the catalyst binds both substrates in a 1:1:1 complex without competition. This 2:1 binding model is in accord with the reactivity results involving **2-1**, **2-3**, and **2-4** previously shown in Figure 2.5, and with the calculated binding energetics in Figure 2.6. As discussed further below, the 2:1 complex may undergo attack by the chlorenium ion donor on either of the two essentially

83

independently bound substrate molecules; it is thus the substrate for attack by the chlorenium ion donor.

An alternative scenario might involve dissociation to an active 1:1 complex, with the catalytically incompetent 2:1 complex serving simply as an off-cycle reservoir. In this scenario, however, the initial rate would not be the same for two reactions with different starting concentrations, such as the different excess experiments carried out in this study. We would anticipate the reaction with a higher concentration of the starting alkene to have a smaller initial rate. This behavior is not observed (see Figure 2.11 and the description of kinetic models in the experimental details).

Although we were unable to obtain crystals of the **resting state** itself, we were able to co-crystallize the catalyst (DHQD)$_2$PHAL with benzoic acid. This crystal structure displayed essentially the conformation deduced from the NMR studies (see SI for crystal structure), with the two H$_a$CCH$_b$ dihedral angle being 73.7° and 77.6°.

2.4   Structural insight into the transition state 2-B

To understand the asymmetric induction achieved in the (DHQD)$_2$PHAL-catalyzed chlorocyclization of **2-1** with DCDMH, a model of the interaction of the chlorenium ion donor with the **resting state** is needed, which must entail both activation and asymmetric specificity. The combination of substrate **2-1** with DCDMH alone is essentially unreactive (at -30 °C); a basic catalyst, such as quinuclidine or (DHQD)$_2$PHAL is needed to promote the reaction. Also, as noted earlier, both rate and stereoselectivity are affected by electronic and stereochemical variations in the dichlorohydantoins used. Thus, the ring-forming reaction involves both the state of carboxylate deprotonation, and the identity of the chlorine donor.

One path that might be envisioned is indirect chlorine transfer to substrate via a chlorinated (DHQD)$_2$PHAL. This can be ruled out as it predicts that the enantioselectivity should be independent of the chlorenium ion source (hydantoin) as the *N*-chloroquinuclidinium form of (DHQD)$_2$PHAL would now serve as the active *in situ* generated halogenating reagent. Also, as assessed in terms of *HalA* (Cl) values, chlorenium ion transfer to the quinuclidine nitrogen in the catalyst would be strongly endothermic (Δ*HalA* (Cl) 24.0 kcal/mol in CHCl$_3$), even when the stabilizing effects of tight ion pairing and solvation are included in the calculation.

2.5 Evidence for concerted addition (*NAAA*) pathway

Without assistance, chlorenium transfer from DCDMH to the alkene would be unfavorable (Δ*HalA* (Cl) = 22.3 kcal/mol in CHCl$_3$) (see *HalA* values in Figure 2.8a). Despite its low *HalA*, alkene **2-1** does slowly react with DCDMH. However, the rate is accelerated greatly in the presence of a basic catalyst such as quinuclidine. This strongly suggests that the catalyzed halocyclization of **2-1** proceeds via a nucleophilic activated alkene addition (*NAAA*) mechanism. Previous reports on chlorolactonization (summarized in Figure 2.8) have noted that a low energy barrier pathway via concerted addition can be triggered when the substrate adopts conformations with the anionic carboxylate oxygen atom near the alkene moiety. This close proximity of the nucleophile sharply enhances the alkene halenium affinity, enabling capture of the chlorenium ion from its donor, as the nucleophile approach now stabilizes for the developing charge in the alkene sp^2 carbon. This view is verified further by the contrasting isotope effects seen in the uncatalyzed reactions of DCDMH with alkenes **2-1** and **2-6** (Figure 2.8a). Here, in **2-1**, replacement of the protons vicinal to the putative carbenium site with deuterium

showed no observable kinetic isotopic effect (k_H/k_D = 1.0).[60] As depicted in Figure 2.8, **2-TS-I** illustrates the concerted transition state with bond distances that indicate a one-step, asynchronous addition of the chlorenium and the carboxylate to the olefin. In the case of **2-6**, the 4-methoxy analog of **2-1**, the alkene's nucleophilicity is inherently enhanced enough that the nucleophile-assisted pathway is unimportant; uncatalyzed reaction of **2-6** with DCDMH is much faster as compared to **2-1**. However, as expected for a stepwise pathway via a carbocationic intermediate, reaction of alkene **2-6** displayed a significant secondary kinetic isotopic effect (k_H/k_D = 1.2). In contrast to the concerted addition calculated for alkene **2-1**, **2-TS-II** depicts the attack to form the carbocation in the stepwise addition of the chlorenium ion to substrate **2-6**. The *HalA* (Cl) values of **2-1** and **2-6** (158.8 and 169.4 kcal/mol) differ by >10 kcal/mol, supporting the formation of a carbocation intermediate. The *HalA* (Cl) value of **2-6** closely matches that of the hydrogen-bonded MCDMH anion (~173 kcal/mol), consistent with unassisted chlorenium capture by **2-6** to form the carbocation, an action too endothermic for olefin **2-1** without further activation.
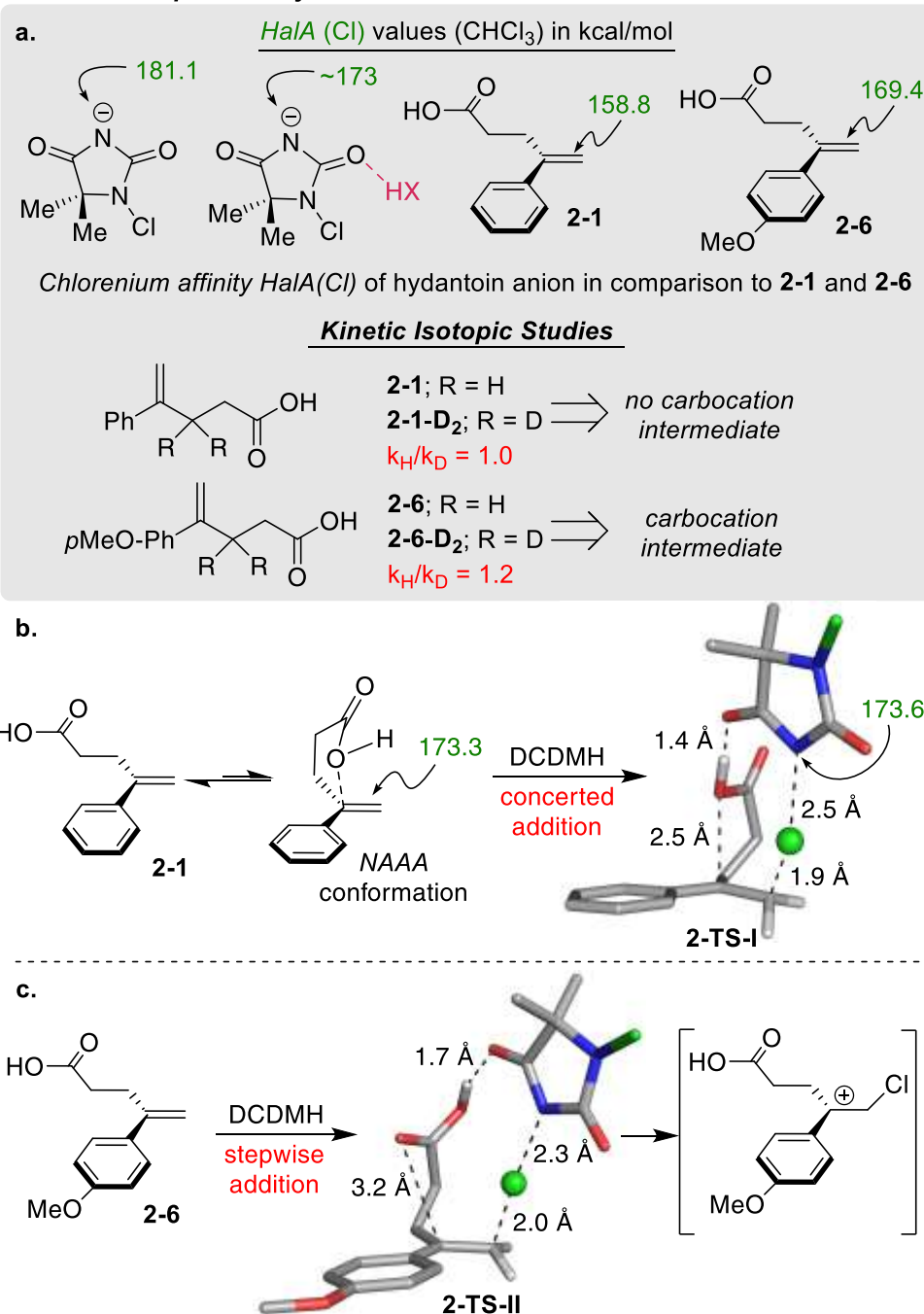
Figure 2.8 Prior work on concerted vs stepwise addition. (a) Evidence for concerted addition from *HalA* (Cl) calculations and KIE experiments. (b) Computationally modeling an uncatalyzed *syn*-concerted addition leading to chlorofunctionalization. (c) Computationally modeling an uncatalyzed *syn*-stepwise addition leading to chlorofunctionalization.

The *m*-NO₂ analogue of **2-1**, alkene **2-3**, is intrinsically deactivated and unreactive

towards DCDMH, hinting that *NAAA* can only offer so much activation if there are strong

inherent factors retarding the intrinsic nucleophilicity of the alkene. Though it appears quite general for otherwise nonpolarized alkenes, the concerted *NAAA* mechanism evidently strikes a fine balance. With the experimental evidence firmly indicating concerted addition to the alkene **2-1**, transition states with quinuclidine as well as (DHQD)$_2$PHAL as a catalyst were computationally modeled and analyzed in the following section.

2.6   Quinuclidine-catalyzed TS for *syn* and *anti* chlorocyclization

For the quinuclidine catalyzed reaction, transition structures for the lowest energy *syn* and *anti* concerted addition pathways were identified and optimized. (Figure 2.9). In search of optimized structures, conformational analyses using the MMFF94 force field provided poses, which were further refined via B3LYP-D3/6-31G*/postSMD (CHCl$_3$) calculations. Though the developing negative charge on the hydantoin ring in the *syn* TS benefits from proximity to the partially positive protonated quinuclidine, that advantage is outweighed by the steric freedom of approach from the far side (*anti* approach). In the CHCl$_3$ "solvent" as represented by the SMD dielectric continuum simulation, the *anti*-addition pathway is found to be 0.7 kcal/mol lower in energy than its *syn* partner, a result consistent with experimental findings. Both structures show similar parameters, with the developing C-Cl and C-O bond lengths slightly longer in the *anti* (2.2, 2.6 Å) than in the *syn* case (2.1, 2.4 Å). All attempts to initiate chlorenium atom transfer from DCDMH to **2-1** were monotonically endothermic in conformations that did not place the nucleophilic carboxylate moiety nearby (Figure 2.9). This implies that a stable *β*-chloromethyl carbenium ion intermediate is not a minimum along the reaction coordinate as would be expected for the stepwise mechanism.
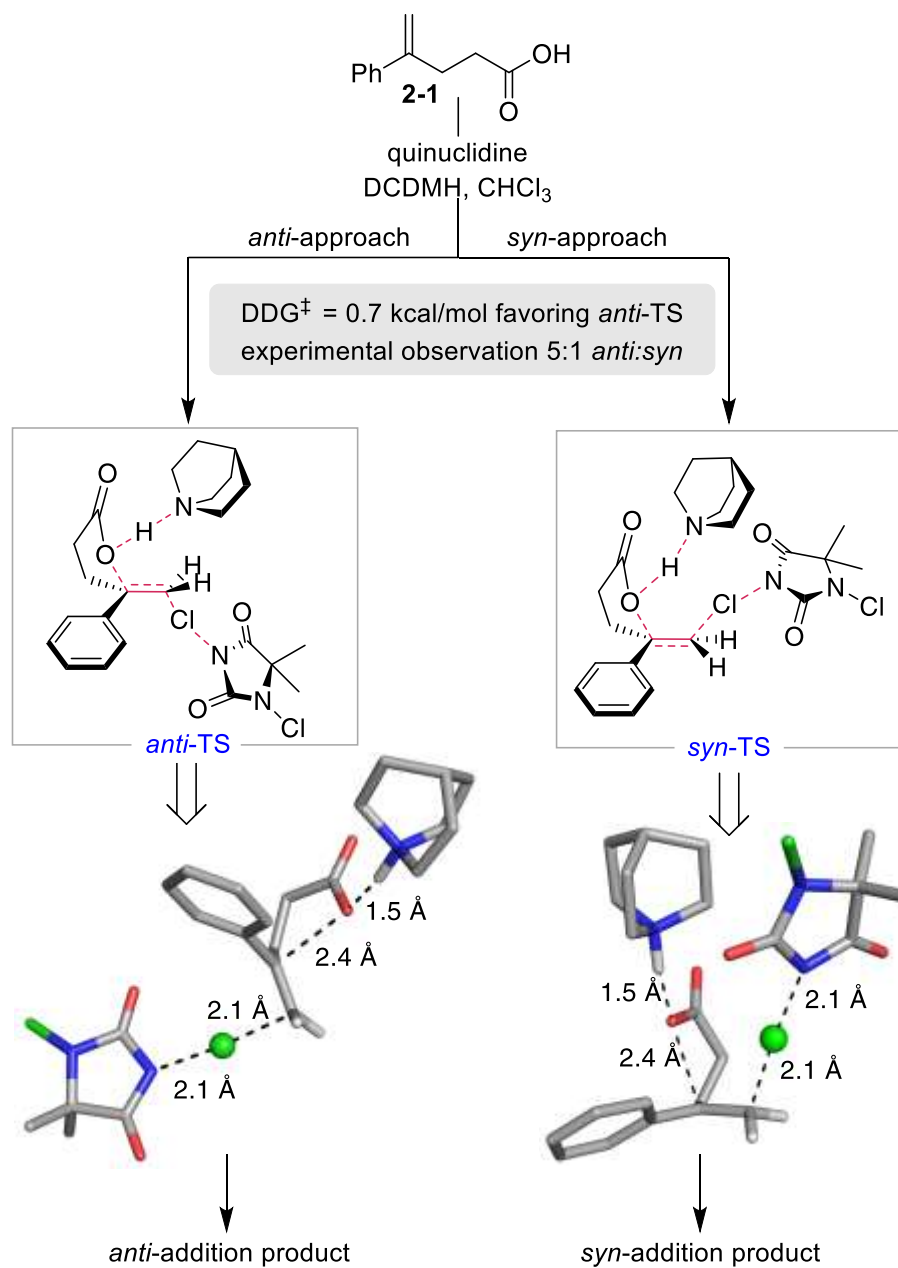
Figure 2.9 Transition states for quinuclidine catalyzed reaction. Transition states leading to *syn* and *anti*-addition for quinuclidine catalyzed chlorolactonization. Calculated using density functionals B3LYP-D3/6-31G* SM8 (CHCl₃)

The experimentally observed *syn*:*anti* ratio for quinuclidine catalyzed chlorocyclization of **2-1-D** is 1:5.[53] This agrees with the discussion above, and also with the calculated difference in activation energies computed for the *syn* and *anti* TS structures shown in Figure 2.9 ($\Delta\Delta G^{\ddagger}$ = 0.7 kcal/mol).

2.7 Modeling of the *syn*-addition TS for (DHQD)$_2$PHAL catalyzed reactions

Having identified the lowest energy TS structures for quinuclidine-catalyzed chlorocyclization of **2-1**, we proceeded to model the *syn* structure into the optimized geometry of (DHQD)$_2$PHAL, reoptimizing at the B3LYP-D3/6-31G* level of theory. The reader is reminded that the asymmetric catalyzed chlorolactonization of **2-1**-**D** favors the *syn* adduct **2-2**-**D** (*syn*:*anti* ratio ~9:1).[53] The energy of activation (10.5 kcal/mol) and partial bond lengths (2.4 Å for C-O and 2.1 Å for C-Cl) for the lowest energy (DHQD)$_2$PHAL catalyzed transition state were comparable to the quinuclidine catalyzed addition (Figure 2.10a). The acute H$_a$CCH$_b$ dihedral angle of 61.7° in the TS effectively oriented the quinuclidine towards the center of the catalyst allowing for the alkenoic acid to sit inside the chiral pocket as it further enjoys π-π-stacking with the phthalazine linker. This dihedral angle also fits well with the NMR studies depicted in Figure 2.6 for (DHQD)$_2$PHAL bound to **2-1**. As illustrated in Figure 2.10a, the *Re* face of the alkene is now readily accessible by both the chlorenium ion donor and the quinuclidine-activated carboxylate nucleophile, the simultaneous addition of which leads to the experimentally observed major *syn* enantiomer. Computational searches for *NAAA*-type TS structures leading to the minor products were much less successful; those products may well arise via more complex stepwise paths, and further studies in this direction are deferred to a future detailed computational analysis.

Prior studies have demonstrated that chlorolactonization using chiral chlorohydantoins exhibits matched-mismatched behavior when used with (DHQD)$_2$PHAL (Figure 2.10b, Table in dashed box). This provides further support for the hydantoin's direct involvement in the rate determining step as the chlorenium source.
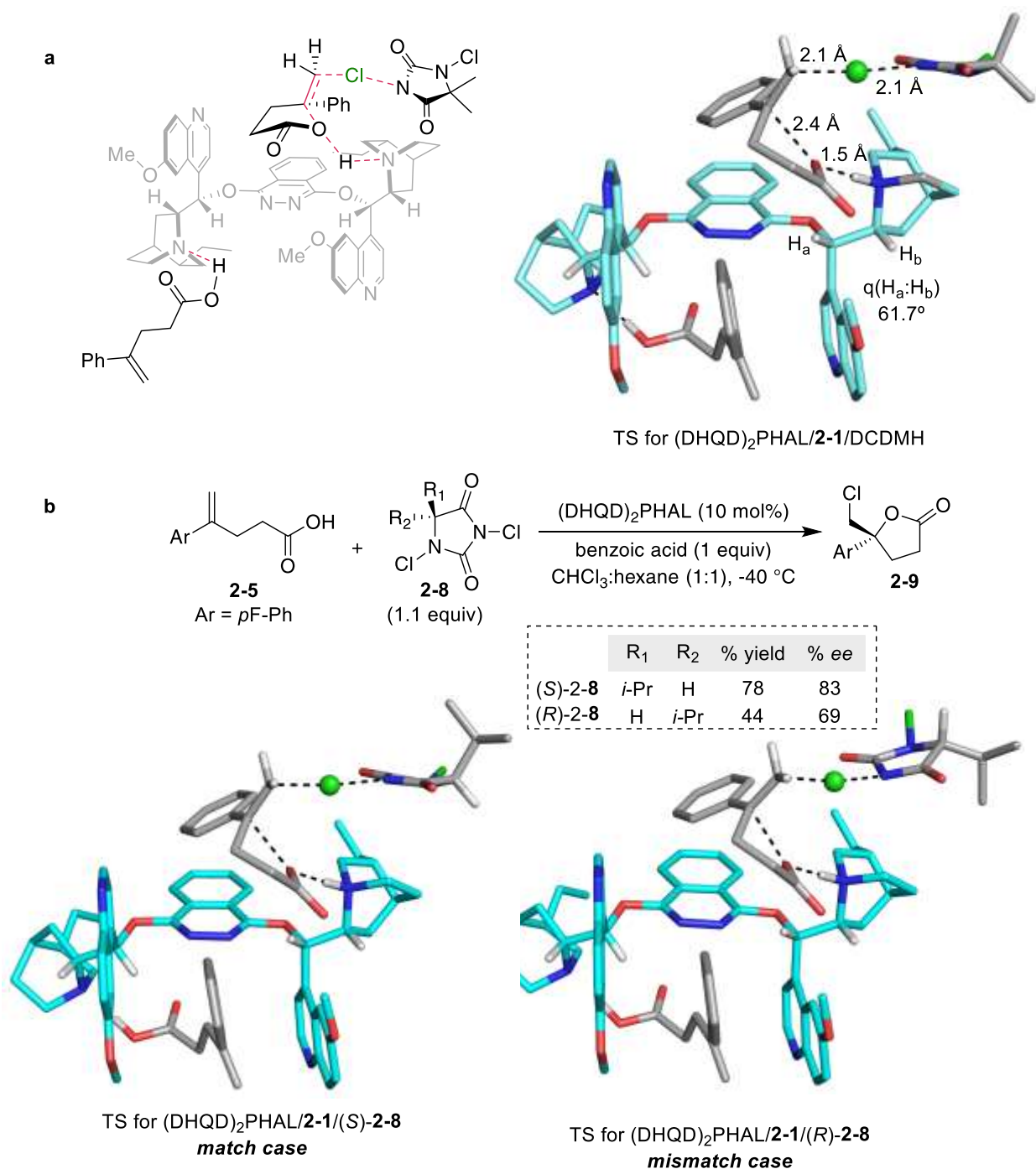
Figure 2.10 Modeling of (DHQD)₂PHAL catalyzed Transition states. (a) Transition states for (DHQD)₂PHAL catalyzed chloro-lactonization using DCDMH and the chiral chlorenium reagent. (b) The non-degeneracy of the two transition states conforms with the previously reported matched-mismatched selectivity. Structures were calculated using the dispersion-corrected density functional method B3LYP-D3, with all optimizations carried out in SMD simulated CHCl₃. This scheme is denoted B3LYP-D3/6-31G*/SMD(CHCl₃).

To connect our computational results to these experimental findings, we reoptimized the (DHQD)$_2$PHAL catalyzed transition state with the two enantiomers of the chiral hydantoin **2-8** and alkene **2-1**. Consistent with the experimental findings, the TS calculated with the (*R*)-**8** (mismatch) shows steric crowding of the isopropyl group with the quinuclidine moiety of (DHQD)$_2$PHAL, presumably magnified as the hydantoin is approaching the **resting state** prior to reaching the TS. The (*S*)-congener (match), however, has a more relaxed approach, having the isopropyl group pointed in the opposite direction. This is also represented in the activation energies for each transition state, with the match TS having a slightly lower barrier ($\Delta\Delta G^{\ddagger} = 0.5$ kcal/mol). Owing to less steric conflict with the catalyst, the approach of (*S*)-**8** to the olefin is also more linear, avoiding the DCDMH distortion seen in the TS from the (*R*) isomer.

2.8   Summary

Reaction progress kinetic analysis (RPKA) and competition studies revealed the delivery of chlorenium ion to the olefin as a key feature of the rate determining step (RDS). These kinetic studies also define the order of each reagent and consequently the rate equation of this catalytic reaction both in the presence and absence of the benzoic acid: rate = k[(DHQD)$_2$PHAL][DCDMH]. Moreover, these studies were conducted at concentrations relevant to the optimized standard protocol, obviating the need for extrapolations outside the range studied. The observed inverse isotope effect (acid catalysis) suggests that the alkene-COOD is more activated for DCDMH attack in **transition state 2-B** than alkene-COOH. Between the kinetic results, ROESY NMR studies, X-ray structures, and DFT analysis, we propose a **resting state** model in which two molecules of substrate **2-1** occupy the binding pockets of (DHQD)$_2$PHAL. In the

proposed catalytic cycle (Figure 2.4), the alkene face that is ultimately chlorinated is exposed to solution, allowing collision with DCDMH. Ring closure is achieved when the backbone chain achieves a conformation placing C-4 near the partially negatively charged carboxylate oxygen, activating the olefin for the concerted *NAAA* closure. The *syn* preference reflects the electrostatic attraction between the developing negative charge on the hydantoin and the positively charged quinuclidinium ion. These mechanistic investigations, coupled with our previously reported labeling studies, suggest that the rate-determining and enantioselectivity-determining events occur together in the predominant pathway. Taken together, the experimental results were combined with an initial DFT analysis that provided structural insight into the **resting state** model and the corresponding **transition state 2-B**. Overall, using the asymmetric chlorolactonization of **2-1** as a proof of principle, a toolbox of analytical techniques has been successfully optimized and applied to probe the nuances underlying the (DHQD)$_2$PHAL catalyzed halofunctionalization of olefins. These mechanistic studies have established an optimal range of alkene *HalA* values over which concerted reactions dominate, firmly defining both relative and absolute stereochemical relationships. This conceptual framework and set of tools for reaction assessment will serve as a guide, in a broad sense, to the emerging field of catalytic stereoselective halofunctionalizations of olefins. More specifically, the localized interactions identified in exploring these chlorolactonization reaction paths point the way to key features needed in the design of simplified organocatalysts.

2.9   Experimental detail

2.9.1 General remarks

Unless otherwise mentioned, solvents were purified as follows. CHCl3 (amylene stabilized) was purchased from Sigma Aldrich and incubated over 4Å MS for 48 h prior to use. Toluene and CH_2Cl_2 were dried over CaH_2 whereas THF and Et_2O were dried over sodium (dryness was monitored by colorization of benzophenone ketyl radical); they were freshly distilled prior to use. NMR spectra were obtained using either a 500 MHz or 600 MHz Varian NMR spectrometer, or an Avance II Bruker 900 MHz instrument, and referenced using the residual 1H peak from the deuterated solvent. Infrared spectra were measured on a Nicolet IR/42 spectrometer FT-IR (thin film, NaCl cells). Waters 2795 (Alliance HT) instrument was used for HRMS (ESI) analysis with polyethylene glycol (PEG-400-600) as a reference.

Column chromatography was performed using Silicycle 60Å, 35-75 μm silica gel. Pre-coated 0.25 mm thick silica gel 60 F254 plates were used for analytical TLC and visualized using UV light, iodine, potassium permanganate stain, p-anisaldehyde stain or phosphomolybdic acid in EtOH stain.

Halofunctionalization reactions were performed in the absence of light. 1,3-Dichloro-5,5-dimethylhydantoin (DCDMH) and 3-chloro-5,5-dimethylhydantoin (MCDMH) were re-crystallized prior to use. Alkenoic acids **2-1**, **2-3**, **2-4**, **2-5**, and **2-6** were prepared as described previously.[38, 67] All other commercially available reagents and solvents were used as received unless otherwise mentioned.

2.9.2 Kinetic studies

2.9.2.i. Sample and NMR instrument preparation for kinetic studies

The probe of the NMR instrument was cooled to -40 °C and allowed to equilibrate for 60 minutes. A stock solution of catalyst and internal standard (toluene, used when benzoic acid was not present) was prepared by dissolving (DHQD)$_2$PHAL (16 mg, 0.0205 mmol) and benzoic acid (62 mg, 0.51 mmol) or toluene (47 mg, 0.51 mmol) in CDCl3 (2 mL). In two additional vials, stock solutions of DCDMH (67.1 mg, 0.34 mmol) and 4-phenyl-4-pentenoic acid (60.4 mg, 0.34 mmol) **2-1** were prepared in CDCl$_3$ (1.5 mL). Kinetic experiments were then performed as follows: To each NMR tube, 0.2 mL of the (DHQD)$_2$PHAL + internal reference (benzoic acid or toluene) solution was added (4 mol% catalyst + 1 equiv. internal standard). The NMR tube solution was then frozen at -78 °C, and the desired amounts of the 4-phenyl-4-pentenoic acid **2-1** and the DCDMH stock solutions were added to the frozen NMR tube, allowing each to freeze in turn. While still frozen, the solution in the NMR tube was made up with CDCl$_3$ to 1 mL total volume. This frozen sample was inserted into the NMR instrument and after 2 min (when the frozen sample had melted at -40 °C), the sample was ejected, very briefly shaken to homogenize the solution, and quickly reinserted into the NMR instrument. After locking and shimming the instrument and setting up the array experiment (six min after shaking the NMR tube), collection of kinetic data ensued either every five or every ten minutes over 10 h.

2.9.2.ii. Reaction Progress Kinetic Analysis (RPKA) data collection and analysis

"Excess" proportions of 0.02 and 0.04 M (Table 1) were chosen for the different "excess" protocol runs, with DCDMH as the limiting reagent in all experiments. The conditions in both experiments were chosen to be close to the optimized conditions, which highlight the advantage of RPKA over classical kinetic methods.3-5 In the first set of

experiments, benzoic acid (1 equiv.) not only assumes the role of the additive, it was also used as the internal standard to normalize the integral values of the product and starting materials during the course of the reaction. In the second set of experiments, toluene (1 equiv.) was used instead of benzoic acid as an internal standard.

Based on the constant concentration of internal standard (benzoic acid or toluene), concentrations of the product 2, DCDMH and 4-phenyl-4-pentenoic acid **2-1** at each data point were calculated. The AB quartet peak at 3.8 ppm (chloromethylene) was used to calculate the concentration of the product, while the resonances for the vinylic protons (s, 5.3 and 5.1 ppm) and methyl groups (s, 1.5 ppm) peaks were used to determine concentrations of 4-phenylpent-4-enoic acid **2-1** and DCDMH, respectively. After fitting a sixth order polynomial function to the plot of product concentration vs. time, the rate at each data point was calculated via the first derivative of the fitted polynomial function.

2.9.2.iii. Kinetic experiments to determine rate equation

Two sets of experiments (Set 1 and Set 2) were designed for RPKA studies (shown in Table 2.2 and Table 2.3). The first set of experiments were conducted in the presence of benzoic acid as an additive (as well as an internal standard), similar to reported optimized condition.[56] The second set of experiments were conducted in the absence of benzoic acid to measure the empirical rate law equation.

2.9.2.iv. Kinetic studies in presence of benzoic acid

The following experiments shown in Table 2.2 were conducted to determine the order of the alkene, catalyst and DCDMH in presence of benzoic acid, and also to determine the effect of any catalyst deactivation of product inhibition.

Table 2.2 RPKA studies in presence of benzoic acid as an additive

Exp	2-1 (M)	DCDMH (M)	Benzoic acid (M)	(DHQD)$_2$PHAL (mol%)	Excess (M)
A	0.071	0.051	0.051	4	0.02
B	0.091	0.051	0.051	4	0.04
C	0.091	0.051	0.051	4	0.02
D	0.091	0.051	0.051	6	0.02
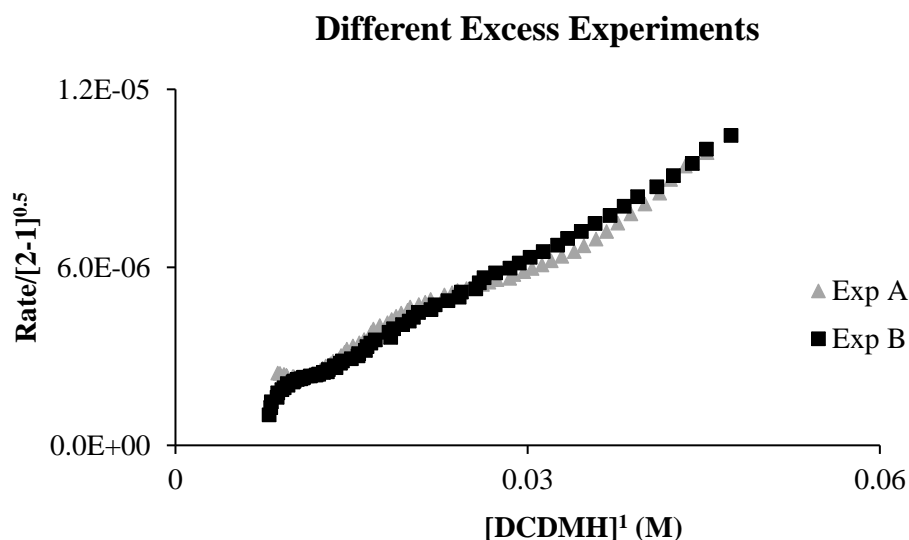
Figure 2.11 Different excess experiments to find order of alkene and DCDMH. RPKA analysis of the order of alkene **2-1** and DCDMH from a set of different excess experiments. The plots corresponding to the two experiments (A and B) overlay when alkene **2-1** and DCDMH are raised to the respective power of 0.5 and 1

Same Excess Experiments
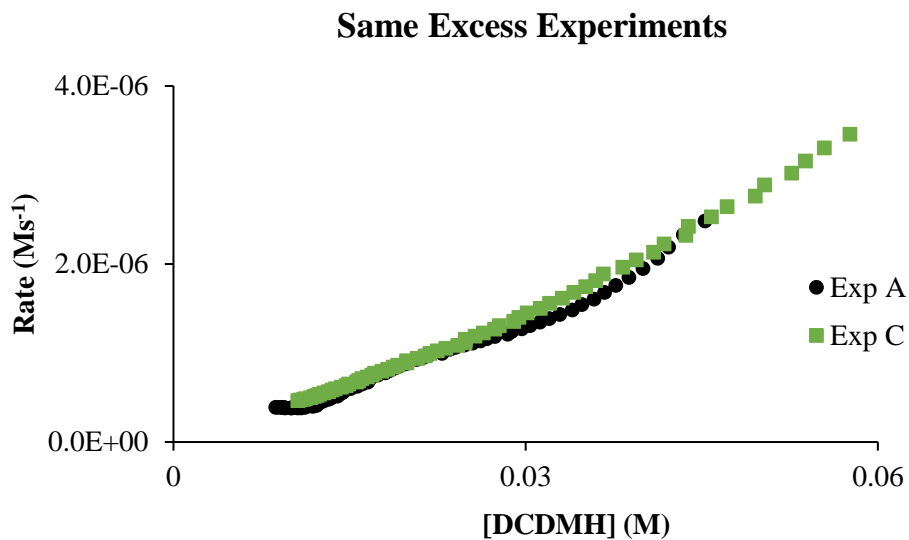
Figure 2.12 Same excess experiment. Overlay of a set of same excess experiments (A and C) indicate that there is neither catalyst deactivation nor product inhibition contributing to the reaction kinetics
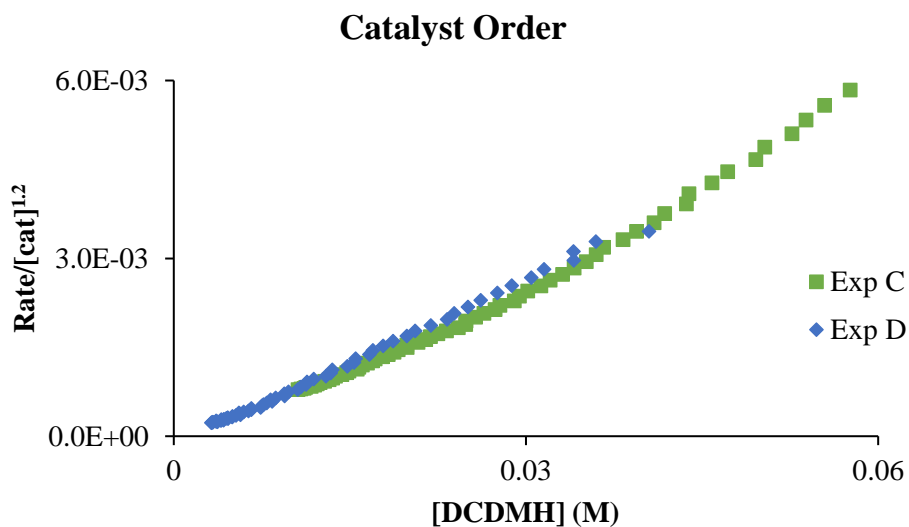
Catalyst Order

Figure 2.13 Finding order of catalyst. Overlay of plots corresponding to a set of same excess experiments (C and D), ran at different catalyst concentration when catalyst is raised to the power of 1.2, indicating that the catalyst is approximately first order

2.9.2.v. Kinetic studies in absence of benzoic acid

The following experiments shown in Table 2.3 were conducted to determine the order of the alkene, catalyst and DCDMH in presence of benzoic acid, and also to determine the effect of any catalyst deactivation of product inhibition.

Table 2.3 RPKA studies in absence of benzoic acid

Exp	2-1 (M)	DCDMH (M)	Benzoic acid (M)	(DHQD)$_2$PHAL (mol%)	Excess (M)
E	0.071	0.051	0.051	4	0.02
F	0.091	0.051	0.051	4	0.04
G	0.091	0.051	0.051	4	0.02

Different Excess Experiments
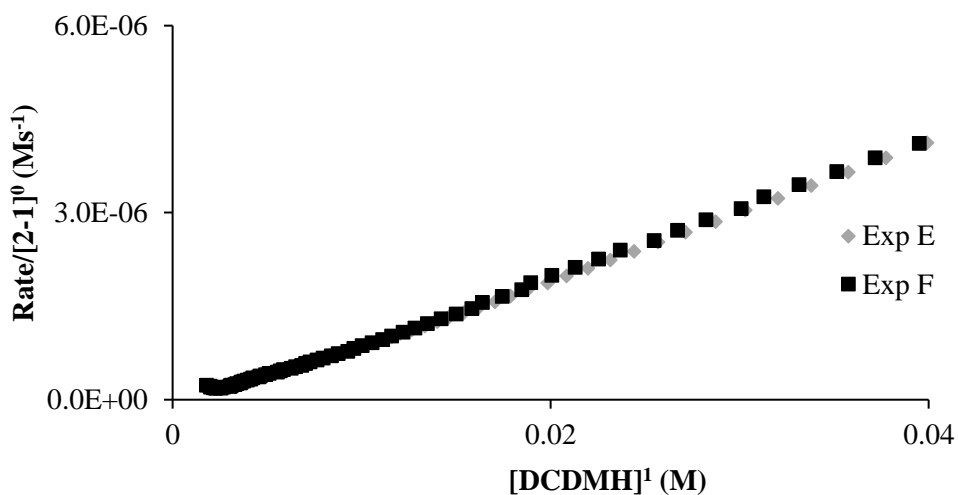
Figure 2.14 Different excess experiments to find order of alkene and DCDMH. RPKA analysis of the order of alkene **2-1** and DCDMH from a set of different excess experiments. The plots corresponding to the two experiments (E and F) overlay when alkene **2-1** and DCDMH are raised to the respective power of 0 and 1

Same Excess Experiments
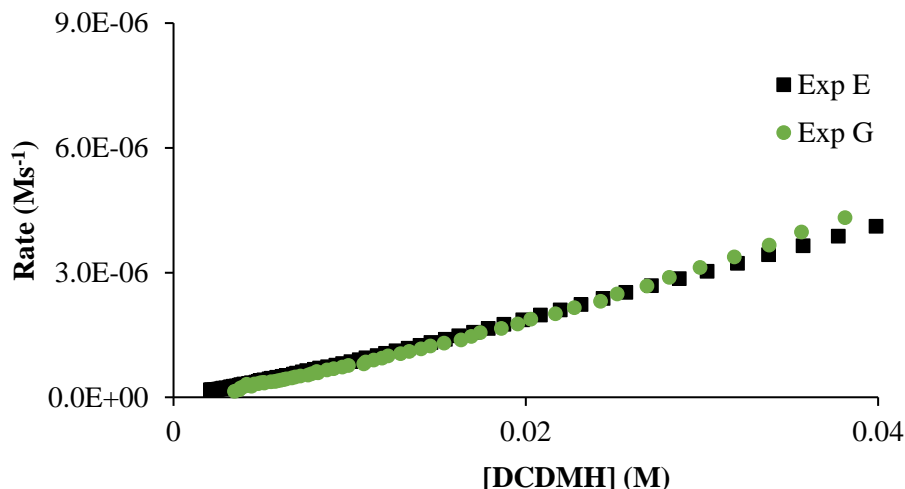
Figure 2.15 Same excess experiment. Overlay of a set of same excess experiments (F and G) indicate that there is neither catalyst deactivation nor product inhibition contributing to the reaction kinetics

2.9.2.vi. Comparison of rates of the reaction with and without benzoic acid

The following plots shows rate effect of benzoic acid.

Rate effect of benzoic acid
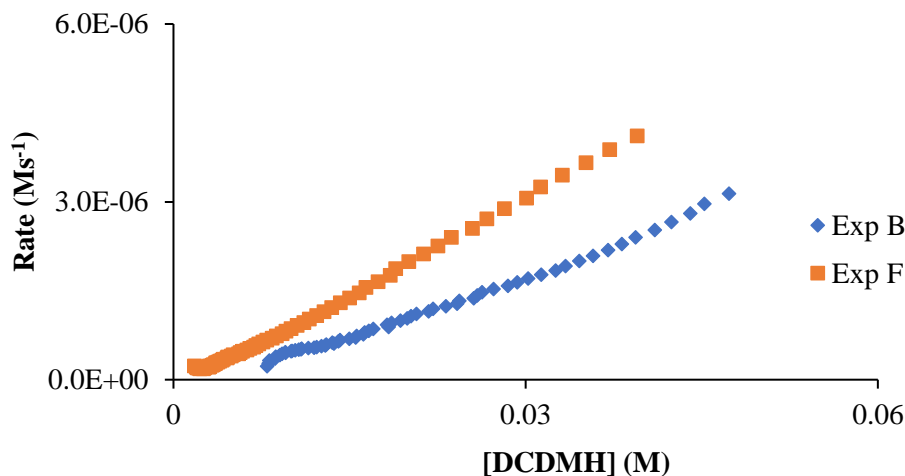
Figure 2.16 Rate comparison with and without benzoic acid. Overlay The rate profiles demonstrate the negative impact of benzoic acid on the rate of the chlorolactonization. Exp B (Table 2.2) is in presence of benzoic acid and is significantly slower than Exp F (Table 2.3)

2.9.2.vii. Discussion on the order of components in the rate law equation

The zeroth order of alkene **2-1** in absence of the benzoic acid indicates that the catalyst $(DHQD)_2PHAL$ is fully saturated with alkene **2-1**. This saturated acid-base complex reacts with the DCDMH leading to the rate determining step. The molecularity of DCDMH in the RDS, equally one from the rate law, indicates the collision of one chlorinating agent with the saturated catalyst, leading to the product. In presence of benzoic acid, which in itself can form an acid-base complex with the catalyst, the alkene now must compete against the benzoic acid for catalyst binding. This competition will favor alkene binding at a higher alkene concentration (assuming similar binding affinities for both species). Therefore, a higher concentration of alkene now leads to a greater concentration of the resting state complex, which ultimately results in the overall rate equation exhibiting a positive dependence on the alkene **2-1** concentration (see next section for a detailed kinetic model).

2.9.3 Kinetic models

2.9.3.i. Model 1: In absence of benzoic acid
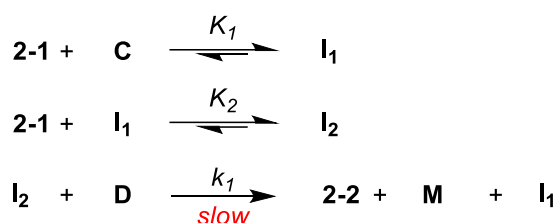
2-1 + **C** $\xrightarrow{K_1}$ **I$_1$**	**2-1** = alkenoic acid	**2-2** = cyclized product
	C = (DHQD)$_2$PHAL	**M** = MCDMH
2-1 + **I$_1$** $\xrightarrow{K_2}$ **I$_2$**	**D** = DCDMH	**I$_1$** = (DHQD)$_2$PHAL:**1** (1:1)
	B = Benzoic acid	**I$_2$** = (DHQD)$_2$PHAL:**1** (1:2)
I$_2$ + **D** $\xrightarrow[slow]{k_1}$ **2-2** + **M** + **I$_1$**	K = equilibrium constants, k = rate constants	

Figure 2.17 Model 1: In absence of benzoic acid. Reaction pathways in absence of benzoic acid.

Acid-base equilibria between catalyst and alkenoic acid **2-1**:

$$K_1 = \frac{[I_1]}{[2-1][C]} \quad \text{-or-} \quad [I_1] = K_1[2-1][C] \qquad\qquad \text{eq (2.1)}$$

$$K_2 = \frac{[I_2]}{[2-1][I_1]} \quad \text{-or-} \quad [I_2] = K_2[1][I_1] \quad \text{-or-} \quad [I_2] = K_1K_2[2-1]^2[C] \qquad \text{eq (2.2)}$$

Total concentration of the catalyst:

$$[C]_0 = [C] + [I_1] + [I_2] \qquad\qquad \text{eq (2.3)}$$

Using eq (1) eq (2) and eq (3)

$$[C]_0 = [C] + K_1[2-1][C] + K_1K_2[2-1]^2[C] \quad \text{-or-} \quad [C] = \frac{[C]_0}{1+K_1[2-1]+K_1K_2[2-1]^2}$$

$$\text{eq (2.4)}$$

Rate of product formation based on model above:

$$\boldsymbol{Rate} = k_1[D][I_2] \qquad\qquad \text{eq (2.5)}$$

Using eq (2.2) and (2.4) to replace [**I$_2$**] and [**C**]

$$\boldsymbol{Rate} = k_1K_1K_2[D][2-1]^2[C] \quad \text{-or-} \quad \boldsymbol{Rate} = \frac{k_1K_1K_2[D][2-1]^2[C]_0}{1+K_1[2-1]+K_1K_2[2-1]^2} \qquad \text{eq (2.6)}$$

The above eq (2.6) represents the derived rate law equation for the proposed catalytic cycle. Since we predict the *resting state* of the catalyst is **I$_2$** based on corroborating data presented in the text, we may assume large equilibrium constants for K_1 and K_2 drive this

binding process. If K_1 and $K_2 \gg 1$, $K_1 K_2 [\textbf{2-1}]^2$ will be the largest component in the denominator, and thus, the above rate law equation can be reduced to the following simplified form, which is in accord with the empirical rate law:

$$\textbf{\textit{Rate}} \approx k_1[\textbf{\textit{D}}][\textbf{\textit{C}}]_0 \quad \text{since} \quad K_1 K_2 [\textbf{2} - \textbf{1}]^2 \gg 1 + K_1[\textbf{2} - \textbf{1}] \qquad \text{eq (2.7)}$$

2.9.3.ii. Model 2: In presence of benzoic acid
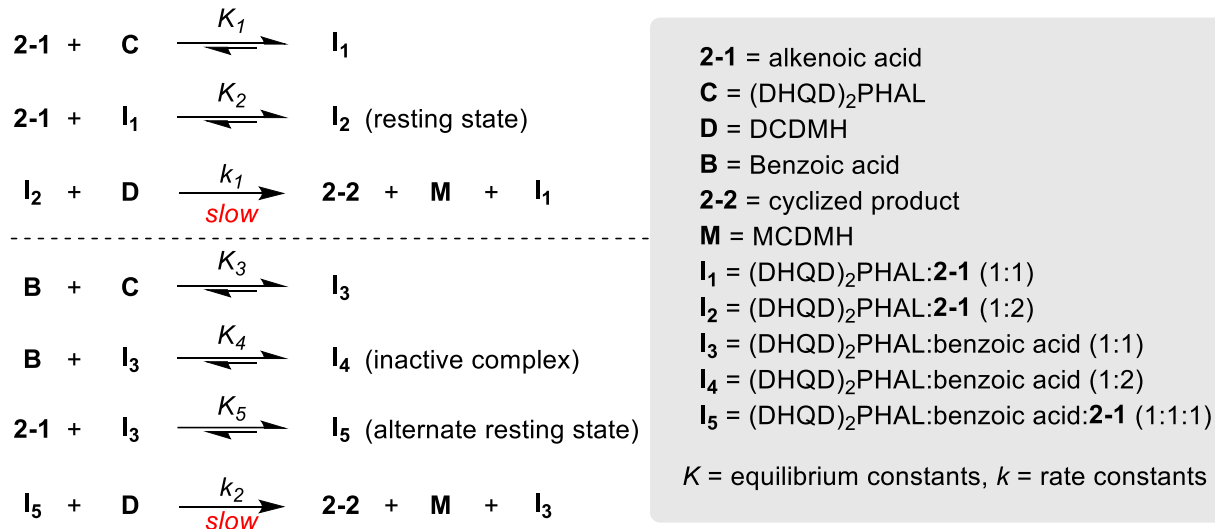
Figure 2.18 Model 2: In presence of benzoic acid. Reaction pathways in presence of benzoic acid.

Acid-base equilibria between catalyst and alkenoic acid **2-1**:

$$K_1 = \frac{[I_1]}{[2-1][C]} \quad \text{-or-} \quad [I_1] = K_1[2-1][C] \qquad\qquad \text{eq (2.8)}$$

$$K_2 = \frac{[I_2]}{[2-1][I_1]} \quad \text{-or-} \quad [I_2] = K_2[2-1][I_1] \text{ -or-} \quad [I_2] = K_1 K_2[2-1]^2[C] \qquad \text{eq (2.9)}$$

Acid-base equilibria between catalyst and benzoic acid:

$$K_3 = \frac{[I_3]}{[B][C]} \quad \text{-or-} \quad [I_3] = K_3[B][C] \qquad\qquad \text{eq (2.10)}$$

$$K_4 = \frac{[I_4]}{[B][I_3]} \quad \text{-or-} \quad [I_4] = K_4[B][I_3] \quad \text{-or-} \quad [I_4] = K_3 K_4[B]^2[C] \qquad \text{eq (2.11)}$$

Acid-base equilibria between catalyst, benzoic acid and alkene **2-1**:

$$K_5 = \frac{[I_5]}{[I_3][2-1]} \quad \text{-or-} \quad [I_5] = K_5[I_3][2-1] \text{ -or-} \quad [I_5] = K_3 K_5[B][2-1][C] \quad \text{eq (2.12)}$$

Total concentration of the catalyst:

$$[C]_0 = [C] + [I_1] + [I_2] + [I_3] + [I_4] + [I_5] \qquad\qquad \text{eq (2.13)}$$

NMR and computational studies discussed in the text demonstrate that the catalyst has

a strong affinity to bind to two carboxylic acids. This implies that the total catalyst

concentration $[C]_0$ approximately equals the summation of its various doubly acid bound states (resting states). Therefore, $[C]$, I_1 and I_3 will be negligible and can be ignored. This enables the simplification of eq (2.13) to the following eq (2.14):

Total concentration of the catalyst:

$$[C]_0 \approx [I_2] + [I_4] + [I_5] \qquad \text{eq (2.14)}$$

Applying eq (2.9), eq (2.11) and eq (2.12) on eq (2.14), we have

$$[C]_0 = K_1 K_2 [2-1]^2 [C] + K_3 K_4 [B]^2 [C] + K_3 K_5 [2-1][B][C] \qquad \text{eq (2.15)}$$

On rearranging that above eq (2.15) we have

$$[C] = \frac{[C]_0}{K_1 K_2 [2-1]^2 + K_3 K_4 [B]^2 + K_3 K_5 [2-1][B]} \qquad \text{eq (2.16)}$$

Rate of the reaction (or product formation) is a summation of the rate of two reactive resting states I_2 and I_5 reacting with DCDMH and leading to the product:

$$Rate = k_1 [D][I_2] + k_2 [D][I_5] \qquad \text{eq (2.17)}$$

Using eq (2.9), eq (2.12) and eq (2.17) we have,

$$Rate = k_1 K_1 K_2 [2-1]^2 [C][D] + k_2 K_3 K_5 [2-1][B][C][D] \qquad \text{eq (2.18)}$$

Using eq (2.16) and eq (2.18)

$$Rate = \left(\frac{k_1 K_1 K_2 [2-1]^2 + k_2 K_3 K_5 [2-1][B]}{K_1 K_2 [2-1]^2 + K_3 K_4 [B]^2 + K_3 K_5 [2-1][B]} \right) [C]_0 [D] \qquad \text{eq (2.19)}$$

The above eq (2.19) represents the derived rate law equation for chlorolactonization in presence of benzoic acid based on the proposed catalytic cycle. If $K_1 \cdot K_2$, $K_3 \cdot K_4$, and $K_3 \cdot K_5$ are comparable in magnitude, a reasonable assumption given that all of them represent a 1:2 binding of (DHQD)$_2$PHAL to carboxylic acids (that assumes the binding affinity for substrate and benzoic acid is similar), the denominator is no longer simplified as described for the case above (Model 1). The presence of [2-1] in the denominator explains the observed fractional order of the alkenoic acid 2-1 (half order), and the presence of [B]

in the denominator explains the rate inhibitory effect of benzoic acid. Furthermore, this model also complies with the first order rate observed for DCDMH and the catalyst.

2.9.3.iii. Model 3: Alternative scenario of 1:1 alkene-catalyst being the reactive intermediate
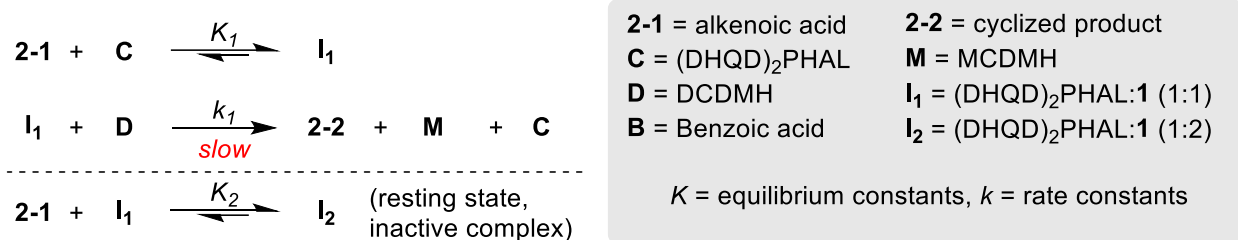
Figure 2.19 Model 2: Alternative scenario of 1:1 alkene-catalyst being reactive intermediate. Reaction pathways for a scenario where 1:1 alkene-catalyst complex is the reactive intermediate.

The following is a scenario where the 1:1 alkene-catalyst complex is the reactive species

in the catalytic cycle and the resting state 2:1 complex is an unreactive off-cycle species.

Acid-base equilibria between catalyst and alkenoic acid **2-1**:

$$K_1 = \frac{[I_1]}{[1][C]} \quad \text{-or-} \quad [I_1] = K_1[2-1][C] \qquad \text{eq (2.20)}$$

$$K_2 = \frac{[I_2]}{[1][I_1]} \quad \text{-or-} \quad [I_2] = K_2[2-1][I_1] \text{ -or-} \quad [I_2] = K_1K_2[2-1]^2[C] \qquad \text{eq (2.21)}$$

Total concentration of the catalyst:

$$[C]_0 = [C] + [I_1] + [I_2] \qquad \text{eq (2.22)}$$

Using eq (20), eq (21) and eq (22)

$$[C]_0 = [C] + K_1[2-1][C] + K_1K_2[2-1]^2[C] \quad \text{-or-} \quad [C] = \frac{[C]_0}{1+K_1[1]+K_1K_2[1]^2} \text{ eq (2.23)}$$

Rate of product formation based on model above:

$$\boldsymbol{Rate} = k_1[D][I_1] \qquad \text{eq (2.24)}$$

Using eq (2.20), eq (2.23) and eq (2.24)

$$\boldsymbol{Rate} = k_1K_1[D][2-1][C] \qquad \text{-or-} \quad \boldsymbol{Rate} = \frac{k_1K_1[D][2-1][C]_0}{1+K_1[2-1]+K_1K_2[2-1]^2} \qquad \text{eq (2.25)}$$

Equation 2.25 represent the rate law in this scenario. Note that the current scenario

results in rate equation having a higher term for the alkene in the denominator. Since the

resting state has already been established to be I_2, we may make similar assumptions of large equilibrium constants of K_1 and K_2. Therefore, similar to model 1, it is reasonable to assume $K_1 K_2 [\mathbf{2\text{-}1}]^2$ will be the large, and thus, the above rate law equation can be reduced to the following simplified form:

$$Rate \approx \frac{k_1[\boldsymbol{D}][\boldsymbol{C}]_0}{K_2[\mathbf{2\text{-}1}]} \qquad\qquad\qquad eq\ (2.26)$$

In this current scenario, rate would have an inverse dependence on alkene **2-1**. This is a result of higher alkene concentration driving the formation of inactive state I_2. Since this behavior is not observed we may rule out this scenario.

2.9.4 ^{1}H NMR analysis of alkenoic acid 2-5 and its complexes with (DHQD)$_2$PHAL and quinuclidine

2.9.4.i. Sample and NMR instrument preparation for ^{1}H NMR studies

The NMR probe was cooled to -40°C and allowed to equilibrate for 60 minutes. Stock solutions of catalyst and different substrates were prepared, and the desired volumes were calculated and added to the NMR tube. In all ^{1}H NMR studies, the volume in the NMR tube was adjusted to 1 mL by addition of CDCl$_3$.

2.9.4.ii. ¹H NMR of alkene 2-5
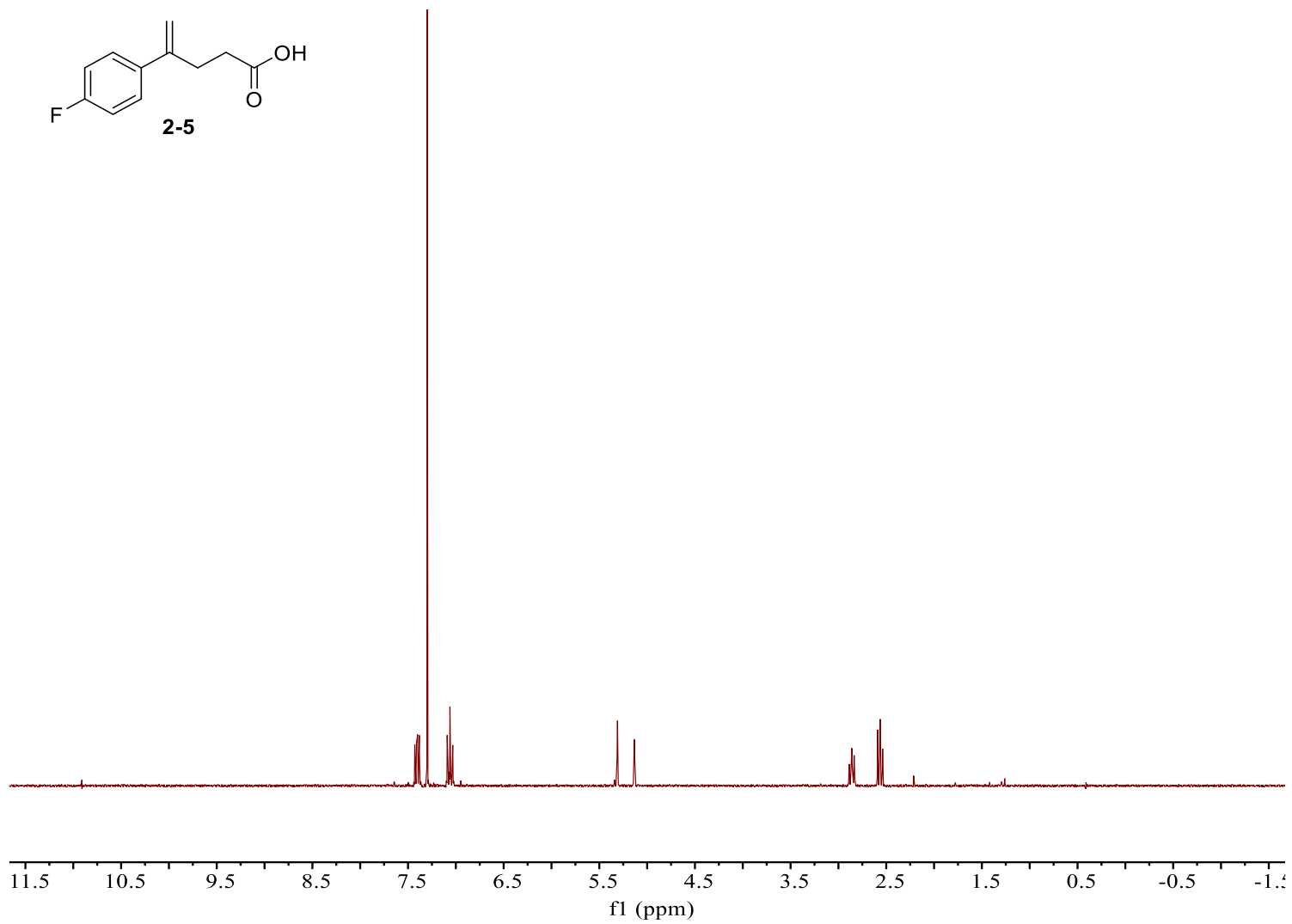
2.9.4.iii. ^1H NMR of alkene 2-5:quinuclidine (1:1) mixture

2-5

quinuclidine

1:1 mixture

f1 (ppm)
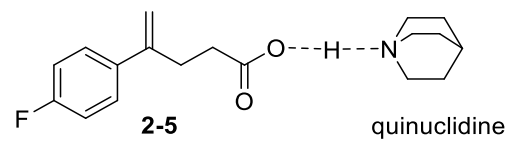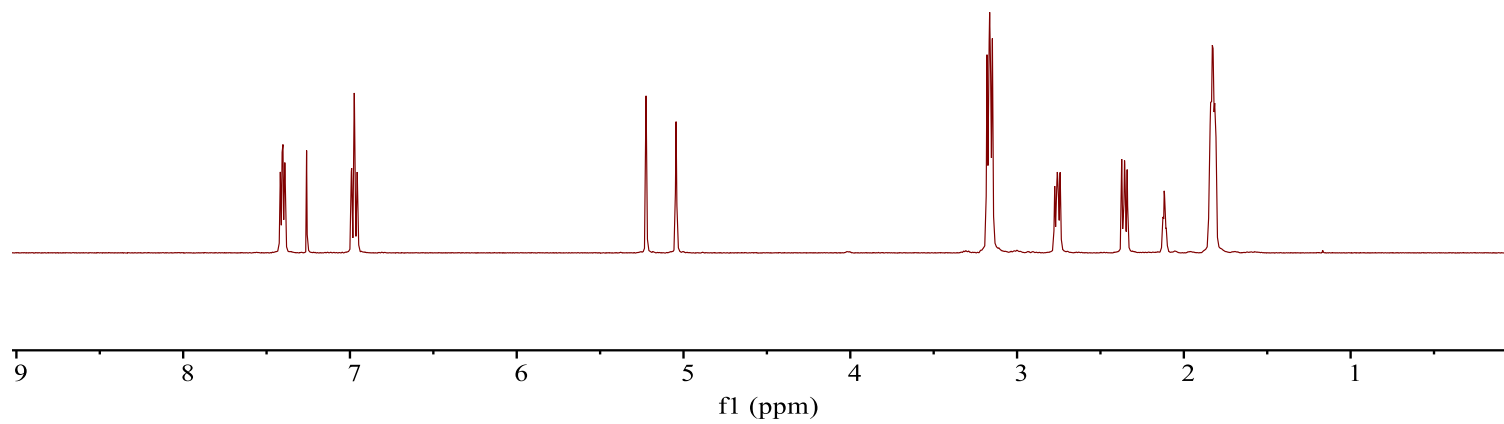
2.9.4.iv. ¹H NMR of quinuclidine

quinuclidine
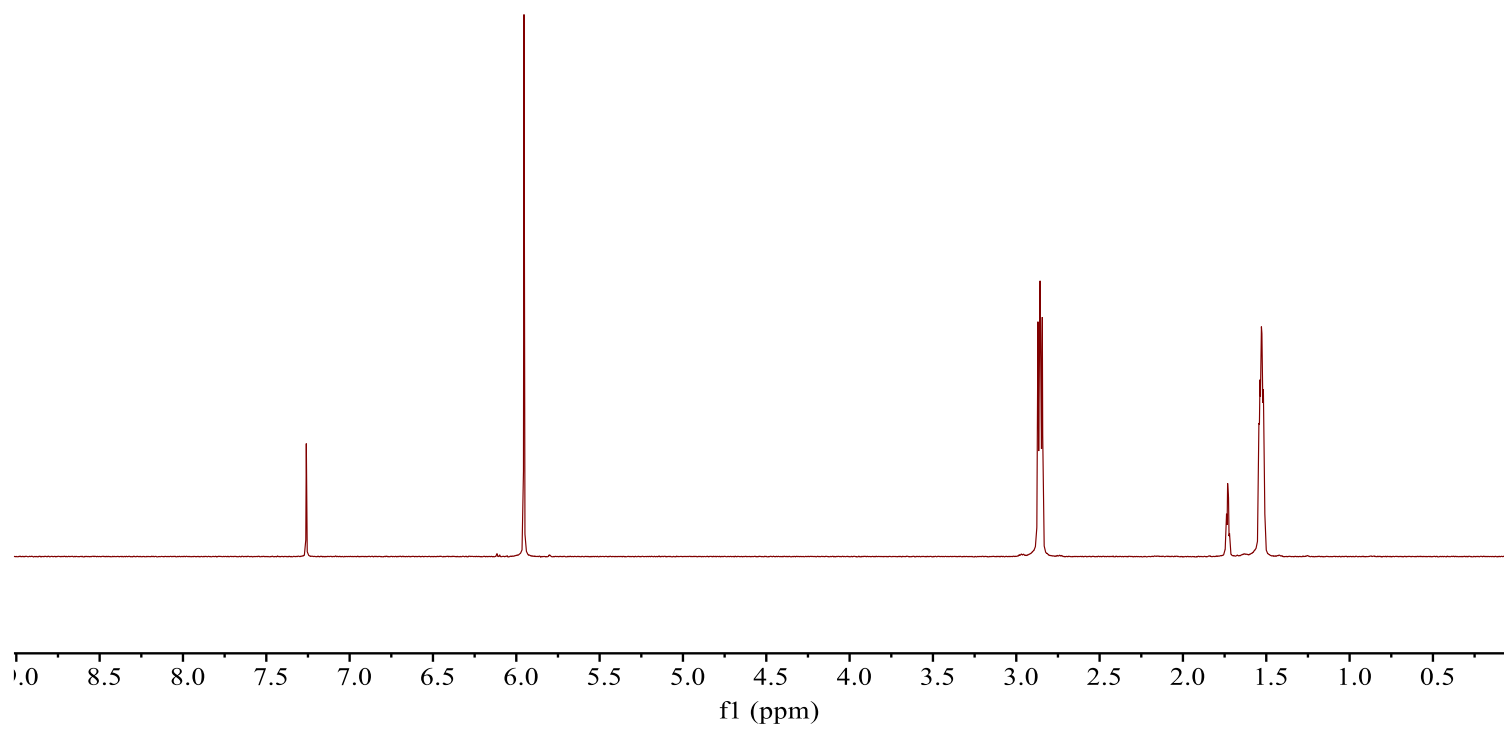
2.9.4.v. ^{1}H NMR of (DHQD)$_2$PHAL and alkene 2-5 (1:2)

i (CHCl$_3$)

(DHQD)$_2$PHAL

5

(1:2 mixture)

f1 (ppm)
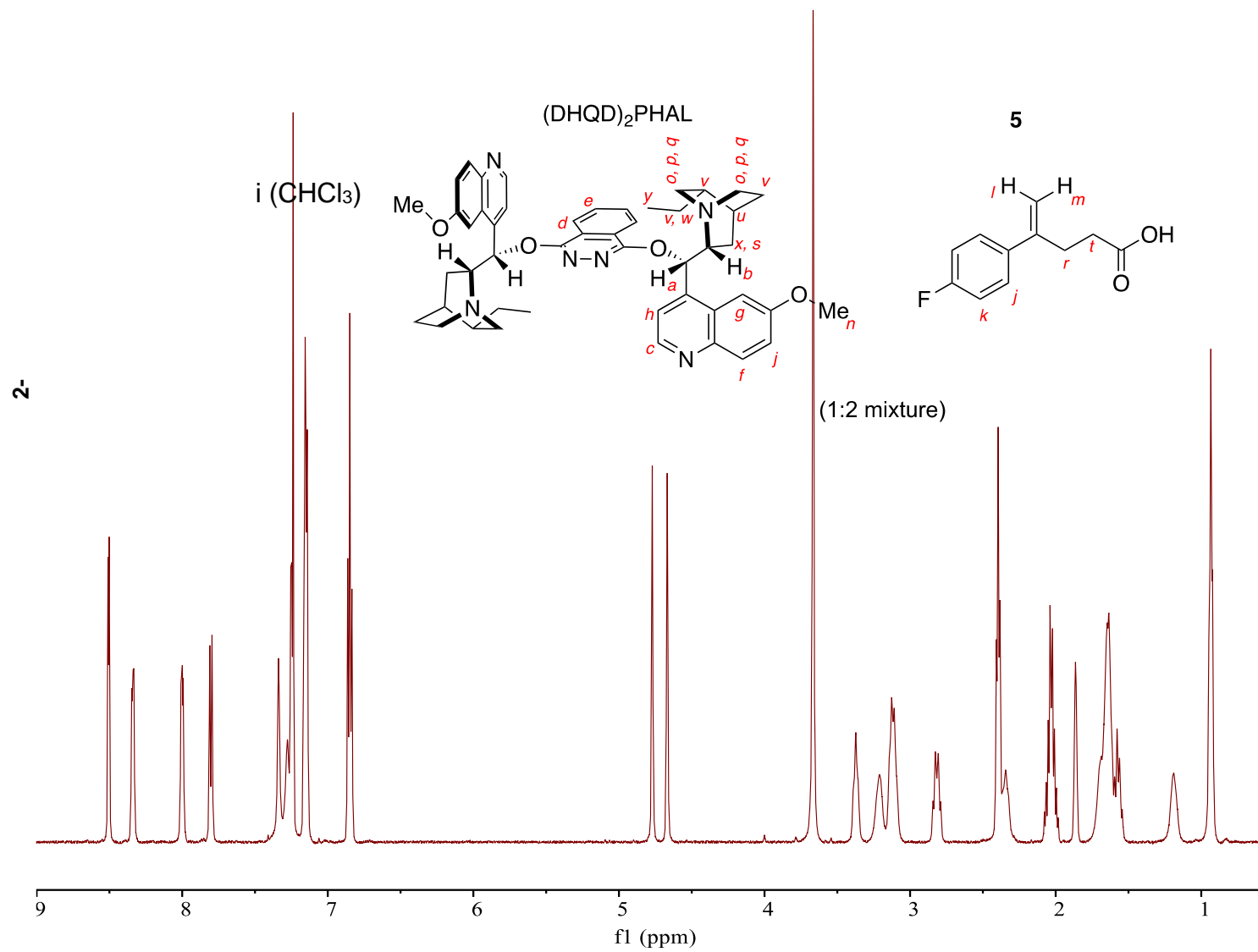
2.9.4.vi. ^{1}H NMR of 0.04 M (DHQD)$_2$PHAL under various concentration of benzoic acid

(DHQD)$_2$PHAL:Benzoic

(DHQD)$_2$PHAL:Benzoic

1,1,2,2-
tetrachloroethylene
(internal standard)

(DHQD)$_2$PHAL

f1 (ppm)

114
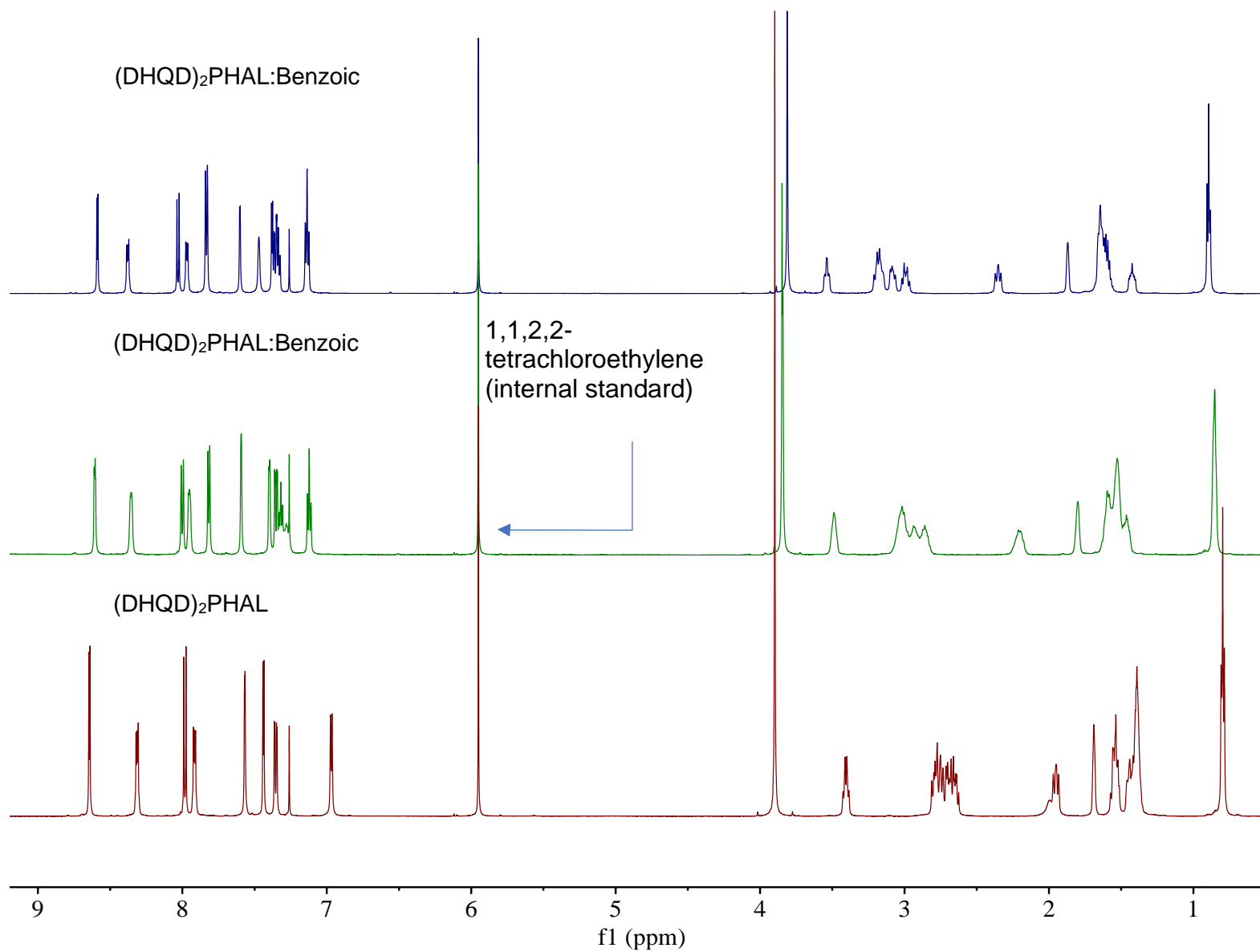
2.9.5   ROESY analysis of (DHQD)₂PHAL:alkene 5 complex

2.9.5.i. Sample and NMR instrument preparation for ROESY studies

The 600 MHz NMR instrument was used for all ROESY studies. Prior to any ROESY experiments, the probe was cooled to -20 ⁰C (the lowest practical temperature on this instrument) and allowed to equilibrate for 2 h. Stock solutions of catalyst and substrate were prepared and the desired volumes of catalyst and substrate were calculated and added to the NMR tube. In all ROESY studies, the solutions in the NMR tubes were equalized to 1 mL by addition of $CDCl_3$. After preparing the sample, dissolved oxygen was removed from the sample via three cycles of freeze-pump-thaw degassing method. The NMR tube was sealed with Teflon tape and inserted in the NMR instrument. The sample was equilibrated in the NMR for 10 min. After tuning the ^{13}C and ^{1}H channels, locking and shimming the sample, PW 90⁰ was measured and used for the study.

2.9.5.ii. Measuring intermolecular distances using ROESY analysis

The intensity-ratio method (developed by Bodenhausen and Ernst and later used by Ammalahti)[64-66] was used to determine the inter-nuclear distances from the ROESY experiments. Several effects such as HOHAHA type magnetization and the offset dependence of the spin-locked conditions can influence the intensities of ROESY cross peaks. ROESY cross peaks can be used to estimate the distances between selected protons by carefully adjusting the measurement conditions. To minimize undesired effects on the ROESY peaks, the spin-lock pulse was positioned at the far low side of the spectrum (3,599 Hz) and a moderate spin-lock field (5,758 Hz) was used.

The following equations illustrate the method to measure the inter-atomic distances. Eq (27) represents the estimated inter-nuclear distances between two nuclei i and j.[64-66] To apply this equation, correction factors based on eq (29) and eq (30) were

115

calculated. Two atom pairs at known, fixed distances were chosen as references to compute and assess the scaling constant. Reference "a", shown in Figure 2.20, was assigned a 1.6 Å fixed distance to calculate the constant. To evaluate the accuracy of this method, reference "b" distance was measured (2.2 Å) by using eq (27) with the calculated constant. The result was then compared with its actual distance from the $(DHQD)_2PHAL$ crystal structure (2.3 Å). This control experiment shows that this method is reliable within acceptable error margins. These calculations are summarized in Table 2.4 and were used to predict the catalyst conformation proposed for the resting state of substrate in the catalyst binding pocket.

Distance between the two nuclei r_{ij} is given by:

$$r_{ij} = \left[C \left\{ \ln \left(\frac{a_{ii}c_{ii} + a_{ij}c_{ij}}{a_{ii}c_{ii} - a_{ij}c_{ij}} \right) \right\}^{-1} \right]^{\frac{1}{6}}$$

eq (27)

$$Constant, C = -2q\tau_{mix} \left(\frac{6\tau_c}{1 + 4\omega^2 \tau_c^2} - \tau_c \right)$$

eq (28)

$$c_{ij} = \frac{1}{sin^2\theta_i sin^2\theta_j}$$

eq (29)

$$c_{ii} = \frac{1}{sin^2\theta_i sin^2\theta_i}$$

eq (30)

$$tan\theta_i = \frac{\gamma B_1}{\omega_i - \omega_0}$$

eq (31)

$$q = 0.1\gamma^4 h^2 \left(\frac{\mu_0}{4\pi} \right)^2$$

eq (32)

Definition of terms:

τ_{mix} = mixing time

a_{ij} = intensity of the cross peak a_{ii} = intensity of the diagonal peak

ω_0 = offset frequency

(DHQD)₂PHAL
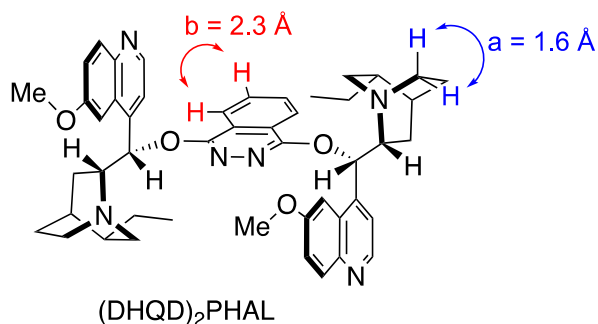
Figure 2.20 ROESY reference distances. Reference distances used for accurately deriving internuclear distances with ROESY analysis

Table 2.4 ROESY correlations

ROESY Correlations (ppm)		Cross peak intensity	Diagonal peak intensity	C_{ij}	C_{ii}	Distances (Å)
Proton i	Proton j					
q (2.80)	*p* (3.11)	8.64	36.4	1.208	1.109	1.6
h (7.30)	*c* (8.50)	3.56	135.5	1.086	1.017	2.3
r (2.40)	*n* (3.67)	0.62	152.6	1.207	1.14	3.2
t (2.03)	*n* (3.67)	0.77	133.7	1.238	1.169	3
n (3.67)	*k* (6.85)	0.29	191.4	1.067	1.059	3.8
e (8.00)	*d* (8.30)	3.24	100	1.106	1.044	2.2
v (1.69)	*d* (8.30)	1.78	125	1.273	1.202	2.6
h (7.25)	*d* (8.30)	0.65	135	1.078	1.017	3.1
d (8.30)	*y* (0.94)	0.46	165	1.354	1.278	3.4
n (3.67)	*j* (7.15)	0.97	191.4	1.075	1.059	3.1

(DHQD)₂PHAL

5
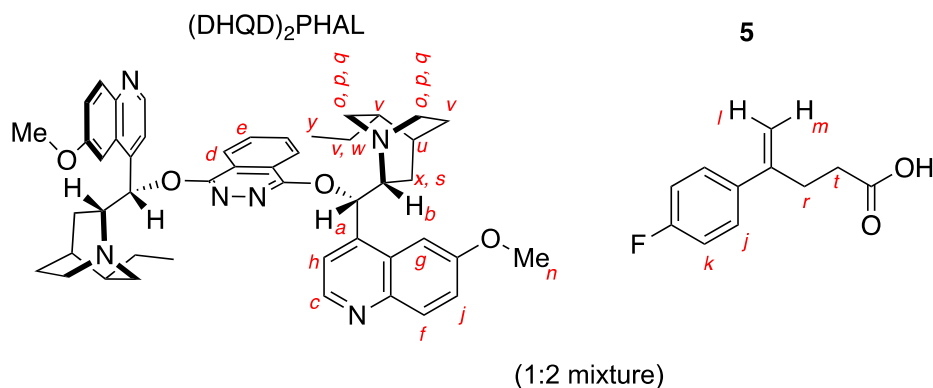
(1:2 mixture)

Figure 2.21 Proton label for ROESY studies. Proton labels in ^{1}H NMR of a 1:2 mixture of (DHQD)₂PHAL and alkene **2-5**

117

2.9.5.iii. Measuring intermolecular distances using ROESY analysis
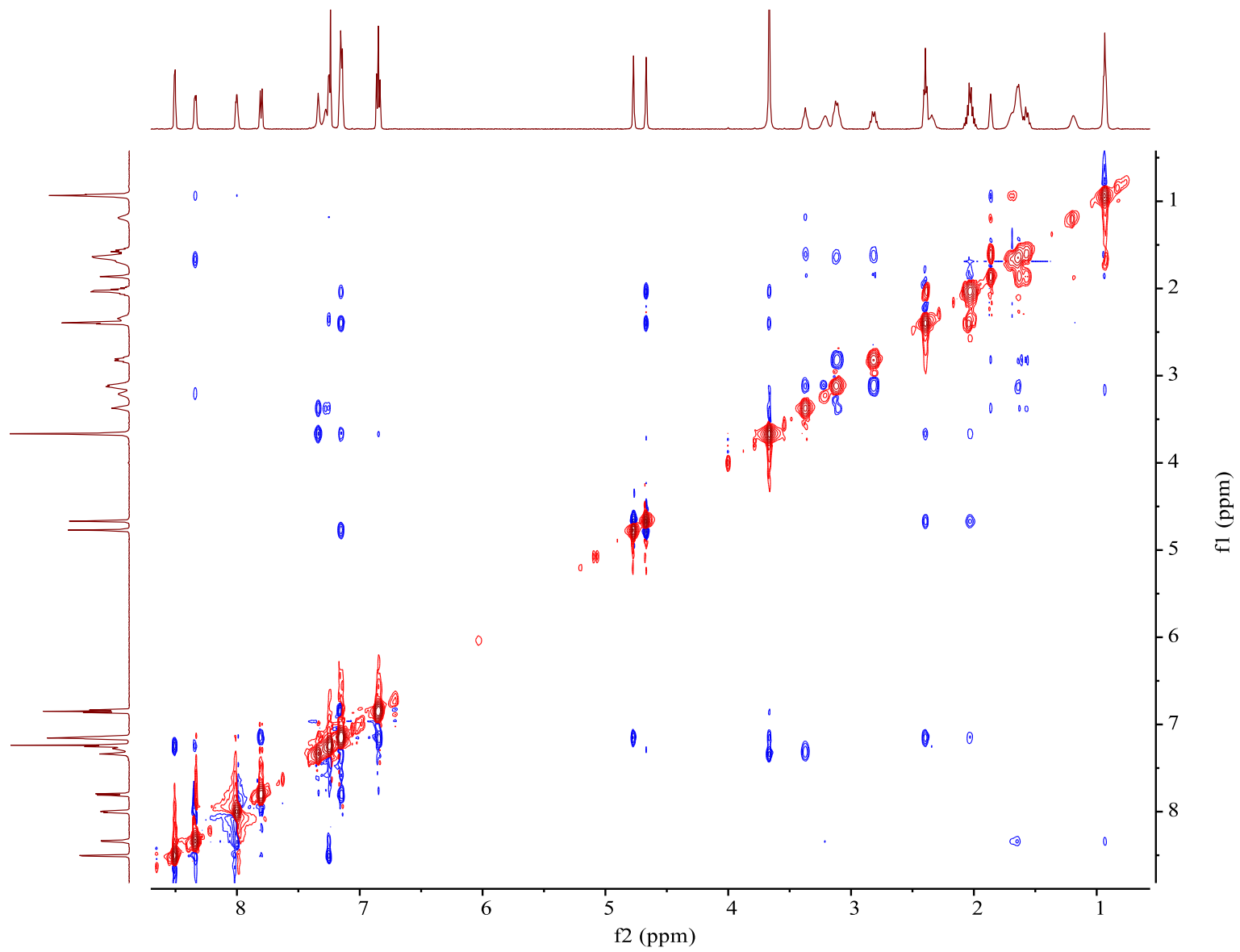
2.9.6 General procedure for kinetic isotopic effect studies

Sample and NMR instrument preparation were the same as that for RPKA kinetic studies. In these experiments $[DCDMH]_o = 0.056$ M and $[\textbf{2-1}]_o = 0.051$ M, were used in the presence of $[toluene]_o = 0.051$ M. Catalyst loading was decreased to 1 mol% to monitor the reaction slowly and collect more data points. Concentration of the product was obtained from the concentration of the internal standard. Product concentration was plotted as a function of time and fitted to an exponential growth curve, utilizing the Excel solver tool using eq (33), and was fitted to the observed data by varying t_o (this accounts for the correct time of the reaction initiation since time elapses from the actual initiation and the first data point acquired by NMR), k, and $[P]_\infty$ (extrapolated product concentration). The completion criterion in Excel solver was a non-linear least squared regression error below 0.00002.

Fitting curve equation:

$$[P]_t = [P]_\infty\left(1 - exp^{-k(t-t_0)}\right) \qquad\qquad \text{eq (33)}$$

$$\frac{k_H}{k_D} = 0.82$$
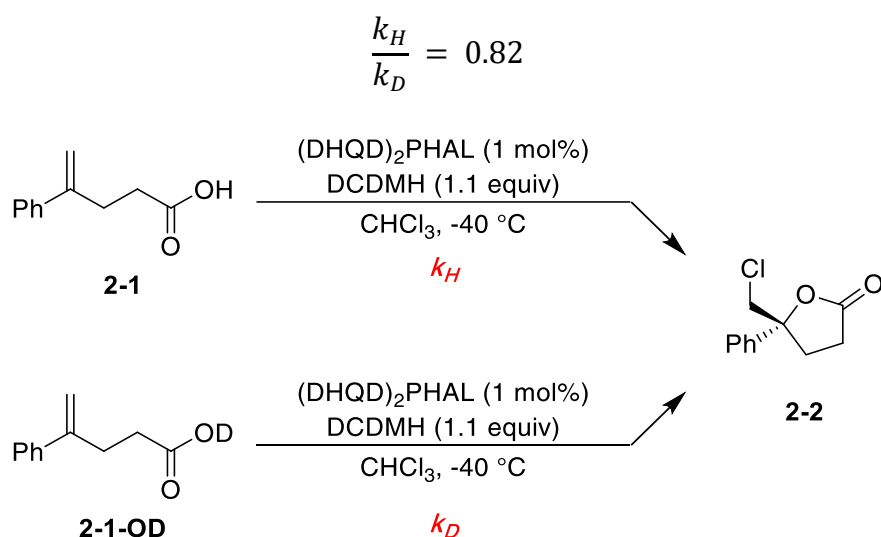
Figure 2.22 Kinetic isotopic effect studies. The figure depicts the kinetic effect of isotopic substitution of OH to OD in substrate **2-1**.
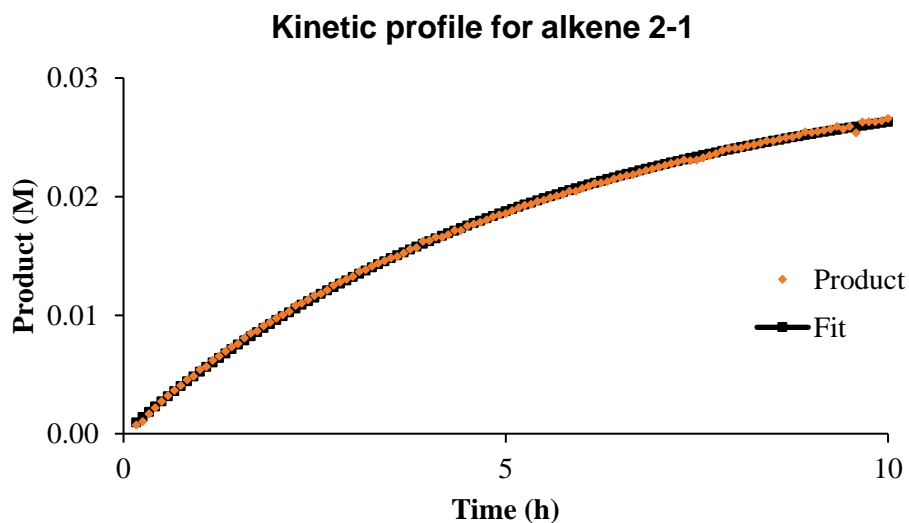
Figure 2.23 Proton label for ROESY studies. Fit of eq (33) to the kinetic profile of product formation from alkene 1. $[P]^\infty$ = 0.031 M, kH = 5.07 x $10^{-5,}$ least squared error = 2.78 x 10^{-6}
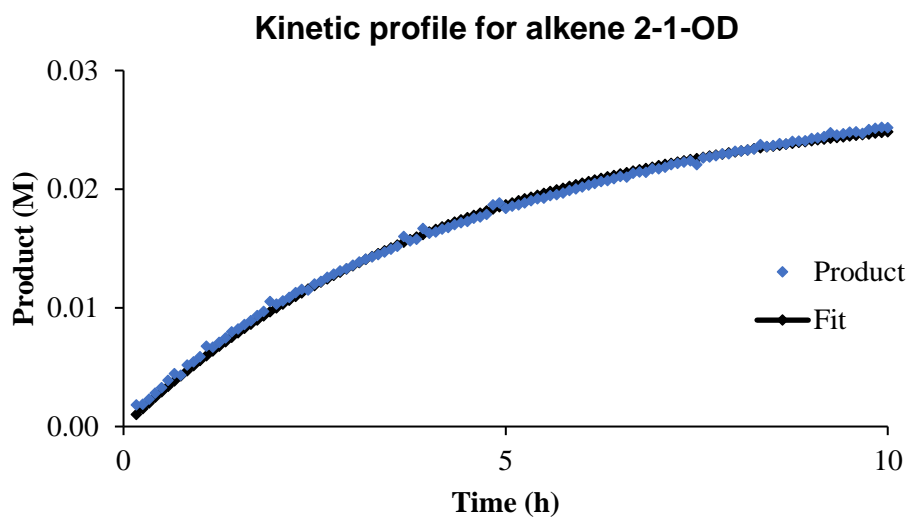
Figure 2.24 Proton label for ROESY studies. Fit of eq (33) to the kinetic profile of product formation from alkene 1-OD. $[P]^\infty$ = 0.027 M, kD = 6.17 x 10^{-5}, least squared error = 1.17 x 10^{-5}

2.9.7 General procedure for the titration of (DHQD)$_2$PHAL with alkene 1

Samples for NMR were prepared using anhydrous CDCl$_3$ inside a dry-box under N$_2$ atmosphere. CDCl$_3$ containing 0.1 μL/g tetramethyl silane was stored over flame dried 3 Å molecular sieves for at least 1 day. The substrate **2-1** was sublimed and the sublimator was opened inside a dry-box. (DHQD)$_2$PHAL was dried under vacuum overnight. All glassware were dried in an oven at 160 °C, and cooled down during transfer to the dry-box under antechamber vacuum. The NMR tube caps were sealed using parafilm to slow down water diffusion and spectra were collected on an Avance II Bruker 900 MHz instrument. The peak profile for proton H$_b$ is shown below. Measurement of H$_a$ was not feasible over the given range of titration since aromatic resonances overlapped with H$_a$ at certain concentrations.
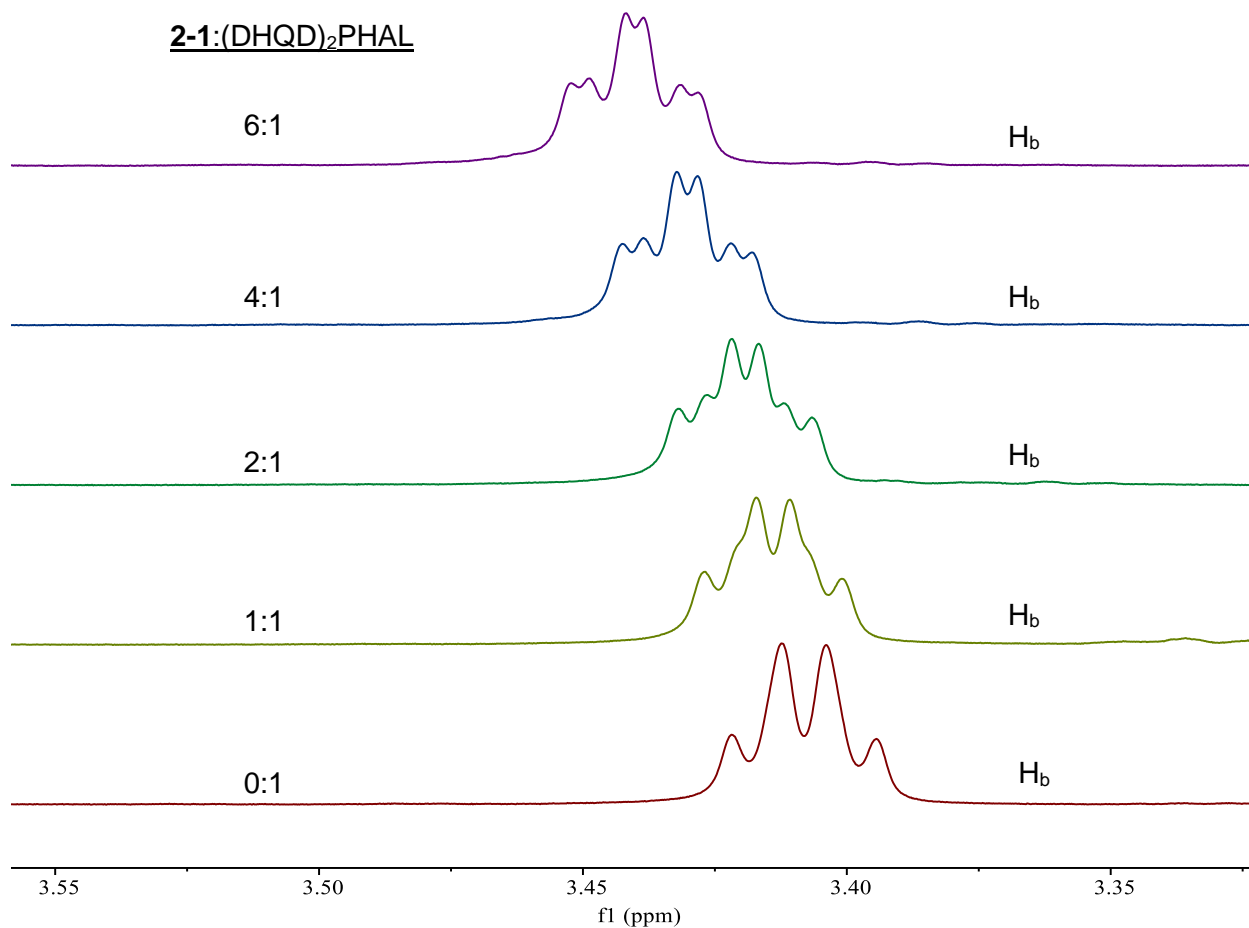
Figure 2.25 Change in chemical shift of H$_b$ on titrating (DHQD)$_2$PHAL with alkene 2-1. The figure depicts the change in chemical shift of the proton in (DHQD)$_2$PHAL when titrated with the alkene **2-1**.

2.9.8   X-Ray crystallography

Cocrystal of (DHQD)$_2$PHAL and benzoic acid was obtained by slow evaporation of

a chloroform solution containing 1:2 ratio of (DHQD)$_2$PHAL and benzoic acid in a capped

NMR tube over three weeks.
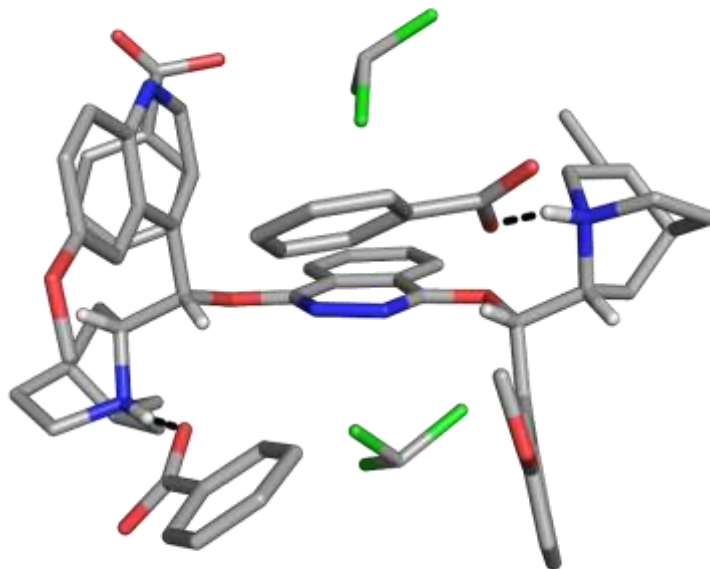
Figure 2.26 Co-crystal of (DHQD)$_2$PHAL with benzoic acid. The figure depicts the co-
crystallized structure of (DHQD)$_2$PHAL with benzoic acid.

2.9.9 General procedures for computational studies

All computations were performed using Gaussian 16.[68] Quantum chemical modeling of reactant, complex, and transition state structures was performed at the B3LYP-D3/6-31G* level.[69-72] All species were fully optimized, with stationary points characterized by vibrational analysis to verify the presence of zero (for minima) and only one (for transition states) imaginary frequencies. At first, energetic contributions of solvation were computed on these "gas phase" optimized structures using the SMD polarizable continuum model of Cramer et al.[73] applied after optimization as additive corrections to the calculated gas-phase enthalpies and free energies. This two-step method is denoted B3LYP-D3/6-31G*/postSMD(CHCl$_3$). However, in the context of this project, where protons and chlorenium ions are potentially transferred, creating or destroying charged sites, we were concerned about structural and energetic differences between structures optimized in vacuum and those optimized in the simulated CHCl$_3$. For this reason, computations that involve uncatalyzed and quinuclidine-promoted reactions were rerun with optimization and vibrational analyses obtained at the B3LYP-D3/6-31G*/SMD(CHCl$_3$) level, in which both the D3 dispersion correction of Grimme et al.[70] and the SMD solvation model were included in the optimization and vibrational analyses. Ultimately, the structures and energies showed little change from the original approach, and conclusions were unchanged.

REFERENCES

REFERENCES

1.   Cresswell, A. J.; Eey, S. T. C.; Denmark, S. E., Catalytic, Stereoselective Dihalogenation of Alkenes: Challenges and Opportunities. *Angew. Chem. Int. Ed.* **2015,** *54* (52), 15642-15682.

2.   Abe, H.; Fukazawa, N.; Kobayashi, T.; Ito, H., Indium chloride mediated chlorolactonization: construction of chlorinated lactone fragments. *Tetrahedron* **2013,** *69* (12), 2519-2523.

3.   Ahmad, S. M.; Braddock, D. C.; Cansell, G.; Hermitage, S. A.; Redmond, J. M.; White, A. J. P., Amidines as potent nucleophilic organocatalysts for the transfer of electrophilic bromine from N-bromosuccinimide to alkenes. *Tetrahedron Lett.* **2007,** *48* (34), 5948-5952.

4.   Brucher, O.; Bergstrasser, U.; Kelm, H.; Hartung, J.; Greb, M.; Svoboda, I.; Fuess, H., Controlling 6-endo-selectivity in oxidation/bromocyclization cascades for synthesis of aplysiapyranoids and other 2,2,6,6-substituted tetrahydropyrans. *Tetrahedron* **2012,** *68* (34), 6968-6980.

5.   Cardillo, G.; Orena, M., Stereocontrolled cyclofunctionalizations of double-bonds through heterocyclic intermediates. *Tetrahedron* **1990,** *46* (10), 3321-3408.

6.   Castellanos, A.; Fletcher, S. P., Current Methods for Asymmetric Halogenation of Olefins. *Chem. Eur. J.* **2011,** *17* (21), 5766-5776.

7.   Chen, F.; Tan, C. K.; Yeung, Y. Y., C-2-Symmetric Cyclic Selenium-Catalyzed Enantioselective Bromoaminocyclization. *J. Am. Chem. Soc.* **2013,** *135* (4), 1232-1235.

8.   Chen, G.; Ma, S., Enantioselective Halocyclization Reactions for the Synthesis of Chiral Cyclic Compounds. *Angew. Chem. Int. Ed.* **2010,** *49* (45), 8306-8308.

9.   Denmark, S. E.; Burk, M. T., Lewis base catalysis of bromo- and iodolactonization, and cycloetherification. *Proc. Natl. Acad. Sci. U.S.A.* **2010,** *107* (48), 20655-20660.

10.   Denmark, S. E.; Kuester, W. E.; Burk, M. T., Catalytic, Asymmetric Halofunctionalization of Alkenes-A Critical Perspective. *Angew. Chem. Int. Ed.* **2012,** *51* (44), 10938-10953.

11.   Dowle, M. D.; Davies, D. I., Synthesis and synthetic utility of halolactones. *Chemical Society Reviews* **1979,** *8* (2), 171-197.

12.   Fang, C.; Paull, D. H.; Hethcox, J. C.; Shugrue, C. R.; Martin, S. F., Enantioselective Iodolactonization of Disubstituted Olefinic Acids Using a Bifunctional Catalyst. *Org. Lett.* **2012,** *14* (24), 6290-6293.

13.   Garnier, J. M.; Robin, S.; Rousseau, G., An approach to enantioselective 5-endo halo-lactonization reactions. *Eur. J. Org. Chem.* **2007,** (20), 3281-3291.

14.   Grossman, R. B.; Trupp, R. J., The first reagent-controlled asymmetric halolactonizations. Dihydroquinidine-halogen complexes as chiral sources of positive halogen ion. *Can. J. Chem.-Rev. Can. Chim.* **1998,** *76* (9), 1233-1237.

15.   Haas, J.; Bissmire, S.; Wirth, T., Iodine monochloride-amine complexes: An experimental and computational approach to new chiral electrophiles. *Chem. Eur. J.* **2005,** *11* (19), 5777-5785.

16.   Haas, J.; Piguel, S.; Wirth, T., Reagent-controlled stereoselective iodolactonizations. *Org. Lett.* **2002,** *4* (2), 297-300.

17.   Ikeuchi, K.; Ido, S.; Yoshimura, S.; Asakawa, T.; Inai, M.; Hamashima, Y.; Kan, T., Catalytic Desymmetrization of Cyclohexadienes by Asymmetric Bromolactonization. *Org. Lett.* **2012,** *14* (23), 6016-6019.

18.   Jaganathan, A.; Garzan, A.; Whitehead, D. C.; Staples, R. J.; Borhan, B., A Catalytic Asymmetric Chlorocyclization of Unsaturated Amides. *Angew. Chem. Int. Ed.* **2011,** *50* (11), 2593-2596.

19.   Jaganathan, A.; Staples, R. J.; Borhan, B., Kinetic Resolution of Unsaturated Amides in a Chlorocyclization Reaction: Concomitant Enantiomer Differentiation and Face Selective Alkene Chlorination by a Single Catalyst. *J. Am. Chem. Soc.* **2013,** *135* (39), 14806-14813.

20.   Kitagawa, O.; Hanano, T.; Tanabe, K.; Shiro, M.; Taguchi, T., Enantioselective halocyclization reaction using a chiral titanium complex. *J. Chem. Soc., Chem. Commun.* **1992,** (14), 1005-1007.

21.   Lee, H. J.; Kim, D. Y., Catalytic enantioselective bromolactonization of alkenoic acids in the presence of palladium complexes. *Tetrahedron Lett.* **2012,** *53* (51), 6984-6986.

22.   Li, L.; Su, C.; Liu, X.; Tian, H.; Shi, Y., Catalytic Asymmetric Intermolecular Bromoesterification of Unfunctionalized Olefins. *Org. Lett.* **2014,** *16* (14), 3728-3731.

23.   Lozano, O.; Blessley, G.; del Campo, T. M.; Thompson, A. L.; Giuffredi, G. T.; Bettati, M.; Walker, M.; Borman, R.; Gouverneur, V., Organocatalyzed Enantioselective Fluorocyclizations. *Angewandte Chemie-International Edition* **2011,** *50* (35), 8105-8109.

24.   Mizar, P.; Burrelli, A.; Gunther, E.; Softje, M.; Farooq, U.; Wirth, T., Organocatalytic Stereoselective Iodoamination of Alkenes. *Chem. Eur. J.* **2014,** *20* (41), 13113-13116.

25.   Moyano, A.; Rios, R., Asymmetric Organocatalytic Cyclization and Cycloaddition Reactions. *Chem. Rev.* **2011,** *111* (8), 4703-4832.

26.   Murai, K.; Matsushita, T.; Nakamura, A.; Fukushima, S.; Shimura, M.; Fujioka, H., Asymmetric Bromolactonization Catalyzed by a C(3)-Symmetric Chiral Trisimidazoline. *Angew. Chem. Int. Ed.* **2010,** *49* (48), 9174-9177.

27.   Murai, K.; Nakamura, A.; Matsushita, T.; Shimura, M.; Fujioka, H., C3-Symmetric Trisimidazoline-Catalyzed Enantioselective Bromolactonization of Internal Alkenoic Acids. *Chem. Eur. J.* **2012,** *18* (27), 8448-8453.

28.   Murai, K.; Fujioka, H., Recent progress in organocatalytic asymmetric halocyclization. *Heterocycles* **2013,** *87* (4), 763-805.

29.   Paull, D. H.; Fang, C.; Donald, J. R.; Pansick, A. D.; Martin, S. F., Bifunctional Catalyst Promotes Highly Enantioselective Bromolactonizations To Generate Stereogenic C-Br Bonds. *J. Am. Chem. Soc.* **2012,** *134* (27), 11128-11131.

30.   Snider, B. B.; Johnston, M. I., Regioselectivity of the halolactonization of gamma,delta-unsaturated acids. *Tetrahedron Lett.* **1985,** *26* (45), 5497-5500.

31.   Tan, C. K.; Le, C. C.; Yeung, Y. Y., Enantioselective bromolactonization of cis-1,2-disubstituted olefinic acids using an amino-thiocarbamate catalyst. *Chem. Commun.* **2012,** *48* (46), 5793-5795.

32.   Tan, C. K.; Zhou, L.; Yeung, Y. Y., Organocatalytic Enantioselective Halolactonizations: Strategies of Halogen Activation. *Synlett* **2011,** (10), 1335-1339.

33.   Tungen, J. E.; Nolsoe, J. M. J.; Hansen, T. V., Asymmetric Iodolactonization Utilizing Chiral Squaramides. *Org. Lett.* **2012,** *14* (23), 5884-5887.

34.   Veitch, G. E.; Jacobsen, E. N., Tertiary Aminourea-Catalyzed Enantioselective Iodolactonization. *Angew. Chem. Int. Ed.* **2010,** *49* (40), 7332-7335.

35.   Wang, M.; Gao, L. X.; Yue, W.; Mai, W. P., Reagent-controlled asymmetric iodolactonization using cinchona alkaloids as chiral sources. *Synth. Commun.* **2004,** *34* (6), 1023-1032.

36.   Wang, Y. M.; Wu, J.; Hoong, C.; Rauniyar, V.; Toste, F. D., Enantioselective Halocyclization Using Reagents Tailored for Chiral Anion Phase-Transfer Catalysis. *J. Am. Chem. Soc.* **2012,** *134* (31), 12928-12931.

37.   Whitehead, D. C.; Fhaner, M.; Borhan, B., A peptide bromoiodinane approach for asymmetric bromolactonization. *Tetrahedron Lett.* **2011,** *52* (18), 2288-2291.

38.   Whitehead, D. C.; Yousefi, R.; Jaganathan, A.; Borhan, B., An Organocatalytic Asymmetric Chlorolactonization. *J. Am. Chem. Soc* **2010,** *132* (10), 3298-3300.

39.   Yin, Q.; You, S.-L., Enantioselective Chlorocyclization of Indole Derived Benzamides for the Synthesis of Spiro-indolines. *Org. Lett.* **2013,** *15* (16), 4266-4269.

40.   Yin, Q.; You, S.-L., Asymmetric Chlorination/Ring Expansion for the Synthesis of α-Quaternary Cycloalkanones. *Org. Lett.* **2014,** *16* (6), 1810-1813.

41.   Yin, Q.; You, S.-L., Asymmetric Chlorocyclization of Indole-3-yl-benzamides for the Construction of Fused Indolines. *Org. Lett.* **2014,** *16* (9), 2426-2429.

42.   Zhang, J. L.; Wang, J.; Qiu, Z. B.; Wang, Y., Highly regio- and diastereoselective halohydroxylation of olefins: a facile synthesis of vicinal halohydrins. *Tetrahedron* **2011,** *67* (36), 6859-6867.

43.   Chen, J.; Zhou, L., Recent Progress in the Asymmetric Intermolecular Halogenation of Alkenes. *Synthesis-Stuttgart* **2014,** *46* (5), 586-595.

44.   Cheng, Y. A.; Yu, W. Z.; Yeung, Y. Y., Recent advances in asymmetric intra- and intermolecular halofunctionalizations of alkenes. *Org. Biomol. Chem.* **2014,** *12* (15), 2333-2343.

45.   Chung, W. J.; Vanderwal, C. D., Stereoselective Halogenation in Natural Product Synthesis. *Angew. Chem. Int. Ed. Engl.* **2016,** *55* (14), 4396-434.

46.   Landry, M. L.; Burns, N. Z., Catalytic Enantioselective Dihalogenation in Total Synthesis. *Acc. Chem. Res.* **2018,** *51* (5), 1260-1271.

47.   Tan, C. K.; Yeung, Y. Y., Recent advances in stereoselective bromofunctionalization of alkenes using N-bromoamide reagents. *Chem. Commun.* **2013,** *49* (73), 7985-96.

48.   Kolb, H. C.; Andersson, P. G.; Sharpless, K. B., Toward an understanding of the high enantioselectivity in the osmium-catalyzed asymmetric dihydroxylation. 1. Kinetics. *J. Am. Chem. Soc.* **1994,** *116* (4), 1278-1291.

49.   Jaganathan, A.; Borhan, B., Chlorosulfonamide Salts Are Superior Electrophilic Chlorine Precursors for the Organocatalytic Asymmetric Chlorocyclization of Unsaturated Amides. *Org. Lett.* **2014,** *16* (14), 3616-3619.

50.   Niu, W.; Yeung, Y.-Y., Catalytic and Highly Enantioselective Selenolactonization. *Org. Lett.* **2015,** *17* (7), 1660-1663.

51.   Nicolaou, K. C.; Simmons, N. L.; Ying, Y.; Heretsch, P. M.; Chen, J. S., Enantioselective Dichlorination of Allylic Alcohols. *J. Am. Chem. Soc.* **2011,** *133* (21), 8134-8137.

52.   Wilking, M.; Mück-Lichtenfeld, C.; Daniliuc, C. G.; Hennecke, U., Enantioselective, Desymmetrizing Bromolactonization of Alkynes. *J. Am. Chem. Soc.* **2013,** *135* (22), 8133-8136.

53.   Yousefi, R.; Ashtekar, K. D.; Whitehead, D. C.; Jackson, J. E.; Borhan, B., Dissecting the Stereocontrol Elements of a Catalytic Asymmetric Chlorolactonization: Syn Addition Obviates Bridging Chloronium. *J. Am. Chem. Soc.* **2013,** *135* (39), 14524-14527.

54.   Yousefi, R.; Whitehead, D. C.; Mueller, J. M.; Staples, R. J.; Borhan, B., On the Chlorenium Source in the Asymmetric Chlorolactonization Reaction. *Org. Lett.* **2011,** *13* (4), 608-611.

55.   Ashtekar, K. D.; Marzijarani, N. S.; Jaganathan, A.; Holmes, D.; Jackson, J. E.; Borhan, B., A New Tool To Guide Halofunctionalization Reactions: The Halenium Affinity (HalA) Scale. *J. Am. Chem. Soc.* **2014,** *136* (38), 13355-13362.

56.   Blackmond, D. G., Reaction progress kinetic analysis: A powerful methodology for mechanistic studies of complex catalytic reactions. *Angew. Chem. Int. Ed.* **2005,** *44* (28), 4302-4320.

57.   Mathew, J. S.; Klussmann, M.; Iwamura, H.; Valera, F.; Futran, A.; Emanuelsson, E. A. C.; Blackmond, D. G., Investigations of Pd-catalyzed ArX coupling reactions informed by reaction progress kinetic analysis. *J. Org. Chem.* **2006,** *71* (13), 4711-4722.

58.   Blackmond, D. G., Kinetic Profiling of Catalytic Organic Reactions as a Mechanistic Tool. *J. Am. Chem. Soc.* **2015,** *137* (34), 10852-66.

59.   Nielsen, C. D. T.; Bures, J., Visual kinetic analysis. *Chem. Sci.* **2019,** *10* (2), 348-353.

60.   Ashtekar, K. D.; Vetticatt, M.; Yousefi, R.; Jackson, J. E.; Borhan, B., Nucleophile-Assisted Alkene Activation: Olefins Alone Are Often Incompetent. *J. Am. Chem. Soc.* **2016,** *138* (26), 8114-8119.

61.   Burgi, T.; Baiker, A., Conformational behavior of cinchonidine in different solvents: A combined NMR and ab initio investigation. *J. Am. Chem. Soc.* **1998,** *120* (49), 12920-12926.

62.   Dijkstra, G. D. H.; Kellogg, R. M.; Wynberg, H., Conformational study of cinchona alkaloids - A combined NMR and molecular-orbital approach. *J. Org. Chem.* **1990,** *55* (25), 6121-6131.

63.   Olsen, R. A.; Borchardt, D.; Mink, L.; Agarwal, A.; Mueller, L. J.; Zaera, F., Effect of protonation on the conformation of cinchonidine. *J. Am. Chem. Soc.* **2006,** *128* (49), 15594-15595.

64.   Ammalahti, E.; Bardet, M.; Molko, D.; Cadet, J., Evaluation of distances from ROESY experiments with the intensity-ratio method. *J. Magn. Reson. A* **1996,** *122* (2), 230-232.

65.   Ammalahti, E.; Bardet, M.; Cadet, J.; Molko, D., NMR assignments and conformational studies of two diastereomeric oxidation products of 2 '-deoxycytidine. *Magn. Reson. Chem* **1998,** *36* (5), 363-370.

66.   Bodenhausen, G.; Ernst, R. R., Direct Determination of Rate Constants of Slow Dynamic Processes by Two-Dimensional Accordion Spectroscopy in Nuclear Magnetic-Resonance. *J. Am. Chem. Soc.* **1982,** *104* (5), 1304-1309.

67.   Meng, C. S.; Liu, Z. H.; Liu, Y. X.; Wang, Q. M., 4-(Dimethylamino)pyridine-catalysed iodolactonisation of gamma,delta-unsaturated carboxylic acids. *Org. Biomol. Chem.* **2015,** *13* (24), 6766-6772.

68.   Frisch, M. J. T., G. W.; Schlegel, H. B.; Scuseria, G. E.; Robb, M. A.; Cheeseman, J. R.; Scalmani, G.; Barone, V.; Petersson, G. A.; Nakatsuji, H.; Li, X.; Caricato, M.; Marenich, A. V.; Bloino, J.; Janesko, B. G.; Gomperts, R.; Mennucci, B.; Hratchian, H. P.; Ortiz, J. V.; Izmaylov, A. F.; Sonnenberg, J. L.; Williams-Young, D.; Ding, F.; Lipparini, F.; Egidi, F.; Goings, J.; Peng, B.; Petrone, A.; Henderson, T.; Ranasinghe, D.; Zakrzewski, V. G.; Gao, J.; Rega, N.; Zheng, G.; Liang, W.; Hada, M.; Ehara, M.; Toyota, K.; Fukuda, R.; Hasegawa, J.; Ishida, M.; Nakajima, T.; Honda, Y.; Kitao, O.; Nakai, H.; Vreven, T.; Throssell, K.; Montgomery, J. A., Jr.; Peralta, J. E.; Ogliaro, F.; Bearpark, M. J.; Heyd, J. J.; Brothers, E. N.; Kudin, K. N.; Staroverov, V. N.; Keith, T. A.; Kobayashi, R.; Normand, J.; Raghavachari, K.; Rendell, A. P.; Burant, J. C.; Iyengar, S. S.; Tomasi, J.; Cossi, M.; Millam, J. M.; Klene, M.; Adamo, C.; Cammi, R.; Ochterski, J. W.; Martin, R. L.; Morokuma, K.; Farkas, O.; Foresman, J. B.; Fox, D. J. *Gaussian 16*, Revision C.01; Gaussian, Inc.: Wallingford, CT, 2016.

69.   Becke, A. D., DENSITY-FUNCTIONAL EXCHANGE-ENERGY APPROXIMATION WITH CORRECT ASYMPTOTIC-BEHAVIOR. *Phys. Rev. A* **1988,** *38* (6), 3098-3100.

70.   Grimme, S.; Antony, J.; Ehrlich, S.; Krieg, H., A consistent and accurate ab initio parametrization of density functional dispersion correction (DFT-D) for the 94 elements H-Pu. *J. Chem. Phys.* **2010,** *132* (15), 19.

71.   Hehre, W. J.; Ditchfield, R.; Pople, J. A., SELF-CONSISTENT MOLECULAR-ORBITAL METHODS .12. FURTHER EXTENSIONS OF GAUSSIAN-TYPE BASIS SETS FOR USE IN MOLECULAR-ORBITAL STUDIES OF ORGANIC-MOLECULES. *J. Chem. Phys.* **1972,** *56* (5), 2257-+.

72.   Lee, C. T.; Yang, W. T.; Parr, R. G., DEVELOPMENT OF THE COLLE-SALVETTI CORRELATION-ENERGY FORMULA INTO A FUNCTIONAL OF THE ELECTRON-DENSITY. *Phys. Rev. B* **1988,** *37* (2), 785-789.

73.   Marenich, A. V.; Cramer, C. J.; Truhlar, D. G., Universal Solvation Model Based on Solute Electron Density and on a Continuum Model of the Solvent Defined by the Bulk Dielectric Constant and Atomic Surface Tensions. *J. Phys. Chem. B* **2009,** *113* (18), 6378-6396.

Chapter 3. Mechanism of catalytic asymmetric chloroetherification of alkene amides

Catalytic asymmetric halofunctionalizations have proliferated over the last decade, yet mechanistic insights into these catalytic processes remain scarce. This article presents a novel mechanism, revealed via detailed kinetic analysis of $(DHQD)_2PHAL$ catalyzed asymmetric chloroetherification. The rate of alkene amide **3-3** undergoing chloromethoxylation showed a first order dependence on the alkene and the methanol. The electrophilic chlorinating agent, DCDMH, showed zeroth order dependence, attributed to its strong binding to and reaction with the catalyst, which only complexes alkene weakly. An inverse secondary kinetic isotopic effect at the site of ether formation pointed to a concerted Ad_E3-type addition of the electrophile and nucleophile components to the alkene. Surprisingly, the catalyst was found to have a zeroth order effect on the reaction rate under the previously reported reaction conditions. This discovery enabled a 10-fold drop in catalyst loading for the chloroetherification with essentially no loss in efficacy or stereocontrol. The kinetic studies were complemented with spectroscopic investigations of reaction intermediates and quantum chemical modeling to further dissect the elementary steps involved in the catalysis. The findings for this catalytic chloroetherification led to a unique kinetic model that contrasts with our prior reported mechanism of chlorolactonization activated by the same catalyst. Exposing this mechanistic diversity among seemingly similar catalytic asymmetric halofunctionalizations underscores the value of such mechanistic investigations and their role in reaction discovery and optimization.

3.1   Introduction

Over the last decade, catalytic asymmetric halofunctionalizations of alkenes have taken their place in the vast arsenal of asymmetric transformations.[1-10] As one would expect in a growing field, a variety of catalysts have shown efficacy for halofunctionalization of different families of olefinic substrates. Most of these catalysts work via Bronsted or Lewis acid/base reactivities, each presumably with unique mechanistic features.[5] Even with the same catalyst, the same mechanism of action is not a foregone conclusion; reaction conditions and changes in substrate functional groups and structures may lead to varied mechanistic pathways. The story reported here highlights this point emphatically.
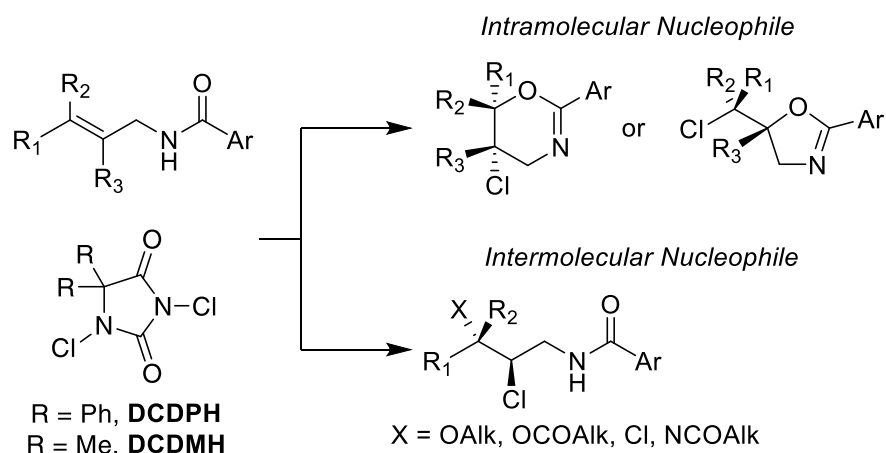
Figure 3.1 (DHQD)$_2$PHAL catalyzed chlorofunctionalization of alkene amides. Various examples of (DHQD)$_2$PHAL catalyzed asymmetric chlorofunctionalizations of alkene amides demonstrating its broad applicability.

Our initial discovery of the asymmetric chlorolactonization of alkene carboxylic acids,[11] catalyzed by the well-known cinchona alkaloid dimer (DHQD)$_2$PHAL,[12] was followed by several halofunctionalization reactions of alkene amide substrates. Some recent examples include chlorocyclizations, chloroetherifications, chloroamidations and alkene amide dichlorinations (Figure 3.1).[13-19] These reactions are broadly classified into

intramolecular and intermolecular cases, with the former requiring a nucleophile tethered to the olefin, while the latter involve external nucleophiles (Figure 3.1). Despite the surge in catalytic chlorofunctionalization processes, there is a dearth of literature insight into their reaction mechanisms. This is most apparent for the intermolecular processes, arguably the more versatile and general of the category. Detailed herein is the discovery of a unique mechanism responsible for the asymmetric chloroetherification of alkene amides (Figure 3.2b), as revealed by kinetic, spectroscopic, and computational tools.
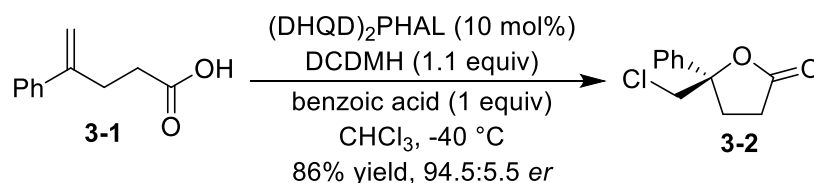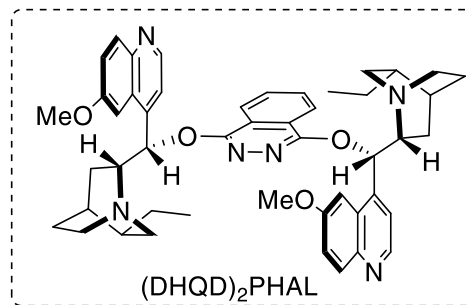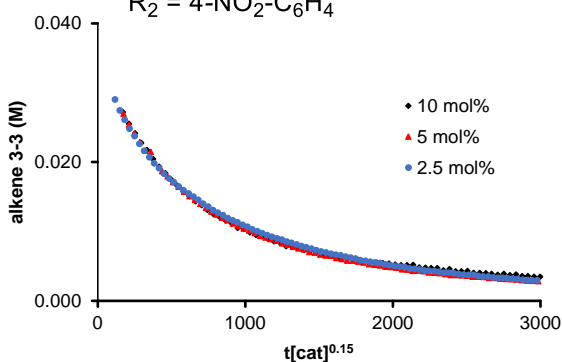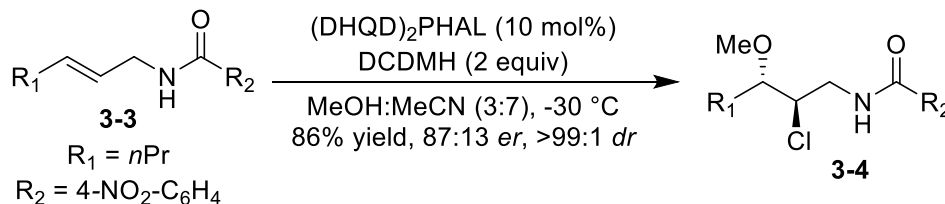
Figure 3.2 Mechanistic study on catalytic chlorofunctionalization of alkene amides. (a) Prior work on the mechanism of chlorolactonization. (b) Current work on mechanism of (DHQD)$_2$PHAL catalyzed chloroetherification of alkene amides.

In a recent article we described the mechanism of chlorolactonization of alkene carboxylic acids, one of the first known catalytic asymmetric halofunctionalization reactions.[20] It is tempting to extrapolate the mechanistic conclusions from that report to other transformations achieved by the same catalyst and chlorenium ion source, such as the chlorofunctionalization of alkene amides. Unfortunately, that logical extension fails, as the present account will show. The reaction conditions for chlorolactonization of alkene **3-1** differ from those of chlorofunctionalization of alkene amides in two key aspects: 1) the nature of the substrate (carboxylic acid vs amide), and 2) the nature of the solvent (non-polar in one case, polar protic in other). Notably, in a previous study, a similar difference was sufficient to invert the stereochemistry.[13, 21, 22] The following observations further differentiate the two systems, suggesting that differing mechanisms are to be expected:

1) Prior investigations have shown that the face selectivity of nucleophile attachment in the chlorofunctionalization of 1,1-disubstituted alkene amides is opposite to that in the analogous reaction with 1,1-disubstituted alkene carboxylic acids.[13, 21, 22]

2) Substrate scope studies have demonstrated that the stereocontrol in chlorofunctionalizations of alkene amides is in general more robust in the face of structural variations than the corresponding chlorolactonizations of alkene carboxylic acids. [11, 14-19]

3) As noted above, polar-protic solvents are optimal for alkene amide chlorofunctionalizations, whereas non-polar solvents are best for chlorolactonization.

4) Carboxylic acid substrates, with their inherently low pK_a values, are strong binders of the basic (DHQD)$_2$PHAL catalyst. This leads to the formation of a key substrate-

catalyst complex at the start of chlorolactonization (the resting state). The alkene amide-catalyst complexation is not as strong. For instance, the B3LYP/6-31G* calculated gas-phase association energy of N-methyl acetamide with trimethylamine is 6-7 kcal/mol weaker than that of acetic acid.

With these differences in mind, an independent investigation into the mechanism of alkene amide chlorofunctionalizations was necessary. In this paper, we describe an extensive mechanistic study on the (DHQD)$_2$PHAL catalyzed intermolecular chloroetherification of alkene amides (Figure 3.2b). A unique mechanistic picture has emerged from this investigation for alkene amide functionalization that differs sharply from that of chlorolactonization. When run at typical catalyst concentrations, the process was found to exhibit a surprising, *zero order dependence* on the concentration of (DHQD)$_2$PHAL. Only at catalyst concentrations an order of magnitude lower did a rate dependence emerge. The amide functional group plays a critical role in engaging the nucleophile for attack on the alkene while the chlorenium ion is first transferred to the catalyst, and then delivered to the alkene. All these observations are in contrast to the (DHQD)$_2$PHAL catalyzed asymmetric chlorolactonization of alkene carboxylic acids.[20] Fortuitously, this investigation has revealed an improvement upon the original reported reaction condition, lowering the catalyst required by 10-fold without impacting the reaction.

3.2   Kinetic studies

Chemical kinetics has always been an indispensable tool for mechanistic investigations. Identifying a complete rate law for any reaction not only limits the number of mechanistic interpretations by setting stringent boundary conditions, but also often

provides critical information regarding the elementary steps involved in a catalytic process. In recent years, the use of kinetic studies has grown among organic chemists with the advent of various visual kinetic analysis protocols such as the Reaction Progress Kinetic Analysis (RPKA) and the Variable Time Normalized Analysis (VTNA) developed by Blackmond and Bures, respectively.[23-28] The popularity of these techniques stem from their highly intuitive nature, as well as their ease of execution and analysis even for organic chemists not adept in chemical kinetics. These protocols often work well with practically relevant reaction conditions, unlike more classical techniques that extrapolate from pseudo first order conditions, where large concentration imbalances are needed for analysis.

We began our mechanistic study with a comprehensive investigation into the chloroetherification kinetics of alkene amide **3-3**. Using the VTNA protocol along with classical kinetic techniques, we established the order of each component, leading to a rate law for the reaction. The standard conditions for these experiments were 0.04 M alkene, 0.08 M DCDMH, 0.004 M (DHQD)$_2$PHAL in 3:7 v:v methanol/acetonitrile at -32 °C. These conditions are nearly identical to those originally reported, and thus negligibly impact the enantioselectivity. Deuterated analogs of the solvents (methanol-d$_4$ and acetonitrile-d$_3$) were used to enable *in situ* reaction monitoring via NMR spectroscopy.

3.2.1 Order of alkene

Two experiments, A and B, shown in Figure 3.3 were executed at different concentrations of alkene with otherwise identical conditions. Analysis of these two experiments utilizing the standard VTNA protocol showed optimal overlay of their respective time-normalized plots when the alkene concentration carried an exponent of 1.1 (Figure 3.3). Thus, the rate of chloroetherification has a first-order dependence on the

138

alkene concentration, which is in contrast to the previous report for chlorolactonization.[20]

In chlorolactonization, the observed zeroth order behavior in alkenoic acid **3-1** originated

from the substrate saturating the catalyst resulting in a bound resting state. The observed

first order dependence on alkene amide **3-3** for the chloroetherification reaction points to

a different substrate-catalyst relationship where the catalyst is no longer saturated with

the alkene. The justification for this hypothesis is explored further in later sections.
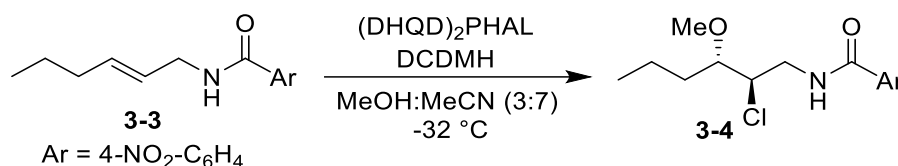
Exp	3-3 (M)	DCDMH (M)	(DHQD)₂PHAL (M)	excess (M)
A	0.04	0.08	0.004	0.04
B	0.06	0.08	0.004	0.02
C	0.04	0.06	0.004	0.02
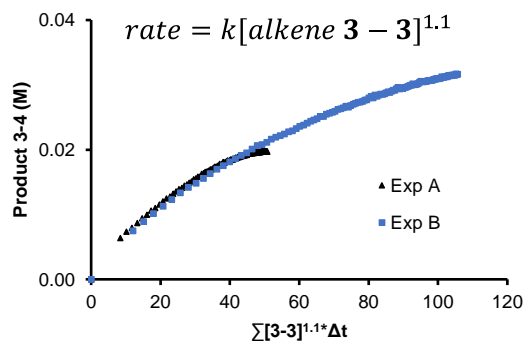
Figure 3.3 Kinetic experiments to determine order of alkene 3-3. (a) A set of different excess experiments analyzed using VTNA protocol to determine order of alkene **3-3**.

3.2.2   Order of DCDMH

Unfortunately, direct determination of the order of DCDMH using experiments A

and C (Figure 3.3) was less straightforward. DCDMH and its dechlorinated by-product, 1-

chloro-5,5-dimethylhydantoin (MCDMH), did not display unique NMR signals during the

course of the reaction. Instead, a combined averaged peak for the two species (DCDMH

and MCDMH) was observed. Thus, as chloroetherification progressed, the observed

averaged peak for the hydantoins moved upfield as the DCDMH:MCDMH ratio decreased (Figure 3.4a). This implied a dynamic equilibrium, presumably due to Cl/H exchange between DCDMH and MCDMH under the reaction conditions. In contrast, both forms are clearly observed under the chlorolactonization conditions.
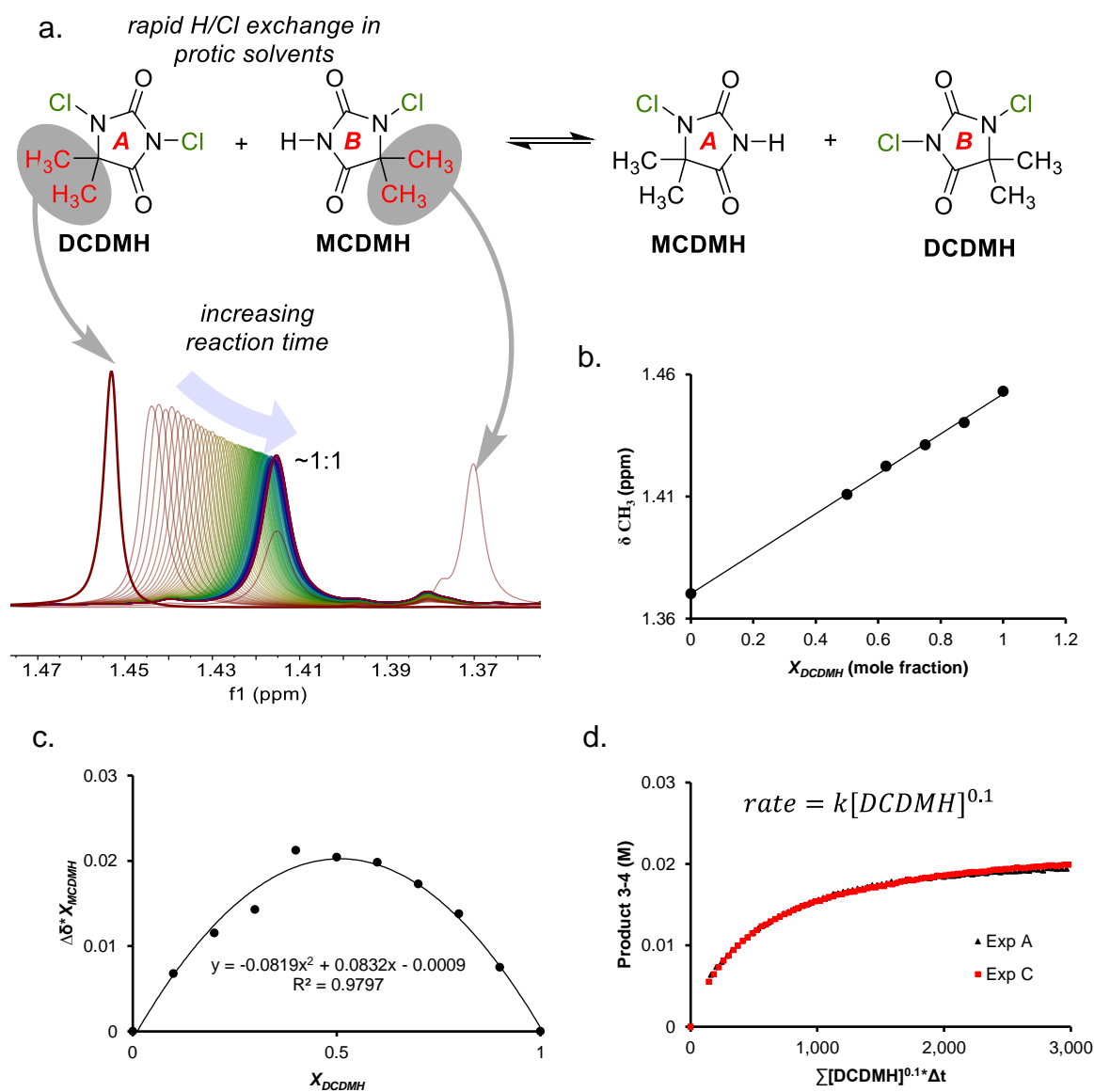
Figure 3.4 Finding order of DCDMH. (a) DCDMH-MCDMH chlorine exchange resulted in averaged ^{1}H NMR spectra for both species. (b) Example of external calibration curves generated prior each experiment to enable quantification of DCDMH and MCDMH with reaction process. (c) A Jobs plot depicting a 1:1 equilibrium between DCDMH and MCDMH. (d) Finding order of DCDMH using VTNA protocols.

Evidently, this Cl/H exchange is triggered by the presence of a protic solvent; it is not observed when pure acetonitrile is used as the solvent. Addition of methanol or fluorinated alcohols such as 1,1,1,3,3,3-hexafluoro-2-propanol (HFIP) lead to immediate coalescence of the peaks. Jobs plot analysis of these two species under the reaction conditions confirmed the 1:1 H/Cl equilibration (Figure 3.4c).[29]

Individual external calibration curves generated prior to each reaction from mixtures with known concentrations of DCDMH and MCDMH (an example shown in Figure 3.4b), allowed quantification of DCDMH and MCDMH concentration during the course of the reaction. This ultimately provided the means to directly evaluate the order of DCDMH, which was found to be nearly zero (Figure 3.4d).

$$rate = k[\mathbf{3-3}]^{1.1}[DCDMH]^{0.1} \hspace{3cm} \text{eq (3.1)}$$

An important note here is that the rate equation evaluated thus far is in stark contrast to our recent report on chlorolactonization of alkene carboxylic acid.[20] In chlorolactonization, the rate was found to be first order with respect to the DCDMH and zero order with respect to alkene **3-1**. As previously mentioned, the zeroth order with respect to alkene **3-1** was a result of saturation kinetics, where **3-1** rapidly binds (DHQD)$_2$PHAL to form a resting complex. This resting complex reacted with DCDMH in the rate determining step, thus exhibiting first order dependence on DCDMH and (DHQD)$_2$PHAL. In chloroetherification of alkene amide **3-3**, the opposite order with respect to the components (**3-3** and DCDMH) indicates that this is certainly no longer the case. The current rate equation could in fact be hinting at a reverse scenario where the DCDMH outcompetes alkene **3-3** for catalyst binding, leading to a saturation of available catalyst as a DCDMH-bound complex.

3.2.3 Product inhibition and catalyst binding

Investigation into the presence of catalyst deactivation or product inhibition provided further clues about the various binding equilibria operating along the reaction pathway. Analysis of a set of "same excess" experiments (Figure 3.5a, Figure 3.5b) revealed the byproduct MCDMH to be an inhibitor of the catalytic chloroetherification. This is yet another finding that directly contradicts the chlorolactonization reaction mechanism, where no product inhibition was observed. More importantly, this reinforces the hypothesis that in chloroetherification of alkene amides, DCDMH binds more strongly than alkene **3-3** to (DHQD)₂PHAL. And perhaps the MCDMH, impotent as a halogenating agent but structurally similar to DCDMH, now competes with DCDMH for catalyst binding to form an inactive complex.

To similarly probe whether amides (alkene substrate or product) show significant catalyst binding, the reaction was doped with 0.5 equivalent of **3-5**, the saturated analog of alkene amide **3-3**. Given their structural similarities, **3-5** should compete with alkene amide **3-3** and/or the reaction product for catalyst binding, provided that binding of **3-3** to catalyst is important to the kinetics. Under this scenario, unreactive **3-5** would siphon off some of the catalyst into an inactive off-cycle complex, acting as a competitive inhibitor and slowing the reaction. However, addition of a 0.5 equivalent (or 0.02 M) of **3-5** had no effect on the rate of chloroetherification of alkene amide **3-3** (Figure 3.5c). This suggests little affinity of the catalyst for any of the amides, substrate **3-3**, product **3-4**, or additive **3-5**. Nonetheless, the amide functionality is essential to achieve high stereoselectivity in asymmetric chlorofunctionalizations.[17, 18] What then is the role of the amide functional group in substrate **3-3**? This question is explored further in a later section via computational studies.

The above studies led to the proposed equilibria shown in Figure 3.5d, illustrating that the total catalyst concentration is effectively shared between a DCDMH-bound active-resting-complex I_1 and an MCDMH bound inactive-resting-complex I_2. The roles of complexes I_1 and I_2 are examined further in the later section using NMR.

a.

3-3
Ar = 4-NO$_2$-C$_6$H$_4$

(DHQD)$_2$PHAL
DCDMH
MeOH:MeCN (3:7)
-32 °C

3-4

Exp	3-3 (M)	DCDMH (M)	(DHQD)$_2$PHAL (M)	MCDMH (M)
B	0.06	0.08	0.004	-
C	0.04	0.06	0.004	-
D	0.04	0.06	0.004	0.02

b.

c.

additives:

MCDMH

3-5
alkane analog

d. (DHQD)$_2$PHAL

inactive complex I_2 ← MCDMH

DCDMH → active complex I_1

inhibition

3-3 or 3-5

no apparent binding
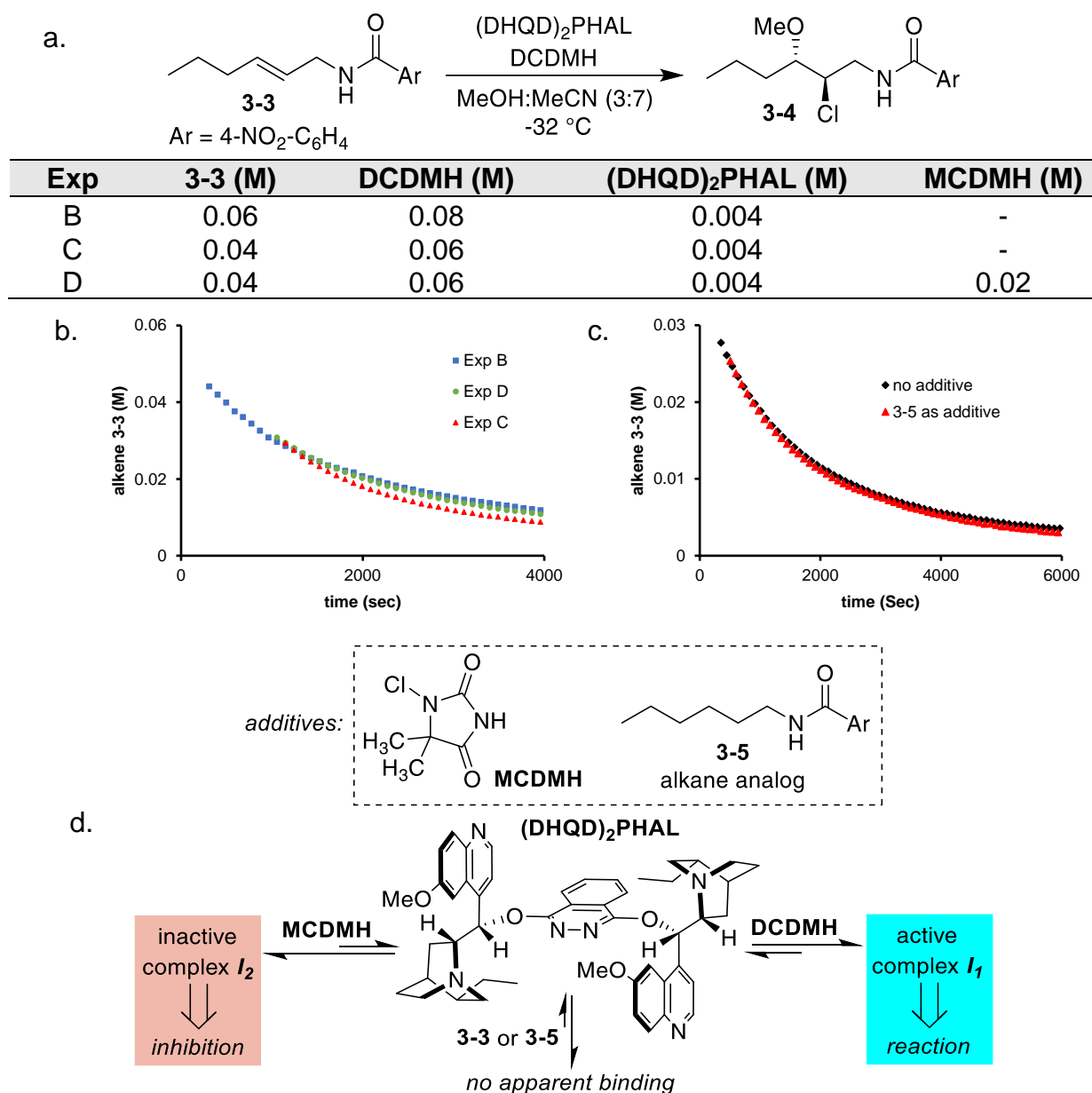
reaction

Figure 3.5 Investigating product inhibition and catalyst deactivation. (a) Same excess experiments conducted to investigate catalyst deactivation of product inhibition. (b) Experiment B, C and D demonstrates a small but noticeable product inhibition from the MCDMH by-product. (c) Addition of structurally similar alkane amide **3-5** to the reaction does not impact the reactivity, indicating amides do not compete for the catalyst

143

(Figure 3.5 (cont'd)) binding. (d) Binding model illustrating competitive binding of DCDMH and MCDMH to the catalyst to generate the active I_1 and inactive I_2 intermediate species respectively.

3.2.4 Role of the nucleophile

The need to investigate the order of nucleophile stemmed from our prior investigations of uncatalyzed halofunctionalizations that indicated a critical role of the nucleophile in alkene chlorofunctionalizations.[30] Prior experimental findings found these alkene additions to occur via a low barrier Ad_E3-type pathway in which the nucleophile and the chlorenium ion donor participate concertedly in preference to a stepwise addition (Figure 3.6a), a process dubbed nucleophile assisted alkene activation (NAAA).[30-32] Although demonstrated for the uncatalyzed reaction, rigorous investigations into the NAAA pathway are lacking for the catalyzed halofunctionalization reactions. For the present reaction, a concerted rate-limiting addition involving the methanol nucleophile predicts a positive reaction order of the alcohol, whereas, zeroth order would indicate its involvement post formation of the high energy carbocation intermediate (Figure 3.6a).

Methanol, the nucleophile in chloroetherification of alkene amides is present in large excess and is practically a constant, as it experiences negligible change in concentration during the course of the reaction. Thus, the order of the methanol in chloroetherification is determined under varying concentrations of methanol by pseudo first-order analysis. Plotting the rate constants (k_{obs}) as a function of methanol concentration yields a linear relationship that indicates a first order dependence (Figure 3.6b, see experimental section for detail). The explicit presence of methanol in the rate further strengthens the idea that the concerted addition of the nucleophile via the NAAA pathway is operational here.

$$rate = k[\mathbf{3-3}]^{1.1}[DCDMH]^{0.1}[MeOH]^1 \qquad\qquad eq\ (3.2)$$

144
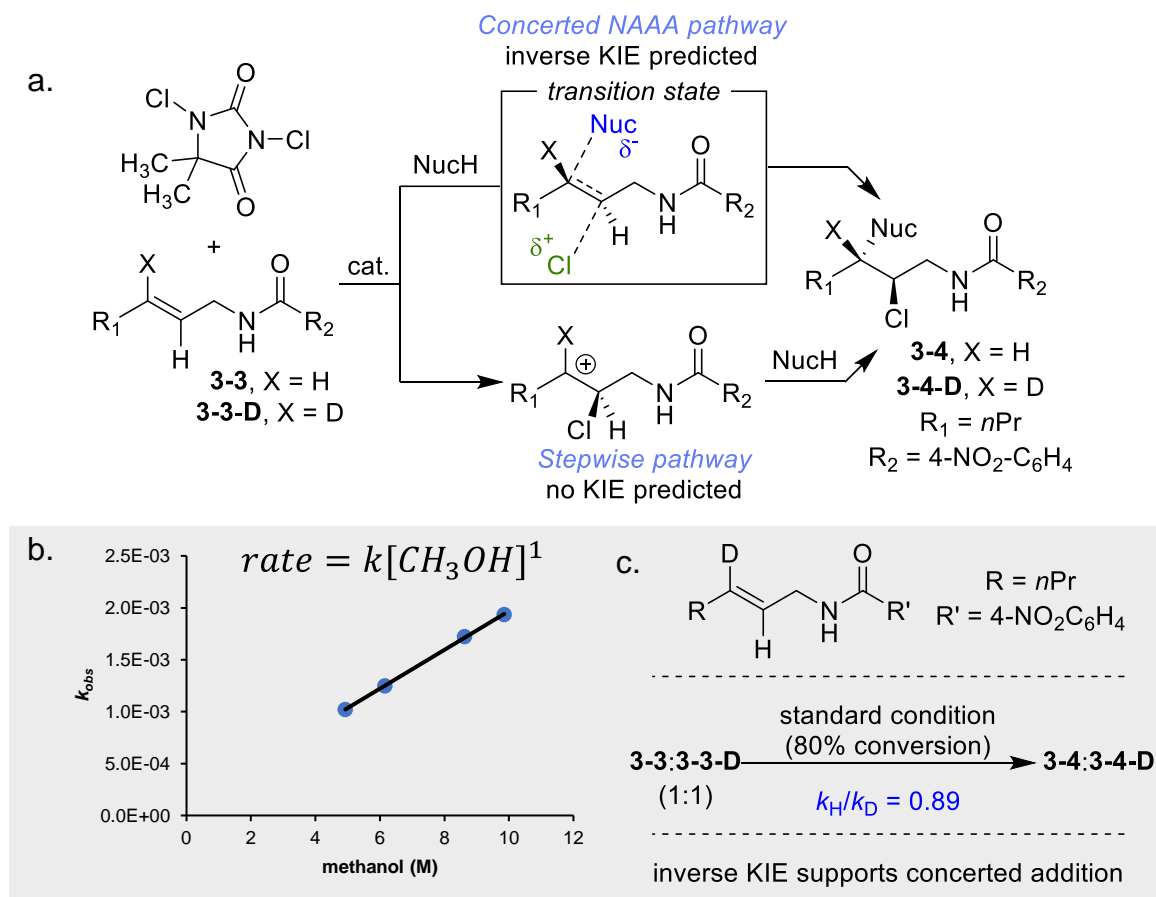
Figure 3.6 Investigating the role of nucleophile. (a) Concerted vs. stepwise alkene chlorofunctionalization. A concerted pathway would involve simultaneous addition of nucleophile (NAAA), while a step wise addition usually involves the nucleophile post chlorenium addition. (b) Finding the pseudo-order of methanol from the rate constant. A first order dependence on methanol concentration supports concerted addition mechanism. (c) Inverse KIE on isotopic substitution center of nucleophilic attack supports a concerted addition pathway over a stepwise addition.

Though it was explored over a range of relatively high concentrations, it could be argued that the observed positive effect of methanol concentration on rate could be an indirect consequence of a change in factors such as solvent polarity and hydrogen bonding. Independent evidence for the direct involvement of the nucleophile as expected in the NAAA pathway was obtained in the form of a kinetic isotopic effect (KIE) study.[33] Specifically, an inverse isotopic effect is anticipated for addition to the deuterated alkene analog **3-3-D** (Figure 3.6c) due to the sp^2 to sp^3 rehybridization during the nucleophilic

145

attack. Little isotopic effect would be expected for a stepwise pathway via a carbocationic or cyclic halonium intermediate, where the center of nucleophilic attack undergoes minimal change in hybridization (Figure 3.6a). In the event, competition experiments conducted with alkenes **3-3** and **3-3-D** resulted in a measured inverse KIE value of 0.89 (Figure 3.6c). Thus, the observed inverse KIE combined with the first-order kinetics in methanol provides conclusive experimental evidence in support of concerted nucleophilic attack (NAAA pathway) in the catalyzed chloroetherification of alkene amide **3-3**.

3.2.5 *Catalyst order*

With the order of alkene **3-3**, DCDMH, and methanol in hand, completing the empirical rate equation required the determination of the order of the catalyst (DHQD)$_2$PHAL. Three experiments with different catalyst loadings of 10 mol% (original condition, 0.004 M), 5 mol%, and 2.5 mol% were investigated while otherwise maintaining identical reaction conditions. Surprisingly, this geometric drop in catalyst loading had little effect on the overall rate of the reaction. Analysis of the data using the VTNA protocol (Figure 3.7a) provided the following completed rate equation, where rate has a near-zero order (0.15) dependence on catalyst:

a.

$$rate = k[(DHQD)_2PHAL]^{0.15}$$

b.
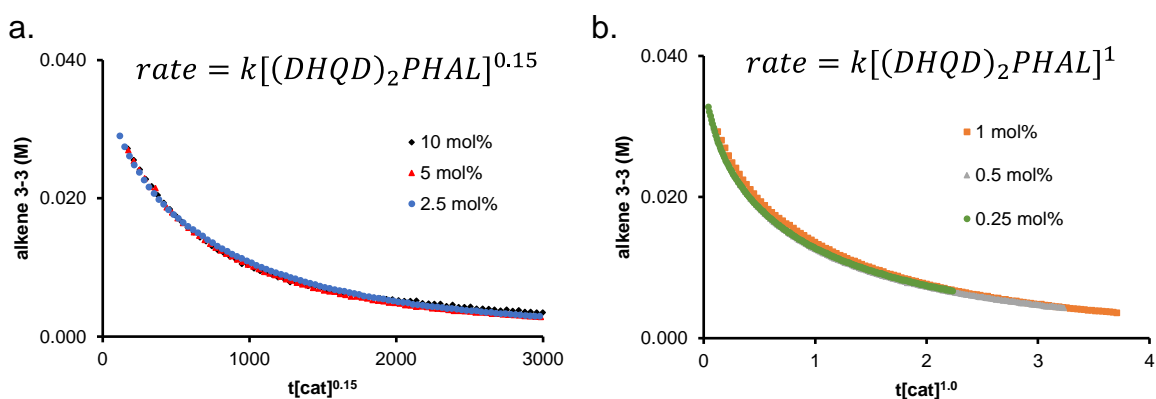
$$rate = k[(DHQD)_2PHAL]^1$$

Figure 3.7 Order of the catalyst (DHQD)$_2$PHAL. (a) Catalyst order is nearly zero (0.15) in the range of 2.5-10 mol% catalyst loading. (b) Lowering the catalyst loading to much value eventually led to an observed first order in catalyst (range 0.25-1.0 mol%).

146

$$rate = k[\textbf{3-3}]^{1.1}[MeOH]^1[DCDMH]^{0.1}[(DHQD)_2PHAL]^{0.15} \qquad eq\ (3.3)$$

Zero-order dependence of a catalyzed reaction rate on catalyst concentration is a rare occurrence. Often the most plausible explanation for such cases is that the rate determining step is outside the catalytic cycle.[34-37] Nonetheless, the first order dependence on alkene and nucleophile indicates that the slowest step for the entire reaction sequence likely precedes the catalytic cycle and involves only the alkene and the nucleophile (methanol, Figure 3.6). This pre-catalytic step could be the association between the alkene and the nucleophile to slowly generate a reactive species, perhaps an NAAA-active conformation, which would be consistent with previous findings with regards to the nucleophile's involvement in a concerted addition mechanism.

3.2.6 Catalytic model

A mechanistic model of catalysis that would fit the findings from the empirically derived rate equation (eq 3.3) is shown in Figure 3.8. This model proposes that alkene amide **3** slowly associates with the nucleophile (methanol) to form a reactive species I_3 in a precatalytic step. I_3 is then quickly siphoned off into the catalytic cycle by the active catalyst complex I_1, the DCDMH-(DHQD)$_2$PHAL bound species. I_1 likely contains an activated chlorenium, which is delivered to the activated alkene complex I_3. This rapidly leads to the chlorofunctionalized product **3-4** along with MCDMH. MCDMH then returns to siphon off some of the catalyst to form an inactive complex I_2, leading to the observed byproduct inhibition as an off-cycle path.

The rate insensitivity to the catalyst concentration begged further examination of the catalyst loading to find the minimum catalyst necessary to maintain the efficiency of the reaction. If a pre-catalytic step is slowly producing a reactive species I_3 that is instantaneously being siphoned off into a catalytic cycle, then at any given moment the

concentration of this reactive species I_3 is exceedingly small. Nonetheless, this would also mean that further lowering catalyst concentration (and in turn I_1) should at some point lead to a small accumulation of I_3, having insufficient I_1 needed for rapid consumption of all I_3. Thus, at a certain lower limit of catalyst loading, the rate should gain a dependence on the catalyst concentration. In fact, this is exactly what was observed; as the catalyst loading was lowered below 1 mol% (0.0004 M), a clear dependence on the catalyst concentration became evident (Figure 3.7b). Lowering the concentration of the catalyst to this range also slightly improved the enantioselectivity of the reaction, allowing for a 10-fold reduction from the previously reported conditions, and importantly, confirming that the reaction is not significantly diluted by background, non-catalyzed processes.
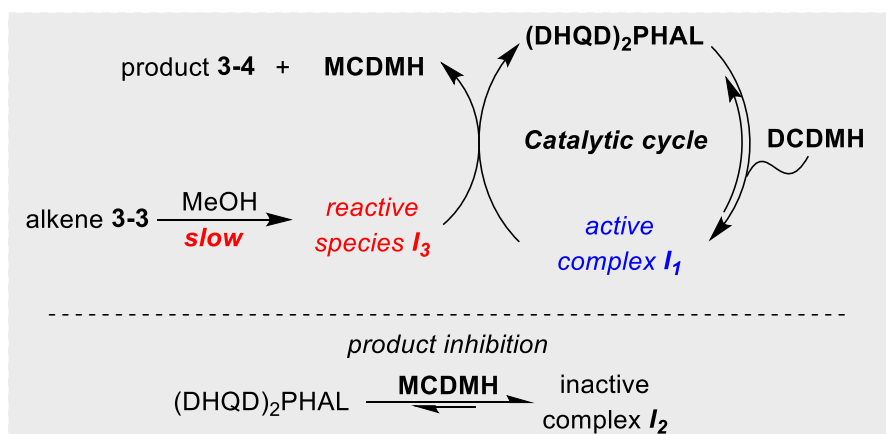
Figure 3.8 Catalytic model. A mechanistic scenario that explains the observed orders of each component, a slow precatalytic step is likely the cause of the observed zero order in catalyst.

The order of every component (alkene, methanol, and DCDMH) was remeasured with 1 mol% catalyst, following the procedures described in previous sections (see SI for details). This led to two distinct rate laws for the two catalyst concentration regimes:

At higher catalyst loading of 2.5-10 mol%

$$rate = k[\mathbf{3-3}]^{1.1}[MeOH]^{1}[DCDMH]^{0.1}[(DHQD)_2PHAL]^{0.15} \qquad \text{eq (3.3)}$$

At lower catalyst loading of 0.25-1.0 mol% catalyst

$$rate = k[\mathbf{3-3}]^{0.9}[MeOH]^1[DCDMH]^{0.8}[(DHQD)_2PHAL]^{1.0} \qquad \text{eq (3.4)}$$

At the lower catalyst loading, the rate now has a first order dependence on DCDMH as well (along with catalyst, alkene and nucleophile). The proposed catalytic cycle (Figure 3.8) does, however, connect the two seemingly disparate rate equations (3.3 and 3.4). A higher catalyst concentration (10 mol%, 0.004 M) drives the formation of I_1, which quickly consumes I_3 as it is slowly generated from alkene amide **3-3** and methanol. The bottleneck for the overall process is the production of I_3 resulting in the observed first order kinetics of alkene **3-3** and methanol, and zero order in catalyst and DCDMH. On the other hand, a drastic cut in the catalyst loading (1 mol%) leads to a significant decline in the concentration of I_1 (due to the reversibility of its formation). This results in an accumulation of I_3 whose consumption now depends on the available concentration of I_1. Thus, now the rate displays a dependence on the concentration of both the catalyst and DCDMH, as amplifying the concentration of either species favors the formation of I_1. This dependence disappears again once the concentration of I_1 exceeds I_3 at high catalyst concentrations.[38]

The combination of the two rate expressions (3.3 and 3.4) along with the inhibition and KIE results presented in prior sections paint a completely novel mechanism for chloroetherification of alkene amides (as shown in Figure 3.8). In the prior model for the chlorolactonization of alkene carboxylic acids, neither zero order catalyst, dual rate law, DCDMH binding of catalyst, nor MCDMH inhibition of reaction were seen.[20] Presumably due to the different solvent systems, (non-polar for chlorolactonization of **3-1**, polar protic for chlorofunctionalization of **3-3**), the two reactions proceed by dramatically different

mechanistic pathways, despite their use of similar reagents. The following sections further investigate the key structural features of the intermediates involved in the reaction.

3.3   Resting state of the catalyst

With kinetics providing insight into the elementary steps of the reaction sequence, further exploration of the nature of the resting state of the catalyst in the catalytic cycle was pursued via NMR spectroscopy. Based on kinetic data, $(DHQD)_2PHAL$ is predicted to have a strong affinity for both DCDMH and MCDMH, resulting in complexes I_1 and I_2 as the active and inactive resting state complexes, respectively (Figure 3.8).

Putatively, $(DHQD)_2PHAL$ and DCDMH form a zwitterionic complex resulting from halogen bonding interaction (Figure 3.9a) between the catalyst's quinuclidine moiety and the chlorenium ion donor. Halogen bond interactions are well-known in the literature with energies that span a range of 2 to 35 kcal/mol.[39] It is conceivable that such an interaction between the nucleophilic quinuclidine nitrogen atom in $(DHQD)_2PHAL$ and the low-lying σ^* of N-Cl in DCDMH, aided by the presence of a polar protic solvent, results in the formation of an ion-pair. In fact, a preliminary look via quantum chemical modeling into this interaction energy between quinuclidine (as a truncated model for the catalyst) and DCDMH revealed a substantially exothermic process of -7.6 kcal/mol (Figure 3.9b). The calculations were performed at the DFT-B3LYP/6-31G*/SM8 (acetonitrile) level. Likewise, MCDMH and quinuclidine formed a halogen bond, albeit weaker (-4.2 kcal/mol. see Figure 3.9b). The lower affinity presumably reflects weaker electrophilicity of the monochloro reagent. Hydrogen bonding with the quinuclidine via the N-H of the MCDMH (see Figure 3.9b) was found to be favored over halogen bonding (-7.8 kcal/mol) and is presumably the preferred mode of catalyst binding and inhibition.
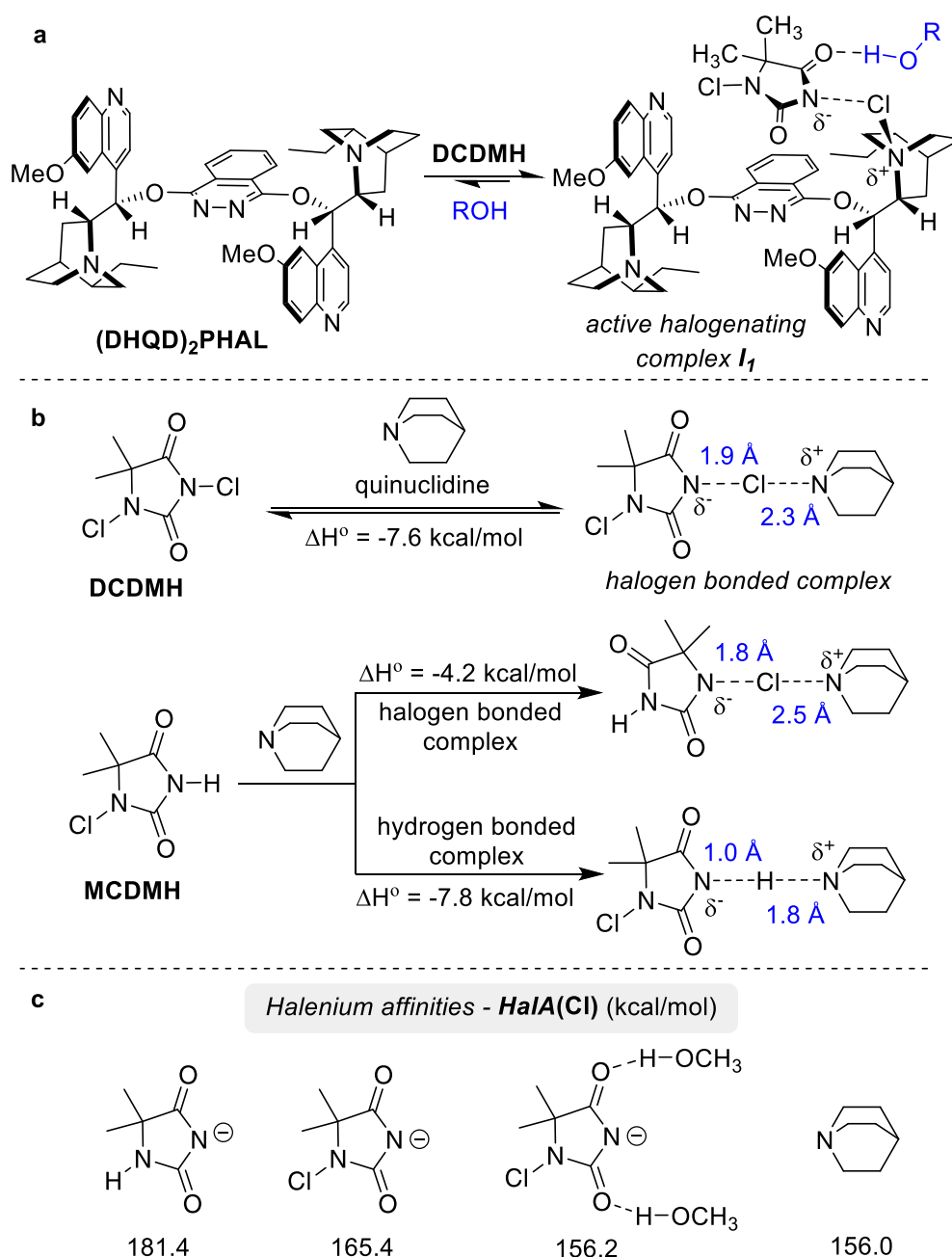
Figure 3.9 Investigating the resting state of the catalyst. (a) DCDMH-(DHQD)$_2$PHAL complexation via halogen bonding to form charge separated intermediate I_1, facilitated in alcoholic solvents. (b) Computational studies suggest significant binding affinity between quinuclidine (truncated catalyst) and chlorenium source DCDMH and MCDMH. Binding enthalpy calculated using DFT-B3LYP/6-31G*/SM8 (acetonitrile) supports the proposed binding model. (c) *HalA*(Cl) calculations further supports chlorenium transfer to quinuclidine nitrogen.

Hydrogen bonding between DCDMH and the protic co-solvent can further facilitate the chlorenium transfer from DCDMH to quinuclidine (Figure 3.9a). Calculations indicate

that a hydrogen bonded 1-chloro-5,5-dimethylhydantoin anion has a much lower halenium ion affinity (*HalA*(Cl) of 156.2 kcal/mol) than one lacking the hydrogen bonded methanol (165.4 kcal/mol), when calculated using DFT-B3LYP/6-31G*/SM8 (acetonitrile) (Figure 3.9c).[40] In fact, under these conditions, the *HalA*(Cl) value of quinuclidine (156.0 kcal/mol) is comparable to that of the hydrogen bonded 1-chloro-5,5-dimethylhydantoin anion. This further supports the hypothesis that, in the polar setting of the chloroetherification reaction, it is feasible for DCDMH to transfer the chlorenium ion to the quinuclidine nitrogen of (DHQD)₂PHAL. This chlorenium transfer to the catalyst nitrogen atom was disfavored in chlorolactonization presumably due to the non-polar solvent conditions which is also supported by prior *HalA*(Cl) calculations.[31]
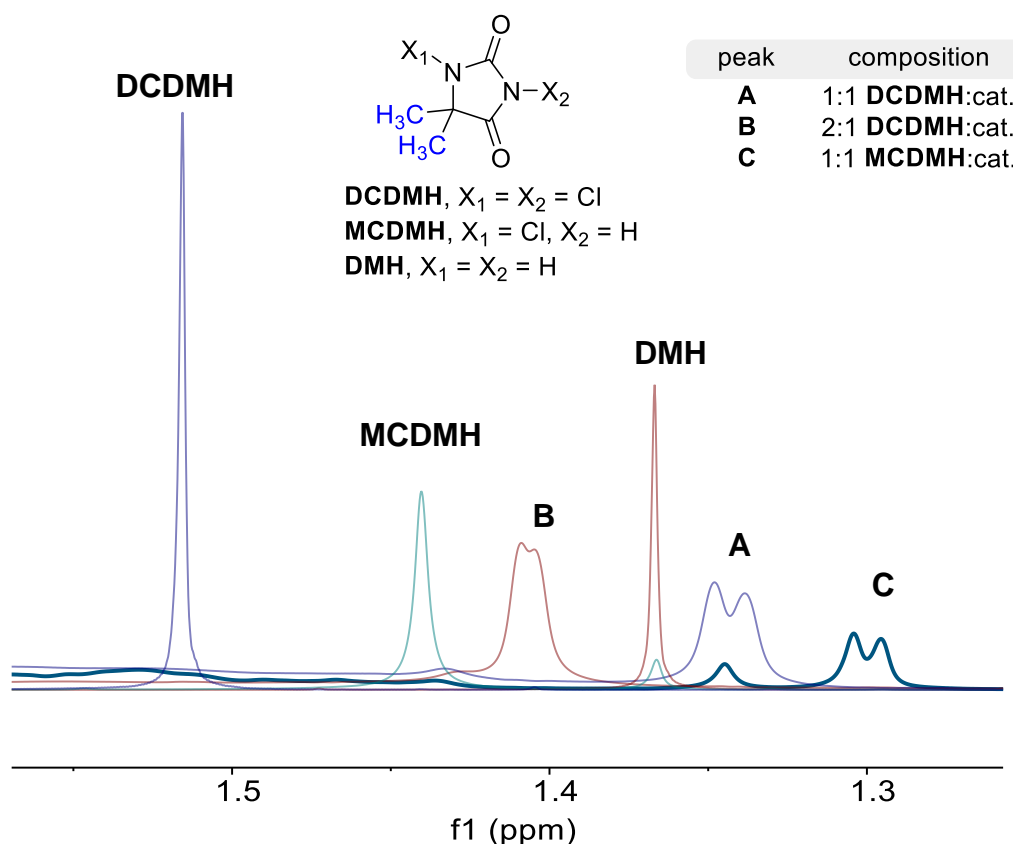
Figure 3.10 NMR evidence towards supporting binding model. Change in ^{1}H NMR chemical shifts of chlorohydantoins DCDMH and MCDMH in presence of catalyst (DHQD)₂PHAL further support the binding model. The spectra were collected at room

(Figure 3.10 (cont'd)) temperature with concentration (DHQD)$_2$PHAL at 0.04 M in acetonitrile-d^3 in 0.4 M HFIP (10 equiv).

The n to σ* donation from catalyst quinuclidine nitrogen to the *N*1-Cl in DCDMH is expected to partially or completely ionize the pair by weakening the *N*1-Cl bond in DCDMH. This should result in an increased negative charge density on DCDMH and positive charge density on the quinuclidine nitrogen atom, an effect that should be reflected in the NMR chemical shift of the respective moieties. Thus, to investigate the (DHQD)$_2$PHAL binding to DCDMH and MCDMH, various mixtures of these species were studied in a series of NMR experiments. The measurements were conducted at room temperature (25 °C) to avoid catalyst precipitation under stoichiometric conditions used for these studies. Methanol was replaced with HFIP (10 equivalents, 0.4 M) as a protic co-solvent with acetonitrile-*d*₃. This was done to avoid DCDMH decomposition to MCDMH, which is prevalent with methanol at room temperature (presumably due to its enhanced nucleophilicity). HFIP and other fluorinated alcohols have been effective as co-solvents in previous reported chlorofunctionalization reactions.[14, 18, 41]

For these experiments, the ^{1}H NMR resonances of the methyl protons in samples of pure DCDMH, MCDMH, and their unchlorinated analog 5,5-dimethylhydantoin (DMH) were measured as controls. The chemical shifts of these methyl protons in various (DHQD)$_2$PHAL-DCDMH and (DHQD)$_2$PHAL-MCDMH mixtures were then remeasured, and their changes were compared against these controls. Figure 3.10 highlights some of the results (for the complete set see SI). The final conclusions are summarized as follows:

1) Addition of 1 equiv. (DHQD)$_2$PHAL to DCDMH shifted the hydantoin's methyl peaks upfield (peak A, Figure 3.10). This large upfield shift suggests negative

charge build up on the hydantoin due to partial or complete de-chlorination at N1 by the nucleophilic nitrogen atom of the catalyst (Figure 3.10).

2)   In the above 1:1 mixture, the DCDMH methyl groups (peak A) are split into two distinct resonances. This diastereotopic splitting indicates that the chlorenium source spends significant time in the chiral cavity.

3)   In the 1:1 mixture, both catalyst and DCDMH resonances exhibit significant line broadening, hinting at a dynamic process. Broadening of the catalyst peaks upon addition of DCDMH is also observed in the spectra from the actual reaction kinetics runs. In the mixture, $(DHQD)_2PHAL$ peaks are broadened to the point where most coupling constants were lost.

4)   In a 2:1 DCDMH-$(DHQD)_2PHAL$ mixture, the DCDMH methyl proton (peak B) shift comes between that of free DCDMH and a 1:1 mixture. This suggests a rapid 1:1 binding exchange between DCDMH-$(DHQD)_2PHAL$ and the free DCDMH, resulting in an averaged chemical shift for DCDMH.

5)   The 1:1 and 2:1 mixtures of MCDMH and $(DHQD)_2PHAL$ display similar trends (upfield chemical shifts of the methyl resonances) along with the induced diastereotopic splitting of the two methyl peaks in MCDMH (1:1 mixture is shown in Figure 3.10, see experimental section for full spectra).

The combined studies strongly suggest that the catalyst $(DHQD)_2PHAL$ undergoes reversible 1:1 binding with DCDMH and MCDMH to form the active and inactive resting state complex I_1 and I_2 respectively, (see Figure 3.8) consistent with the kinetic findings. Unlike the chlorolactonization of alkene carboxylic acids, here the highly polar environment for chloroetherification of alkene amides evidently facilitates formation of the

154

charge separated species present in the complexation of I_1 and I_2. Furthermore, under the reaction conditions, where the concentrations of DCDMH and MCDMH are much higher than the that of catalyst, the total catalyst concentration can be assumed to be effectively shared entirely between I_1 and I_2.

Table 3.1 DOSY NMR of chlorohydantoin-catalyst complexes

composition	^{1}H NMR (ppm)	DOSY coefficient[a]
DCDMH	1.516	0.9375
DCDMH: (DHQD)₂PHAL	1.343 (peak A)[b]	0.5625
MCDMH	1.440	0.5738
MCDMH: (DHQD)₂PHAL	1.300 (peak C)[b]	0.4546

[a]DOSY coefficients were normalized against the solvent acetonitrile; [b]See SI for full DOSY spectra (all DOSY experiments were conducted at 0 °C).

Finally, the ^{1}H NMR studies were complemented with DOSY NMR experiments. Interaction between DCDMH and (DHQD)₂PHAL should slow the diffusion of the smaller, lighter DCDMH resulting in a smaller diffusion coefficient approaching that of the (DHQD)₂PHAL. In order to investigate the extent of binding, DOSY experiments of DCDMH, MCDMH and their 1:1 mixture with (DHQD)₂PHAL (see SI) with 10 equivalents of HFIP were conducted at 0 °C in acetonitrile-d_3. The diffusion coefficients for DCDMH and MCDMH obtained from a mono-exponential were normalized against the diffusion of acetonitrile to compensate for interexperimental differences.[42] As expected, free DCDMH demonstrated a faster diffusion rate (0.9375) as compared to DCDMH in the presence of (DHQD)₂PHAL (0.5625). This 40% drop in the relative rate of diffusion is indicative of DCDMH binding to the (DHQD)₂PHAL. Consistent with formation of I_1 and I_2, a similar effect was observed on the diffusion coefficient of MCDMH (Table 3.1); the slow diffusion of MCDMH itself can be understood in terms of the known tendency of the lactam-type functionality found in MCDMH to self-associate into dimers.[43, 44]

3.4   Catalytic cycle for chloroetherification
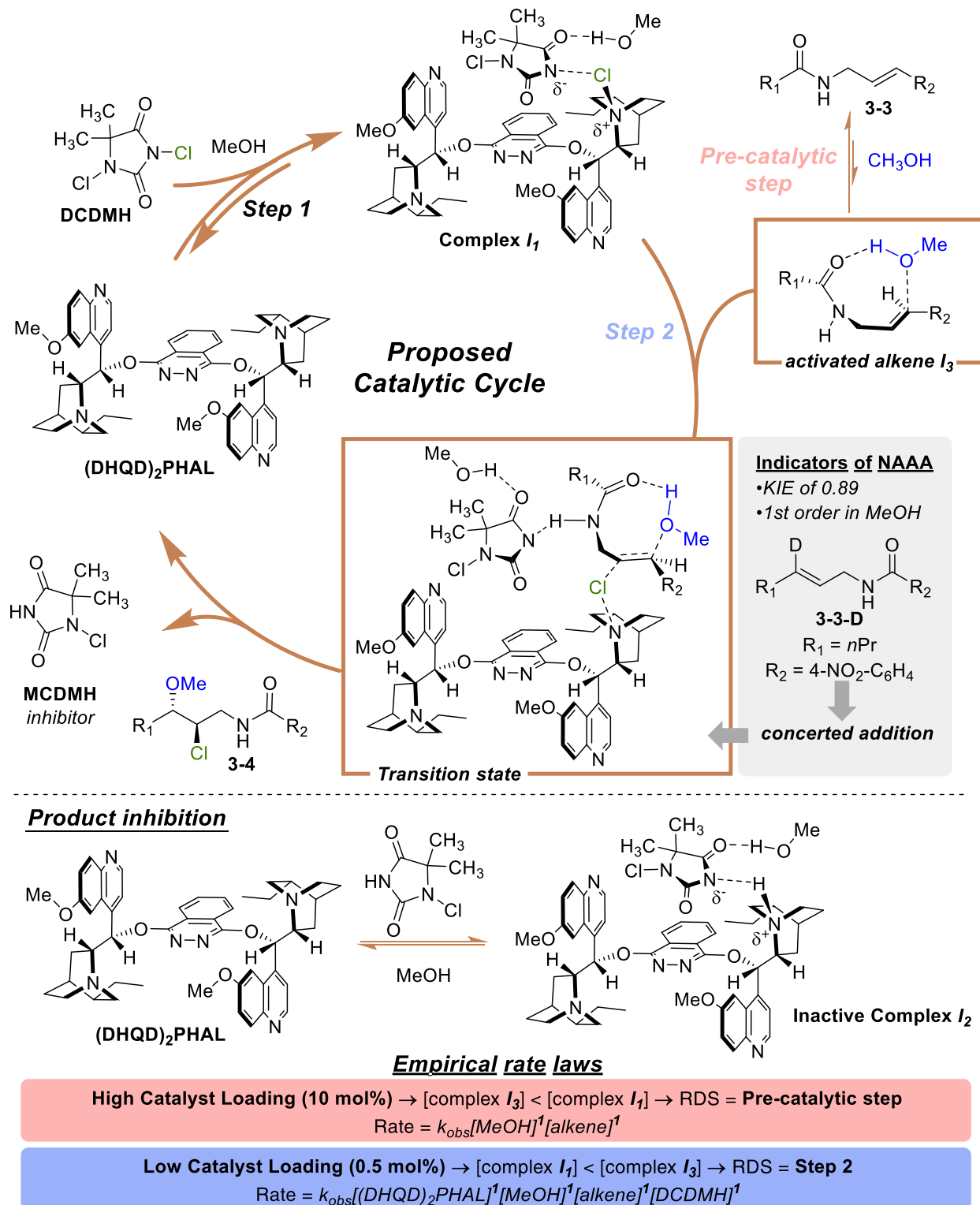
Figure 3.11 Catalytic cycle for chlorofunctionalization of alkene amides. Proposed catalytic cycle for (DHQD)$_2$PHAL catalyzed chloroetherification. The inset in the top left corner presents the empirically estimated rate laws at high and low catalyst concentration

(Figure 3.11 (cont'd)) regimes. The catalytic cycle illustrates that how DCDMH and the MCDMH competes for catalyst binding, with the former leading to a productive intermediate I_1 in the catalytic cycle, while the later leads to an inactive species I_2. Kinetic studies suggest that amide mediated methanol (nucleophile) activation of the alkene, to generate an NAAA active conformation I_3 is likely the slow precatalytic step. Evidence for concerted addition of the methanol is presented in the bottom right shaded box.

To rationalize the combined results of the studies described above, we propose the catalytic cycle illustrated in Figure 3.11. The reaction begins with alkene amide **3** and nucleophile, methanol, forming an activated species I_3, in a pre-catalytic step as supported by the first order dependence of both species on the rate. I_3 is presumably an "NAAA-active" conformation that is primed for the concerted addition of the nucleophile. The rapidly generated DCDMH-(DHQD)$_2$PHAL complex I_1 (Step 1) siphons the nucleophile-activated alkene species I_3 (Step 2, Figure 3.11) into the catalytic cycle, leading to the chlorofunctionalized product **3-4**. The first order rate dependence on methanol, and the observed inverse KIE (Figure 3.6c) supports an NAAA-type concerted addition of the nucleophile and chlorenium ion to the alkene amide **3-3.** This is also in agreement with prior analyses of uncatalyzed chlorofunctionalization of alkene carboxylic acids.[30] Instead of an uncomplexed DCDMH, I_1 is the effective chlorenium ion source, presumably the catalyst chlorinated at the quinuclidine nitrogen atom (Figure 3.11).

Thus, in contradistinction to chlorolactonization of alkene carboxylic acids, which involves direct chlorenium ion transfer from DCDMH to the catalyst-bound alkene center,[19, 20] the chlorinated catalyst here plays the role of chlorenium ion delivery agent in chloroetherification of alkene amides. Consistent with this scenario, our prior studies of (DHQD)$_2$PHAL-catalyzed chloroetherification found essentially identical enantioselectivities, regardless of chlorenium ion donor.[17] The by-product MCDMH exchanges chlorenium ion with DCDMH, and also acts as a weak competitive inhibitor to

the catalyst (Figure 3.11). The proposed catalytic model supports the variable dependence on the concentration of the catalyst, as depicted by the empirical rate laws shown in Figure 3.11 shaded box. At high catalyst concentrations, formation of I_3, via an equilibrium outside of the catalytic cycle, is rate limiting.   But at low catalyst concentrations, Step 2 is the RDS, and the rate shows the expected dependencies on catalyst and chlorenium source, along with the nucleophile and the starting material.

3.5   Investigation into the transition states

While a full-scale computational investigation exploring the labyrinthine route to chloroetherification is beyond the scope of this paper, a few key preliminary findings can be presented to support the discussion. Exploring the possible reaction trajectories while imposing the boundary conditions set by the experimental results, led to the proposed transition state **3-TS1** shown in Figure 3.12a. The calculations were performed at the B3LYP/6-31Gd* level,[45-48] finding an enthalpic barrier of 4.2 kcal/mol for passage over the transition state **3-TS1**. This low barrier explains the fast rate of the chloroetherification of alkene amides (30 min to 2 hours at -30 °C, <1 min at room temp) relative to chlorolactonization (>12 h to completion at -30 °C). In **3-TS1,** the amide functional group directs the nucleophilic attack of methanol via hydrogen bonding, enabling the concerted addition pathway by pre-organizing the NAAA complex (in Figure 3.12a). The concerted addition places the methanol 2.4 Å above the reacting alkenoic center. The chlorenium ion, now delivered by the quinuclidine nitrogen atom to the alkene, is nearly equidistant from the two centers at about 2.2 Å, while the aromatic ring is positioned away from the catalytic center, consistent with the observed tolerance for various aryl substitutions in chlorofunctionalization of alkene amides.[15, 17]

a. Transition state 1 (3-TS1)

1.7 Å

Explicit solvents used as hydrogen bond partners

2.4 Å   2.2 Å   2.2 Å

Quinuclidine-mediated chlorenium ion transfer

Low enthalpic barrier
$\Delta H^\dagger$ = 4.2 kcal/mol (favored)

b. Transition state 2 (3-TS2)

2.3 Å

2.2 Å

2.1 Å   1.7 Å

High enthalpic barrier
$\Delta H^\dagger$ = 12.5 kcal/mol (disfavored)
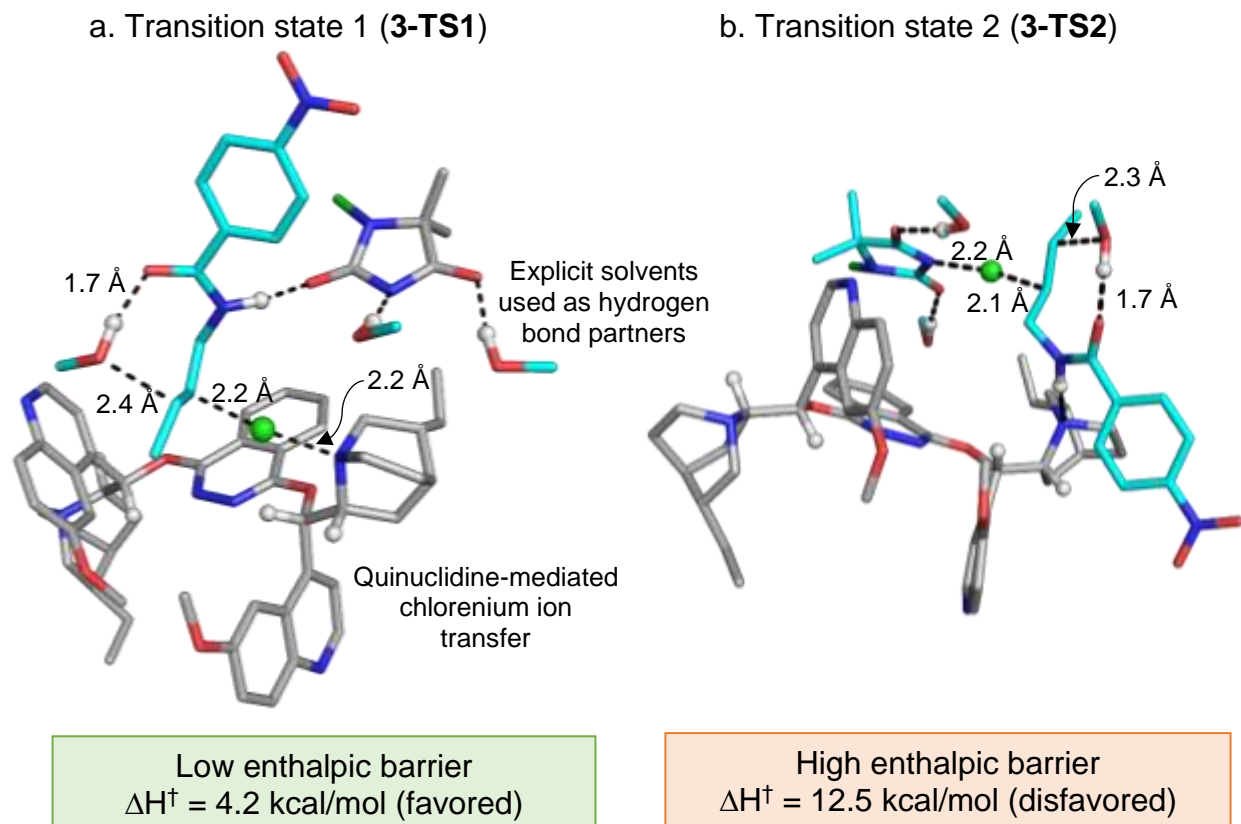
Figure 3.12 Transition state calculations. (a) Computational investigation of the chlorofunctionalization step in (DHQD)$_2$PHAL catalyzed chloroetherification reaction, revealed **3-TS1** to be the most favored transition state. **3-TS1** involved a (DHQD)$_2$PHAL mediated chlo-renium transfer. (b) **3-TS2** represents a low energy alternative transition state that is disfavored over **3-TS1**, in **3-TS2** chlorenium is directly transfer from DCDMH to alkene similar to prior mechanistic reports.

An alternative pathway, where DCDMH transfers the chlorenium ion directly to the alkenoic center (as in chlorolactonization) rather than via quinuclidine was also explored (Figure 3.12b). However, such transition states were disfavored by a minimum of 8 kcal/mol. Similarly, alternative transition states for pathways where the amide is not involved in directing the methanol or those that involved stepwise addition via carbenium or chloriranium ion intermediates were disfavored over the proposed **3-TS1**.

The above transition states were complemented with an experimental exploration into the activation energy barriers using Eryring plots (Figure 3.13). The reaction was studied under a temperature range of -36 to -12 °C. The low enthalpic barrier for the

chloroetherification process (-7.28 kcal/mol) were in alignment with the computational findings. Entropy was found to be the predominant contributor to the overall free energy barrier further supporting the highly organized transition states displayed in Figure 3.12a. The selectivities were found to be negligibly impacted by in the temperature range studied for the eyring plot.

y = -3.67E+03x + 1.94E+00
R² = 9.81E-01
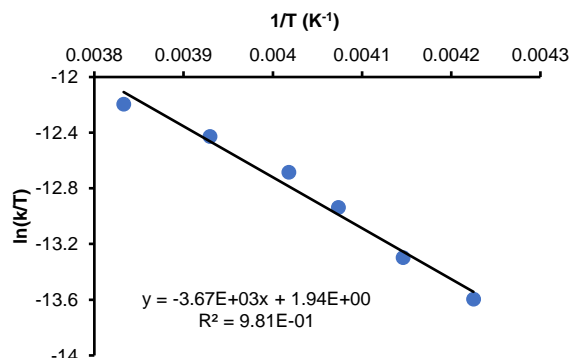
T (°C)	k_{obs}	ln(k/T)	TΔS‡ (kcal/mol)	ΔH‡ (kcal/mol)	ΔG‡ (kcal/mol)
-31.8	4.05E-04	-13.30	-10.46	7.28	17.74
-36.3	2.95E-04	-13.60	-10.26	7.28	17.55
-27.5	5.91E-04	-12.94	-10.64	7.28	17.93
-24.1	7.71E-04	-12.68	-10.79	7.28	18.08
-18.5	1.02E-03	-12.43	-11.03	7.28	18.32
-12.1	1.32E-03	-12.20	-11.31	7.28	18.60

Figure 3.13 Eyring plot. Dissecting the enthalpic vs entropic contribution for chloroetherification using an Eyring plot at 10 mol% catalyst loading.

3.6   Summary

Detailed in this article is a comprehensive mechanistic investigation of (DHQD)$_2$PHAL catalyzed chloroetherification of alkene amides. The study used a combination of modern kinetic techniques, NMR spectroscopy, isotope effects and computations to reveal a novel mechanism of chloroetherification of alkene amide system. The kinetic studies revealed rate to have a first order dependence on the concentration of alkene and a zeroth order dependence on the concentration of DCDMH

under the originally reported reaction condition. This behavior stems from the preferential binding of the DCDMH to the catalyst, resulting in the chlorinating reagent saturating the catalyst. The first order dependence on methanol and the observed inverse kinetic isotopic effect point to a concerted addition of the nucleophile for chloroetherification. Further exploration revealed a zeroth-order dependence in catalyst when the reactions were run under the prior reported conditions (10 mol% catalyst). The study has illustrated two distinct rate laws for the reaction under two different catalyst loading regimes. These discoveries have demonstrated that reaction efficacy is preserved even after a 10-fold lowering in catalyst loading, improving upon the original reported conditions. The study has also dissected out several on- and off-cycle equilibria modulating the reactivity of the species involved in the reaction, such as inhibition by the by-product MCDMH. The spectroscopic and computational investigation found the chlorenium ion to take a completely novel route to reach the alkene from its source by shuttling via the quinuclidine moiety of the catalyst. Finally, the amide functional group appears to activate the methanol for its nucleophilic attack via hydrogen bonding.

These mechanistic discoveries in (DHQD)$_2$PHAL catalyzed chloroetherification stand in contrast to the prior mechanistic report of chlorolactonization in almost every aspect. Furthermore, the mechanistic differences between these two ostensibly similar reactions encourage vigilance in extrapolating mechanistic conclusions. Consistent with earlier findings of selectivity inversion,[13] these differences can be associated to the drastic changes in the nature of solvent (polar protic vs non-polar) and substrate (alkene amide vs alkene carboxylic acid) functional groups in the two reactions. Though the greatest lesson of this work is to avoid facile generalization of mechanisms from one reaction to

another, we hope that the present account will prove valuable in analysis and reaction design, especially for the fast-growing family of (DHQD)$_2$PHAL-catalyzed alkene amide chlorofunctionalizations, which are typically run under similar media and conditions.

3.7   Experimental detail

3.7.1 General remarks

Unless otherwise mentioned, solvents were purified as follows. Molecular sieves (4 Å) were dried at 160 °C under 0.25 mtorr pressure prior to use. CHCl$_3$ (amylene stabilized) was purchased from Sigma Aldrich and incubated over 4 Å MS for 48 h prior to use. Toluene and CH$_2$Cl$_2$ were dried over CaH$_2$, whereas THF and Et$_2$O were dried over sodium (dryness was monitored by colorization of benzophenone ketyl radical); all were freshly distilled prior to use. Deuterated solvents such as acetonitrile-d_3, methanol-d_4 and CDCl$_3$ were purchased from Sigma Aldrich but were dried further over 4 Å molecular sieves for 48 h prior to use.

All NMR spectra were obtained using an autosampler-equipped Agilent 500 MHz NMR, Varian Inova 500 MHz NMR, and Varian Inova 600 MHz NMR instruments and referenced using the residual ^{1}H peak from the deuterated solvent. All kinetic experiments were run on the Varian Inova 500 MHz NMR and Varian Inova 600 MHz NMR instruments fitted with chillers. Infrared spectra were measured on a JASCO 6600 FT-IR fitted with an ATR probe. Waters 2795 (Alliance HT) instrument was used for HRMS (ESI) analysis with polyethylene glycol (PEG-400-600) as a reference.

Column chromatography was performed using Silicycle 60Å, 35-75 µm silica gel. Pre-coated 0.25 mm thick silica gel 60 F254 plates were used for analytical TLC and visualized using UV light, iodine, potassium permanganate stain, *p*-anisaldehyde stain or phosphomolybdic acid in EtOH stain.

162

Chlorofunctionalization reactions were performed in the absence of light. 1,3-Dichloro-5,5-dimethylhydantoin (DCDMH) and 3-chloro-5,5-dimethylhydantoin (MCDMH) were recrystallized prior to use. Alkenoic amide **3-3** was prepared as described previously.[17] All other commercially available reagents and solvents were used as received unless otherwise mentioned.

3.7.2 Kinetic Studies

3.7.2.i Experimental procedure

The NMR probe was cooled to -32 °C and allowed to equilibrate for at least for 1 hour prior to use. The volume of reaction mixture in each NMR experiment was 0.8 mL after addition of all the substrates, reagents, catalyst, internal standard, additive or additional solvent. A 0.16 M stock solution of the internal standard, 1,1,2,2-tetrachloroethane (TCE), was prepared by dissolving 34 µl (0.32 mmol) of TCE in 1966 µL of the solvent (deuterated methanol:acetonitrile, 3:7 v/v). From this solution, 0.2 mL was used for each experiment to attain the final molarity of 0.04 M. A 0.16 M stock solution of the alkene **3-3**, was prepared by dissolving 0.32 mmol (79.4 mg) of alkene in 2 mL of the solvent, from which an appropriate amount was used for each experiment. Similarly, a 0.016 M stock solution of the (DHQD)$_2$PHAL was prepared by dissolving 0.032 mmol (24.9 mg) of the catalyst in 2 mL of the solvent, from which an appropriate amount was used for each experiment. The stock solution of DCDMH was prepared fresh in small batches before each experiment by dissolving 0.128 mmol (25.2 mg) of DCDMH in 0.4 mL of solvent, which was frozen immediately until use. From the stock solution, appropriate amounts of alkene, internal standard and catalyst were syringed into a dry NMR tube under nitrogen. This NMR tube was placed in the temperature equilibrated NMR and was subsequently tuned, locked and shimmed to collect a pre-reaction

spectrum. Further spectral collection parameters for the kinetic study were set at this point. The sample was then ejected and immediately placed in -78 °C bath. The appropriate amount of DCDMH was then added from its thawed solution to start the reaction. The entire mixture was shaken to homogeneity, wiped, and placed back in the -32 °C NMR. The NMR was quickly locked and shimmed and the array of spectral collection was begun. The exact time of addition of the DCDMH to the reaction mixture was noted down in seconds and was marked as the start of the reaction. The time of each NMR spectrum collected during the experiment was normalized to this exact time of DCDMH addition to accurately define the starting point of every reaction.

3.7.2.ii Kinetic analysis protocols

The spectra collected were analyzed using the MestReNova software package. Each spectrum was phased, and baseline corrected prior to integration. Figure 3.14a depicts an example of the concentration profile extracted from the spectral analysis of a kinetic experiment run under the standard condition. Vinylic proton of the alkene **3-3** (H_a) was chosen for analysis of its concentration, the corresponding proton for the product **3-4** (H_b) was used to calculate the product concentration (Figure 3.14b). Figure 3.14b also depicts a pair of replicate experiments (Exp 1 and 2 are replicates) illustrating reproducibility of the obtained concentration profile.
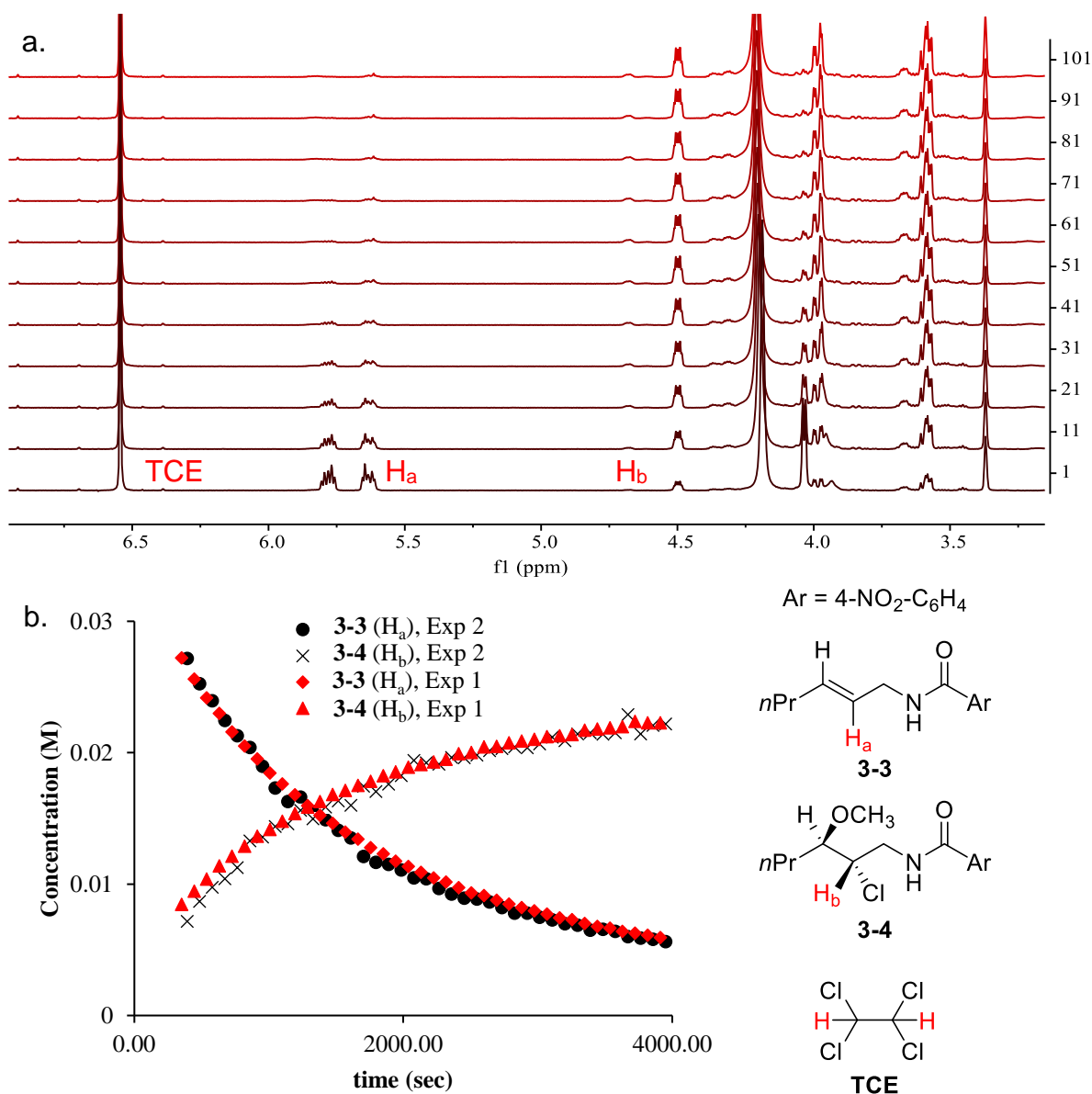
Figure 3.14 Kinetic study procedures. (a) Sample NMR spectra from kinetic study used to generate the concentration profile. (b) Concentration profile of alkene and product.

In accord with the reaction progress kinetic analysis (RPKA) methods,[23, 24] *"different excess"* experiments were conducted to establish the orders of the alkene and the DCDMH. The *"excess"* amounts of DCDMH were chosen as 0.02 and 0.04 M (Table 3.3), with the alkene being the limiting substrate. Similarly, *"same excess"* experiments were conducted to show the effect of any product inhibition or catalyst deactivation (Table 3.4). A set of experiments with varying concentrations of catalyst enabled the

determination of catalyst reaction order (Table 3.5). The variable time normalized analysis (VTNA) protocols were used to analyze the reaction kinetics.[26-28] Based on VTNA, visual overlay of the different datasets enables the determination of the order of each of these components. These plots will be shown in the following sections.

Methanol, being a solvent component, is expected to have a pseudo order impact on rate. The order of methanol was determined from the rate constant measurements from a series of reactions run with varying concentration of methanol. This procedure will be discussed in more detail in following sections.

Two sets of experiments were conducted to determine the order of the alkene, DCDMH and methanol. The first set was run with 10 mol% catalyst (DHQD)$_2$PHAL and second set with 1 mol% (DHQD)$_2$PHAL. In all studies, 0.04 (M) TCE was used as an internal standard.

3.7.2.iii Measuring concentration of DCDMH and MCDMH

Concentrations of the alkene **3-3** or the product **3-4** could be easily determined from peak integration against the internal standard (TCE). However, since DCDMH and MCDMH displayed a combined averaged peak (Figure 3.15a, also discussed in the main text), measuring their concentrations required a separate approach. External calibration curves had to be generated prior to every experiment to quantify their concentrations (Figure 3.15b). Each calibration curve related the averaged chemical shift of the methyl peaks of DCDMH and MCDMH at varying mole fraction (**X**) ratios totaling 0.08 M for their combined concentration, measured under the corresponding reaction conditions. This allowed their actual concentrations to be determined from the observed chemical shift during the course of the reaction. A reasonable assumption here is that the total

concentration of DCDMH + MCDMH during the reaction course is the same as the initial

concentration of DCDMH for that reaction. An example is shown below (Figure 3.15).

Table 3.2 Calibration curve table for a reaction using initial concentration of 0.08 M for DCDMH

DCDMH (M)	MCDMH (M)	X_{DCDMH}	δ (ppm)
0	0.08	0	1.3702
0.08	0	1	1.4531
0.04	0.04	0.5	1.4108
0.07	0.01	0.875	1.4403
0.06	0.02	0.75	1.4312
0.05	0.03	0.625	1.4224
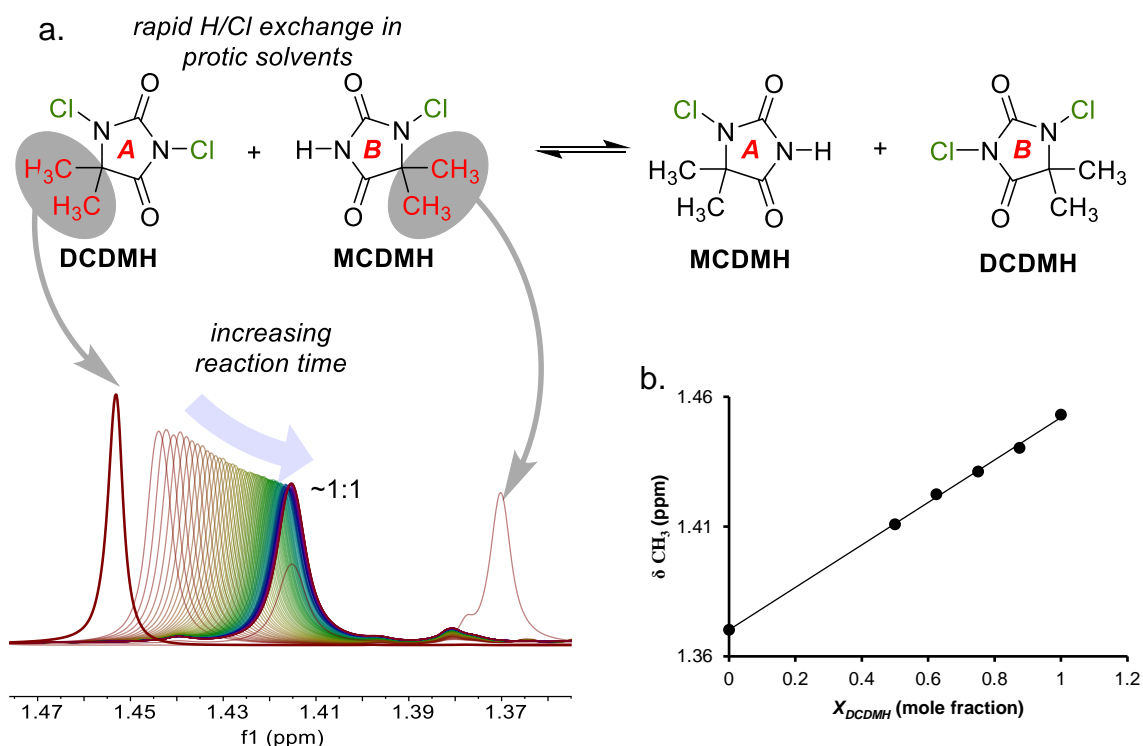
Figure 3.15 Quantifying concentration of DCDMH. (a) Displayed above is the change in chemical shift of the averaged methyl peak of DCDMH and MCDMH over the course of the reaction. (b) Example of a calibration curve used to quantify DCDMH and MCDM concentrations for the kinetic study.

3.7.3 Kinetic analysis results

3.7.3.i Order of alkene 3-3 and DCDMH in 10 mol% (DHQD)$_2$PHAL

The following experiments shown in Table 3.3 were utilized to find the order of the alkene **3-3** and DCDMH using VTNA protocols.

Table 3.3 Different excess experiments for VTNA studies

Exp	3-3 (M)	DCDMH (M)	(DHQD)$_2$PHAL (mol%)	Excess (M)
A	0.04	0.08	10	0.04
B	0.06	0.08	10	0.02
C	0.04	0.06	10	0.02
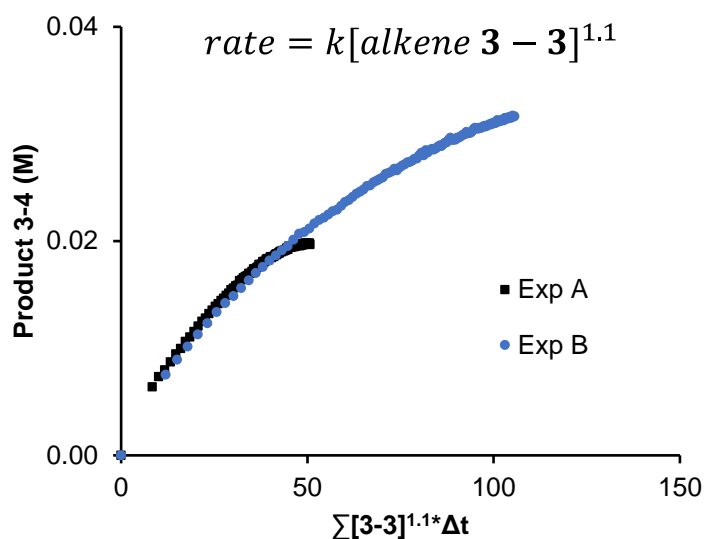
Figure 3.16 Finding Order of alkene amides 3-3 at high catalyst loading. The plot represents the VTNA analysis of a pair of different excess experiments conducted to find the order of alkene **3-3**. The plots corresponding to experiments A and B overlay when the alkene term in the time-normalized axis is raised to the power of 1.1, revealing it to be the correct order for the alkene.

The time normalized (*x*-axis) axis utilized for VTNA analysis represent the time integral form of the concentration of the respective species.[26] For the above case, it is represented by:

$$\Sigma[3-3]^{1.1} * \Delta t = \int_{t=0}^{t=n}[3-3]^{1.1}dt = \Sigma_{i=1}^{n}\left(\frac{[3-3]_i - [3-3]_{i-1}}{2}\right)^{1.1}(t_i - t_{i-1}) \qquad \text{eq (3.5)}$$
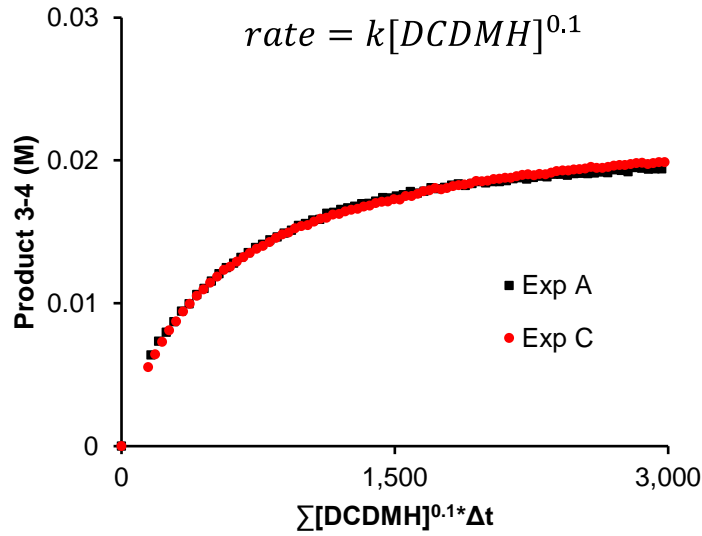
Figure 3.17 Finding order of DCDMH at high catalyst loading. The plot represents the VTNA analysis of a pair of different excess experiments conducted to find the order DCDMH. The plots corresponding to experiments A and C overlay when the DCDMH term in the time-normalized axis is raised to the power of 0.1, revealing it to be the order for DCDMH.

The time normalized axis is represented by:

$$\sum [DCDMH]^{0.1} * \Delta t = \int_{t=0}^{t=n} [DCDMH]^{0.1} dt = \sum_{i=1}^{n} \left(\frac{[DCDMH]_i - [DCDMH]_{i-1}}{2} \right)^{0.1} (t_i - t_{i-1})$$

eq (3.6)

3.7.3.ii Same excess experiments

The experiments in Table 3.4 were utilized to determine the effect of product inhibition or catalyst deactivation using VTNA protocols.

Table 3.4 Same excess experiments for VTNA studies

Exp	3-3 (M)	DCDMH (M)	(DHQD)$_2$PHAL (mol%)	Excess (M)	Additive (M)
B	0.06	0.08	10	0.02	-
C	0.04	0.06	10	0.02	-
D	0.04	0.06	10	0.02	0.02, MCDMH
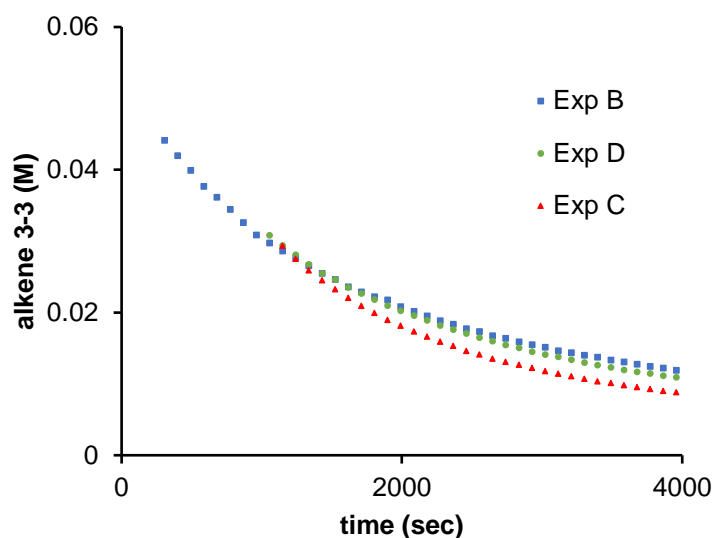
Figure 3.18 Same excess experiments. The above are a set of same-excess experiments. The non-overlay of the concentration vs time profiles of experiments B and C indicates either catalyst deactivation or product inhibition during the reaction course. Overlay of experiment D, which is identical to experiment C with the exception of the added MCDMH, indicates product inhibition by MCDMH.

3.7.3.iii Order of (DHQD)₂PHAL in the 2.5-10 mol% loading regime

The following experiments in Table 3.5 were utilized to determine the order of the

catalyst using VTNA protocols.

Table 3.5 Experiments with different catalyst concentration

Exp	3-3 (M)	DCDMH (M)	(DHQD)₂PHAL (mM)	Excess (M)
A	0.04	0.08	4.0 (10.0 mol%)	0.04
E	0.04	0.08	2.0 (5.0 mol%)	0.04
F	0.04	0.08	1.0 (2.5 mol%)	0.04
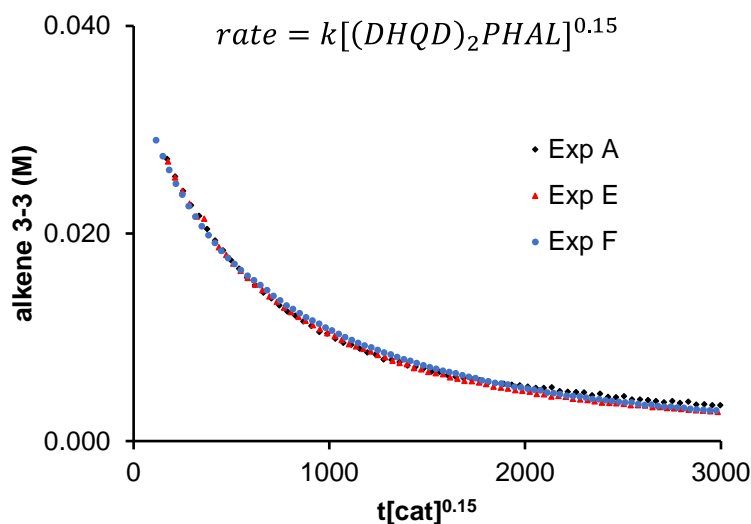
Figure 3.19 Order of catalyst (DHQD)₂PHAL at high catalyst loading. The plot represents the VTNA analysis of a series of experiments with varying concentrations of the catalyst (DHQD₂PHAL to find its order. The plots corresponding to experiments A, E, and F overlay when the catalyst term in the time-normalized axis is raised to the power of 0.15, revealing its order to be nearly zero.

171

3.7.3.iv Order of methanol at 10 mol% (DHQD)$_2$PHAL

For a general rate law equation, Rate = k_{obs}[**3-3**]^x[DCDMH]^y where the [methanol] is much greater than [alkene] or [DCDMH], the order of the methanol will be included in the observed rate constant $k_{obs}=k'$[CH$_3$OH]^z. To extract the order of methanol from the observed rate constant (k_{obs}) the following steps were taken.

1) To determine the order of methanol a series of four kinetic experiments were run with different concentrations of methanol (Table 3.6). For each experiment different methanol-acetonitrile ratios were used while maintaining a constant total solvent volume of 0.8 mL. This held the concentration of the reaction components identical in each case (0.04 M alkene, 0.08 M DCDMH and 4.0 mM (DHQD)$_2$PHAL).

Table 3.6 Experiments with different concentration of methanol

Exp	Methanol (M)	k_{obs}	ln[CH$_3$OH]	ln(k_{obs})
1	4.92	1.02E-03	1.59	-6.89
2	6.15	1.23E-03	1.82	-6.69
3	8.62	1.72E-03	2.15	-6.36
4	9.85	1.93E-03	2.29	-6.25

2) The concentration profile for each of these experiments were fitted with a 6th order polynomial. Rate was determined from the derivative of this 6th order polynomial (Figure 3.20 shows the concentration profile for experiment 2 of Table 3.6).
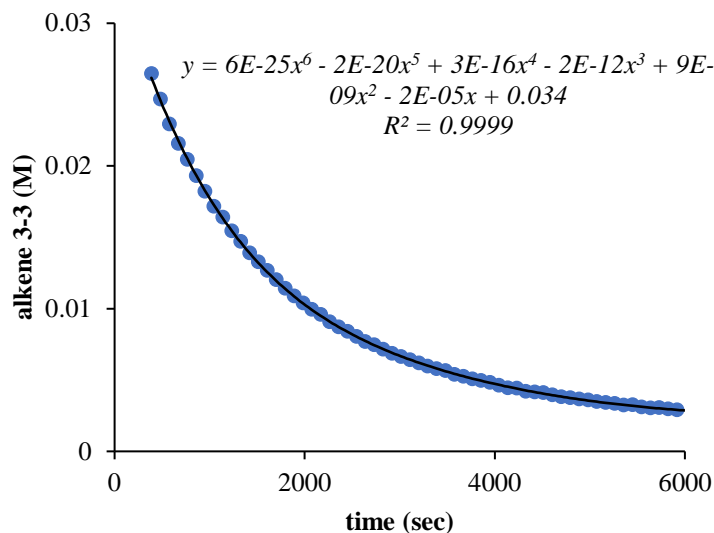
Figure 3.20 Concentration profiles used to find rate constants. An example of the concentration profile of alkene **3-3** fitted with a 6th order polynomial, which will be subsequently used to determine rate as a function of reaction time.

3)   Based on the rate equation, rate = k[**3-3**]^x[DCDMH]^y, rate is expected to be linear

function of the variable [**3-3**]^x[DCDMH]^y. Thus, the slope of the rate vs [**3-3**]^x[DCDMH]^y plot is expected to yield the observed rate constant (k_{obs}). The

following is an example of such a plot with the slope of the linear fit used as the

rate constant (Figure 3.21).
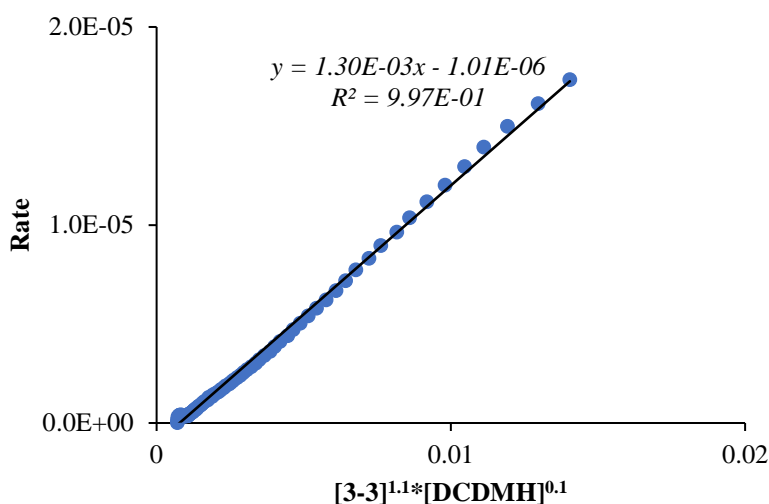
Figure 3.21 Rate profiles used to extract the rate constants. An example of rate vs [**3-3**]^x[DCDMH]^y plot used to extract the observed rate constant.

173

4) The order of methanol can now be obtained in two ways. First by plotting the concentration of methanol against the rate constant (k_{obs}) (Figure 3.22a). A linear change of k_{obs} with methanol would indicate a first order effect. Second, a log of the obtained rate constant against the log of the concentration of the methanol (Figure 3.22b). In this case the slope of the trend would indicate the methanol order. This was found to be 0.9.

a.

b.
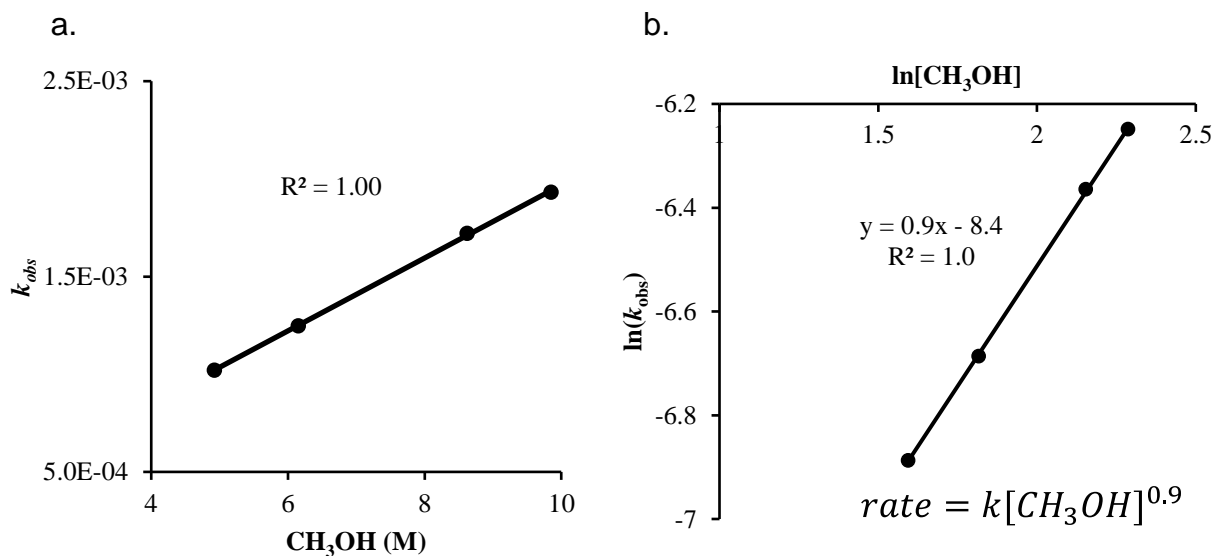
Figure 3.22 Finding order of methanol (nucleophile) at high catalyst loading. (a) Plot of k_{obs} vs CH3OH to find the order of methanol. (b) Plot of lnk_{obs} vs ln[CH3OH] to find the order of methanol.

3.7.3.v Order of alkene 3-3 and DCDMH in 1 mol% (DHQD)₂PHAL

The following experiments shown in Table 3.7 were utilized to find the order of the alkene **3-3** and DCDMH using VTNA protocols.

Table 3.7 Different excess experiments for VTNA studies

Exp	3-3 (M)	DCDMH (M)	(DHQD)₂PHAL (mol%)	Excess (M)
G	0.04	0.08	1	0.04
H	0.06	0.08	1	0.02
I	0.04	0.06	1	0.02

$$rate = k[alkene\ \mathbf{3-3}]^{0.9}$$
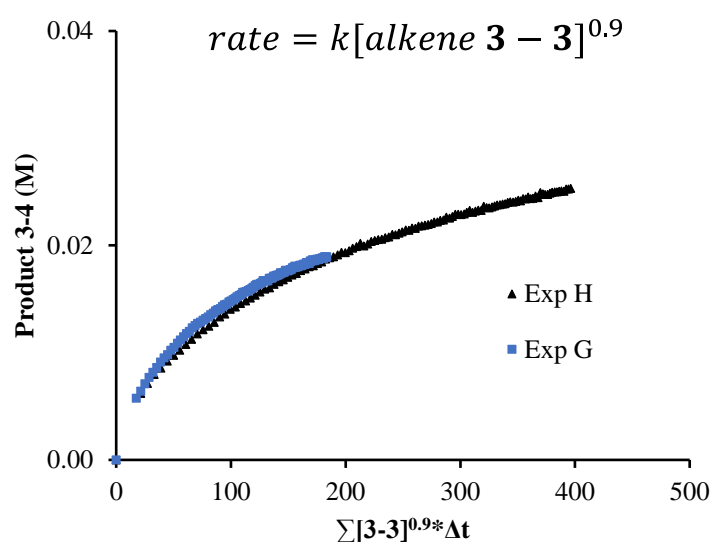
Figure 3.23 Finding order of alkene amide 3-3. The plot represents the VTNA analysis of a pair of different excess experiments conducted to find the order of alkene **3-3**. The plots corresponding to experiments G and H overlay best when the alkene term in the time-normalized axis is raised to the power of 0.9, which is taken to be the reaction order of the alkene.

The time normalized axis is represented by:

$$\sum[\mathbf{3-3}]^{0.9} * \Delta t = \int_{t=0}^{t=n}[\mathbf{3-3}]^{0.9}dt = \sum_{i=1}^{n}\left(\frac{[3-3]_i - [3-3]_{i-1}}{2}\right)^{0.9}(t_i - t_{i-1}) \qquad \text{eq (3.7)}$$
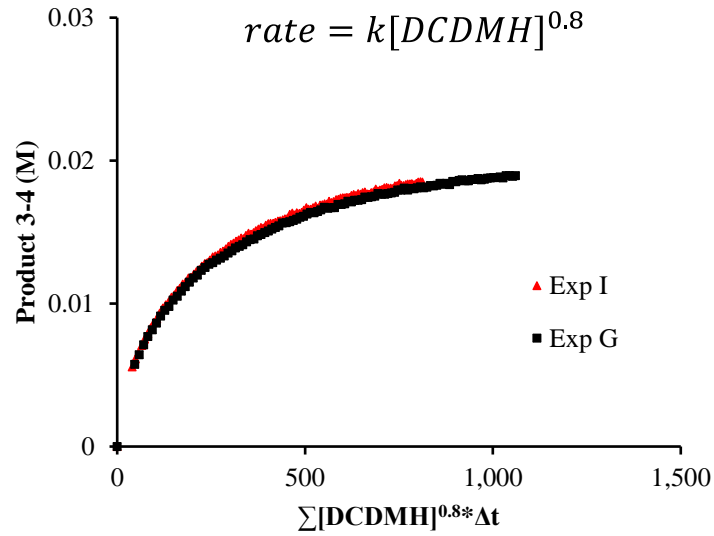
Figure 3.24 Finding order of DCDMH. The plot represents the VTNA analysis of a pair of different excess experiments conducted to find the order of DCDMH. The plots corresponding to experiments G and I overlay when the DCDMH term in the time-normalized axis is raised to the power of 0.8, which is taken to be the order of the DCDMH.

The time normalized axis is represented by:

$$\sum[\boldsymbol{DCDMH}]^{0.8} * \Delta t = \int_{t=0}^{t=n}[\boldsymbol{DCDMH}]^{0.8} dt = \sum_{i=1}^{n}\left(\frac{[\boldsymbol{DCDMH}]_i - [\boldsymbol{DCDMH}]_{i-1}}{2}\right)^{0.8}(t_i - t_{i-1})$$

eq (3.8)

3.7.3.vi Order of (DHQD)₂PHAL in the 2.5-10 mol% loading regime

The following experiments in Table 3.8 were utilized to determine the order of the catalyst using VTNA protocols.

Table 3.8 Experiments with different catalyst concentration

Exp	3-3 (M)	DCDMH (M)	(DHQD)₂PHAL (mM)	Excess (M)
G	0.04	0.08	0.4 (1.0 mol%)	0.04
J	0.04	0.08	0.2 (0.5 mol%)	0.04
K	0.04	0.08	0.1 (0.25 mol%)	0.04

$$rate = k[(DHQD)_2 PHAL]^1$$
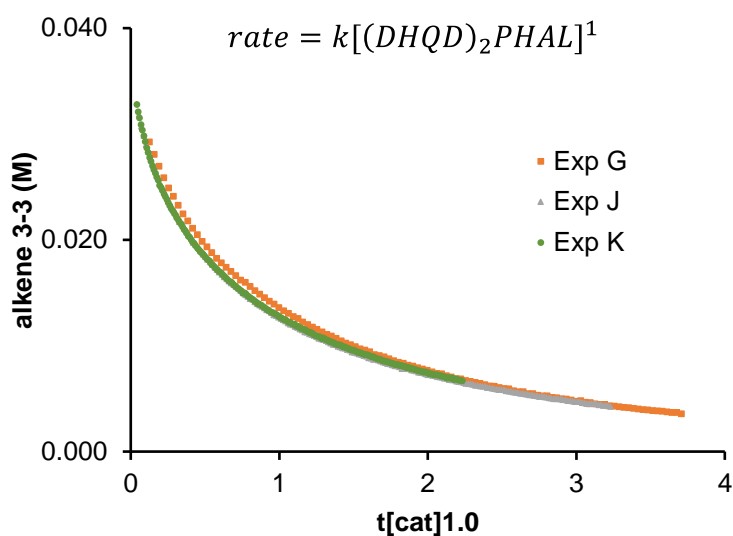
Figure 3.25 Finding order of (DHQD)₂PHAL at low catalyst loading. The plot represents the VTNA analysis of a series of experiments with varying concentrations of the catalyst (DHQD)₂PHAL to find its order. The plots corresponding to experiments G, J, and K overlay when the catalyst term in the time-normalized axis is raised to the power of 1.0.

3.7.3.vii Order of methanol at 10 mol% (DHQD)₂PHAL

The order of methanol was determined using the same procedure as depicted in Section iv. The following represents the final two plots leading to the order of methanol from k_{obs}.
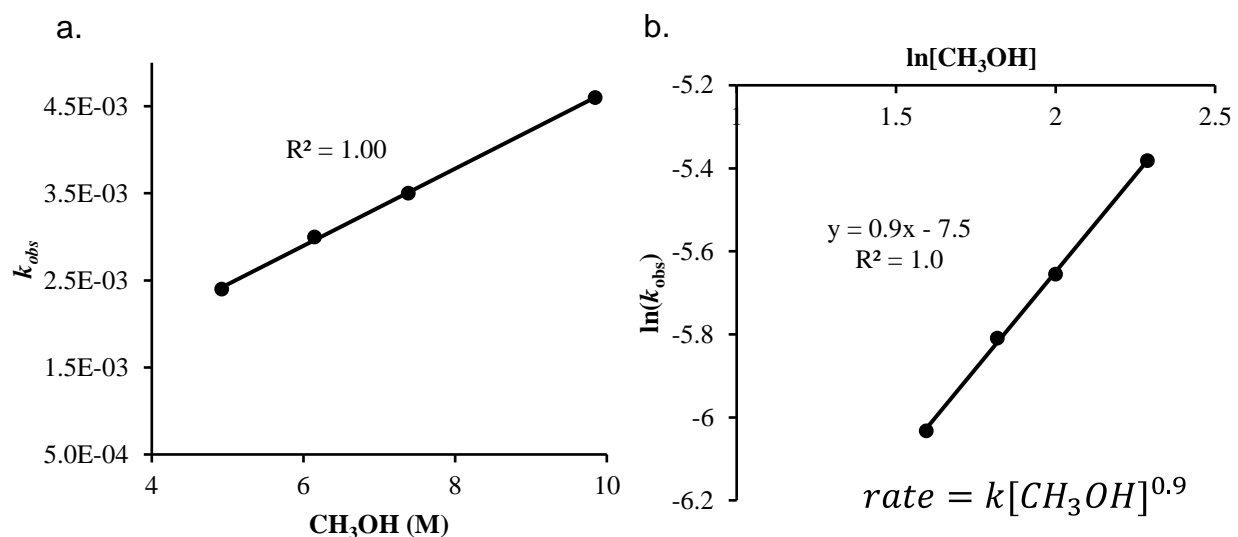
Figure 3.26 Finding order of methanol (nucleophile) at low catalyst loading. (a) Plot of k_{obs} vs CH₃OH to find the order of methanol. (b) Plot of lnk_{obs} vs ln[CH₃OH] to find the order of methanol.

3.7.3.viii Empirical rate laws in different catalyst loading regime

The following represent the rate law equations at the two catalyst concentration regime:

Rate law equation at high catalyst loading of <u>2.5-10.0 mol%</u>

$$Rate = k[\mathbf{3-3}]^{1.1}[MeOH]^{0.9}[DCDMH]^{0.1}[(DHQD)_2PHAL]^{0.15} \qquad \text{eq (3.9)}$$

Rate law equation at lower catalyst loading of <u>0.25-1.0 mol% catalyst</u>

$$Rate = k[\mathbf{3-3}]^{0.9}[MeOH]^{0.9}[DCDMH]^{0.8}[(DHQD)_2PHAL]^{1.0} \qquad \text{eq (3.10)}$$

3.7.3.ix Effect of additives

To explore possible binding of amide to the catalyst (DHQD)₂PHAL, the reaction was doped with 0.5 equivalent of alkane amide **3-5** (experiment L, Table 3.9). This additive had a negligible impact of the kinetic profile of the reaction indicating that amides **3-3** or **3-5** do not competitively bind to the catalyst, in contrast to the behavior of MCDMH.

Table 3.9 Experiments with different catalyst concentration

Exp	3-3 (M)	DCDMH (M)	(DHQD)₂PHAL (mol%)	Additive
A	0.04	0.08	10	-
L	0.04	0.08	10	0.02 (M) of **3-5**
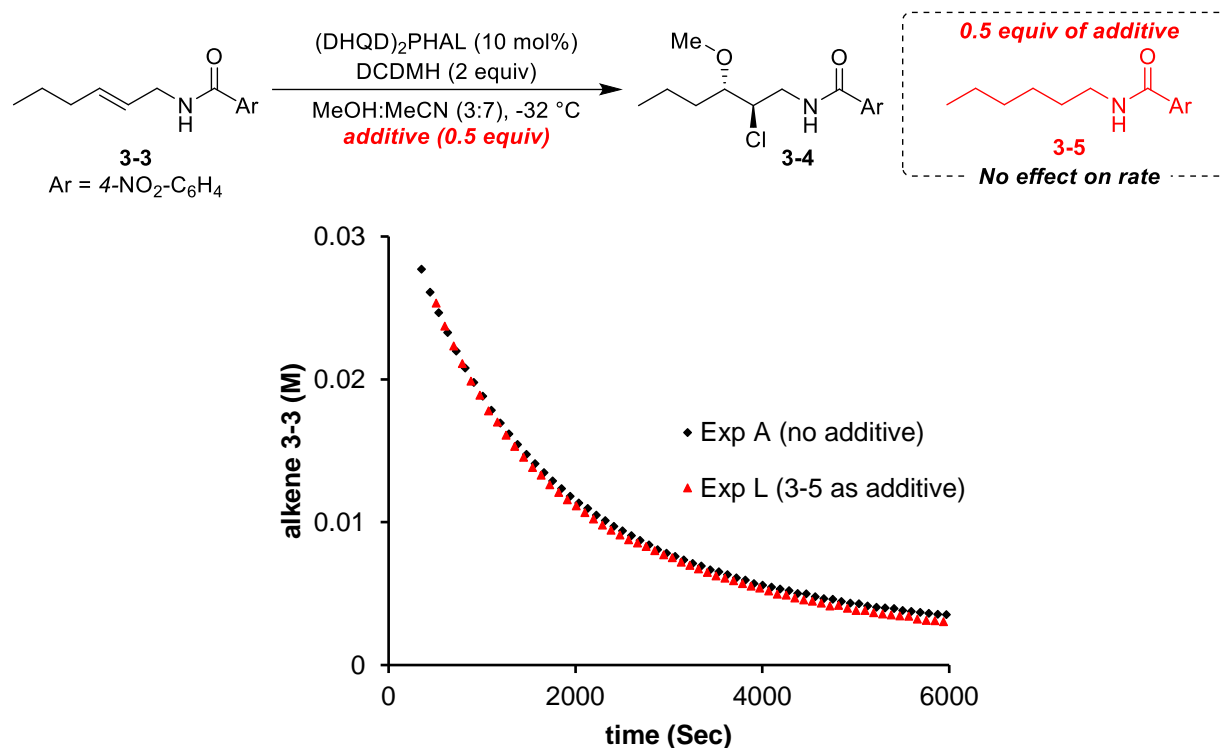
Figure 3.27 Effect of additive on chloroetherification. Kinetic profiles of (DHQD)₂PHAL catalyzed chloroetherification with and without the additive **3-5**.

3.7.3.x Kinetic isotopic effect studies

The kinetic isotopic effect (KIE) of deuterium at the ether-forming carbon was measured using competition experiment protocols well-established in literature.[33] A ~1:1 mixture of alkene amide **3-3** and **3-3-D** (0.02 M, each) were subjected to the typical reaction conditions used for kinetic studies (0.08 M DCDMH, 4 mM or 0.4 mM (DHQD)$_2$PHAL in a 3:7 mixture of methanol-acetonitrile at -32 °C). To allow only partial conversion, the reaction was quenched after 30 min using saturated aqueous sodium thiosulfate. The aqueous layer was extracted with dichloromethane (2 mL x 3). The combined organic layer was evaporated to obtain the crude product. The crude solid was passed through a short bed of silica with ethyl acetate-hexane (1:1) to filter out the catalyst and hydantoin by-products. This provided a mixture of products **3-4** and **3-4-D**, along with the unreacted alkene amides **3-3** and **3-3-D**. The pre-reaction and the post-reaction isotopic mixtures were analyzed using ^{1}H NMR to measure the change in isotopic composition using equation 3.11. TCE was used as internal standard and methanol-d$_4$:acetonitrile-d$_3$ (3:7) was used as the NMR solvent of choice.
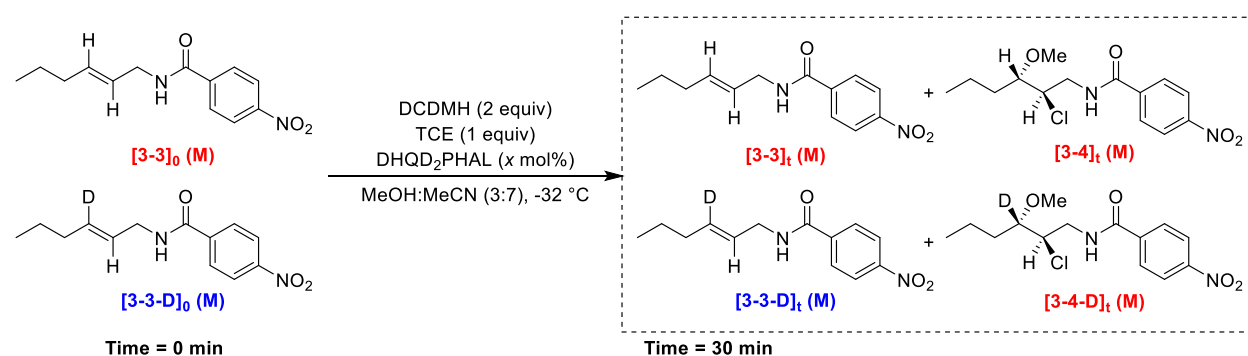
Figure 3.28 Kinetic isotopic effect study. Competition between isotopes of alkene amide 3-3 revealed an inverse kinetic isotopic effect on the (DHQD)$_2$PHAL catalyzed chloroetherification reaction.

$$KIE = \frac{k_H}{k_D} = \frac{\log(1-F_H)}{\log\left[(1-F_H)\left(\frac{R_f}{R_0}\right)\right]}$$ eq (3.11)

Where F_H, R_f and R_0 are:

$$F_H = \frac{([3-3]_0 - [3-3]_t)}{[3-3]_0}$$ eq (3.12)

$$R_f = \frac{[3-3]_t}{[3-3D]_t}$$ eq (3.13)

$$R_0 = \frac{[3-3]_0}{[3-3D]_0}$$ eq (3.14)

At high catalyst loading of 10.0 mol%:

kinetic isotopic effect (k_H/k_D): 0.89

At low catalyst loading of 1.0 mol%

kinetic isotopic effect (k_H/k_D): 0.87

3.7.4 Kinetic model

The kinetic model for the proposed catalytic cycle is illustrated below:

$$C + D \xrightleftharpoons{K_1} I_1 \quad (active\ complex)$$

$$3\text{-}3 + S \underset{k_2}{\overset{k_1}{\rightleftharpoons}} I_3$$

$$I_1 + I_3 \xrightarrow{k_3} 3\text{-}4 + M + C$$

$$C + M \xrightleftharpoons{K_2} I_2 \quad (inactive\ complex)$$

3-3 = alkene **3-3**, **3-4** = product **3-4**
D = DCDMH, **M** = MCDMH
C = (DHQD)$_2$PHAL
I_1 = (DHQD)$_2$PHAL:DCDMH (1:1)
I_2 = (DHQD)$_2$PHAL:MCDMH (1:1)
I_3 = activated alkene complex
S = solvent (methanol)

K = equilibrium constants, k = rate constants
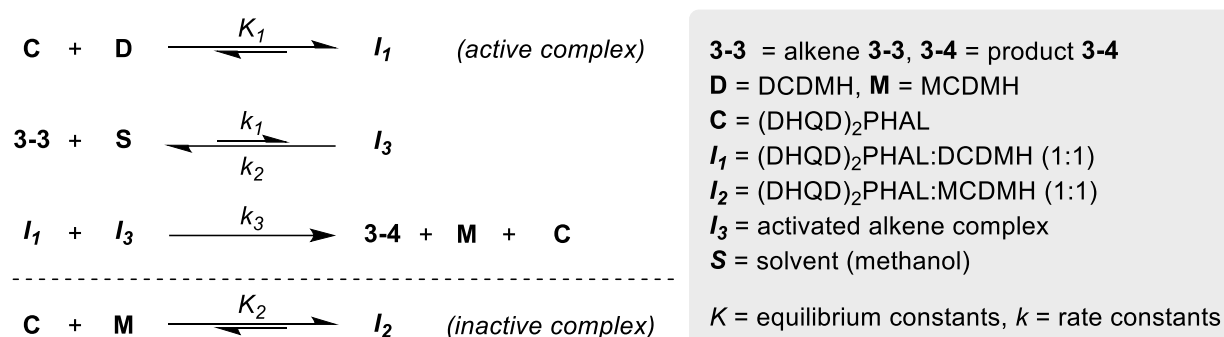
Figure 3.29 Kinetic model. Reaction pathways for the proposed kinetic model.

DCDMH-(DHQD)$_2$PHAL binding equilibrium to form the active halogenating complex:

$$K_1 = \frac{[I_1]}{[C][D]} \quad \text{-or-} \quad [I_1] = K_1[C][D] \qquad \text{eq (3.15)}$$

MCDMH-(DHQD)$_2$PHAL binding equilibrium to form the inactive complex:

$$K_2 = \frac{[I_2]}{[C][M]} \quad \text{-or-} \quad [I_2] = K_2[C][M] \qquad \text{eq (3.16)}$$

Total concentration of the catalyst:

$$[C]_0 = [C] + [I_1] + [I_2] \qquad \text{eq (3.17)}$$

Using eq (3.15), eq (3.16), and eq (3.17)

$$[C]_0 = [C] + K_1[C][D] + K_2[C][M] \quad \text{-or-} \quad [C] = \frac{[C]_0}{1 + K_1[D] + K_2[M]} \qquad \text{eq (3.18)}$$

Formation of I_3 is hypothesized to be a slow, reversible pre-catalytic step. This implies $k_1 \ll k_2$ or k_3, which results in the rapid consumption of I_3 as it is formed. Therefore, rather than a true equilibrium, the low concentration of I_3 is in a steady state. This leads to the following steady state approximation:

$$\frac{d[I_3]}{dt} = k_1[3\text{-}3][S] - k_2[I_3] - k_3[I_1][I_3] = 0 \qquad \text{eq (3.19)}$$

183

Using equations (3.15) and (3.19)

$$\frac{d[I_3]}{dt} = k_1[\mathbf{3-3}][\mathbf{S}] - k_2[I_3] - k_3K_1[\mathbf{C}][\mathbf{D}][I_3] = 0 \qquad \text{eq (3.20)}$$

Rearranging the above equation, we have,

$$[\boldsymbol{I_3}] = \frac{k_1[\mathbf{3-3}][\mathbf{S}]}{k_2 + k_3K_1[\mathbf{C}][\mathbf{D}]} \qquad \text{eq (3.21)}$$

Rate of product formation based on the proposed catalytic cycle is given by:

$$\boldsymbol{Rate} = k_3[\boldsymbol{I_1}][\boldsymbol{I_3}] \qquad \text{eq (3.22)}$$

Using equations (3.21) and (3.15) to replace [I$_3$] and [I$_1$]

$$\boldsymbol{Rate} = \frac{k_3k_1K_1[\mathbf{C}][\mathbf{D}]}{k_2 + k_3K_1[\mathbf{C}][\mathbf{D}]}[\mathbf{3-3}][\mathbf{S}] \qquad \text{eq (3.23)}$$

Substituting in eq (3.18) to eq (3.23) provides the final equation:

$$\boldsymbol{Rate} = \frac{k_3k_1K_1[\mathbf{C}]_0[\mathbf{D}]}{k_2 + k_2K_1[\mathbf{D}] + k_2K_2[\mathbf{M}] + k_3K_1[\mathbf{C}]_0[\mathbf{D}]}[\mathbf{3-3}][\mathbf{S}] \qquad \text{eq (3.24)}$$

Equation (3.24) represents the rate law equation governing the proposed catalytic cycle. This equation is consistent with variation of empirical rate equations at differing concentrations of catalyst. Note that equation (3.24) has a denominator term for MCDMH, indicating that the presence of MCDMH slows down the reaction rate. This accounts for the inhibitory activity of MCDMH from its competitive binding to (DHQD)$_2$PHAL.

The denominator of the derived rate equation (3.24) contains a catalyst concentration term. Thus, at a relatively high catalyst loading the $k_3K_1[\mathbf{C}]_0[\mathbf{D}]$ term becomes the dominant factor in the denominator. This reduces the above rate equation to the approximate form:

$$\boldsymbol{Rate} \approx k_1[\mathbf{3-3}][\mathbf{S}] \qquad \text{eq (3.25)}$$

This now explains the observed rates showing near zeroth order dependence on [catalyst] and [DCDMH], but first order on [methanol] and [alkene **3-3**] at high [catalyst]. The reverse is true in the low catalyst regime, where the $k_3K_1[\textbf{C}]_0[\textbf{D}]$ term is now negligible, leading to apparent first order dependence on [catalyst] and a positive order (0.8) for [DCDMH]. This reduces the above rate equation 3.24 to the approximate form:

$$\textbf{\textit{Rate}} \approx \frac{k_3k_1K_1[\textbf{\textit{C}}]_0[\textbf{\textit{D}}]}{k_2+k_2K_1[\textbf{\textit{D}}]+k_2K_2[\textbf{\textit{M}}]}[\textbf{3}-\textbf{3}][\textbf{\textit{S}}] \qquad\qquad \text{eq (3.26)}$$

3.7.5 ¹H NMR studies

¹H NMR studies were conducted at 25 °C, in acetonitrile-d_3 (0.8 mL total volume) as the deuterated solvent with 0.04 M of the reagents or catalyst (DCDMH, MCDMH and (DHQD)$_2$PHAL). A 0.16 M stock solution of the DCDMH, MCDMH and (DHQD)$_2$PHAL was prepared by dissolving 0.32 mmol of each species in 2 mL of deuterated solvent. Appropriate volumes of reagents (0.2 mL aliquots for 0.04 M final concentration) from these stock solutions, were syringed into a clean, dry NMR tube under nitrogen. 0.32 mmol (or 34 µL, equals 10 equiv. to mimic reaction conditions) of 1,1,1,3,3,3-hexafluoroisopropanol (HFIP) was added to each sample directly using a gas tight micro syringe, as the protic additive (as a replacement for methanol). Total volume of each sample solution was adjusted to 0.8 mL by adding the appropriate amount of the deuterated solvent. Each spectrum was a result of 16 scan accumulating with 10 seconds of recycle delay. The spectra with mixed hydantoin and catalyst (Exp 5-8, Table 3.10) were not labeled due to broadening of peaks.

Table 3.10 Experiments with different catalyst concentration

Exp	Hydantoin (M)	HFIP (M)	(DHQD)$_2$PHAL (M)
1	0.04 M, DCDMH	0.4	-
2	0.04 M, MCDMH	0.4	-
3	0.04 M, DMH	0.4	-
4	-	0.4	0.04
5	0.04 M, DCDMH	0.4	0.04
6	0.08 M, DCDMH	0.4	0.04
7	0.04 M, MCDMH	0.4	0.04
8	0.08 M, MCDMH	0.4	0.04

3.7.5.i ^{1}H NMR of DCDMH (Exp 1, Table 3.10)

DCDMH

HFIP (C-H)

HFIP (O-H)

DCDMH

CH$_3$CN

f1 (ppm)
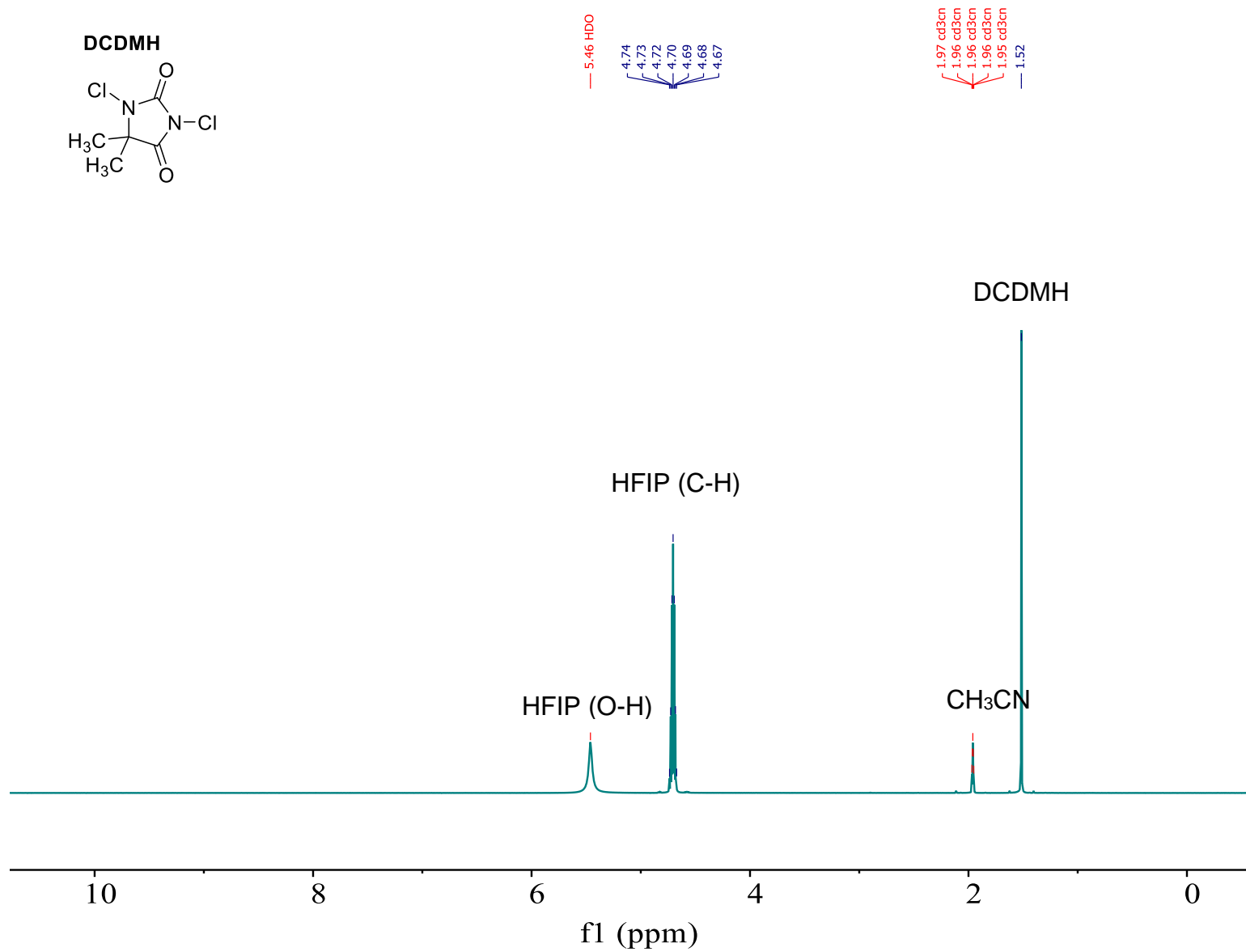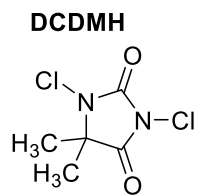
3.7.5.ii ¹H NMR of MCDMH (Exp 2, Table 3.10)

MCDMH

5.65

4.74
4.73
4.72
4.71
4.70
4.70
4.69
4.69
4.68

1.97
1.96
1.96
1.96
1.95
1.44
1.37

HFIP (C-H)

MCDMH

HFIP (O-H)

CH₃CN

10   8   6   4   2   0

f1 (ppm)
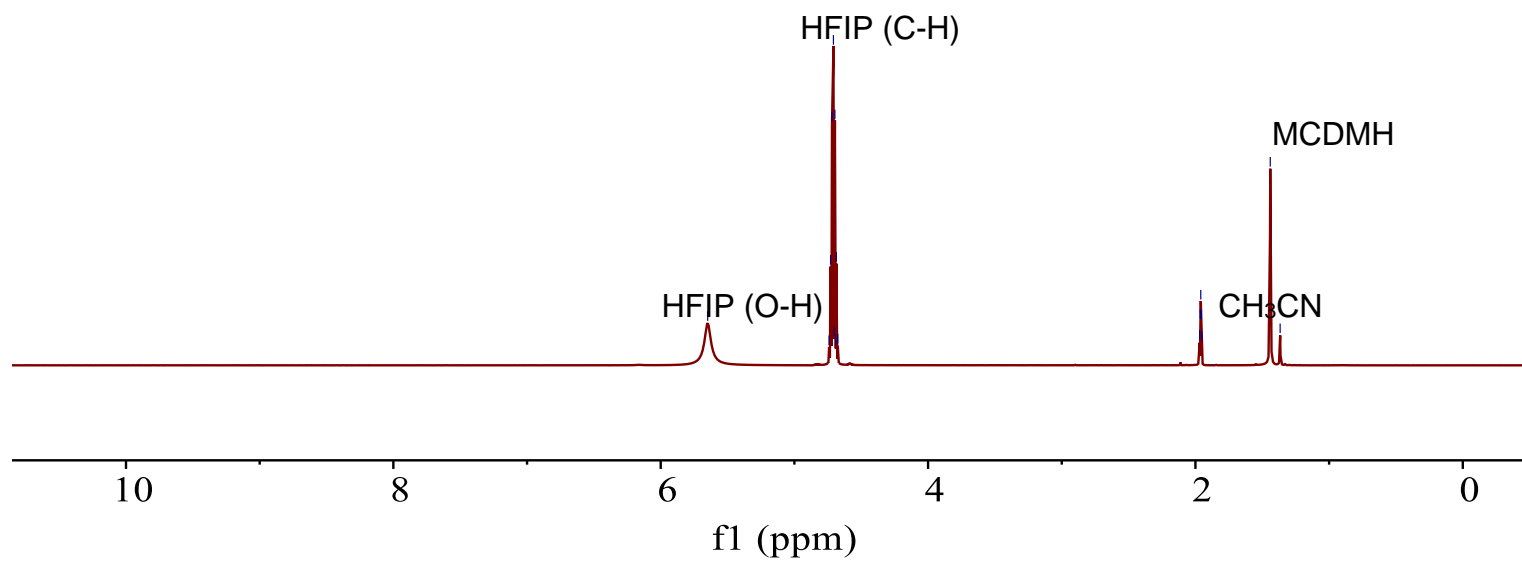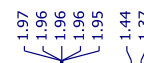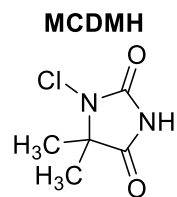
3.7.5.iii ¹H NMR of DMH (Exp 3, Table 3.10)

DMH

5.65

4.74
4.73
4.72
4.71
4.70
4.70
4.69
4.69
4.68

1.97
1.96
1.96
1.96
1.95

1.44
1.37

fl (ppm)
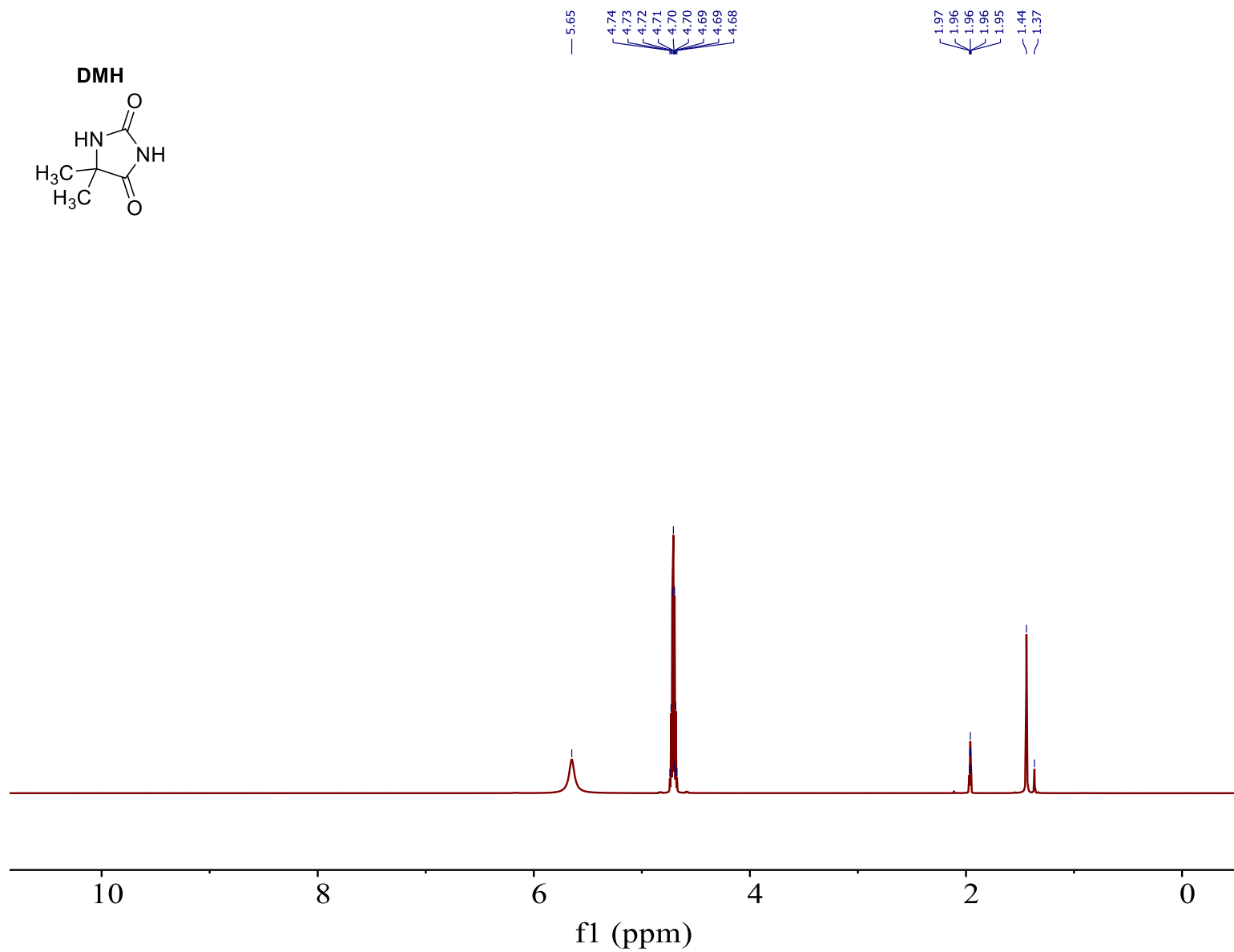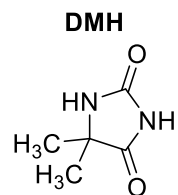
3.7.5.iv ¹H NMR of (DHQD)₂PHAL (Exp 4, Table 3.10)

190
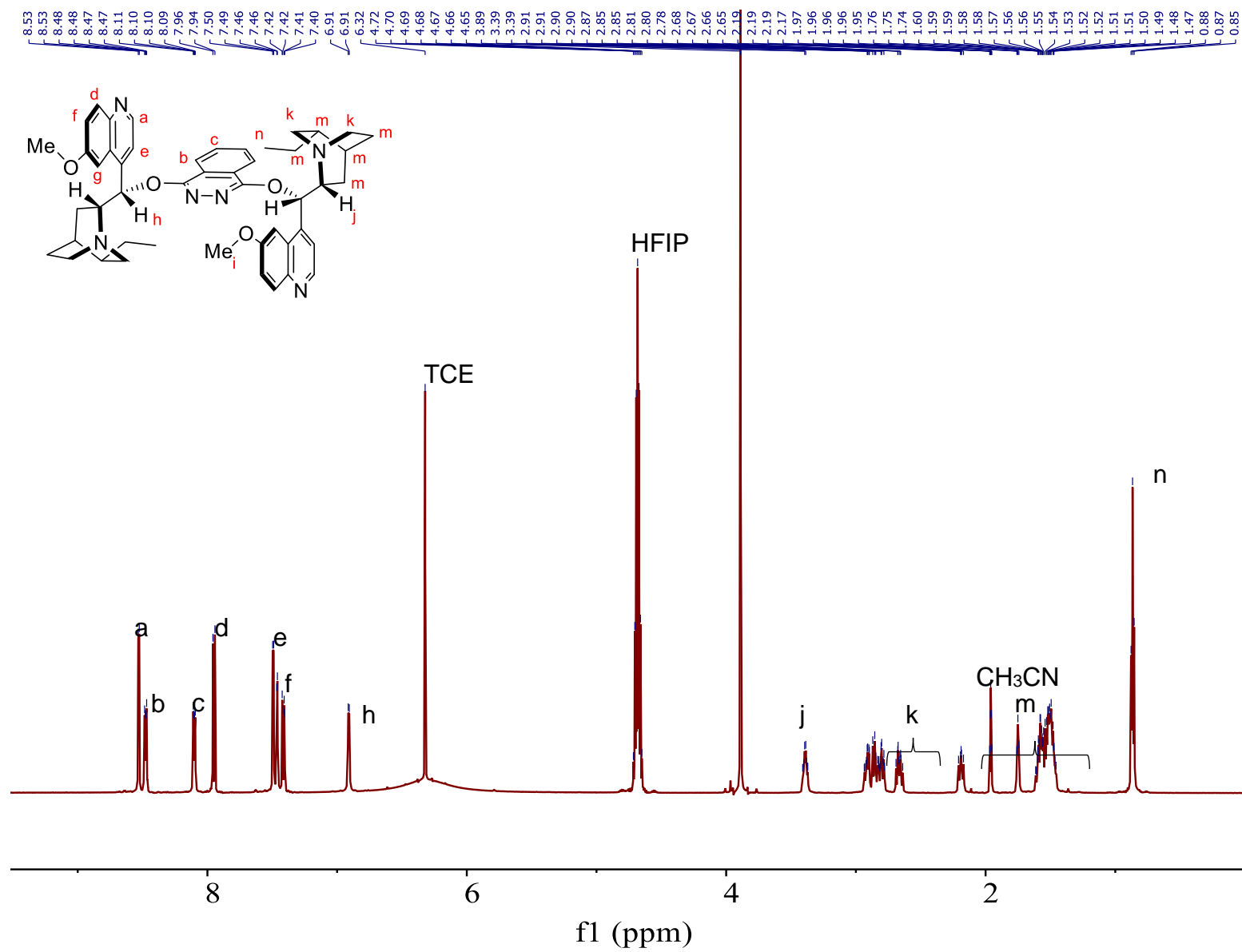
3.7.5.v ^{1}H NMR of DCDMH + (DHQD)$_2$PHAL 1:1 mixture (Exp 5, Table 3.10)

(DHQD)$_2$PHAL

DCDMH

(1:1)

TCE

HFIP

CH$_3$CN

f1 (ppm)
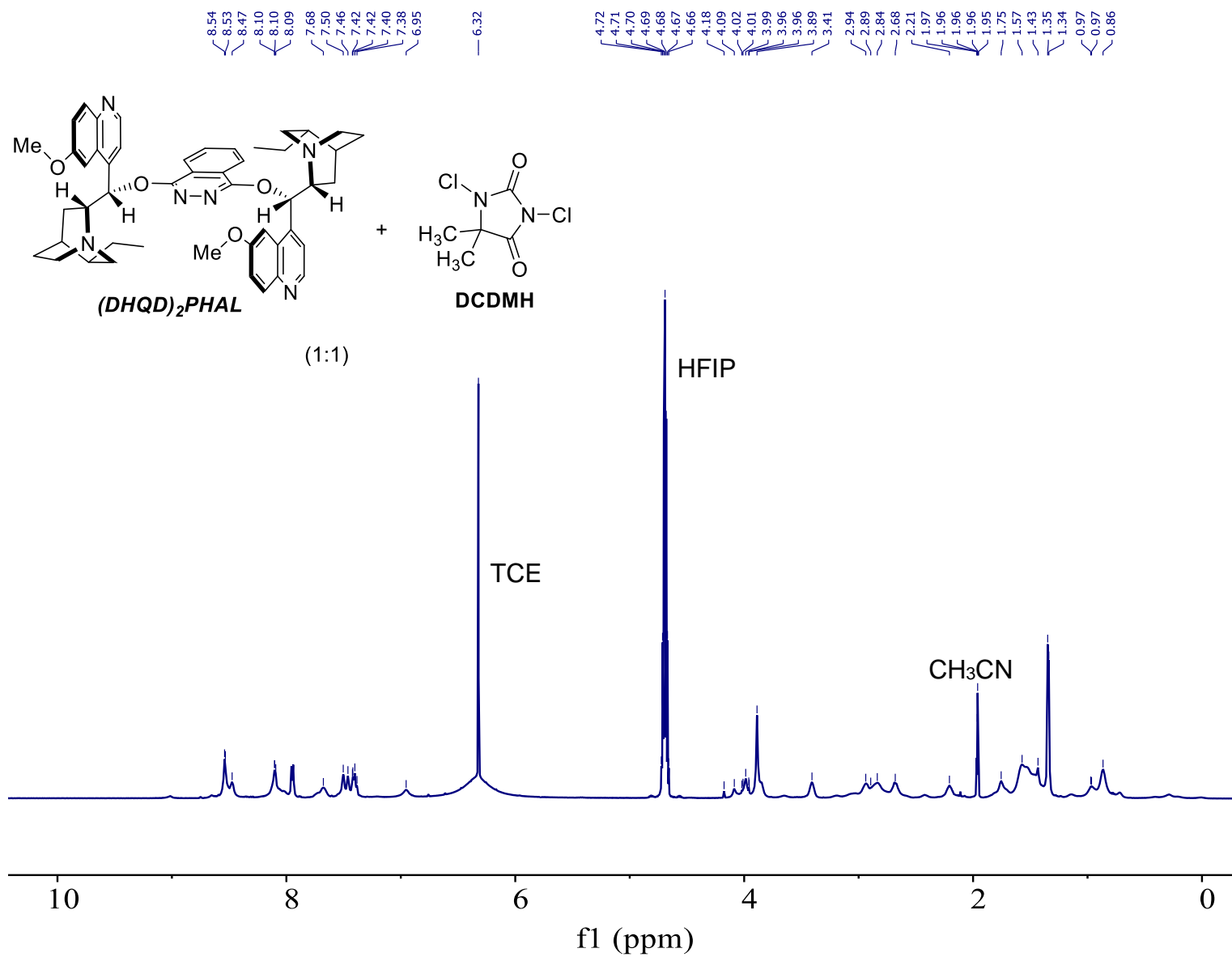
3.7.5.vi ^{1}H NMR of DCDMH + (DHQD)$_2$PHAL 2:1 mixture (Exp 6, Table 3.10)

(DHQD)$_2$PHAL

+

DCDMH

(1:2)

TCE

HFIP

CH$_3$CN

f1 (ppm)
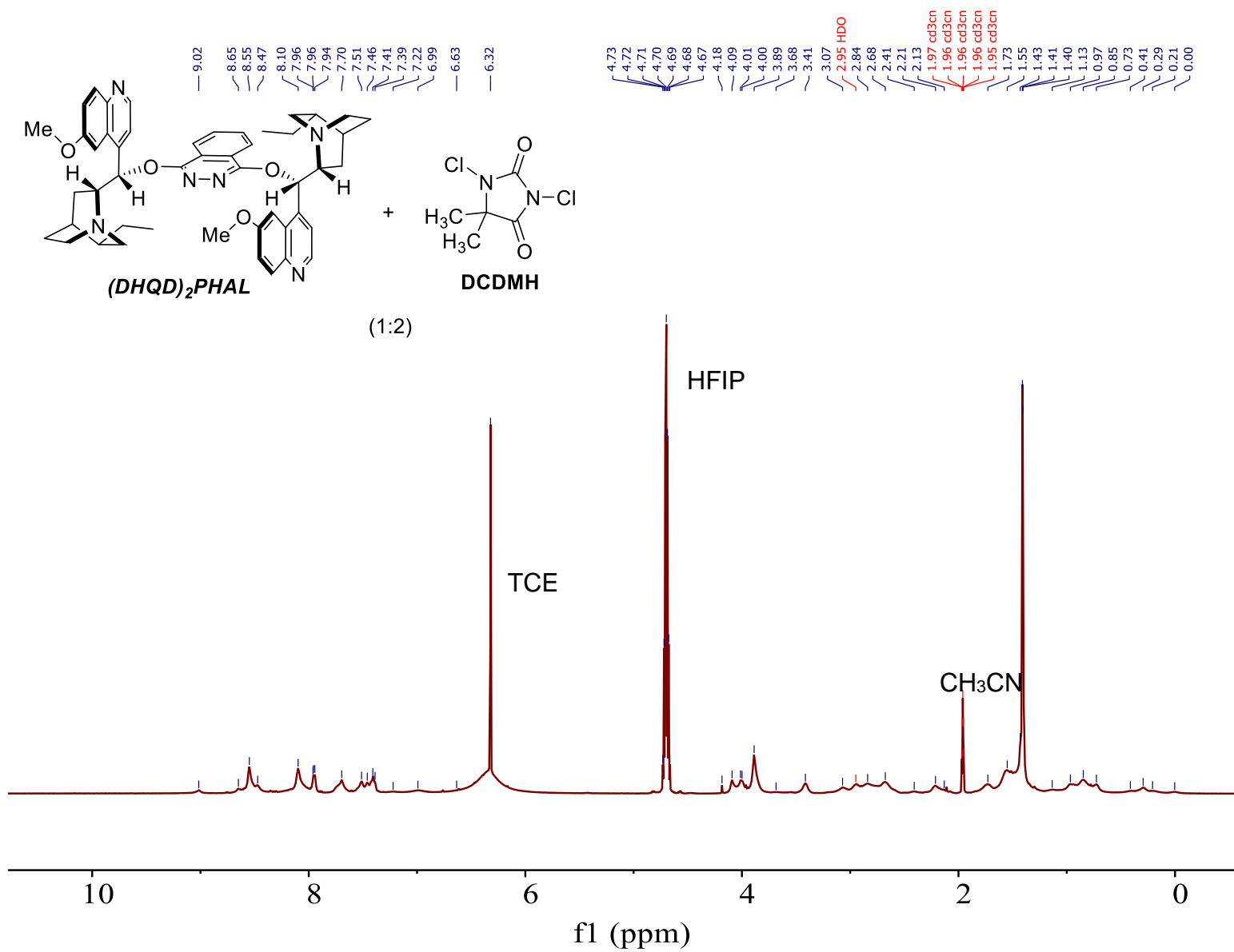
3.7.5.vii ^{1}H NMR of MCDMH + (DHQD)$_2$PHAL 1:1 mixture (Exp 7, Table 3.10)

(DHQD)$_2$PHAL

MCDMH

(1:1)

HFIP

TCE

CH$_3$CN
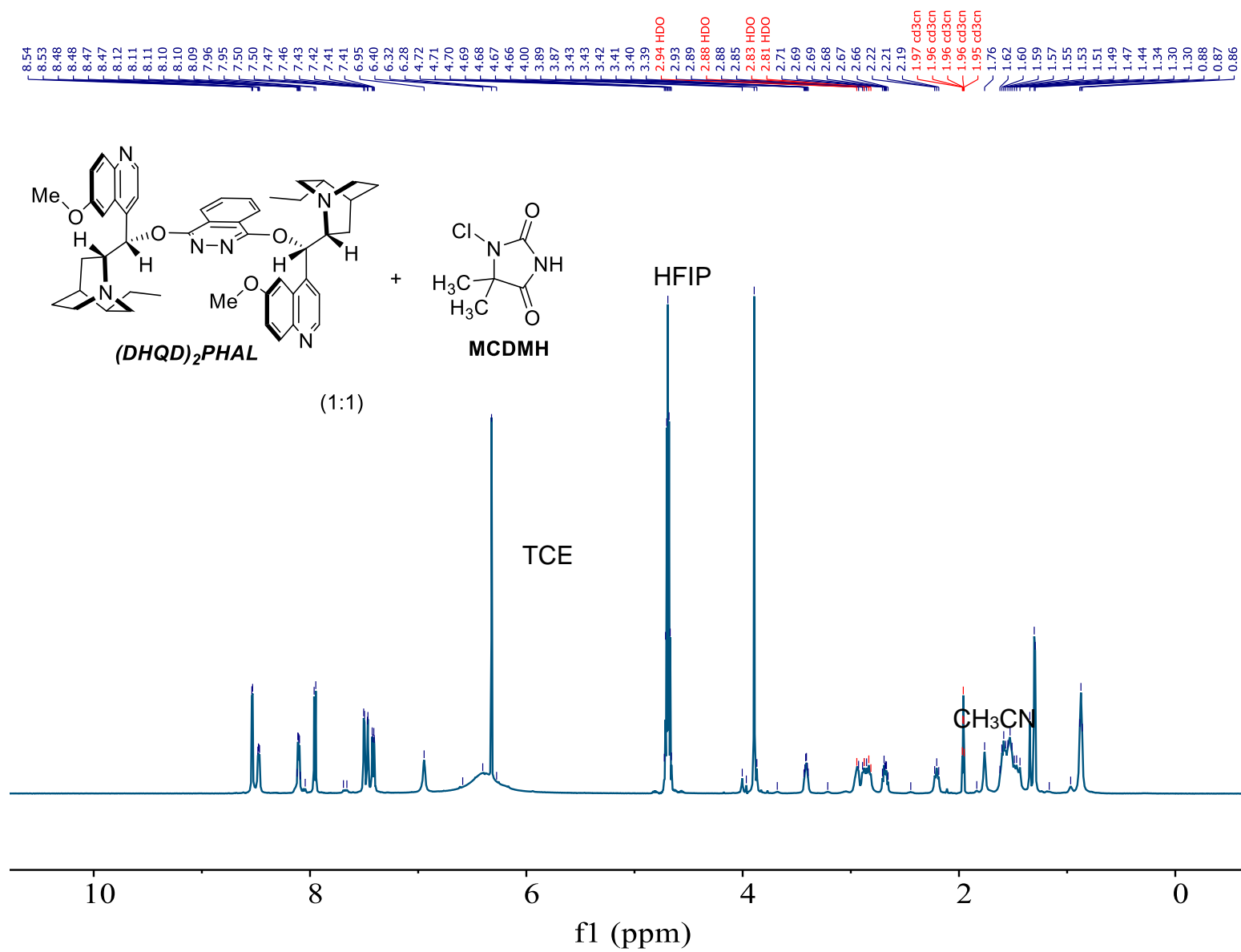
3.7.5.viii ^{1}H NMR of MCDMH + (DHQD)$_2$PHAL 2:1 mixture (Exp 7, Table 3.10)
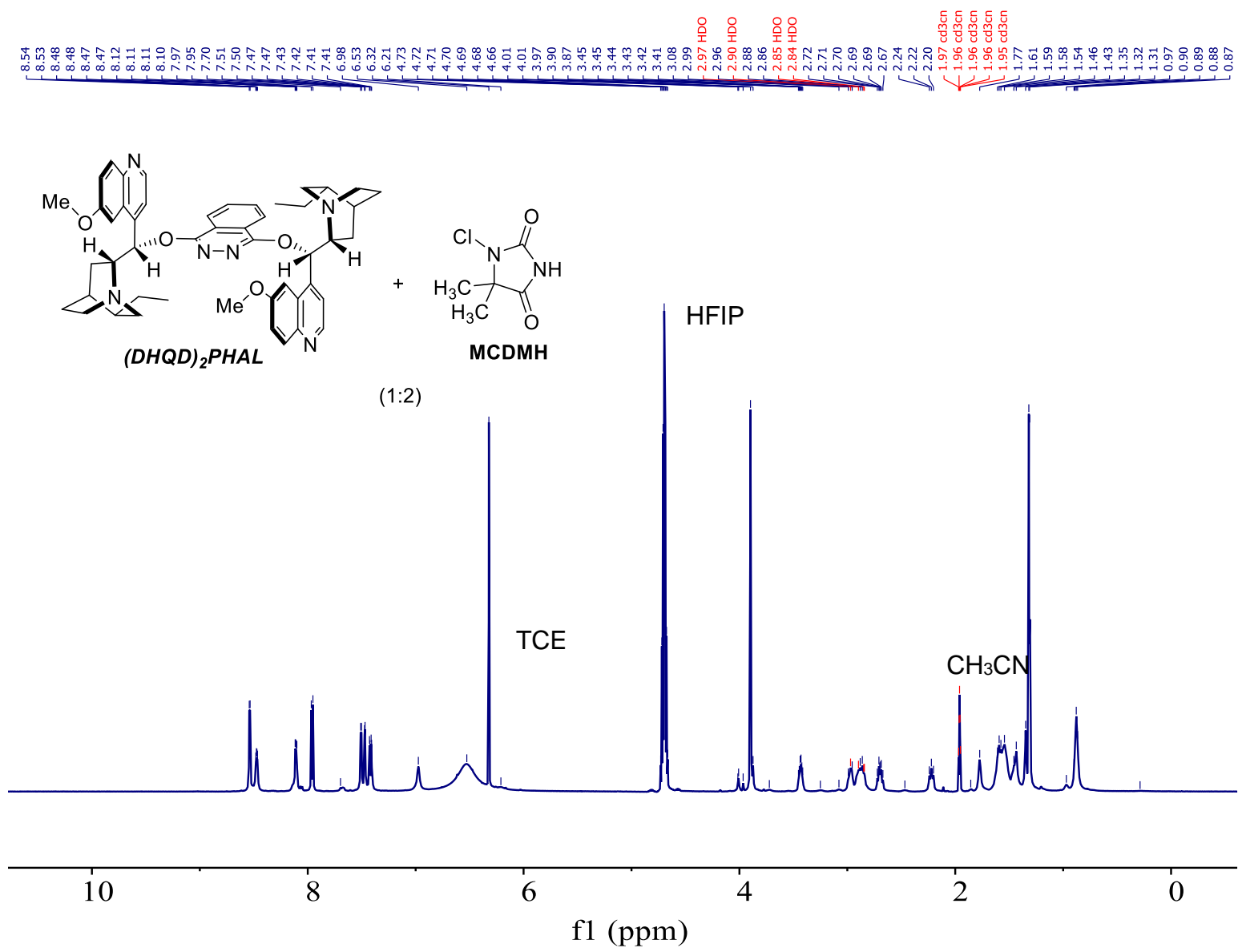
3.7.5.ix Spectra i-viii (Exp 1-8, Table 3.10) gem-dimethyl region
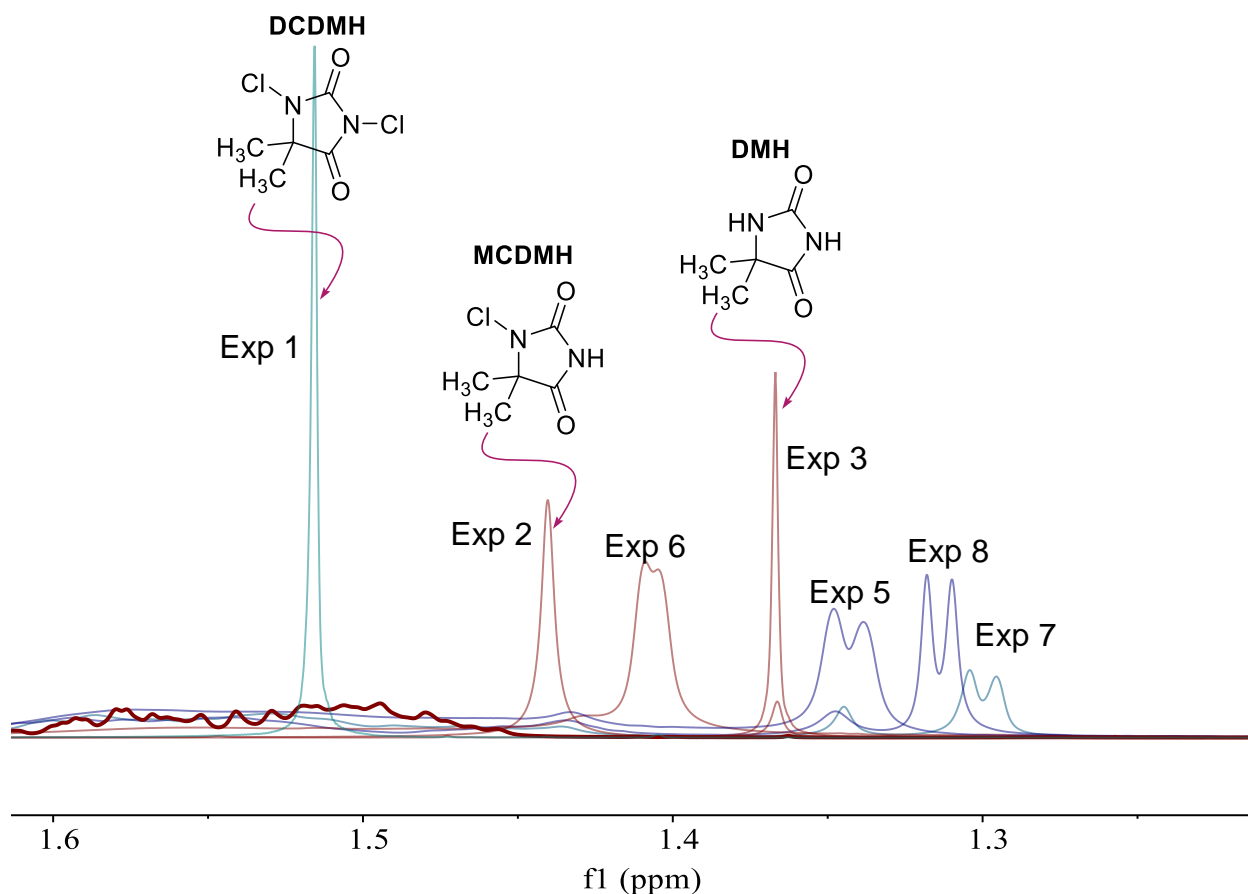
Figure 3.30 Chemical shift change of chlorohydantoins in presence of catalyst. The above overlay of spectra demonstrates the change in chemical shift of the methyl protons of DCDMH and MCDMH with various equivalents of (DHQD)$_2$PHAL indicating a reversible binding (Table 3.10, Exp 1-8). Also note the doubling of the two methyl signals in the presence of the catalyst, indicates the diastereotopic environment experienced by them inside the chiral pocket.

3.7.6 DOSY NMR studies

3.7.6.i Sample preparation

DOSY NMR studies were conducted at 0 °C in acetonitrile-d_3 (0.8 mL total volume of the sample) as the deuterated solvent. The NMR probe was cooled to 0 °C and allowed to equilibrate for at least 1 h prior to use. Stock solutions (0.16 M) of DCDMH, MCDMH and (DHQD)$_2$PHAL each were prepared by dissolving 0.32 mmol of each species in 2 mL of deuterated solvent. Appropriate volumes of reagents (0.2 mL for 0.04 M final concentration) from these stock solutions were syringed into a clean, dry NMR tube under nitrogen. 1,1,1,3,3,3-hexafluoroisopropanol (HFIP, 0.32 mmol or 34 μL) was added to each sample directly using a gas tight micro syringe as the protic additive (as a replacement for methanol). Total volume of each sample was adjusted to 0.8 mL by adding the appropriate amount of the deuterated solvent. The pulse sequence used for the DOSY experiment is dbppste_cc (Bipolar Pulse Pair Stimulated Echo with convection compensation with 15 increments, gradient strength incremented from 2.4 to 56.6 G/cm).[49] Each spectrum was a collection of 16 scans, with 10 second recycle delay, 20 ms diffusion delay, and 1.0-1.4 ms diffusion gradient length. Gradient strengths, diffusion delays, and gradient lengths were set such that the signal intensity of the spectrum with the highest gradient power was 10-20% of that of the spectrum with the lowest gradient power.

3.7.6.ii DOSY analysis

The DOSY NMRs were analyzed using MestReNova 12.0 and 14.1. The diffusion coefficients for the chlorohydantoins (DCDMH and MCDMH) were obtained from mono-exponential fits. The coefficients from the mono-exponential were normalized against the diffusion of acetonitrile, as an internal standard to compensate for interexperimental differences).[42]

Table 3.11 Experiments with different catalyst concentration

Exp	Chlorohydantoin (M)	HFIP (M)	(DHQD)$_2$PHAL (M)	Gradient length (ms)	Chlorohydantoin NMR ^{1}H NMR (ppm)	Chlorohydantoin NMR DOSY coefficient*
1	0.04 M, DCDMH	0.4	-	1.0	1.516	0.9375
2	0.04 M, DCDMH	0.4	0.04	1.2	1.343	0.5625
3	0.04 M, MCDMH	0.4	-	1.4	1.440	0.5738
4	0.04 M, MCDMH	0.4	0.04	1.3	1.300	0.4546

* DOSY coefficients were normalized with respect to the solvent acetonitrile set to 1.0
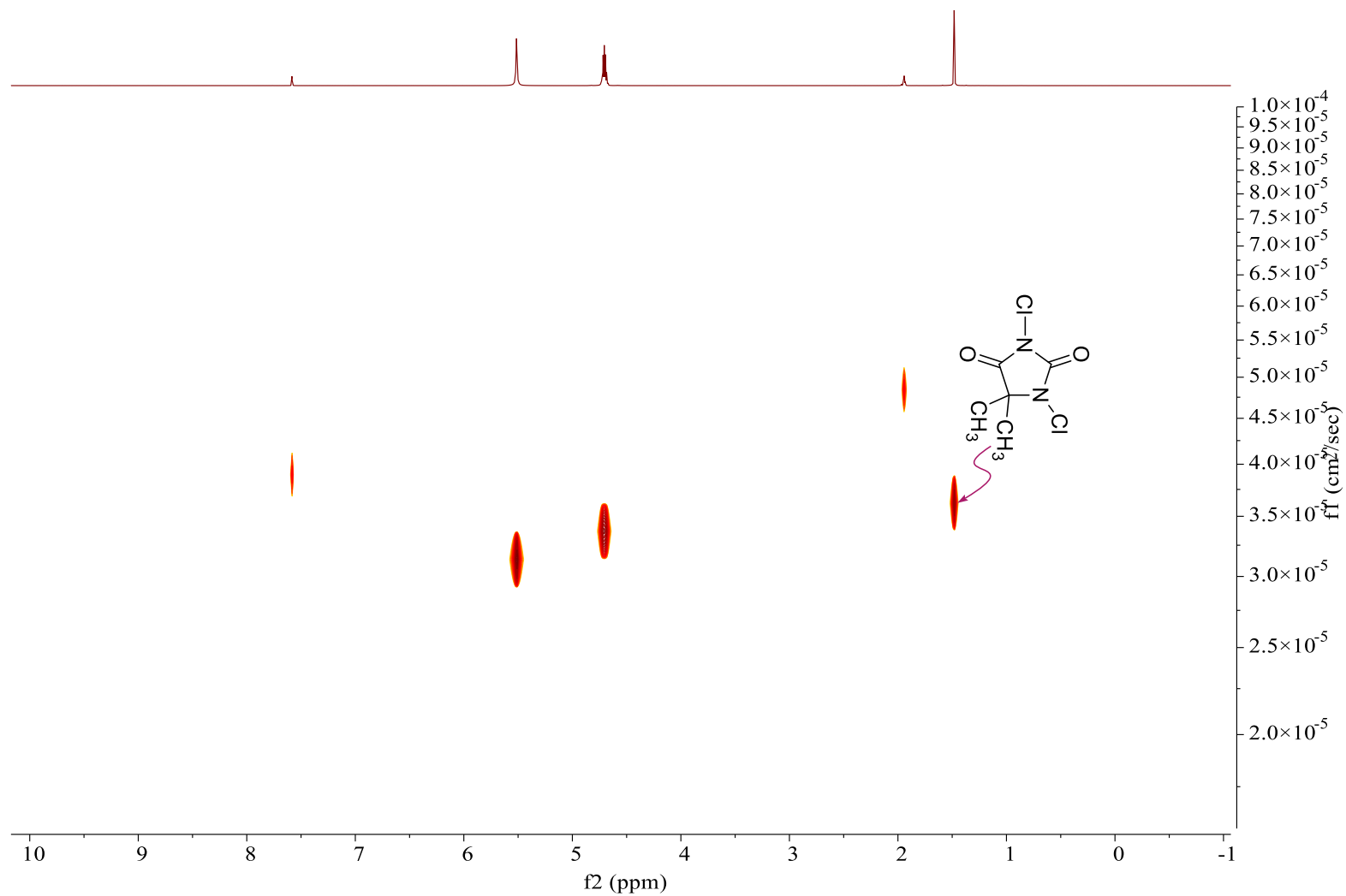
3.7.6.v DOSY NMR spectra of MCDMH (Exp 3, Table 3.11)
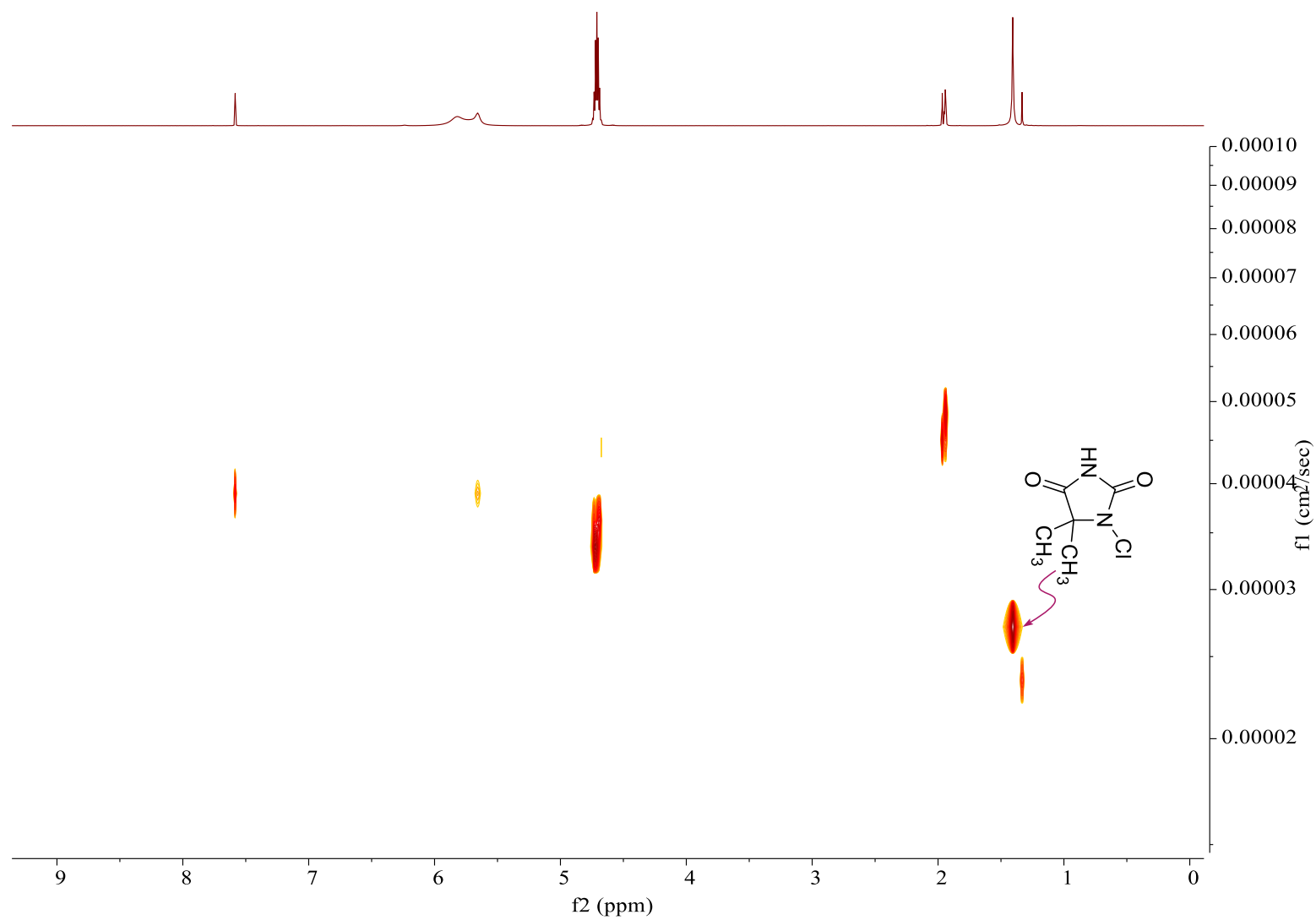
3.7.6.vi DOSY NMR spectra of MCDMH-(DHQD)₂PHAL (Exp 4, Table 3.11)
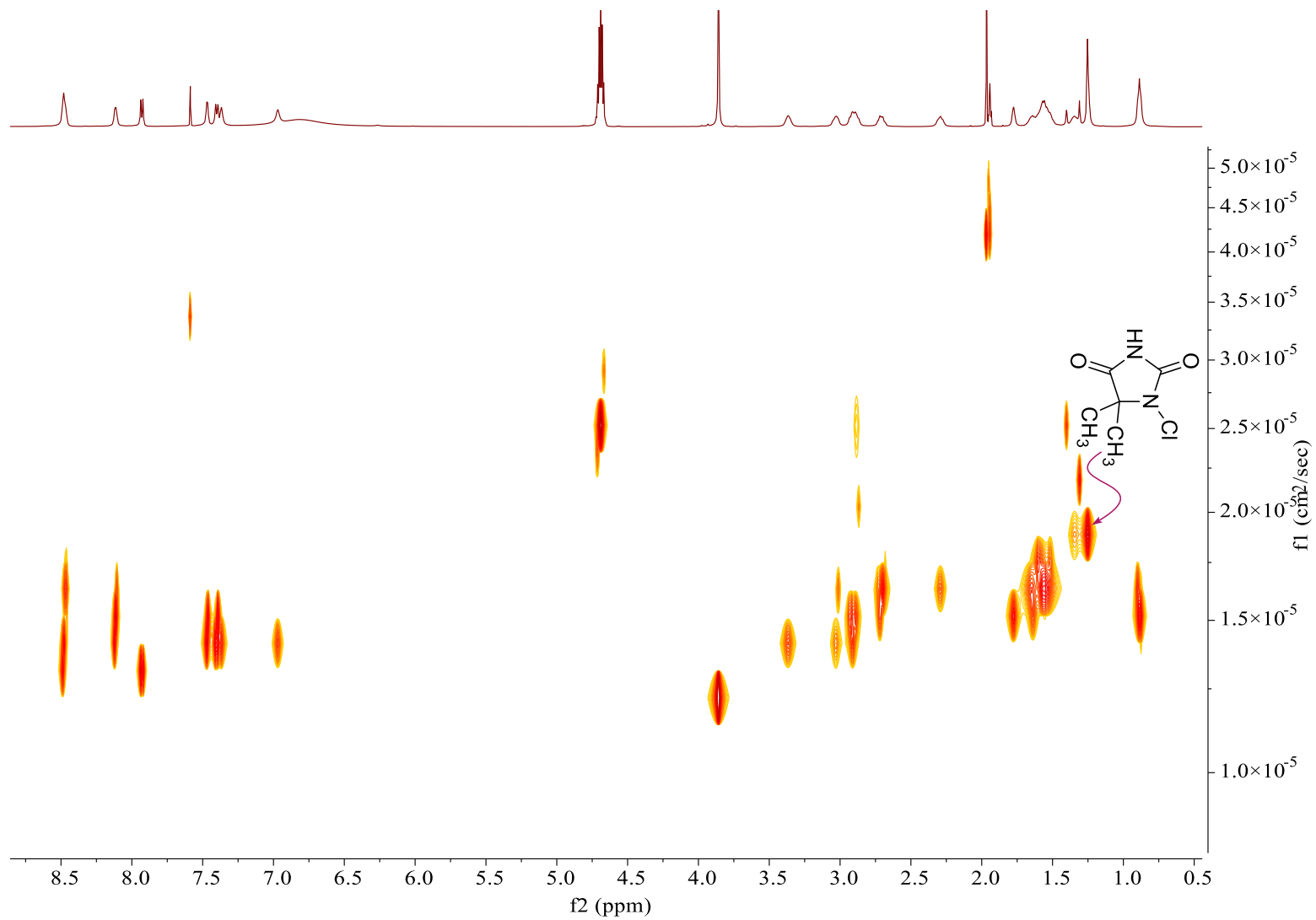
3.7.6.vii DOSY analysis to determine bound ratio

Under the assumption that chlorohydantoins (DCDMH and MCDMH) exist in two states in presence of the catalyst (DHQD)$_2$PHAL (1:1 bound and an unbound state), one may derive the approximate bound to unbound ratio of chlorohydantoin in these 1:1 chlorohydantoin:catalyst mixtures. This is done by fitting the average diffusion decay of the chlorohydantoin with a linear combination of two exponentials (eq 3.27), one corresponding to the catalyst from the 1:1 complex and one corresponding to the chlorohydantoin in the "free state" pure chlorohydantoin spectra. The coefficients (S_{0A} and S_{0B}) of the linear combination of these two exponentials approximately represents the free to bound ratio.

A modified version of the Stejskal-Tanner equation,[50] which compensates for non-uniform pulse field gradients, was used in the single exponential DOSY analyses. The necessary calibrations and equations were implemented as provided by the instrument vendor, Varian. Details can be found in "High-Resolution Diffusion-Ordered Spectroscopy (DOSY) User Guide", Pub No. 9100094300 Rev.B 2/23/10, Varian, Inc.

Biexponential fitting of the decay of hydantoin peaks in the hydantoin-catalyst mixture was performed using a slight modification of the standard Stejskal-Tanner equation:

$$S = S_{0A}e^{-D_A\gamma^2\delta^2g^2\Delta'} + S_{0B}e^{-D_B\gamma^2\delta^2g^2\Delta'} \qquad \text{eq (3.27)}$$

S is the signal amplitude, S_0 is the echo amplitude for no diffusion, D is the diffusion coefficient, δ is the gradient pulse width, γ is the gyromagnetic ratio, g is the gradient amplitude, Δ′ is the diffusion time corrected for the effects of finite gradient pulse width, and a and b are the fractional contribution from the two diffusing species.

Prior to DOSY coefficient calculation, 1.0 Hz line broadening, zero-filling to 64k data points, and Whittaker Smoother baseline correction as employed in Mnova 14.1 were performed on all data. DOSY coefficients were calculated using the maximum peak calculation for relevant peaks including a biexponential calculation for the reagent, chlorohydantoins (DCDMH and MCDMH).[51] The diffusion of the deuterated solvent, CD_3CN, was used as an internal standard and diffusion values were adjusted to compensate for differences in CD_3CN between experiments. The biexponential is calculated assuming that the reagent diffusion is a combination of diffusion as the free reagent and as that bound to the catalyst. The diffusion coefficients for the biexponential were set from the diffusion coefficient of the reagent without catalyst and the average of the aromatic diffusion coefficients of the catalyst in the presence of the reagent. The relative ratios between the two exponentials were free variables, allowed to be determined by MNova. The resulting biexponential is a good fit giving the ratios of bound to free in Table 3.12.

Table 3.12 Extracting the free-to-bound ratio from a biexponential fitting

Exp	Chlorohydantoin (M)	(DHQD)$_2$PHAL (M)	S_{0A}	S_{0B}	Free to bound ratio of chlorohydantoins
1	0.04 M, DCDMH	-	-	-	100:0
2	0.04 M, DCDMH	0.04	14.79	10.38	59:41
3	0.04 M, MCDMH	-	-	-	100:0
4	0.04 M, MCDMH	0.04	26.26	31.14	46:54

The biexponential coefficient (S_{0A} and S_{0B}) represents the bound vs. free ratio. Another interpretation could be that it's purely free reagent on top of only catalyst and a biexponential fit is not appropriate. This would make sense if both peaks were superimposed and had similar linewidths making deconvolution impossible. Since the data shows that the catalyst has much broader peaks than that of the reagent, indicating

slower dynamics (larger, slower moving molecules or assemblies have shorter T_2 time constants and broader peaks), the bound vs. free is the more credible model. The effect of the 1,1,1,3,3,3-hexafluoroisopropanol (HFIP) was not addressed in these calculations. The HFIP is present in excess (10 equiv) for all experiments and is assumed that its influence, if any, on binding and diffusion is averaged out.

3.7.7 General procedure for computational studies

General remarks: All calculations presented in this article were performed using the Spartan'18 (Spartan 18; Wavefunction Inc.: Irvine, CA) software package. Density functional theory was used to optimize all structures at the B3LYP/6-31G* level.[45, 47, 48]

Chlorohydantoin-quinuclidine binding enthalpies: Structures were optimized using density functional theory at the B3LYP/6-31G* level in the gas phase. The optimized structures were then reoptimized using the SM8 polarizable continuum solvent model[40] with acetonitrile as the solvent. Vibrational analysis was performed to ensure the absence of imaginary frequencies for optimized minima. Binding enthalpies were calculated from the enthalpic differences of the respective bound and unbound species.

(DHQD)$_2$PHAL transition states and substrate-bound complexes: Both transition state and substrate-bound complex structures were optimized using density functional theory at the B3LYP/6-31G* level in the gas phase. Structural optimization was followed by vibrational analysis to verify the structure's character as either a "saddle point" (transition structure, with a single imaginary frequency) or a minimum (no imaginary frequency). Explicit solvent methanol molecules were utilized as hydrogen bond partners of DCDMH.

Halenium affinity calculations: Structures used for halenium affinity calculations were optimized using density functional theory at the B3LYP/6-31G* level in the gas phase. The optimized structures were then reoptimized using the SM8 model with acetonitrile as the solvent of choice. Vibrational analysis was performed to ensure the absence of imaginary frequencies for optimized minima. Halenium affinities were calculated from the enthalpic differences of the respective chlorinated and dechlorinated species using the prior illustrated method.[31]

REFERENCES

REFERENCES

1.   Chen, J.; Zhou, L., Recent Progress in the Asymmetric Intermolecular Halogenation of Alkenes. *Synthesis-Stuttgart* **2014,** *46* (5), 586-595.

2.   Cheng, Y. A.; Yu, W. Z.; Yeung, Y. Y., Recent advances in asymmetric intra- and intermolecular halofunctionalizations of alkenes. *Org. Biomol. Chem.* **2014,** *12* (15), 2333-2343.

3.   Chung, W. J.; Vanderwal, C. D., Stereoselective Halogenation in Natural Product Synthesis. *Angew. Chem. Int. Ed.* **2016,** *55* (14), 4396-4434.

4.   Cresswell, A. J.; Eey, S. T. C.; Denmark, S. E., Catalytic, Stereoselective Dihalogenation of Alkenes: Challenges and Opportunities. *Angew. Chem. Int. Ed.* **2015,** *54* (52), 15642-15682.

5.   Denmark, S. E.; Kuester, W. E.; Burk, M. T., Catalytic, Asymmetric Halofunctionalization of Alkenes-A Critical Perspective. *Angew. Chem. Int. Ed.* **2012,** *51* (44), 10938-10953.

6.   Khalid, M.; Mohammed, S., Recent Halocyclization Reactions of Alkenes - A Review. *Indian J. Heterocycl. Chem.* **2018,** *28* (4), 507-527.

7.   Landry, M. L.; Burns, N. Z., Catalytic Enantioselective Dihalogenation in Total Synthesis. *Acc. Chem. Res.* **2018,** *51* (5), 1260-1271.

8.   Murai, K.; Fujioka, H., Recent Progress in Organocatalytic Asymmetric Halocyclization. *Heterocycles* **2013,** *87* (4), 763-+.

9.   Nolsoe, J. M. J.; Hansen, T. V., Asymmetric Iodolactonization: An Evolutionary Account. *Eur. J. Org. Chem.* **2014,** *2014* (15), 3051-3065.

10.   Tan, C. K.; Yeung, Y. Y., Recent advances in stereoselective bromofunctionalization of alkenes using N-bromoamide reagents. *Chem. Commun.* **2013,** *49* (73), 7985-7996.

11.   Whitehead, D. C.; Yousefi, R.; Jaganathan, A.; Borhan, B., An Organocatalytic Asymmetric Chlorolactonization. *J. Am. Chem. Soc.* **2010,** *132* (10), 3298-+.

12.   Boratynski, P. J., Dimeric Cinchona alkaloids. *Mol. Divers.* **2015,** *19* (2), 385-422.

13.   Garzan, A.; Jaganathan, A.; Marzijarani, N. S.; Yousefi, R.; Whitehead, D. C.; Jackson, J. E.; Borhan, B., Solvent-Dependent Enantiodivergence in the Chlorocyclization of Unsaturated Carbamates. *Chem. Eur. J.* **2013,** *19* (27), 9015-9021.

14.   Jaganathan, A.; Borhan, B., Chlorosulfonamide Salts Are Superior Electrophilic Chlorine Precursors for the Organocatalytic Asymmetric Chlorocyclization of Unsaturated Amides. *Org. Lett.* **2014,** *16* (14), 3616-3619.

15.   Jaganathan, A.; Garzan, A.; Whitehead, D. C.; Staples, R. J.; Borhan, B., A Catalytic Asymmetric Chlorocyclization of Unsaturated Amides. *Angew. Chem. Int. Ed.* **2011,** *50* (11), 2593-2596.

16.   Jaganathan, A.; Staples, R. J.; Borhan, B., Kinetic Resolution of Unsaturated Amides in a Chlorocyclization Reaction: Concomitant Enantiomer Differentiation and Face Selective Alkene Chlorination by a Single Catalyst. *J. Am. Chem. Soc.* **2013,** *135* (39), 14806-14813.

17.   Soltanzadeh, B.; Jaganathan, A.; Staples, R. J.; Borhan, B., Highly Stereoselective Intermolecular Haloetherification and Haloesterification of Allyl Amides. *Angew. Chem. Int. Ed.* **2015,** *54* (33), 9517-9522.

18.   Soltanzadeh, B.; Jaganathan, A.; Yi, Y.; Yi, H.; Staples, R. J.; Borhan, B., Highly Regio- and Enantioselective Vicinal Dihalogenation of Allyl Amides. *J. Am. Chem. Soc.* **2017,** *139* (6), 2132-2135.

19.   Yousefi, R.; Whitehead, D. C.; Mueller, J. M.; Staples, R. J.; Borhan, B., On the Chlorenium Source in the Asymmetric Chlorolactonization Reaction. *Org. Lett.* **2011,** *13* (4), 608-611.

20.   Yousefi, R.; Sarkar, A.; Ashtekar, K. D.; Whitehead, D. C.; Kakeshpour, T.; Holmes, D.; Reed, P.; Jackson, J. E.; Borhan, B., Mechanistic Insights into the Origin of Stereoselectivity in an Asymmetric Chlorolactonization Catalyzed by (DHQD)$_2$PHAL. *J Am Chem Soc* **2020,** *142* (15), 7179-7189.

21.   Marzijarani, N. S.; Yousefi, R.; Jaganathan, A.; Ashtekar, K. D.; Jackson, J. E.; Borhan, B., Absolute and relative facial selectivities in organocatalytic asymmetric chlorocyclization reactions. *Chem. Sci.* **2018,** *9* (11), 2898-2908.

22.   Yousefi, R.; Ashtekar, K. D.; Whitehead, D. C.; Jackson, J. E.; Borhan, B., Dissecting the stereocontrol elements of a catalytic asymmetric chlorolactonization: syn addition obviates bridging chloronium. *J. Am. Chem. Soc.* **2013,** *135* (39), 14524-7.

23.   Blackmond, D. G., Reaction progress kinetic analysis: A powerful methodology for mechanistic studies of complex catalytic reactions. *Angew. Chem. Int. Ed.* **2005,** *44* (28), 4302-4320.

24.   Blackmond, D. G., Kinetic Profiling of Catalytic Organic Reactions as a Mechanistic Tool. *J. Am. Chem. Soc.* **2015,** *137* (34), 10852-10866.

25.   Bures, J., A Simple Graphical Method to Determine the Order in Catalyst. *Angew. Chem. Int. Ed.* **2016,** *55* (6), 2028-2031.

26.   Bures, J., Variable Time Normalization Analysis: General Graphical Elucidation of Reaction Orders from Concentration Profiles. *Angew. Chem. Int. Ed.* **2016,** *55* (52), 16084-16087.

27.   Bures, J., What is the Order of a Reaction? *Top. Catal.* **2017,** *60* (8), 631-633.

28.   Nielsen, C. D. T.; Bures, J., Visual kinetic analysis. *Chem. Sci.* **2019,** *10* (2), 348-353.

29.   Renny, J. S.; Tomasevich, L. L.; Tallmadge, E. H.; Collum, D. B., Method of Continuous Variations: Applications of Job Plots to the Study of Molecular Associations in Organometallic Chemistry. *Angew. Chem. Int. Ed.* **2013,** *52* (46), 11998-12013.

30.   Ashtekar, K. D.; Vetticatt, M.; Yousefi, R.; Jackson, J. E.; Borhan, B., Nucleophile-Assisted Alkene Activation: Olefins Alone Are Often Incompetent. *J. Am. Chem. Soc.* **2016,** *138* (26), 8114-8119.

31.   Ashtekar, K. D.; Marzijarani, N. S.; Jaganathan, A.; Holmes, D.; Jackson, J. E.; Borhan, B., A New Tool To Guide Halofunctionalization Reactions: The Halenium Affinity (HalA) Scale. *J. Am. Chem. Soc.* **2014,** *136* (38), 13355-13362.

32.   Denmark, S. E.; Ryabchuk, P.; Burk, M. T.; Gilbert, B. B., Toward Catalytic, Enantioselective Chlorolactonization of 1,2-Disubstituted Styrenyl Carboxylic Acids. *J. Org. Chem.* **2016,** *81* (21), 10411-10423.

33.   Lars, M.; Hundley, S. W., Reaction Rates of Isotopic Molecules. John Wiley & Sons: New York, 1979; pp 91-102.

34.   Pandey, R. N.; Henry, P. M., Palladium(II) Catalyzed Exchange Reactions .9. Vinyl Propionate Exchange with Acetic-Acid Catalyzed by Palladium(II) Acetate. *Can. J. Chem.* **1975,** *53* (15), 2223-2231.

35.   Tanaka, Y.; Takahara, J. P.; Lempers, H. E. B., Research and Development of the Catalytic Oxidation of Methylacrylate to 3,3-Dimethoxy Methyl Propionate. *Org. Process Res. Dev.* **2009,** *13* (3), 548-554.

36.   Whitaker, D.; Bures, J.; Larrosa, I., Ag(I)-Catalyzed C-H Activation: The Role of the Ag(I) Salt in Pd/Ag-Mediated C-H Arylation of Electron-Deficient Arenes. *J. Am. Chem. Soc.* **2016,** *138* (27), 8384-8387.

37.   Yayla, H. G.; Peng, F.; Mangion, I. K.; McLaughlin, M.; Campeau, L. C.; Davies, I. W.; DiRocco, D. A.; Knowles, R. R., Discovery and mechanistic study of a photocatalytic indoline dehydrogenation for the synthesis of elbasvir. *Chem. Sci.* **2016,** *7* (3), 2066-2073.

38.   The structure of the kinetic intermediate *I₃* is not immediately obvious, and deserves comment. The rate behavior demands such an entity, and our current working model is the complex shown in Figure 7. Computational explorations find such a structure to lie just 4 kcal/mol above the lowest energy amide-methanol complex, suggesting that at any given moment, it would only be present in sub micromolar concentrations.

39.   Cavallo, G.; Metrangolo, P.; Milani, R.; Pilati, T.; Priimagi, A.; Resnati, G.; Terraneo, G., The Halogen Bond. *Chem. Rev.* **2016,** *116* (4), 2478-2601.

40.   Marenich, A. V.; Olson, R. M.; Kelly, C. P.; Cramer, C. J.; Truhlar, D. G., Self-Consistent Reaction Field Model for Aqueous and Nonaqueous Solutions Based on Accurate Polarized Partial Charges. *J. Chem. Theory. Comput.* **2007,** *3* (6), 2011-33.

41.   Liang, X. W.; Zheng, C.; You, S. L., Catalytic Asymmetric Chlorinative Dearomatization Reaction of Benzofurans. *Adv. Synth. Catal.* **2016,** *358* (13), 2066-2071.

42.   Neufeld, R.; Stalke, D., Accurate molecular weight determination of small molecules via DOSY-NMR by using external calibration curves with normalized diffusion coefficients. *Chem. Sci.* **2015,** *6* (6), 3354-3364.

43.   Kakeshpour, T.; Bailey, J. P.; Jenner, M. R.; Howell, D. E.; Staples, R. J.; Holmes, D.; Wu, J. I.; Jackson, J. E., High-Field NMR Spectroscopy Reveals Aromaticity-Modulated Hydrogen Bonding in Heterocycles. *Angew. Chem. Int. Ed.* **2017,** *56* (33), 9842-9846.

44.   Kakeshpour, T.; Wu, J. I.; Jackson, J. E., AMHB: (Anti)aromaticity-Modulated Hydrogen Bonding. *J. Am. Chem. Soc.* **2016,** *138* (10), 3427-3432.

45.   Becke, A. D., Density-Functional Exchange Energy Approximation with Correct Asymptotic Behavior. *Physical Review A* **1988,** *38* (6), 3098-3100.

46.   Grimme, S.; Antony, J.; Ehrlich, S.; Krieg, H., A consistent and accurate ab initio parametrization of density functional dispersion correction (DFT-D) for the 94 elements H-Pu. *J. Chem. Phys.* **2010,** *132* (15), 19.

47.   Hehre, W. J.; Ditchfield, R.; Pople, J. A., Self—Consistent Molecular-Orbital Methods.12. Further Extensions of Gaussian-Type Basis Sets for use in Molecular-Orbital Studies of Organic Molecules. *J. Chem. Phys.* **1972,** *56* (5), 2257-+.

48.   Lee, C. T.; Yang, W. T.; Parr, R. G., Development of the Colle-Salvetti Correlation Engery Formulation into a Functional of the Electron Density. *Phys. Rev. B* **1988,** *37* (2), 785-789.

49.   Jerschow, A.; Muller, N., Suppression of convection artifacts in stimulated-echo diffusion experiments. Double-stimulated-echo experiments. *J Magn Reson* **1997,** *125* (2), 372-375.

50.   Stejskal, E. O.; Tanner, J. E., Spin Diffusion Measurements: Spin Echoes in the Presence of a Time-Dependent Field Gradient. *J. Chem. Phys.* **1965,** *42* (1), 288-+.

51.   Nilsson, M.; Connell, M. A.; Davis, A. L.; Morris, G. A., Biexponential fitting of diffusion-ordered NMR data: practicalities and limitations. *Anal. Chem.* **2006,** *78* (9), 3040-5.